UNIVERSITY OF OKLAHOMA

GRADUATE COLLEGE

GENETIC ARCHITECTURE AND INFLUENCE OF SWITCHGRASS INTERNODE ANATOMY ON BIOFUEL PRODUCTION-RELEVANT TRAITS

A DISSERTATION

SUBMITTED TO THE GRADUATE FACULTY

in partial fulfilment of the requirements for the

Degree of

DOCTOR OF PHILOSOPHY

By

DAVID J. THOMAS
Norman, Oklahoma
2022

GENETIC ARCHITECTURE AND INFLUENCE OF SWITCHGRASS INTERNODE ANATOMY ON BIOFUEL PRODUCTION-RELEVANT TRAITS

A DISSERTATION APPROVED FOR THE DEPARTMENT OF MICROBIOLOGY AND PLANT BIOLOGY

BY THE COMMITTEE CONSISTING OF

Dr. Heather McCarthy, Chair

Dr. Laura E. Bartley

Dr. John P. Masly

Dr. Abigail Moore

Dr. Scott Russell

Acknowledgements

I would first like to thank Dr. Laura E. Bartley for giving me this opportunity. When I started in the Bartley lab, I had no experience in plant biology at all, but she gave me a chance and I am grateful. She has spent countless hours discussing data and methods and has pushed me to be a better scientist at every step. It is hard to put into words how thankful I am for this opportunity and for all her continued support toward reaching this goal.

I want to thank my committee members for their support and guidance; Dr. Masly, Dr. McCarthy, Dr. Moore, Dr. Russell, and previous member, Dr. Marc Libault. I also want to thank the University of Oklahoma Department of Microbiology and lant Biology and the Graduate College.

I want to express my deepest gratitude to my wife, Molly, for always supporting me and listening to my long and often too detailed descriptions of my projects. I never could have reached this accomplishment without Molly's love and support. I want to thank my mother, Cathryn, for her unending encouragement. When I doubted myself, she never did, and made that very clear. I also want to thank her for instilling in me the will to always better myself and to seek out ways to make the world a better place for everyone. I want to thank my grandfather, John Wallace, for his encouragement and joy he expressed when he saw me pursue a graduate degree in plant biology. I want to thank my grandmother, Jeri, whose spirit I evoke whenever I stroll through the woods and wildflower meadows, whose impact on me as a child in Colorado summers is no doubt evident in my deep appreciation for the beauty of nature. Thank you to my brother, Jess, and sister, Anna, who have always greeted my every aspiration with excitement and invigorating discussion. I want to thank my dad, James, for his support and enthusiasm, especially when I chose to attend his alma mater. I

also want to thank the many friends and additional family who have always shown great interest in this direction I have taken and shown their support.

I want to thank collaborators Dr. Thomas Juenger, Dr. Felix Fritschi, Dr. David Lowry, and Jason Bonnette, additional switchgrass common gardens co-PIs and the many technicians involved who without their efforts, this work would not be possible.

I want to thank the many past and present members of the Bartley lab. Firstly, thanks to the patience and guidance of Sandra Thibivilliers, who played an integral role when I first started in plant biology and taught me so much. Those first few years were formative under her instruction and leadership within the Bartley lab. Past lab mates Dr. Kangmei Zhao, Dr. Fan Lin, and Dr. Chengcheng Zhang, thank you for teaching me so much and always greeting my questions with eagerness to help me learn. I want to thank Dr. Mariela Monteoliva for her many discussions and insights about plant biology and methods - and all the laughs, too. I want to thank undergrads Daniel, Mary, Alice, and Phuong; working with you all in the lab was one of my favorite aspects of graduate school.

I want to thank Dr. Gordon Uno for advice and frequent reminders to keep improving when I first started at OU. I want to thank Dr. Jon Giddens, whose friendship started with him as my intro botany TA but grew beyond that as we become colleagues who discussed research, attended conferences together, brainstormed methods, and even co-TA'd intro botany. I want to thank Dr. Daniel Jones and Dr. Zac Myers who were always a wealth of information and great to bounce around ideas with, along with Adam Wilson and many other students in MPBIO.

Table of Contents

List of Tables

List of Figures

Abstract

Biofuels produced from plant biomass, such as switchgrass, have the potential to mitigate the increasing pace of rising atmospheric CO_2 and global temperatures caused in part by the burning of fossil fuels. Biofuels produced from photosynthetically sequestered carbon in plant cell walls represent a contemporary capture-and-release cycle of carbon, compared to the net increase of carbon released into the atmosphere when burning fossil fuels. The main needs of biomass improvement for biofuels to become a viable alternative to fossil fuels are to (1) increase biomass yield and (2), improve biomass composition to increase biomass deconstruction efficiency. The anatomy of switchgrass tiller internodes remains intact even after standard mechanical deconstruction of biomass prior to chemical deconstruction. However, the impact of internode anatomy on biomass deconstruction efficiency is poorly understood. Furthermore, current understanding of internode anatomy plasticity in genotype clones caused by varied conditions across environments in this context is also lacking. Therefore, our goal is to explore the influence of internode anatomy variation on biofuel-relevant traits in switchgrass biomass and to increase our understanding of genetic control of internode anatomy variation.

This research analyzed internode anatomy of lowest above ground internodes in clones of upland (VS16, DAC) and lowland (AP13, WBC) switchgrass genotypes at three common garden sites in: South Texas, Central Missouri, and Central Michigan. Cortical cell wall thickness (CWT) varies independently of 21 other traits measured and suggests unique genetic control may be present for optimization. Cortical cell wall thickness also negatively correlates with digestion efficiency and mild resistance to loss of hydraulic conductivity. Next, we narrowed our focus to establish a genetic basis of internode anatomy

variation with quantitative trait loci (QTL) analysis in the F_2 progeny of a four-way outbred mapping population grown at a single site. Anatomical measurements of the F_2 mapping population were utilized in QTL analysis to identify eight QTLs for six internode anatomy traits including cortical cell wall thickness, cortex radius, chlorenchyma radius, annulus area, epidermis cell count, and cortex-to-rind ratio. Candidate genes involved in various processes from cell cycle and hormone regulation to cell wall biosynthesis are present in the QTL intervals. Next we found that all biomass composition traits of lowland WBC vary significantly in clones grown across ten environments and 17 degrees of latitude. Lastly, we provide a detailed description of our hand sectioning method and present a 3D-printed microtome, "The Rapid-Tome", specifically designed to effectively section hollow and tough materials such as switchgrass and woody stems up to 8 mm thick.

In total, this dissertation provides a valuable morphometric analysis of switchgrass internode anatomy and supports the long-term goal of enhancing biomass for biofuel production. This work identified variable internode anatomy traits that impact biomass digestibility and provide evidence that internode anatomy is an important factor of biomass tissue characteristics. This work shows that internode anatomy variation across environments shows potential to match genotype to specific environments to optimize internode anatomy for biomass conversion efficiency into biofuels. Furthermore, the QTL and candidate genes identified provide guidance for selectively breeding favorable internode anatomy phenotypes and presents a genetic basis for future genetic engineering of biofuel production-relevant traits.

Keywords: Switchgrass, grass anatomy, bioenergy, cell wall

Chapter 1: Introduction

Switchgrass is a warm season perennial tall grass native to North America under development as a biomass source for the production of biofuels (Vogel, Sarath, et al., 2011). In North America, switchgrass has a wide geographical range across which there are several climatic and environmental gradients driving intraspecies diversity and functional trait plasticity (Lowry et al., 2014). The names of the ecotypes reflect their origin, uplands were originally found in upland habitats, often characterized by droughty soils adapted to hardiness zones 3-7, while lowland ecotypes originated along riverine habitats and flood plains of southern US adapted to hardiness zones 5 through 9 (Casler et al., 2011). Broad species adaptation from the Rocky Mountains to the Atlantic Ocean, high biomass yield across distribution, and high tolerance to marginal conditions such as low fertility and drought are favorable traits that led to switchgrass selection as a biomass feedstock for biofuel production (Casler et al., 2011). Switchgrass shows widespread variability across its range between different ecotypes at the phenotypic and genotypic levels because of genetic variation that make switchgrass a genetic resource and poised for artificial crop evolution and improvement (Casler et al., 2007).

1.1 Switchgrass as a biomass source for biofuel production

Switchgrass is described as a high-potential energy crop fit for biofuel production (Wright, 2007). A baseline study found that net energy of cellulosic ethanol form switchgrass produced 540% more renewable energy than nonrenewable energy with technology and switchgrass genetic material available in the year 2000 (Schmer et al., 2008). This is an especially impressive figure when taking into account that switchgrass cultivars are derived from natural populations and are only a few generations removed from

wild collections (Lowry et al., 2019). Major crop improvements are likely possible in a short amount of time with selective breeding. Interest in switchgrass in the United States is heavily focused on growing switchgrass as a feedstock for biofuel production, though other utilization efforts also exist. Traditionally, switchgrass has been used as a feed for grazers, restoration of rangelands, and erosion control (Nageswara-Rao et al., 2013; Perrin et al., 2008) However, switchgrass is also being investigated for producing biomass in a variety of settings including along waterway buffers (Gu & Wylie, 2018), reclaimed mine lands (Brown et al., 2016; Scagline-Mellor et al., 2018), and even nuclear test sites in Kazakhstan (Sagyndyk et al., 2007). From a breeder's perspective for bioenergy switchgrass, the main objective for biomass improvement is to develop superior varieties that are suitable for economic production in commercial cropping systems with a focus in switchgrass on biomass yield and composition (Brown & Caligari, 2008). Therefore, our understanding of the entire process from biomass to fuel can lead to a more efficient process, and help researchers and breeders select the most favorable traits not just for producing a lot of biomass but producing an optimal biomass that can be efficiently processed. For example, environmental gradients can have an impact on cell wall compositional traits with downstream effects on processing that include inhibition of microbial biofuel production of drought-stressed switchgrass hydrolysate while rain variability reducing production (Ong et al., 2016; Reichmann et al., 2018). Understanding the biomass components affected by environmental gradients and resistance to potential water stress due to uncertain water availability are both major goals that require large scale projects that span these gradients and conditions.

1.2 Common diversity gardens project

Reciprocal planting studies reveal there are disparities between locally adapted and displaced populations that may guide selection of high-performance ecotypes, cultivars, and traits (Hereford, 2009; Lowry, 2012). Multi-site field trials establish the opportunity to explore the influence of genotype by environments (G x E) interactions on biomass yield and composition. Novel allelic combinations clonally propagated across a latitude gradient can reveal favorable traits that are not bound by typical source population survivorship constraints (Hartman et al., 2011; Lowry et al., 2014). Extending the reciprocal planting rationale to multiple sites, 10 common gardens have been established across 16.7 degrees of latitude in the Midwest and populated with a known-four-way cross and F_2 mapping population of two uplands from the northern great plains (genotypes VS16 and DAC6), and two lowlands from the southern great plains (genotypes AP14 and WBC3) (Lowry et al., 2019; Milano et al., 2016). This large multisite project designed to investigate switchgrass trait variability across genotypes along a latitude gradient serves as an extremely valuable resource from which to sample. The plants in these gardens serve as a library of diversity and trait plasticity in a diverse genotype mapping population. Switchgrass exhibits phenotypic diversity across its range that includes large differences in height, tiller diameter, tiller count, phenology, cell wall composition, and total biomass yield among different switchgrass genotypes with different latitudes of origin. By looking at correlations in genetic markers with biomass traits, anatomical traits, and physiological traits we can learn more about how genetically diverse switchgrass respond differently to the same environmental stimuli. Identification of site-genotype high performance

combinations for site-specific biofuel feedstock switchgrass genotypes has the potential to further reduce the costs of biofuel production.

When different genotypes produce phenotypic traits across environments and in some cases appear as rank changes in traits among genotypes across environments, this is considered (G x E) interactions (Des Marais et al., 2013). Understanding the variability of switchgrass internode anatomy across environments and impacts on biomass yield and quality in the context of genotype x environment is a valuable step to take towards developing this biofuel feedstock. This is because locally optimized varieties in terms of conversion efficiency and yield reduce the total cost of biofuel production. Identifying biomass yield and quality, including functional impacts of internode anatomy plasticity, across common gardens is a valuable way to identify local adaptation as a result of evolutionary and natural selective pressures in plant populations (Kawecki & Ebert, 2004).

Numerous efforts to improve switchgrass as a biofuel feedstock have focused on biomass production as a primary breeding target (Sanderson et al., 2006; Schmer et al., 2008). As a fine scale feature of biomass, cell wall composition is known to vary among different cell types, primary vs. secondary cell walls, and secondary cell wall thickness (Vogel, 2008). Switchgrass conversion efficiency is largely a factor of tissue characteristics (DeMartini et al., 2013), with tissue characteristics directly impacted by internode anatomy. However, the relationship of switchgrass internode anatomical variation with biomass conversion efficiency remains underrepresented in the literature.

1.3 The switchgrass internode

The grass internode is made up of four main tissue types with specialized functions that collectively contribute to plant survival, proliferation, and biomass production towards

reproductive success at the end of the growing season (Esau, 1960). The four tissue types are the dermal, hypodermal, ground, and vascular tissues systems. Internodes, which make up 50.4% of total switchgrass biomass yield and 44.9% total glucose yield as seen in the Alamo cultivar (AP13 is a specific genotype of Alamo), provide structural support to leaves, which also includes the panicle after floral transition (Hu & Ragauskas, 2011). Cells with thick secondary cell walls represent a substantial carbon sink and in most grasses, provide a dominant fraction cell wall components lignin, cellulose, and hemicellulose found in biomass (Chen et al., 2002; Jung & Casler, 2006a, 2006b). The abundance of cell with secondary walls and the actual cell wall thickness both ultimately influence biomass yield directly and indirectly. The abundance of cells with accumulated cell wall directly add to the total yield, while the function of these strong cells provides structural support required to maintain stature for photosynthesis. Internodes are also implicated in physiological drought response because they are largely comprised of numerous vascular bundles that contain water transport cells (metaxylem) that supply the plant with water and nutrients from the soil. The epidermis protects the internal cells from pathogenic attack while restricting gas exchange and moisture loss to the stomatal openings of photosynthetically active chlorenchyma just under the epidermis. The interfasicular fiber cell layer is characterized by extensive secondary cell wall accumulation and provides strength to the tiller while acting as a carbon sink. Individual vascular bundles are distributed within the cortical parenchyma cells that fill in the rest of the internode inward toward the central hollow pith. The range in size of water conducting vessels (xylem), abundance of interfasicular fiber cells and the thickness of their walls contribute to water

transport and vessel embolism-expansion of air bubbles or introduction of air into vessels that break the water column and deactivate water flow (Venturas et al., 2017).

1.4 Native ecoregions drive local adaptation and water relations

Air temperature and soil water status influence plant growth and survival that work in tandem with the capabilities of the plant to withstand stress. Under high evaporative demands, vapor pressure deficit of the air surrounding the leaf quickly pulls water molecules out of the leaf at a rate that induces increasingly negative pressure in the xylem the drier and hotter the air is. The "cohesion-tension" theory explains that water molecules that evaporate from the leaf through the stomata are replaced by new ones entering the plant through the roots (Dixon & Joly, 1895; Pickard, 1981). As water evaporates from the internal cavities within the leaf and out through stomata, a liquid water meniscus forms between mesophyll cells. The meniscus retreats slightly as the volume is reduced with each evaporating water molecule, but the surface tension of the water molecules in the meniscus resists this retreat and transfers this surface tension into the water continuum (Venturas et al., 2017). Tension manifests in the form of internal negative pressure in the water column within the xylem when the evaporative demand exceeds the incoming water supply in the roots. At a certain point of drought stress, the negative pressure is enough to induce a break in the water column within 50% of the plant's vessels, (a measure called P_{50}). When the water column breaks air bubbles in the water expand to fill the span of the vessel (embolism), or air is seeded through pits in the vertical sidewalls from neighboring cells.

Moisture and temperature conditions across environments have driven switchgrass adaptation and plasticity (Vogel, Sarath, et al., 2011). Underlying phenotypic adaptation are anatomical adaptations that may include internode and vascular cell variations in order

to handle or resist water stress. The capability of plants to withstand stress is driven by its structure and functional capacity of its tissues and cells. Metaxylem size is negatively correlated with embolism resistance (Blackman et al., 2010; Ocheltree et al., 2016), and plants with smaller metaxylem will therefore possess a P_{50} that is closer to zero. However, a recent report found that interfasicular fibers and bundle fibers both correlate positively with more negative P_{50} in several grass species (Lens et al., 2016; Volaire et al., 2018). Upland ecotypes are characteristically adapted to drier soils and have on average smaller metaxylem, with metaxylem diameter negatively correlated with embolism resistance (Blackman et al., 2010). Vascular bundle anatomy and reinforcing fibers are prominent factors of moisture and nutrient transport from the soil throughout the plant's many tissues. The maximum stem conductance (K_S) varies considerably between species and is dependent on xylem diameter, dissolved solutes, soil water potential and atmospheric conditions (Taiz et al., 2015).

1.5 Cell wall composition and modifications influence biomass digestibility

Successful efforts to improve composition have led to increased digestibility (Fu et al., 2011; Li et al., 2018; Saha & Ramachandran, 2013) through a greater understanding of genes involved in cell wall biosynthesis and a greater understanding of switchgrass transcriptional networks (Chen et al., 2010; Somleva et al., 2002; Tu et al., 2010; Zuo et al., 2018). The modification of the lignin biosynthesis pathway by down regulating a gene that codes for a monolignols (lignin precursors) resulted in the reduction of lignin content and a 38% increase in ethanol yield (Fu et al., 2011). Additionally, altering the composition of lignin without affecting total lignin content produced increased digestibility as well (He et al., 2018). Furthermore, changes in cell wall architecture in terms of altered lignin and

other structural components appear to correlate to improved ethanol yields as well (Sarath et al., 2011). These studies show that with a greater understanding of genes that are involved with cell wall biosynthesis, it is possible to improve cell wall traits to increase digestibility and ethanol yields.

Cell wall composition is known to vary among different cell types, primary vs. secondary cell walls, and secondary cell wall thickness (Vogel, 2008). Bamboo axial stiffness relates to the size and arrangement of sheaths of fiber cells surrounding the vascular bundles in addition to the arrangement of crystalline cellulose microfibrils in secondary cell walls (Mannan et al., 2017). Numerous studies show that alkaline pretreatment hydrolyzes ester bonds connecting some subunits of lignin and breaks the ether bonds of lignin and hemicellulose, which increases access to the remaining polysaccharides for enzymatic digestion (Hu & Wen, 2008; Loow et al., 2016; Xu et al., 2010). Taken in account together, variations in cell wall thickness and the composition that accompanies that combined with cell type differences likely impact total cell wall content and therefore digestibility.

High value polysaccharides that can be processed into fuel are locked away inside the cell walls of plants. The cell wall is primarily composed of a matrix of cellulose, hemicellulose, and lignin. Lignin is a structural heteropolymer, which in grasses primarily consists of two monolignol subunits syringyl (S), and guaiacyl (G) (Fu et al., 2011). Lignin inhibits enzymatic activity and severely limits cell wall digestion and the release of cell wall bound polysaccharides (Vermaas et al., 2015). The Maule reaction reveals striking variation in the interfasicular fiber of cross sections. Maule staining differentiates between lignin rich in S and G lignin subunits by staining s subunits red (Chen et al., 2002). S-rich

lignin has previously been shown to be less recalcitrant than G-rich lignin to degradation during biomass pretreatments (Chen & Dixon, 2007).

Exploring the presence of mixed linkage glucans (MLG) in the cell walls of genotypes with different internode anatomies can establish a connection with digestibility that we can test. Immunolocalization utilizes the ability of an antibody to detect and bind to a specific antigenic molecule. The target antigen of interest, in this case MLG, is injected into a small mammal which then identifies the antigen and produces antibodies against it. Indirect immunofluorescence utilizes two antibodies to detect the presence of a molecule. The primary antibody targets the molecule of interest. The secondary antibody is fused to a fluorescent tag and targets the primary antibody. Indirect detection gives a larger signal per target molecule because several tagged secondary antibodies can bind to each single primary antibody, thus increasing the fluorescent signal (Knox, 1997).

Chemically processing large amounts of biomass for theoretical and actual ethanol quantification is a time intensive endeavor that requires expensive and complex assays (Vogel, Dien, et al., 2011). Near-infrared reflectance spectroscopy (NIRS) is a high-throughput, low-cost method to predict agricultural product composition(Vogel, Dien, et al., 2011). However, accurate composition prediction relies on consistent biomass preparation quality and can be influenced by several physical features of the milled and ground biomass. Compositional prediction with NIRS of wheat shows that ground wheat kernel produces more accurate predictions than whole wheat kernels because of the influence of kernel curvature, topography, and surface roughness on the spectra (Caporaso et al., 2018) In projects with disparate field sites, it is imperative that any processing variation that may exist be eliminated or controlled.

1.6 Identification of Quantitative Trait Loci for marker selected breeding

Advancements in switchgrass biomass yields have been accomplished through conventional breeding (Bhandari et al., 2010; Casler, 2010). Conversely, marker assisted breeding can be done on seedlings and can greatly increase the pace of advancement that is typically restricted by multi-year mature plant selection cycles (Serba et al., 2015). Quantitative trait loci (QTL) analysis utilize polymorphic markers to provide a framework map around which variability in DNA can be linked to phenotypic, quantitative traits (Kearsey & Farquhar, 1998) Recently, two QTL studies have explored biomass yield and the root economic spectrum in switchgrass (Chen et al., 2021; Lowry et al., 2019). QTL were identified that significantly associate with biomass yield, flowering traits, and root traits that may contribute to biomass yield and other indirectly related biomass traits. Though multiple significant QTL and connections were established in both studies, neither discuss or analyze the anatomy of internodes, especially in the context of biomass conversion efficiency or biomass quality. Furthermore, a common next step after identifying significant QTL for traits of interest is to explore this genetic basis by identifying candidate genes within neighboring genetic marker intervals.

1.7 Exploring candidate genes with transcription factor phylogeny

Characterizing and establishing a genetic basis for these internode anatomy traits and the extent of their variation within a mapping population is an important step towards enhancing switchgrass biomass for biofuel production. Understanding the genetics of numerous internode anatomy traits will lead to a better understanding of biomass conversion efficiency, echoing advancements made by applying this approach towards cell wall composition (Bouton, 2007). The organization of cell types within a plant, its

anatomical architecture, is a result of several processes within plant development and morphogenesis. Internode anatomy begins with meristematic tissues that are the site of cell division and cell differentiation, followed by cell elongation and secondary cell wall accumulation (Taiz et al., 2015). Cell fate determination and secondary cell wall formation are also impacted by hormone and regulatory factors signaling between cells as well as environmental stimuli. Considering these aspects together produces the final organization, abundance, and proximity of the numerous cell types found within vegetative and reproductive plant structures. Establishing a connection with these factors and internode anatomy is imperative and relies largely on functional characterizations of genes and phylogenetic resources that identify homologs across species.

1.8 Sample preparation with 3D-printed tools

Processing of the internodes is straightforward but time consuming, advances in sample processing and preparation would greatly impact the type of research questions possible, and the magnitude of sampling achievable. Several recent studies utilized 3D-printing to enhance plant tissue sectioning methods. Other analyses have recently explored the use of 3D-printing to increase the throughput of plant tissue sectioning (Atkinson & Wells, 2017). Atkinson et al. describe a 3D-printed embedding mold to embed plant roots in agarose for sectioning but is not applicable for harder tissues. Another group created a 3d -printed sectioning tool to simply produce sections of plant material but has not sample advancement mechanism to control section thickness (Giannini, 2017). Additive manufacturing and advancements in 3D printing technology make it possible to download files from the internet and print all kinds of objects and tools, including a hand-held microtome.

1.9 Aim and focus of the study

In this dissertation, I have studied the genetic architecture and influence of internode anatomy of switchgrass on biofuel production-relevant traits.

Chapter 2 presents a morphometric analysis of internode anatomy in four genotypes clonally propagated and established in six environments. We analyzed implications of internode anatomy with biomass digestibility and hydraulic conductivity. This analysis explores internode anatomy as an important component of biomass for utilization as a biofuel feedstock.

Chapter 3 describes a focus morphometric study of switchgrass internode anatomy as a single environment. The main goal of this project was to identify a genetic basis for internode anatomy traits utilizing quantitative trait loci (QTL) analysis on the F_2 progeny of a four-way outbred mapping population. This analysis also includes a phylogenetic reconstruction of the multifunctional NAC transcription factors in switchgrass, rice, and *Arabidopsis thaliana*.

In Chapter 4, we analyzed biomass composition of the lowland WBC genotype across latitudes and ten environments to evaluate biomass composition variation with near infrared spectroscopy (NIRS) across field sites. Furthermore, this analysis discusses the impact of multisite milling on biomass composition predictions with NIRS of single plant switchgrass biomass.

Chapter 5 details an improved hand sectioning technique for generating high-quality plant sections for microscopic analyses. This chapter also introduces a novel microtome design that can be 3D-printed specifically designed to section hollow and tough plant stems, common in grasses.

1.10 References

Atkinson, Jonathan A. and Wells, Darren M. (2017), 'An Updated Protocol for High Throughput Plant Tissue Sectioning', *Frontiers in Plant Science,* 8.

Bhandari, HS, et al. (2010), 'Variation among half-sib families and heritability for biomass yield and other traits in lowland switchgrass (Panicum virgatum L.)', *Crop science,* 50 (6), 2355-63.

Blackman, Christopher J, Brodribb, Tim J, and Jordan, Gregory J (2010), 'Leaf hydraulic vulnerability is related to conduit dimensions and drought resistance across a diverse range of woody angiosperms', *New Phytologist,* 188 (4), 1113-23.

Bouton, Joseph H (2007), 'Molecular breeding of switchgrass for use as a biofuel crop', *Current opinion in genetics & development,* 17 (6), 553-58.

Brown, Carol, et al. (2016), 'Switchgrass biofuel production on reclaimed surface mines: I. Soil quality and dry matter yield', *BioEnergy Research,* 9 (1), 31-39.

Brown, Jack and Caligari, Peter DS (2008), 'Breeding schemes', *An Introduction to Plant Breeding*, 34-59.

Caporaso, Nicola, Whitworth, Martin B., and Fisk, Ian D. (2018), 'Near-Infrared spectroscopy and hyperspectral imaging for non-destructive quality assessment of cereal grains', *Applied Spectroscopy Reviews,* 53 (8), 667-87.

Casler, Michael D (2010), 'Changes in mean and genetic variance during two cycles of within-family selection in switchgrass', *BioEnergy research,* 3 (1), 47-54.

Casler, Michael D, et al. (2011), 'The switchgrass genome: tools and strategies', *The Plant Genome,* 4 (3), 273-82.

Casler, Michael D, et al. (2007), 'Latitudinal and longitudinal adaptation of switchgrass populations', *Crop Science,* 47 (6), 2249-60.

Chen, Fang and Dixon, Richard A (2007), 'Lignin modification improves fermentable sugar yields for biofuel production', *Nature biotechnology,* 25 (7), 759.

Chen, Lei, et al. (2002), 'Lignin deposition and associated changes in anatomy, enzyme activity, gene expression, and ruminal degradability in stems of tall fescue at different developmental stages', *Journal of Agricultural and Food Chemistry,* 50 (20), 5558-65.

Chen, Weile, et al. (2021), 'The genetic basis of the root economics spectrum in a perennial grass', *Proceedings of the National Academy of Sciences,* 118 (47).

Chen, Xinlu, et al. (2010), 'A high-throughput transient gene expression system for switchgrass (Panicum virgatum L.) seedlings', *Biotechnology for biofuels,* 3 (1), 9.

DeMartini, Jaclyn D, et al. (2013), 'Investigating plant cell wall components that affect biomass recalcitrance in poplar and switchgrass', *Energy & Environmental Science,* 6 (3), 898-909.

Des Marais, David L, Hernandez, Kyle M, and Juenger, Thomas E (2013), 'Genotype-by-environment interaction and plasticity: exploring genomic responses of plants to the abiotic environment', *Annual Review of Ecology, Evolution, and Systematics,* 44, 5-29.

Dixon, Henry Horatio and Joly, John (1895), 'XII. On the ascent of sap', *Philosophical Transactions of the Royal Society of London.(B.),* (186), 563-76.

Fu, C., et al. (2011), 'Genetic manipulation of lignin reduces recalcitrance and improves ethanol production from switchgrass', *Proc Natl Acad Sci U S A,* 108 (9), 3803-8.

Giannini, John 'The OPN Microtome: An Inexpensive, Open Source Hand-Held Mini Microtome', <https://pages.stolaf.edu/wp-content/uploads/sites/803/2017/04/Giannini_OPN_Microtome_Manual_20170415.pdf>, accessed.
Gu, Yingxin and Wylie, Bruce K (2018), 'Mapping cropland waterway buffers for switchgrass development in the eastern Great Plains, USA', *GCB Bioenergy,* 10 (6), 415-24.
Hartman, Jeffrey C, et al. (2011), 'Potential ecological impacts of switchgrass (Panicum virgatum L.) biofuel cultivation in the Central Great Plains, USA', *biomass and bioenergy,* 35 (8), 3415-21.
He, Yuan, et al. (2018), 'Lignin composition is more important than content for maize stem cell wall degradation', *Journal of the Science of Food and Agriculture,* 98 (1), 384-90.
Hereford, Joe (2009), 'A quantitative survey of local adaptation and fitness trade-offs', *The American Naturalist,* 173 (5), 579-88.
Hu, Zhenhu and Wen, Zhiyou (2008), 'Enhancing enzymatic digestibility of switchgrass by microwave-assisted alkali pretreatment', *Biochemical Engineering Journal,* 38 (3), 369-78.
Hu, Zhoujian and Ragauskas, Arthur J (2011), 'Hydrothermal pretreatment of switchgrass', *Industrial & Engineering Chemistry Research,* 50 (8), 4225-30.
Jung, HG and Casler, MD (2006a), 'Maize Stem Tissues: Cell Wall Concentration and Composition during Development [Erratum: 2009 Nov-Dec, v. 49, no. 6, p. 2412.]'.
--- (2006b), 'Maize stem tissues: impact of development on cell wall degradability', *Crop Science,* 46 (4), 1801-09.
Kawecki, Tadeusz J and Ebert, Dieter (2004), 'Conceptual issues in local adaptation', *Ecology letters,* 7 (12), 1225-41.
Knox, J Paul (1997), 'The use of antibodies to study the architecture and developmental regulation of plant cell walls', *International review of cytology* (171: Elsevier), 79-120.
Lens, Frederic, et al. (2016), 'Herbaceous angiosperms are not more vulnerable to drought-induced embolism than angiosperm trees', *Plant Physiology*.
Li, Guotian, et al. (2018), 'Overexpression of a rice BAHD acyltransferase gene in switchgrass (Panicum virgatum L.) enhances saccharification', *BMC biotechnology,* 18 (1), 54.
Loow, Yu-Loong, et al. (2016), 'Typical conversion of lignocellulosic biomass into reducing sugars using dilute acid hydrolysis and alkaline pretreatment', *Cellulose,* 23 (3), 1491-520.
Lowry, David B (2012), 'Local adaptation in the model plant', *New Phytologist,* 194 (4), 888-90.
Lowry, David B, et al. (2014), 'Adaptations between ecotypes and along environmental gradients in Panicum virgatum', *The American Naturalist,* 183 (5), 682-92.
Lowry, David B, et al. (2019), 'QTL× environment interactions underlie adaptive divergence in switchgrass across a large latitudinal gradient', *Proceedings of the National Academy of Sciences,* 116 (26), 12933-41.

Mannan, Sayyad, Paul Knox, J, and Basu, Sumit (2017), 'Correlations between axial stiffness and microstructure of a species of bamboo', *Royal Society open science,* 4 (1), 160412.
Milano, Elizabeth R, Lowry, David B, and Juenger, Thomas E (2016), 'The genetic basis of upland/lowland ecotype divergence in switchgrass (Panicum virgatum)', *G3: Genes, Genomes, Genetics,* 6 (11), 3561-70.
Nageswara-Rao, Madhugiri, Stewart, C Neal, and Kwit, Charles (2012
), 'Genetic diversity and structure of natural and agronomic switchgrass (Panicum virgatum L.) populations', *Genetic resources and crop evolution,* 60 (3), 1057-68.
Ocheltree, Troy W, Nippert, Jesse B, and Prasad, PV (2015), 'A safety vs efficiency trade-off identified in the hydraulic pathway of grass leaves is decoupled from photosynthesis, stomatal conductance and precipitation', *New Phytologist*.
Ong, Rebecca Garlock, et al. (2016), 'Inhibition of microbial biofuel production in drought-stressed switchgrass hydrolysate', *Biotechnology for biofuels,* 9 (1), 1-14.
Perrin, Richard, et al. (2008), 'Farm-scale production cost of switchgrass for biomass', *BioEnergy Research,* 1 (1), 91-97.
Pickard, William F (1981), 'The ascent of sap in plants', *Progress in biophysics and molecular biology,* 37, 181-229.
Reichmann, Lara G, et al. (2018), 'Inter-Annual Precipitation Variability Decreases Switchgrass Productivity from Arid to Mesic Environments', *BioEnergy Research,* 11 (3), 614-22.
Sagyndyk, KS, Aidossova, SS, and Prasad, MNV (2007), 'Grasses tolerant to radionuclides growing in kazakhstan nuclear test sites exhibit structural and ultrastructural changes-implications for phytoremedaition and involved risks', *Terrestrial and Aquatic Ecotoxicology,* 1, 70-77.
Saha, S. and Ramachandran, S. (2013), 'Genetic improvement of plants for enhanced bio-ethanol production', *Recent Pat DNA Gene Seq.,* 7.
Sanderson, Matt A, et al. (2006), 'Switchgrass as a biofuels feedstock in the USA', *Canadian Journal of Plant Science,* 86 (Special Issue), 1315-25.
Sarath, Gautam, et al. (2011), 'Ethanol yields and cell wall properties in divergently bred switchgrass genotypes', *Bioresource technology,* 102 (20), 9579-85.
Scagline-Mellor, Steffany, et al. (2018), 'Switchgrass and Giant Miscanthus Biomass and Theoretical Ethanol Production from Reclaimed Mine Lands', *BioEnergy Research*, 1-12.
Schmer, Marty R, et al. (2008), 'Net energy of cellulosic ethanol from switchgrass', *Proceedings of the National Academy of Sciences,* 105 (2), 464-69.
Serba, Desalegn D, et al. (2015), 'Quantitative trait loci (QTL) underlying biomass yield and plant height in switchgrass', *BioEnergy research,* 8 (1), 307-24.
Somleva, MN, Tomaszewski, Z, and Conger, BV (2002), 'Agrobacterium-mediated genetic transformation of switchgrass', *Crop Science,* 42 (6), 2080-87.
Taiz, Lincoln, et al. (2015), *Plant physiology and development* (Sinauer Associates Incorporated).
Tu, Yi, et al. (2010), 'Functional analyses of caffeic acid O-methyltransferase and cinnamoyl-CoA-reductase genes from perennial ryegrass (Lolium perenne)', *The Plant Cell,* 22 (10), 3357-73.

Venturas, Martin D., Sperry, John S., and Hacke, Uwe G. (2017), 'Plant xylem hydraulics: What we understand, current research, and future challenges', *Journal of Integrative Plant Biology,* 59 (6), 356-89.
Vermaas, Josh V, et al. (2015), 'Mechanism of lignin inhibition of enzymatic biomass deconstruction', *Biotechnology for biofuels,* 8 (1), 217.
Vogel, John (2008), 'Unique aspects of the grass cell wall', *Current opinion in plant biology,* 11 (3), 301-07.
Vogel, Kenneth P, et al. (2011), 'Switchgrass'.
Volaire, Florence, et al. (2018), 'Embolism and mechanical resistances play a key role in dehydration tolerance of a perennial grass Dactylis glomerata L', *Annals of Botany,* 122 (2), 325-36.
Wright, Lynn (2007), 'Historical perspective on how and why switchgrass was selected as a "model" high-potential energy crop', *ORNL/TM-2007/109 Oak Ridge, TN: Bioenergy Resources and Engineering Systems*.
Xu, Jiele, et al. (2010), 'Sodium Hydroxide Pretreatment of Switchgrass for Ethanol Production', *Energy & Fuels,* 24 (3), 2113-19.
Zuo, Chunman, et al. (2018), 'Revealing the transcriptomic complexity of switchgrass by PacBio long-read sequencing', *Biotechnology for Biofuels,* 11 (1), 170.

Chapter 2: The Influence of Switchgrass Internode Anatomy on Biofuel Production-relevant Traits

Authors: David J. Thomas[1], Jason Bonnette[2], Millicent Sanciangco[3], Rahele Panahabadi[5]

David B. Lowry[4], Heather R. McCarthy[1], Thomas E. Junger[2], and Laura E. Bartley[5]

1- University of Oklahoma
2- University of Texas at Austin
3- Great Lakes Bioenergy Research Center
4- Michigan State University
5- University of Washington

Publication Status: This chapter is in preparation to be submitted for publication in Plant Physiology

Authors Contributions: DT, LB, and TJ conceived of and designed the study, DT helped with sample harvest, prepared samples, and conducted the analyses, DT and LB wrote the manuscript. JB and TJ directed field collections

MS and DL conducted the deconstruction assays

HM advised on physiology and provided parts of the experimental set up.

Acknowledgements

Felix Fritschi helped coordinate the 2018 harvest at CLMB and provided project insight. Anna Jacobsen helped with hydraulic conductivity troubleshooting. Lisa Vormwald harvested tillers at KBSM for the hydraulic conductivity analysis. Grace John contributed physiological and anatomical insight. Phuong Phi and Alice McCaskill contributed to internode anatomy sectioning and image analysis.

Funding sources

NSF grant (IOS 1444533)
DOE grant (DE-SC0014156, DE-SC0021126)
CBI

2.1 Abstract

Switchgrass (*Panicum virgatum* L.) is a perennial C4 warm-season tallgrass and a promising feedstock for production of lignocellulosic biofuels. Local environmental conditions produce phenotypic variation across the geographical range of switchgrass. We hypothesize that internode anatomy plasticity, representing evolutionarily driven local adaptation, modulates traits important for efficient biofuel production, including biomass yield (e.g., height), drought tolerance, and biomass digestibility. We analyzed internode anatomy of lowest above ground internodes in clones of upland (VS16, DAC) and lowland (AP13, WBC) switchgrass genotypes at three common garden sites in: South Texas, central Missouri, and central Michigan. Lowlands are larger in many traits including height, average xylem diameter, and annulus radius. A few traits such as cortical cell wall thickness (CWT) and sclerenchyma radial thickness deviate from this pattern, lack isometry with height or internode diameter, and rank differently among genotypes across sites. Hydraulic conductance measurements in tiller segments from the Michigan site revealed that mild pressures induce 50% loss of conductivity in all four genotypes, yet averages are statistically different ($P<0.001$) by ecotype; Lowland (-0.25 MPa), and upland (-0.59 MPa). Comparing different digestion treatment parameters revealed that thin (4 μm) CWT and milder treatment produces similar glucose yield as thick (8 μm) CWT and harsher treatment. Significant anatomical plasticity represents local adaptation among genotypes across environments with minimal impact on hydraulic conductivity loss resistance, providing leeway to optimize internode anatomy to favor cell wall deconstruction efficiency for lignocellulosic biorefining.

2.2 Introduction

Switchgrass is a warm season, perennial species native to the tallgrass prairie of North America that is under development as a biorefining crop due to its large annual biomass production and relative abiotic stress tolerance (Casler et al., 2011). Biomass yield and yield stability are key phenotypic targets in this effort (Sanford et al., 2017). Breeding efforts have developed "cultivars" that exhibit increased biomass (Saha et al., 2013) and studies have identified loci that increase biomass across both upland and lowland ecotypes (Casler et al., 2007; Lovell et al., 2016). Progress has also been made in identifying genes (Li et al., 2018; Rao et al., 2019; Shen et al., 2009), genetic loci (Lowry et al., 2019; Lowry et al., 2015; Serba et al., 2016) that increase the quality of switchgrass biomass to enable efficient utilization for biorefining (DeMartini et al., 2013; Sarath et al., 2011). However, the interactions between the desired traits of high yield and high-quality biomass are unclear. Here we examine internode anatomy phenes, (fundamental units of a phenotype, i. e. cell diameter, cell wall thickness, (Lynch, 2011; Schneider et al., 2021)) the understanding of which we hypothesized would enable simultaneous improvement of multiple bioenergy-relevant traits and understanding of the fitness tradeoffs between different internode-related phenotypes.

Biomass yield is a major target for improvement to increase switchgrass viability as a biofuel feedstock (Sanderson et al., 2006). A metanalysis found that switchgrass biomass yield (mean ± SD) was higher in plants of the taller and fewer tiller count lowland ecotype (12.9 ± 5.9 Mg ha–1), but showed significant overlap with plants of the shorter yet numerous tiller count upland ecotype (8.7 ± 4.2) depending on the environment (Wullschleger et al., 2010). However, the positive relationship of biomass yield and height

is consistent across ecotypes and provides an important benchmark for comparison (Price & Casler, 2014). In addition to the visible plant architecture traits, e.g., height and internode diameter, that can predict biomass yield, microscopic analysis of internode cross-sections present anatomical phenes that may impact the efficiency of cell wall digestibility due to cell dimensions, relative cell type abundance, and cell wall composition variation across cell types. We want to test the hypothesis that internode anatomy plasticity leads to differences in biomass yield and deconstruction efficiency across genotypes and latitudes.

Internode anatomy phenes might be especially important for hydraulic conductivity and maintaining photosynthesis under drought. Hydraulic conductivity itself is influenced by internode vascular bundle anatomy phenes and transports water through a plant as a complete soil to atmosphere continuum incorporating numerous cell types and transport mechanisms (Taiz et al., 2015). There is also evidence of stem fiber abundance positively correlated with resistance to water stress (Lens et al., 2016). Dissolved gas within a transport vessel can expand and break the water column as negative pressure builds during high evaporative demand. Disruption of water transport can lead to stomatal closure that reduces carbon fixation and prolonged conductivity failure under severe drought leads to plant mortality. Internode anatomy phenes also impact photosynthesis. The abundance of stem photosynthetic cells, chlorenchyma, provides a source of non-foliar photosynthesis (Aschan & Pfanz, 2003), which is beneficial to survive leaf dieback due to severe drought effects (Cernusak & Cheesman, 2015). Furthermore, chlorenchyma is abundant in wheat cultivars found to be most tolerant to drought conditions (Al-maskri et al., 2014).

Cell type abundance and cell wall thickness might also impact biomass deconstruction by contributing primary and secondary cell wall fractions that have variable

digestion efficiency. Cell wall deconstruction, in which cell walls are degraded into useable oligosaccharide and lignin fragments is well known to depend on relative composition of structural cell wall components lignin, cellulose, and hemicellulose (Chundawat et al., 2011; Himmel et al., 2007). Biomass composition studies generally focus on digestion of total plant biomass and only some consider leaf to stem ratio, but the impact of different internode cell types or individual phenes like cell wall thickness is poorly represented, though not entirely absent. Analysis of cell wall digestion shows the thicker secondary cell walls of switchgrass sclerenchyma fibers were not completely degraded even with 100-fold concentrations of enzyme and 7 day digestions (Ding et al., 2012). Another study shows that microbial access to the inner cell wall surface of the cell lumen has a larger impact on digestion than lignin content (Wilson & Mertens, 1995).

To test the hypothesis that internode anatomy phenes influence biofuel production relevant traits, we conducted an internode anatomical morphometric analysis of two upland and two lowland genotypes clonally propagated to common gardens at three latitudes in the United States. Switchgrass has historically been divided into upland and lowland ecotypes with recent genetic and morphological evidence of a third ecotype in the Gulf coast region (Lovell et al., 2021). Uplands were originally found in upland habitats, often characterized by droughty soils adapted to U.S.D.A. hardiness zones 3-7 while lowland ecotypes originated along riverine habitats and flood plains of southern US adapted to hardiness zones 5 through 9 (Casler et al., 2011). Phenotypic plasticity is the ability of a single genotype to produce multiple phenotypes in response to the environment (Schlichting, 1986). Switchgrass exhibits phenotypic plasticity across its wide geographical range as a result of interaction of each genotype with environmental

conditions in North America from Northern Mexico to Southern Canada, and East of the Rocky Mountains to the Gulf and Atlantic coasts (Lowry et al., 2014). The development and function of switchgrass anatomical phenes are driven by the interactions between genotype and environment (G x E).

We evaluated internode anatomy phenes at 20 genotype-site-year combinations, cell wall deconstruction variation under eleven different digestion treatment conditions, and hydraulic conductivity and resistance to loss of hydraulic conductivity of four genotypes at one site. We provide evidence of internode anatomy plasticity across latitudes and among genotypes that show internode anatomy variation is an important genotypic feature to consider for the utilization of switchgrass lignocellulosic biorefining into transportation fuels.

2.3 Results

2.4 Internode anatomy plasticity across genotypes and environments

To test the hypothesis that internode anatomy is important for biofuel traits, we measured internode anatomy in representative switchgrass genotypes in previously established common gardens in 2015 (Chen et al., 2021; Lowry et al., 2019; Milano et al., 2016). Tillers from four clonally propagated genotypes, lowlands AP13 and WBC, and uplands VS16 and DAC, were harvested from three sites (Figure 2.1 A), Michigan (KBSM), Missouri (CLMB), and southern Texas (PKLE). Anatomy was analyzed in cross section between 1 and 2 cm above the lowest above ground node (Figure 2.1 B and C)

In total, we harvested tillers from six different site-year environments and 20 unique genotype-site-year designations (e.g., KBSM20, Table 2.1, S2.1) for a total number of 71 samples with replication. Figure 2.2 shows representative cross sections from each of the

genotypes. Ten raw internode anatomy traits and two calculated traits (rind percent annulus radius and cortex percent annulus radius), as well as maximum plant height were measured at all six environments (Table 2.1, right column). Table 2.1 also contains descriptions for ten additional traits that were not measured at all sites as part of different harvest and analysis campaigns. Based on expected phenotypic effects, we divided the traits into four non-exclusive categories—plant architecture, biomass yield, hydraulic conductivity, and cell wall digestibility (Table 2.1). Data collection across traits varied somewhat due to the nature of each trait. For example, only one tiller height and internode diameter measurement was made for each tiller. Data collection on traits that show a range of values required multiple measurements to be representative, for example xylem diameter or annulus radius. Though there are numerous observations to discuss, we focus on the most significant relationships and traits that are most or least variable.

The first analysis addresses the hypothesis that internode anatomical variation is indicated by plant architectural variation (e.g., tiller height and internode diameter). Table 2.2 summarizes internode anatomy variation of the four genotypes across six environments, showing that all twelve traits differ significantly across genotype-environment combinations ($p<0.01$), though Tukey's and Dunn's tests indicate only a few different groups for some traits and many groups for others. Trait variation is present among genotypes at each site and within genotypes across latitudes (Table 2.3). The AP13 cell wall proportion of the area of each fiber cell at PKLE16/17 is 0.88 (+/- 13), but only 0.70 +/- 0.05 at KBSM16 (Figure S2.1, S2.2). AP13 is the most variable in this trait across three sites (SD = 0.13) VS16 the least variable (SD = 0.04) while VS16 shows the highest

proportion of cell wall in the entire dataset, 0.94 +/- 0.001 at CLMB16. WBC is more consistent across sites than AP13, but less so than either upland.

Lowland genotypes are the largest in most internode anatomy traits across sites. Though the uplands are generally smaller, cortical cell wall thickness, nearest vascular bundle neighbor in the sclerenchyma, and sclerenchyma radial thickness are similar in both ecotypes and in some cases were larger in the uplands. The calculated traits, cortex percent annulus radius and rind percent annulus radius, are similar across the genotypes and sites. Average xylem diameter is largest in AP13 across all environments except CLMB16 where VS16 is largest (Figure 2.3 A). The two classes of xylem diameters present in the different vascular bundle sizes of the cortex create the bimodal shape seen in the violin plots of Figure 2.3. On the other hand, cortical cell wall thickness shows rank change across sites, with VS16 the largest at KBSM16 and DAC largest at KBSM20, while AP13 is largest at CLMB16 and CLMB18, and WBC largest at PKLE17 (Figure 2.3 B). Sclerenchyma radial thickness is largest in AP13 across environments and DAC consistently the smallest, while VS16 overtakes WBC is KBSM16 and CLMB16 (Figure 2.3 C).

Several reports relate the latitude of origin to growth characteristics (Hereford, 2009; Lowry, 2012). All four genotypes, uplands displaced southward, and lowlands displaced northward, show a decrease in average cortical cell wall thickness when grown further from latitude of origin (Figure S2.5 A). Similarly, Sclerenchyma radial thickness show the same negative trend with latitude displacement (Figure S2.5 B). However, not all traits show this pattern with nearest neighbor vascular bundle distance in the cortex and xylem diameter exhibiting an increase in both traits for lowlands, and a decrease for uplands with latitude displacement (Figure S2.5 C, D). This suggests that atypical

environmental conditions have a similar global influence that reduces cortical cell wall thickening, and differently among ecotypes. Furthermore, this variation among genotypes in some but not all traits substantiate the decoupling of genotype trait responses to be strictly driven by environmental conditions. The fact that some traits show an increasing trend with latitude displacement, while others are decreasing, shows that the variation observed in the dataset is not solely dependent on displacement from origin, but also on the interaction of the genotypes with the environment to show varying degrees of trait plasticity independently of each other.

Consistent with the general statistical analysis that showed differences among genotypes, non-metric multi-dimensional scaling (NMDS) analysis of the internode anatomy traits shows that the ecotypes separate in the first dimension with ellipses representing each series of points, colored by genotype-site (Figure 2.4 A, S2.3 A). Several but not all traits were found to deviate from a normal distribution, which NMDS is an extremely flexible technique for analyzing different types of data ((Dexter et al., 2018). In NMDS, stress is calculated as a quantitative measure of ordination fit ((Kruskal, 1964a, 1964b). The stress measure indicates how well the algorithm has managed to arrange the points in the ordination while preserving the rank-order distances ((Dexter et al., 2018). K.R. Clarke describes the rule of thumb to decide when a value if stress is sufficiently high to caution against biological interpretation of the ordination, setting the stress values cutoff at +/- 0.20 ((Clarke, 1993). This background leads us to interpret the range of stress levels above and below 0.3 to reason that traits with stress below 0.2 have their ranks preserved while those traits with stress>0.2 do not. This means that many traits do rank consistently while several of the traits vary independently and deviate from the ranks of the other traits.

NMDS stress shows four traits with stress that exceeds +/- 0.2 which suggests these traits do not rank with the traits that have stress levels below the 0.2 threshold (Figure S2.3 A). To reduce high stress, the traits were scaled to their respective annulus radii (Figure S2.3 B). The stress is reduced after scaling though cortical cell wall thickness, nearest vascular bundle neighbor in the sclerenchyma chlorenchyma radial thickness and xylem diameter of cortex vascular bundles all remain above the 0.2 threshold. These results further indicate a lack of consistent trait rankings. Figure S2.4 B shows that the PKLE16/17 is the least dissimilar yet overlaps completely with both CLMB16 and KBSM16 sites.

We next examined correlation among traits using Spearman rank correlations since only two traits, cortical cell wall thickness and xylem diameter in the cortex, are normally distributed. Though many traits positively correlate with each other and with outer internode diameter, we observed only weak relationships with tiller height (Figure 2.4 B). Neither cortical cell wall thickness nor nearest neighbor VB in SCLR have any correlation above 0.5 with any trait. Tiller height is mildly correlated with the outer diameter (SCC = 0.43), average xylem diameter (SCC = 0.37), cortex radius (SCC = 0.33), and annulus radius (SCC = 0.31). Thus, the internode anatomy phenes might contribute to some extent to tiller height and outer diameter or height across genotypes and environments, internode anatomy does not seem to be a major.

We also explored internode anatomy traits after scaling to the annulus radius (trait/annulus radius) per sample. Annulus radius itself highly correlates with outer diameter (SCC = 0.91) and thus provides justification for scaling to annulus radius. Ecotype dissimilarity is reduced but is still clearly present in the NMDS after scaling traits to annulus radius (Figure 2.4 C, S2.4 C). The traits that are most dissimilar in the first

dimension of the scaled data remain the same as the unscaled data, yet the magnitude of stress decreases in most traits (Figure S2.3 B). This means that dissimilarity in the ranked trait data is not simply driven by annulus radius and shows adherence to the ecotype designation. Figure S2.4 D shows that the PKLE16/17 site in Texas remains the least dissimilar, yet dissimilarity of the other sites is reduced. After scaling, cortical cell wall thickness positively correlates with xylem diameter (SCC = 0.79) and nearest neighbor distance of vascular bundles in both the cortex (SCC = 0.73) and the sclerenchyma (SCC = 0.57), as well as sclerenchyma radial thickness (SCC = 0.67) (Figure 2.4 D). By scaling each raw cortical cell wall thickness values to their respective genotype-site annulus radius, multiple positive correlations (SCC>0.55) emerge that represent a specific genotype and site relationship rather than a broad relationship across all genotypes. Interestingly, when evaluating internode anatomy traits as a factor of latitude displacement from their origin, ecotypes differ in some cases in their regression slopes and level of significance (Figure S2.5) Cortical cell wall thickness in all four genotypes shows a negative trend with displacement and is significant in all but DAC ($P < 0.05$) Figure S2.5 A). However, sclerenchyma radial thickness, nearest vascular bundle in the cortex, and xylem diameter are not significant, though opposing trends are detected (Figure S2.5 B – D).

For the final examination of phene relationships, we examined the allometry among phenes, which is the quantitative relationship of growth and allocation (Weiner, 2004). Most traits lack isometry when scaled to height, outer diameter, or annulus radius, and produce different slopes when individual genotypes are compared across latitudes. The overall slope of annulus radius vs. outer diameter (m = 0.95) is isometric and reflects the reported correlation coefficient of 0.91 in Figure 2.5 A, yet the individual slopes of VS16

especially (m = 0.81), and DAC (0.55) are greater compared to AP13 (0.49) and WBC (0.47), Figure 2.4 B. The low correlation of annulus radius and tiller height (0.31) in Figure 2.4 B, reflects the wide 95% confidence interval on Figure 2.5 C. Cortical cell wall thickness and outer diameter lack a significant correlation, (Figure 2.4 B), and show a flat, (hypoallometric), scaling relationship overall (m = 0.024) in which cortical cell wall thickness changes independently of outer diameter (Figure 2.5 B). For annulus radius vs tiller height, the trend is again overall isometric (m = 0.55) but the genotype slopes are again different, but this time not separated by ecotype, DAC (m = 0.62) and WBC (m = 0.35) positive and VS16 (m = -0.24) and AP13 (m = -0.45) negative (Figure 2.5 C). As for cortical cell wall thickness and height, no relationships are significant among the genotypes (Figure 2.5 D). This indicates that genotypes can exhibit scaling that deviates from the combined genotype trend and reveals limitations on predicting internode anatomy traits by larger phenotypic traits as they differ across environments by traits observable without microscopic analysis.

2.5 Percent loss of hydraulic conductivity and internode anatomy

A potentially important indicator of switchgrass yield under water restriction, we next examined the relationship between internode anatomy and internode hydraulic properties. For example, switchgrass under water limitation exhibits a diminished growth phenotype of internode in cross section with smaller outer diameter, annulus radius, and cortical cell wall thickness that likely reduces biomass yield (Figure S2.6). For the subset of samples in this analysis, we added several additional traits for whole tillers (KBSM20 in Table 2.1 & S2.1). Internode anatomy measurements were completed on separate tiller segments on which hydraulic conductivity was measured. We used the standard centrifuge

method to induce loss of conductivity that in some cases produces "r-shape" percent loss of conductivity curves, perhaps as a result of the so-called "open-vessel artifact". Though there is controversy that these r-shaped PLCs are invalid, several studies show that multiple methods agree with the standard centrifuge method in some species (i.e. *Olea europaea* and *Prunus persica*) even with vessel lengths longer than the stem segment spun in the rotor (Hacke et al., 2015; Yin et al., 2019). Our data shows two r-shaped (Figure S2.10 B, C), two sigmoidal PLCs (Figure S10 A, D), and significant differences by ecotype ($P<0.001$) (Figure 2.6 C, S2.7 B and C).

We found that percent loss of conductivity (PLC) in lower tiller segments varied significantly across four genotypes with the uplands (VS16 and DAC) more resistant than the lowlands (AP13 and WBC) (Figure 2.6 C, S2.7 B and C). Since we only discuss the hydraulics of the tiller segment, rather than the intact tiller, we will use the term "segment" to specifically indicate we are strictly referring to the hydraulic conductivity characteristics of an excised tiller segment. The pressure required to induce 20 percent loss of conductivity in the tiller segment ($P20_{segment}$) across the measured segments is statistically indistinguishable for AP13, WBC, and VS16 at -0.19 MPa with DAC showing more resistance, requiring an average of -0.48 MPa. However, genotypes began to separate at 30 PLC and fit into two groups by ecotype ($P< 0.05$ Tukey test). Mild pressures induce 50 PLC in all four genotypes, yet averages are statistically different ($P<0.001$) by ecotype; AP13 (-0.21 MPa), WBC (-0.30 MPa), DAC (-0.57 MPa), and VS16 (-0.62 MPa). Though the resistance to loss of conductivity is statistically different across ecotypes, the range of average pressure to induce 50% PLC in a 13 cm tiller segment ($P50_{segment}$) is minor (0.4 MPa) and does not provide as much variation in protection from conductivity loss as

hypothesized according to the variability of internode anatomy. Finally, we also examined the pressure at the extreme side of the conductivity curve, PLC 90. VS16 and DAC maintained conductivity at highest pressures. VS16 showed the highest resistance to conductivity loss by requiring -1.9 MPa to induce 90% loss of conductivity, compared to DAC (-1.0 MPa), AP13 (-0.29 MPa), and WBC (-0.72 MPa).

Numerous significant relationships were found between internode anatomy traits, maximum stem specific hydraulic conductance (K_S), and percent loss of hydraulic conductivity shown by Spearman correlations (Figure 2.6 A). Maximum conductance and $P50_{segment}$ show opposite correlations with internode anatomy and leaf traits consistent with well-known trade-offs between efficacy (i.e., resistance to embolism) and efficiency (i.e., bulk flow volume) of hydraulic conductivity (Ocheltree et al., 2016) . In general, tillers with larger total leaf area and are of the first leaf below the flag leaf ($flag^{-1}$), height, outer diameter, annulus radius, and average xylem diameter had larger conductance and milder $P50_{segment}$. The larger the distance between vascular bundles, the greater the conductance and milder $P50_{segment}$, which is explained by the observed positive correlation of average xylem diameter and distance between cortical vascular bundles (SCC = 0.82). Sheath radial thickness also highly positively correlates with stem-specific conductivity K_S (SCC = 0.94) and negatively with $P50_{segment}$ (SCC = -0.78) (Figure 2.6 A). Most correlations are negative with $P50_{segment}$ and only three are positive—cortical cell wall thickness (SCC = 0.83) (Figure 2.6 D), sclerenchyma cell wall thickness (SCC = 0.75), and rind percent annulus radius (SCC = 0.81) Figure 2.6 A, S2.7 F). Additionally, cortical cell wall thickness negatively correlates with maximum stem hydraulic conductivity (K_S) (Figure 2.6 E), as well as rind % annulus radius (Figure S2.7 D).This is consistent with the hypothesis that

genotypes with more fibers in cross section, measured as sclerenchyma radial thickness and sclerenchyma cell wall thickness, have greater resistance to embolism (Lens et al., 2016). Negative correlations of traits with resistance to segment hydraulic conductivity loss include nearest neighbor distance of vascular bundles in the cortex (SCC = -0.76), average xylem diameter (SCC = -0.71), and annulus radius (SCC = -0.73).

To explore the relationships between Ks in terms of stem capacitance traits, we found several significant relationships with K_s vs. leaf traits and annulus radius scaled internode anatomy (Figure S2.8). First we looked at hydraulic conductivity and traits that influence the water requirements of the plant: the leaf. Total leaf area (SCC = 0.82) vs. Ks shows that lowlands are larger than the uplands in both features (Figure S2.8 A). Sheath maximum thickness is also largest in the lowlands and shows a highly significant positive correlation (SCC = 0.94), with AP13 the largest (Figure S2.8 B). Considering traits that influence stem water storage capacity (capacitance) in relation to K_s is best to do so with scaled data to annulus radius. This way we can compare the differences in proportion of tissues and cells relative to genotype size differences, etc, rather than raw values. Cortex % of the annulus radius is not significant with all four genotypes (data not shown in figure) but is significant with DAC removed (SCC = 0.72, Figure S2.8 C). The distance between vascular bundles in the cortex scaled to annulus radius is negatively correlated with K_s (SCC = -0.71, Figure S2.8 D) and is largest in DAC, while the other genotypes all overlap. Cortex cell lumen diameter scaled to annulus radius is also negatively correlated (SCC = -0.71, Figure S2.8 E), with DAC again having the largest proportion of cortex lumen diameter / annulus radius. Lastly, xylem diameter in cortex vascular bundles scaled to annulus radius negatively correlates with K_s (SCC = -0.82, Figure S2.8 F). Although the

lowlands have larger cortex radius % annulus radius, the uplands have larger proportion of cortex lumen and distance between cortex vascular bundles scaled to annulus radius. Combining these traits together to calculate a theoretical capacitance reveals that raw capacitance related trait values are higher in lowlands and significantly different from uplands ($p < 0.001$) (Figure S2.9 A). However, differences are no longer significant when the features are scaled to annulus radius with genotypes practically indistinguishable from each other (Figure S2.9 B).The takeaway here is that the uplands have greater lumen storage and further distance between vascular bundles than the lowlands yet have larger xylem diameter scaled to annulus radius. Therefore, the uplands have greater theoretical capacitance relative to their size than the lowlands do, yet the uplands also have larger xylem diameter than the lowlands. Furthermore, K_s scaled to annulus radius of the two lowlands and VS16 are statistically different ($p < 0.01$) from DAC, which had lower conductivity.

2.6 Deconstruction of biomass across genotypes and environments

Switchgrass biomass conversion efficiency into biofuels is largely a function of tissue characteristics (DeMartini et al., 2013). Cell wall composition in switchgrass is found to vary by cell type and cell wall thickness observable with histological staining. The Maule reaction reveals lignin that is rich in syringyl units stained bright red, while the gold cell walls are predominately guaiacyl rich lignin. However, the images in Figure S2.18 clearly show that the most recently deposited secondary walls on the inner most cell wall surface observed in fiber cells of all four genotypes is predominately rich in syringyl units. AP13 exhibits a unique sclerenchyma cell file layer that is rich in S-lignin that is absent in other genotypes (Figure S2.18 E). The two uplands also stain red for S-rich lignin in the

entirety of the cortex, while WBC only shows S-rich in the outer half of the cortex (Figure S2.18 B-D, I-K). Furthermore, AP13 shows greater S-rich lignin in the cortex when grown at PKLE with no S-rich Sclerenchyma cell file layer, though present at KBSM, and both AP13 and VS16 show altered S/G lignin ratio under rain exclusion (Figure S2.6). Interestingly, the S-rich lignin sclerenchyma cell layer in AP13 also uniquely has mixed linkage glucans (MLG) detected with immunolocalization (Figure S2.17). Based on these observations, we designed a digestion experiment to explore the impact of variable internode anatomy and cell wall composition on cell wall deconstruction.

Particle size of switchgrass biomass is hypothesized to influence digestion efficiency. Prior to chemical digestion in the process of biomass deconstruction, mechanical deconstruction by milling and cryo-grinding (chilled with liquid nitrogen) pulverizes the biomass into tiny particles, yet internode anatomy is still intact (Figure S2.13). Particles of AP13 and WBC internode biomass grown at PKLE site in Texas have multiple thick-walled fiber shards visible ranging from <1 μm to <20 μm in width, with fibrous shards commonly greater than 50 μm in length (Figure S2.13 A and B), while a single cortical cell with attached walls from neighboring cells is visible in Figure S2.13 C. Furthermore, particles size differences are quantifiable as shown in Figure S2.13 D-F.

To we examine the relationship between internode anatomy and biomass deconstruction, we digested biomass from six environments and four genotypes at various pretreatment severities and cellulase loadings. Reaction conditions are reflected by codes with higher numbers reflecting harsher treatments where P indicated the pretreatment NaOH molarity, T the pretreatment temperature, and E the enzyme concentration (Table S2.2). Two traits show a mild positive correlation with glucose yield across different

digestion treatments: nearest neighbor distance to vascular bundles in the cortex (up to 0.45) and the in the sclerenchyma (up to 0.28) depending on the treatment (Figure 2.7 A). This may indicate that glucose yield is increased by increased cortical cells and sclerenchyma fiber cells because of further distances between vascular bundles. In contrast, several anatomical traits negatively correlate with glucose yield and the relationship increases with treatment severity. As expected, if cell wall thickness limits enzyme accessibility, cortical cell wall thickness and sclerenchyma radial thickness show the strongest correlations across treatment conditions. Cortical cell wall thickness shows the strongest correlations with glucose yield at P2T2E2 (-0.72), while sclerenchyma radial thickness is strongest at P3T2E2 (-0.59) (Figure 2.7 A). Additionally, the two mildest treatments, P1T1E1 and P1T2E1, highly correlate with the harshest treatment (P3T2E2) with 0.81 and 0.79, respectfully. This result shows that the mildest treatment yields may serve as an indicator for yields with harsher treatments when deconstructing switchgrass biomass. Comparing across genotypes and digestion treatments, WBC and AP13 have significantly higher glucose yield ($P < 0.001$) (Figure S2.14 A). Furthermore, looking within genotypes across sites shows that AP13 has higher glucose yield at KBSM ($p < 0.01$) compared to CLMB and PKLE (Figure S2.14 B), and WBC has higher glucose yield at CLMB ($p < 0.01$) than PKLE and KBSM (Figure S2.14 C). Percent pentose yield mg/g was also determined and is positively correlated with glucose yield (0.95) across all treatments with NaOH pretreatment (Figure S2.15 A and B), though the correlation is reduced to 0.87 after removing the P3T2E2 high yielding treatments (Figure S2.15 C and D). Additionally, the groupings of the data by treatment reveal that the pretreatment

conditions of H2SO4 show minimal range (0.02 %) glucose yield relative to the P3T2E2 treatment (0.18 %) with similar pentose yield (Figure S2.15 E and F).

Thin cortical cell wall thickness (4 µm) and mild pretreatment (P2T2E2) produces similar yield (0.04 % glucose mg/g biomass) with thick cortical cell wall thickness (8 µm) and harsher pretreatment (P3T2E1) (Figure 2.7 B). This does not support our hypotheses that trends with internode anatomy and yield would decrease with harsher treatments. Similar yields and relationships with anatomical traits are evident when comparing P2T2E1 to P2T2E2, and P1T2E2 to P1T2E3 despite the tenfold difference of enzyme in both cases. Cell wall area per lignified fiber show minimal patterns similar to previous traits, while annulus radius shows a mild relationship only under the harshest treatment (P3T2E2), (Figure 2.7 D and E). Glucose yield varied among genotypes by site across digestion treatments with WBC showing significantly higher yield after the P3T2E2 treatment compared to AP13 and VS16 ($p < 0.0005$), (Figure S10 A). Lowlands both had higher glucose yields with AP13 significantly higher at KBSM vs. CLMB and PKLE ($p <0.01$) and WBC significantly higher at KBSM and CLMB vs. PKLE ($p < 0.005$) after P3T2E2, with both uplands not significantly different across sites (Figure S10 B - E).

Acetyl bromide soluble lignin (ABSL) and cellulose content in three site biomass show an overall lack of significant relationships with cortical cell wall thickness (CWT) and digestibility (Figure S2.16). CWT is significantly positively correlated with cellulose content ($p = 0.021$) (Figure S2.16 A). However, ABSL lacks any meaningful relationship with CWT Figure S2.16 B), or average glucose yield % mg/g after P2T2E2 (Figure S2.16 D), or P3T2E2 Figure S2.16 F) digestion treatment. Average cellulose mg/g of biomass is negatively correlated though not significantly with glucose % yield mg/g after P2T2E2

(Figure S2.16 C), or P3T2E2 (Figure S2.16 E) digestion treatment. Though CWT and cellulose content are significantly correlated, no clear genotype specific relationship or trend across sites is observed.

2.7 Discussion

This study set out to identify internode anatomy variation in four characteristic genotypes of two ecotypes across common gardens spanning 17 degrees of latitude. The results revealed several significant trends that relate traits to plant processes that functionally impact plant water stress response and cell wall deconstruction. Not only does internode anatomy vary among genotypes, we also found significant plasticity in numerous traits within each genotype across common gardens. Based on genotypic plasticity, we evaluated hydraulic conductivity of tiller segments from four genotypes grown at KBSM20 in Michigan to find mild but statistically significant variation in the $P50_{segment}$ and numerous correlations with internode anatomy phenes. Furthermore, biomass deconstruction analyses tested the hypothesis that internode anatomy can modify the effectiveness of treatment severity parameters: NaOH molarity, incubation temperature, and enzyme concentration.

2.8 Internode anatomy plasticity across genotypes and environments

The internode anatomy analysis tests the hypothesis that visible plant architecture traits indicate underlying internode anatomy plasticity among genotypes and across environments. Generally, internode anatomy showed similarities within the ecotypes in plant architecture. However, numerous internode anatomy phenes vary among genotypes at each site and within genotypes across sites (Figure 2.2, tables 2.2 and 2.3). This represents a genotype specific response to environment that may impact biofuel relevant

traits and could direct where each genotype is suited for biomass quality in terms of internode anatomy. To interpret the impact of phene variation on biomass, we need to consider the function of phenes that show the highest variation as well as those that are consistent across genotypes and or sites.

The impact of trait plasticity depends on the function(s) of each trait. Cell type and abundance serve a particular evolved purpose for the plant yet can also serve as attractive features that enhance biomass for biofuels. Water and nutrient transport are crucial for plant growth and ultimately impacts total biomass yield. Average xylem diameter is largest in the lowlands which may reflect the semi-riparian conditions this ecotype is adapted to, and this trend is generally observed across latitudes (Figure 2.3). Departing from this trend is the cell wall thickness of cortical cells and one case, sclerenchyma fiber radial thickness. This shows that the uplands have thicker walls in many cases and VS16 has larger cell files of sclerenchyma than WBC. The difference in trends of different traits led us to explore trait scaling relationships in greater detail.

Cortical cell wall thickness (CWT) is emerging as a trait of special interest and had the highest stress in both scaled and unscaled NMDS. Additionally, CWT lacked significant correlations without scaling, suggesting there isn't a broad relationship but is rather specific to each genotype and environment combination (Figure 2.4 B, C). The thickness of the cell wall of the cortex can have an impact on both cell wall digestion and water storage in the internode (capacitance). Furthermore, the inconsistent thickness of this trait not only across genotypes and sites, combined with the fact that it shows rank change across sites independently from other internode anatomy phenes, suggests that this trait may be regulated separately and could be targeted for optimization.

2.9 Multiple internode anatomy traits show non-isometric trait relationships indicative of alternative resource allocation among genotypes

Based on the variable trends of several traits among genotypes across latitudes, we next tested the hypothesis that internode anatomy phenes scale differently among genotypes across latitudes. At any point in time, a plant has a given amount of resources and allocates these resources to different structures. This fact implies that there may be trade-offs in allocation to cell types that result in different plant performance under stress and in the efficiency with which we want to convert biomass into biofuels.

Different types of allometric relationships between plant architecture and internode anatomy across latitudes represent differential allocation of resources into different cell and tissue types (Weiner, 2004). Allometric analyses are present in literature that look at cell wall thicknesses described in the context of functional implications in the leaves of diverse angiosperms (Scoffoni et al., 2017), but are lack analyses in the internode. We found that in many cases, scaling relationships across latitudes differ among genotypes and from the overall relationship when the genotypes are combined (Figure 2.5).

Differences in allocation of resources to leaves reflects the growing season length and winter die back in northern latitudes. Likewise, switchgrass under water limitation exhibits a diminished growth phenotype of internode in cross section with reduced internode anatomy traits (Figure S2.6). This not only reflects the influence of the limitation of water on early vegetive growth directed by turgor pressure and cell expansion, but also limits future performance of these tissues should water become abundant. Similarly, lignification of cells increases with maturity and varies across cell types that alter biomass

deconstruction efficiency, i.e., cortical cell wall thicknesses and cell type abundance (rind % and cortex radius).

Reciprocal planting studies reveal there are disparities between locally adapted and displaced populations that may guide selection of high performance ecotypes, cultivars, and traits (Hereford, 2009; Lowry, 2012). Previously established common gardens across 16.7 degrees of latitude in the Midwest that were populated with a known-four-way cross and F_2 mapping population of two uplands from the northern great plains (genotypes VS16 and DAC6), and two lowlands from the southern great plains (genotypes AP14 and WBC3) ((Lowry et al., 2019; Milano et al., 2016). When different genotypes produce phenotypic traits that rank change across environments, this is considered a genotype x environment interaction (Des Marais et al., 2013). Figure 2.3 shows rank change in both metaxylem diameter and cortical cell wall thickness. Winter die-off increases and biomass production decreases relative to displacement of genotypes from native locale (Lovell et al., 2021). Similarly, drier and warmer conditions in southern latitudes may have a similar kill off effect on displaced northern uplands. Comparisons of latitude displacement against internode anatomy traits among genotypes revealed a subtle trend that may reflect the observed differences in biomass yield. Cortical cell wall thickness showed a negative relationship with latitude displacement across all genotypes (Figure S2.5 A. Interestingly, this trend is not observed in all traits. Understanding the variability of switchgrass internode anatomy across environments and impacts on biomass yield and quality in the context of genotype x environment is a valuable step to take towards developing this biofuel feedstock.

2.10 Reduction of hydraulic conductivity under mild pressure may be explained by plant segmentation theory

Plant segmentation theory suggests leaf die-back and sacrificial death of disposable plant regions increase likelihood of whole plant survival (Cochard et al., 1996; Davis et al., 2002; Lo Gullo et al., 2004; Vilagrosa et al., 2003). In ryegrass, it only takes approximately 21 days to regrow the maximum three leaves it typically supports (Holloway-Phillips & Brodribb, 2011). One study analyzing cross sections with cryo-SEM also found daily embolism in the roots of Maize even in wet soil, suggesting that the impact of stem emboli may be larger if roots embolize and soil moisture content is too low to facilitate root refilling (McCully et al., 1998). However, alternative strategies may be present in maize as it is an annual, compared to perennial grasses such as switchgrass.

Though hydraulic capacitance was not directly measured, its definition of water storage capacity for introduction into the transpiration stream affords us to make assumptions based on internode anatomy traits that are associated with water storage. The larger the distance between vascular bundles, the greater the conductance and milder $P50_{segment}$, which is explained by the observed positive correlation of average xylem diameter and distance between cortical vascular bundles (SCC = 0.82), which translate to higher stem capacitance. The thickness of the cell wall also directly impacts the amount of water the cells are capable of storing, and thicker walls mean more area of the cell is not free for water storage (McCulloh et al., 2019). Another source of above ground water storage is the leaf sheath that surrounds much of the length of the internode in many grasses, including switchgrass. Sheath radial thickness highly correlates with K_S (0.94) and

$P50_{segment}$ (-0.78) suggesting that sheath thickness is correlated with greater conductivity and vulnerability to loss of conductivity.

2.11 Loss of conductivity may be restored by positive root pressure

Plants grown under water stress conditions are smaller, while periodic water limitation ultimately impacts gas exchange once the stomata close due to low turgor pressure (Nunes et al., 2020). We want to test the hypothesis that switchgrass internode anatomy plasticity effects hydraulic conductivity to understand the potential impact these traits may have on plant biomass yield by impacting resistance to water limitation stress. We found that mild pressures induce 50 PLC in all four genotypes, yet averages are statistically different ($P<0.001$) by ecotype; AP13 (-0.21 MPa), WBC (-0.30 MPa), DAC (-0.57 MPa), and VS16 (-0.62 MPa). VS16 showed the highest resistance to conductivity loss by requiring -1.9 MPa to induce 90% loss of conductivity, compared to DAC (-1.0 MPA), AP13 (-0.29 MPA), and WBC (-0.72 MPa).

Reduction of hydraulic conductivity, usually due to vessel embolism, occurs during times of peak transpiration due to plant exposure to sunlight, warm temperatures, and wind. When evaporative demand subsides, positive root pressure in the roots has been shown in several grasses to mediate xylem refilling and the repair of failed vessels. For example, rice (Stiller et al., 2003), and sugarcane (Neufeld et al., 1992) show that over 60% of hydraulic conductivity may be lost during peak transpiration that can be restored by overnight root pressure (Holloway-Phillips & Brodribb, 2011). Furthermore, the maximum tiller height of bamboo (more than 30m tall) is observed to be determined by positive root pressure, that is, height is closely predicted by maximum root pressure needed to repair hydraulic dysfunction that occurred during diurnal gas exchange (Cao et al., 2012). In maize, mid-

day leaf water potential of -1.98 MPa resulted in 68% loss of stem-specific conductivity that reduced to 24% overnight after returning the Ψ_{soil} to ~0 MPa (Gleason et al., 2017). This indicates recovery of stem-specific conductance overnight from positive root pressure during low rate of transpiration. The mild resistance to conductivity loss in switchgrass is speculated to be diurnal embolism and positive root pressure mediated refilling, a common phenomenon in herbaceous plants (Holloway-Phillips et al. 2011). It is possible that our data represents this same phenomenon occurring in switchgrass and warrants detailed measurements of root pressure in switchgrass under various conditions to elucidate this process.

2.12 Cell wall thickness and deconstruction

Enzyme access to substrate is the key element in biomass deconstruction kinetics that is a rate-limiting step of cell wall digestion (Arantes & Saddler, 2010; Donohoe & Resch, 2015; Hall et al., 2011). There is evidence that lignin content in secondary cell walls is a major barrier to efficient enzymatic deconstruction and a reduction in lignin concentration will improve enzymatic hydrolysis and utilization of structural polysaccharides (Grabber, 2005). Our results in Figure 7 and Figure S2.15 show that there is also a component of internode anatomy that impacts glucose and pentose yields present across different treatment severities. The strongest relationship is found with the thickness of cortical cell walls, where glucose yield per mg of biomass increases with treatment severity. This result refutes our hypothesis that the influence of internode anatomy on digestion efficiency would only have an effective on mild to medium treatments, and then not make any difference when harsher treatments are applied.

Thermochemical treatments typically increase accessibility of cellulose microfibrils for enzymatic digestion, which produced the more pronounced relationships and steeper slopes of the 6.25 mM and 62.5 mM NaOH treatments. An explanation for this is that the composition of the thicker cell walls is less digestible due to increased lignification that comes with maturity. The other is that the reduced inner cell wall surface area that results from thicker walls reduces enzyme access to begin digestion. Cell wall digestion experiments show the thicker secondary cell walls of switchgrass sclerenchyma fibers were found to not completely degrade even with 100-fold larger concentration of enzyme, compared to the standard, and 7 day digestions (Ding et al., 2012), and another study suggests that in the rumen of cattle, microbial access to the inner cell wall surface of the cell lumen has a larger impact on digestion than lignin content (Wilson & Mertens, 1995). Precisely which feature, cell wall surface or composition, is the predominate factor requires further analysis.

We tested the hypothesis that thick cell walls and fiber cell abundance each reduce cell wall deconstruction efficiency. Similar yields were found with 4 μm cortical cell wall thickness and milder treatment as 8 μm thickness and harsher treatment (Figure 2.7 A). A similar relationship was observed in sclerenchyma radial thickness, and less but still present in cell wall area per fiber cell yet is absent in annulus radius. These results suggest that internode anatomy has a greater impact on digestion efficiency than the plant architectural trait of annulus radius. Cortical cell wall thickness is only weakly correlated with plant height (-0.11) and not significantly with outer diameter in the six-environment analysis (Figure 2.4 B) and shows rank change among genotypes across

environments. This suggests that this high impact trait varies according to genotype x environment interactions.

Visualization of cell wall composition with histology and immunolocalization suggest that lignin and mixed-linkage glucans (MLG) vary among genotypes and cell types that modulate cell wall deconstruction. As mentioned above, the secondary cell wall is made of cellulose, hemicellulose, and lignin. The Maule reaction reveals lignin that is rich in syringyl units-stained bright red, while the gold cell walls are predominately guaiacyl rich lignin. However, the images in Figure S2.18 clearly show that the most recently deposited secondary walls on the inner most cell wall surface observed in fiber cells of all four genotypes is predominately rich in syringyl units. Studies show that a reduction of S rich lignin through RNAi constructs increased cell wall digestibility (Tu et al., 2010). *Brachypodium distachyon* lines with 22% reduction of S/G ratio showed the largest ethanol yield increase (17%) relative to the control (Trabucco et al., 2013). The different patterns of s-rich lignin across genotypes and cell types likely impact deconstruction, with the S-rich cells and innermost walls being less digestible. Furthermore, MLG occurs in mature, senescing tissues of various grasses including switchgrass (Vega-Sanchez et al., 2013). Immunolocalization of MLG in AP13 and VS16 show different patterns in the sclerenchyma, a region in AP13 that is rich in S lignin (Figure S2.17). The different MLG content across internode anatomies associated with AP13 and VS16 likely impact the deconstruction of these cells. This provides another aspect towards understanding the connection between digestion yields and cell wall thickness in terms of cell wall composition.

To draw some conclusions about the relationship of internode anatomy and cell wall deconstruction, we combined the traits to calculate an internode anatomy "quality" metric. We used the product of cortical cell wall thickness and cortex radius, and the product of cell wall area per sclerenchyma fiber ratio and sclerenchyma radial width and multiplied them to produce this "quality" metric for comparison (Figure S2.19) which includes images of the internodes of the exact samples represented by the data. Cell wall area per fiber is negatively correlated with digestion yield and increases this trend when adjusted for size when multiplied by sclerenchyma radial thickness (Figure S2.19 A and B). When exploring this type of analysis with cortical cell wall thickness and cortex radius, we again see a negative relationship with digestion yield (Figure S2.19 C). combining these measures together produces the correlation of quality and glucose yield in Figure S2.19 D shows a strong relationship with internode anatomy and deconstruction. Connecting cell wall thickness and relative cell type abundance in the context of biomass deconstruction and yield are presented in Figure 2.8. As the previous regressions and correlations show (Figure 7), the CWT and SCLR radial thickness traits are negatively correlated with digestion yield. The slope of the relationship is more pronounced in response to treatment severity (Figure 2.6). The model shows that thin walls and smaller sclerenchyma radial thickness (low cell count) are the easiest samples to digest and produce the highest yield, even at treatment mild treatments (P1T1E2) and above. Figure 2.8 summarizes the strongest relationships of internode anatomy and digestion efficiency with the conclusion that biomass that consists of thinner cortical cell walls (< 6 μm) and thinner sclerenchyma radial thickness will be more efficiently deconstructed.

Significant internode anatomy plasticity was found across environments within genotypes and among genotypes at the same environment. The plasticity of internode anatomy represents different resource allocation among genotypes because of local adaptation. Plasticity was found in trats that are categorized into biomass yield, physiology, and cell wall deconstruction. The plasticity of vascular traits was found to have the anticipated relationship with maximum stem conductance and potentially represent embolism resistance, though resistance was mild in all genotypes. The fiber and cell wall thickness traits were found to significantly influence cell wall deconstruction efficiency. Taking these two major results into consideration, optimization of internode anatomy should favor cell wall deconstruction efficiency for lignocellulosic biorefining due to the minimal impact on resistance to segment hydraulic conductivity. Furthermore, by analyzing traits independently of genotype and growing location, we have presented relationships with numerous internode anatomy traits that can be included in analyses for prediction purposes. Decoupling traits from genotypes and considering the traits alone may provide an additional and perhaps more valuable metric of predicting switchgrass performance and biomass deconstruction efficiency. This approach should be applied to a more genetically and morphologically diverse population.

2.13 Materials and Methods

2.14 Internode and whole tiller harvests

Plant materials were harvested a total of six different times at three different sites. Five collections of lower tiller segments 10 cm long were made and one collection of whole tillers. The segment harvests were made at the end of season in late summer before the first killing frost at each site. Each segment included 2 cm of internode below the lowest node

above soil level and approximately 8 cm of internode above the node or as much length until the next node. Segments were stored in 50% EtOH in 15 ml screw cap tubes and mailed to OU.

Lower tiller segments 10 cm long were harvested from common gardens in 2016 in Texas, Missouri, and Michigan, and repeated in Texas in 2017. All four genotypes were harvested in 2016 from Michigan and Missouri but only AP13 in Texas. Only AP13, WBC and VS16 were harvested at the Texas site in 2017, all DAC had died. The segments harvested in 2016 and 2017 were used in the digestibility analysis (see biomass deconstruction methods section). Lower tiller segments 10 cm long were harvested from the Missouri site in 2018 end of season in late September for internode anatomy analysis.

Whole tillers of AP13, WBC, VS16, and DAC for hydraulic conductivity were harvested from Michigan on July 28th (AP13 and DAC), and August 2nd (WBC and VS16) of 2020. Tillers were sealed in plastic bags with damp paper towels to maintain moisture status and shipped overnight. Tillers were harvested 5 days apart to allow for time to conduct hydraulic conductivity and measurements as well as to limit storage time of harvested plant material before analysis.

2.15 Sectioning, histology, and microscopy

Hand sectioning method was used to take cross sections of each internode beginning at 1 cm above the node, taking sections as needed no further than 2 cm above the node. Acriflavine hydrochloride was used predominately on the sections as a general cell wall stain to enhance visibility of cell walls.

The Maule reaction stains S lignin units bright red and G lignin units dull-brown (Trabucco et al., 2013). Reagents were prepared according to Mitra *et al* 2014 (Mitra &

Loqué, 2014) and all steps carried out at room temperature in 1.5 ml Eppendorf tube. Sections were first incubated in 1 milliliter of 0.05% potassium permanganate for two minutes at room temperature. Sections were then washed by pipetting replacing 700 ml of potassium permanganate with an equal volume of distilled water and repeated 3-5 times until solution is clear. Sections were then incubated in 1 ml of 3.7% hydrochloric acid for two minutes. After HCL was removed, 1 ml concentrated ammonium hydroxide (14.8 M) was added to the tube. Sections were mounted in the ammonium hydroxide on a standard glass slide.

The monoclonal antibody targeting MLG, described in (Meikle et al., 1994), was diluted to 10ng/mL from the stock solution. After 24-hour incubation, samples were washed in 1x TBST buffer twice at ten-minute intervals. 200 µl of 1/200 dilution (in TBST) of secondary monoclonal antibody (isotype IgG) coupled to the alexafluor 647 fluorophore was placed in each well and incubated under slight agitation in 4°C for 24 hours. Sections were again washed in 1x TBST buffer twice at ten-minute intervals. Individual sections were then placed on a size 0 coverslip, immersed in approximately 50-60 µl mowiol (polyvinyl alcohol solution) mounting media. Immersed sections were covered with a size zero coverslip and placed in 4°C in the dark until imaging. Sections were mounted between two coverslips to facilitate imaging from either side if needed.

All microscopy was completed on a Nikon Eclipse Ni microscope and a Nikon Ds-Qi1Mc camera (brightfield), and for fluorescence with GFP filter cube. Sections were tagged with the secondary antibody coupled with the alexa 647 fluorophore tag with excitation/emission at 594nm/633nm were imaged through the CY5 filter.

2.16 Morphometric analysis

All anatomical trait measurements were carried out in FIJI image software (Schindelin et al., 2012). Replicate images were measured for each genotype-location. In all cases, three images were measured per individual genotype, with three to six individuals measured except only two AP13 at PKLE16. Distances between two points were measured using the line tool unless otherwise described below. Nearest neighbor distance of vascular bundles was determined in all visible vascular bundles that fit into either cortex or sclerenchyma categories defined by >50% vascular bundle area location within either tissue. This led to different total counts of vascular bundles measured but was never less than 25 per image. Phloem area was measured using the trace tool to draw around the perimeter of the phloem areas of each visible vascular bundle in the cortex only with no fewer than 25 phloem areas measured per image. Cell wall area per fiber cell was determined by selecting a representative sclerenchyma fiber region, dividing the total cell wall area by the total area, and then dividing by cell count described in Figure S2.2. Tiller height of all but the KBSM20 samples were obtained from shared database within the common gardens group. Outer internode diameters were measured with digital calipers at the site of sectioning, 1 cm above the node.

2.17 Hydraulic conductivity measurements

Methods are described in detail in Supplemental text 1 and shown in Figure S2.11 and S2.12. We designed the use of foam and cyanoacrylate glue to seal the hollow pith of switchgrass. Pressure was applied to segments using the traditional centrifuge method with the Sperry style rotor (Alder et al., 1997). After centrifugation, the segments were connected to the hydraulic conductivity apparatus, adapted from (Jacobsen, 2011).

Hydraulic conductivity was measured using the R program (R Development Core Team, 2022; RStudio Team (2020)), conductR (https://mcculloh.botany.wisc.edu/methods/). PLC curves were generated for a total of 23 tiller segments with AP13 (5), WBC (5), VS16 (6) and DAC (7).

2.18 Biomass deconstruction

Remaining internode segments from a total of 43 harvested tiller segments harvested in 2016 and 2017 from the Michigan, Missouri, and South Texas sites were Wiley milled with a 2mm screen and cryo-ground for 3 minutes at 1000 rpm. De-starched alcohol insoluble residue (AIR) was prepared and sent to Great Lakes Bioenergy Research Center (GLBRC) for deconstruction and sugar yield analysis in triplicate 2 mg technical replicates.

Deconstruction parameters consist of three concentrations of NaOH pretreatment, 0.62 mM (P1), 6.25 mM (P2), 62.5 mM (P3); two heating treatments while biomass is in the NaOH for three hours, 45 C (T1) and 90 C (T2); and three enzyme treatments all at 50 C for 20 hours at three concentrations of Accellerase which contains multiple glycolytic activities (Sigma-Aldrich C9870) at 0.05 uL (E1), 0.50 uL (E2), and 5.00 uL (E3). Nomenclature of deconstruction treatments increase in number and reflects a tenfold increase in parameter severity in NaOH or enzyme concentration and a doubling of temperature (Table S2). Due to limitations in biomass because of differences in genotype size, not all treatments were applied to every genotype, namely DAC was very limited. Each sample was measured in three technical replicates.

Acetyl bromide soluble lignin (ABSL) and cellulose were performed on de-starched alcohol insoluble residue (dsAIR) following (Bartley et al., 2013). ABSL content

was used as a proxy for lignin content (Fukushima & Hatfield, 2004).For ABSL, 2-3 mg of dsAIR were incubated for 3 hours at 1050 rpm in 100 ul of 25% acetyl bromide in glacial acetic acid. While cooling on ice, 400 ul of 2M sodium hydroxide and 70 ul of freshly prepared 0.5 M hydroxylamine hydrochloride is added, then 1430 ul of water. Solution is centrifuged then 200 ul taken and read at 280 nm in UV specific 96 well plate. Cellulose was quantified following TFA hydrolysis of dsAIR pellet(Bartley et al., 2013).

2.19 Statistical analyses

All analyses were performed in R studio (R Development Core Team, 2022; RStudio Team (2020)). Internode anatomy traits were analyzed with MANOVA to identify traits of significant variance. ANOVA and Tukey tests and the Dunn's test were used to identify the factor source of the variation in normal and non-normally distributed traits, respectively. Non-metric multidimensional scaling (NMDS) was used to analyze internode anatomy data as a rank-based approach due to the non-linear, non-normally distributed, and wide magnitudes ranges across trait measurements. All correlation plots represent only statistically significant ($p<0.05$) Spearman correlations with blank spaces representing non-significance.

Traits were Log10 transformed prior to allometric regressions to remove the influence of magnitude differences (Mascaro et al., 2013).

Table 2.1 | Internode anatomy trait descriptions

Trait	Functional Importance	Trait Measurement	Established Relationship* or Hypothesis	Reference Or Rationale	Data set
Plant Architecture					
Height	Biomass yield	Ground level to inflorescence apex	Positively correlates with biomass yield*	Price 2014	All
Internode diameter *(Outer Diameter)*	Biomass yield	Measured at 1 cm above the first node above soil line with digital calipers	Positively correlates with biomass yield	Larger diameter {more biomass}	All
Internode length	Biomass yield	Measured at the first node above soil line to next node	Positively correlates with biomass yield	Longer internodes {total height}	KBSM20
Node count	Biomass yield	Number of nodes present	Positively correlates with biomass yield	More nodes {total height}	KBSM20
Flag leaf -1 area	Biomass yield	Next leaf below the flag leaf, scanned and area measured in FIJI/Image J	Positively correlates with biomass yield	More leaf area {higher carbon capture}	KBSM20
Total leaf area	Biomass yield	All leaves present measured as above	Positively correlates with biomass yield	More leaf area {higher carbon capture}	KBSM20
Internode Anatomy	All measurements made on 3 cross sections per individual plant taken between 1 and 2 cm above the first node above the soil line. Three individual plants per genotype per environment. See Figure 1 for highlighted measurements				
Internode annulus radius *(Annulus radius)*	Biomass yield	Straight line distance drawn perpendicular to epidermis, drawn from epidermis to pith, N = 8 per section	Positive correlation with biomass yield	Thicker annulus radius {more biomass}	All
Chlorenchyma radial thickness *(CHLR Radial Thickness)*	Biomass Yield	Straight line distance drawn perpendicular to epidermis, drawn across maximum Chlorenchyma cavity. N = 10 per section	Increases net photosynthesis* and may mediate drought response	Aschan 2003, Cernusak 2015, Nilsen 1990	All
Sclerenchyma radial thickness *(SCLR Radial Thickness)*	Physical stress and water stress	Straight line distance drawn perpendicular to epidermis, drawn across maximum Chlorenchyma cavity. N = 10 per section	Positive correlation with embolism resistance*, contributes to internode cell wall density*	Lens 2016, Jung and Casler	All

Vascular bundle fiber % area of vascular bundle	Biomass yield,	Area of vascular bundle fibers / Vascular bundle area (proto & meta xylem, proto & phloem) N =25+ / section See supp. #	Strengthens xylem and phloem, contributes to internode cell wall density	More fiber area {greater protection against cavitation}	All
Xylem diameter *(Xylem Diameter Cortex)*	Biomass yield, water Stress	Horizontal width of metaxylem, bisected xylem not measured, cortex vascular bundles only. N = 25+ per section	Positively correlates with conductivity and embolism vulnerability*	Ocheltree 2016, Hacke and Sperry 2006	All
Phloem area	Biomass yield	Phloem area traced per cortical vascular bundle, N = 15+ per section	Positively correlates with biomass yield *	Natrova 1991, More phloem area {more phloem transport capacity}	CLMB18 3-site 16/17
Cortical parenchyma cell wall thickness *(Cortex Cell Wall Thickness)*	Biomass yield, cell wall digestibility, water stress	Straight line measured from lumen to lumen, N =10 per section	Positively correlates with biomass yield, negatively with cell wall digestibility, negatively correlated with capacitance*	J.R.Wilson 1995, Jacobsen 2005, McCulloh 2014	All
Sclerenchyma cell wall thickness *(SCLR Cell Wall Thickness)*	Biomass yield	Straight line distance drawn perpendicular to epidermis, drawn across representative Sclerenchyma, excluding embedded vascular bundle widening. N =10 per section	Positively correlates with biomass yield, negatively with cell wall digestibility, negatively correlated with capacitance	J.R.Wilson 1995, Jacobsen 2005, McCulloh 2014	KBSM18
Cell wall area per lignified fiber	Water stress and biomass yield	Cell wall area / cell area of sclerenchyma fibers. See supp. Fig #	Positively correlates with conduit embolism resistance and biomass yield*	Lens 2016	3-site 16/17
Epidermis & hypodermis	Water stress and biotic stress	Cell layer count from epidermis to chlorenchyma cavity	Cell file thickness positively correlates with drought resistance and pathogens*	Javelle 2010	All
Nearest cortical vascular bundle neighbor *(Nearest VB Neighbor Cortex)*	Nutrient and moisture transport, water stress	All distances measured from center point of each vascular bundle surrounded by >50% cortical parenchyma. Nearest neighbor distance Averaged. See fig. 1E N = 50+ per section	Associated with hydraulic conductivity and negatively correlated to stem hydraulic capacitance	Near vascular bundle neighbor {high VB density and fewer cortical cells in between and small water storage capacity}	All

Nearest sclerenchyma vascular bundle neighbor *(Nearest VB Neighbor SCLR)*	Nutrient and moisture transport, water stress	Only vascular bundles <50% surrounded by sclerenchyma fibers measured as above.	Associated with hydraulic conductivity stem hydraulic capacitance	Near vascular bundle neighbor {high VB density and fewer sclerenchyma cells in between and smaller water storage capacity}	All
	Cell wall digestibility	(Chlorenchyma radial thickness + Sclerenchyma radial thickness) / Annulus radius	Negatively correlated with biomass digestibility	Barros-Rios 2012, Jung 2006	All
Cortex radial thickness % of internode annulus radius *(Cortex Percent Annulus Radius)*	Cell wall digestibility	(Annulus radius-(Chlorenchyma radial thickness + Sclerenchyma radial thickness)) / Annulus radius	Positively correlated with biomass digestibility	Barros-Rios 2012, Jung 2006	All
Cortex lumen diameter	Cell wall digestibility	Lumen span diameter. N =10 per section	Positively correlates with cell wall digestibility*, and stem hydraulic capacitance*	J.R.Wilson 1995, Jacobsen 2005, McCulloh 2014	KBSM20
Sclerenchyma lumen diameter	Cell wall digestibility	Lumen span diameter. N =10 per section	Positively correlates with cell wall digestibility*, and stem hydraulic capacitance*	J.R.Wilson 1995, Jacobsen 2005, McCulloh 2014	KBSM20
Embolism Resistance					
Pressure to induce 50% loss of hydraulic conductivity of internode *(P50)*	Water stress and biomass yield	Sperry rotor and conductivity apparatus. See supp fig. 10 and methods for description	Drought induced embolism negatively correlates with productivity*	Griffin 2012, Porier 2012	KBSM20

Established relationships denoted by *
Alternate trait names used in figures in ( ) where it applies

Table 2.2 | Summary of internode anatomy traits across six environments

Genotype	Environment	Ecotype	Cortex Cell Wall Thickness (µm)	Nearest VB Neighbor Cortex (µm)	Nearest VB Neighbor SCLR (µm)	Xylem Diameter Cortex (µm)	CHLR Radial Thickness (µm)	SCLR Radial Thickness (µm)
AP13	KBSM16	L	5 ± 1 ab	283 ± 26 a	76 ± 12 ab	40 ± 5 a	107 ± 44 a	126 ± 13 ab
AP13	CLMB16	L	7 ± 1 ab	253 ± 23 abc	78 ± 22 ab	31 ± 1 abcd	77 ± 68 ab	94 ± 39 bcd
AP13	PKLE16	L	6 ± 0 ab	258 ± 14 abc	121 ± 33 a	32 ± 0 abcd	88 ± 11 ab	115 ± 5 abc
AP13	PKLE17	L	6 ± 1 ab	281 ± 33 a	72 ± 6 ab	34 ± 3 ab	88 ± 27 ab	158 ± 36 a
AP13	CLMB18	L	7 ± 2 ab	253 ± 56 abc	78 ± 9 ab	34 ± 4 ab	82 ± 49 ab	101 ± 32 bc
AP13	KBSM20	L	3 ± .3 b	264 ± 50 ab	94 ± 14 ab	35 ± 4 ab	48 ± 23 ab	104 ± 23 abc
WBC	KBSM16	L	4 ± 1 ab	209 ± 26 abcd	92 ± 14 ab	31 ± 1 bcd	47 ± 12 ab	52 ± 8 cde
WBC	CLMB16	L	4 ± 1 ab	200 ± 17 bcde	117 ± 18 a	28 ± 2 bcde	18 ± 3 b	40 ± 5 de
WBC	PKLE17	L	8 ± 1 ab	220 ± 18 abc	90 ± 15 ab	30 ± 4 bcd	93 ± 23 ab	105 ± 5 abc
WBC	CLMB18	L	6 ± 1 ab	218 ± 28 abc	87 ± 20 ab	33 ± 3 abc	59 ± 43 ab	72 ± 17 cde
WBC	KBSM20	L	5 ± 1 ab	273 ± 9 ab	81 ± 7 ab	35 ± 2 ab	78 ± 13 ab	79 ± 13 bcde
VS16	KBSM16	U	7 ± 1 ab	191 ± 17 bcdef	74 ± 7 ab	30 ± 3 bcd	24 ± 6 b	73 ± 14 cde
VS16	CLMB16	U	6 ± .6 ab	162 ± 18 cdef	73 ± 13 ab	28 ± 3 bcde	27 ± 4 ab	80 ± 25 bcde
VS16	PKLE17	U	4 ± 1 ab	101 ± 22 f	77 ± 5 ab	17 ± 2 e	29 ± 19 ab	46 ± 18 cde
VS16	CLMB18	U	4 ± 2 ab	123 ± 10 ef	91 ± 15 ab	28 ± 4 bcde	12 ± 3 b	39 ± 15 de
VS16	KBSM20	U	7 ± 1 ab	131 ± 12 def	85 ± 10 ab	24 ± 1 cde	24 ± 12 ab	70 ± 15 cde
DAC	KBSM16	U	6 ± 2 ab	133 ± 9 def	73 ± 16 ab	21 ± 2 e	17 ± 4 b	34 ± 5 e
DAC	CLM16	U	4 ± 1 ab	124 ± 4 ef	75 ± 2 ab	22 ± 3 de	24 ± 22 b	31 ± 9 e
DAC	CLMB18	U	7 ± 2 ab	130 ± 42 ef	72 ± 7 ab	27 ± 5 bcde	20 ± 7 b	39 ± 14 de
DAC	KBSM20	U	8 ± 5 a	114 ± 11 f	55 ± 5 b	20 ± 1 e	20 ± 10 b	53 ± 22 cde
Total Average & SD			5.6 ± 1.4	196 ± 62	83 ± 15	29 ± 6	49 ± 31	76 ± 34
MANOVA x Genotype*Environment			**^{T}	***^{D}	***^{D}	***^{T}	***^{D}	***^{D}
Shapiro Wilks Test for Normality			Normal	Non-normal	Non-normal	Normal	Non-normal	Non-normal

N = 3 to 6 clonal replicates per genotype at each environment except AP13 PKLE16 n = 2
Averages and standard deviation for each genotype environment
^{T} = Tukey groups at alpha= 0.05
^{D} = Dunn's test

Table 2.2 Continued | Summary of internode anatomy traits across six environments

Genotype	Environment	Ecotype	Annulus Radius (µm)		Cortex Radius (µm)		Rind Percent Annulus Radius		Cortex Percent Annulus Radius		Outer Diameter (mm)		Height (cm)	
AP13	KBSM16	L	1093 ± 143	ab	861 ± 99	a	0.21 ± 0.03	ab	0.79 ± 0.03	bc	8 ± 1	a	216 ± 5	abc
AP13	CLMB16	L	992 ± 174	abc	821 ± 142	a	0.17 ± 0.08	abc	0.83 ± 0.08	abc	6 ± 1	abc	100 ± 5	hi
AP13	PKLE16	L	937 ± 196	abcd	734 ± 180	ab	0.22 ± 0.03	ab	0.78 ± 0.03	bc	7 ± 1	ab	128 ± 25	efghi
AP13	PKLE17	L	1144 ± 135	a	898 ± 102	a	0.22 ± 0.04	ab	0.79 ± 0.04	bc	7 ± 1	a	155 ± 34	cdefgh
AP13	CLMB18	L	879 ± 243	abcd	697 ± 171	ab	0.2 ± 0.04	ab	0.8 ± 0.04	bc	8 ± 1	a	250 ± 11	a
AP13	KBSM20	L	919 ± 144	abcd	767 ± 101	ab	0.16 ± 0.02	abc	0.84 ± 0.02	abc	8 ± 1	a	175 ± 9	cdefg
WBC	KBSM16	L	763 ± 144	bcde	663 ± 129	ab	0.13 ± 0.01	bc	0.87 ± 0.01	ab	6 ± 1	abc	211 ± 5	abcd
WBC	CLMB16	L	699 ± 63	cdef	641 ± 64	ab	0.08 ± 0.01	c	0.92 ± 0.01	a	5 ± 0	bcd	190 ± 4	bcde
WBC	PKLE17	L	953 ± 125	abcd	754 ± 112	ab	0.21 ± 0.03	ab	0.79 ± 0.03	bc	6 ± 1	abc	210 ± 43	abcde
WBC	CLMB18	L	793 ± 179	bcd	662 ± 126	ab	0.16 ± 0.04	abc	0.84 ± 0.04	abc	6 ± 0	ab	248 ± 11	ab
WBC	KBSM20	L	880 ± 96	abcd	724 ± 73	ab	0.18 ± 0.01	abc	0.82 ± 0.01	abc	6 ± 1	ab	179 ± 14	cdef
VS16	KBSM16	U	570 ± 15	defg	473 ± 26	bc	0.16 ± 0.02	abc	0.84 ± 0.02	abc	4 ± 1	cde	112 ± 17	fghi
VS16	CLMB16	U	547 ± 37	defg	441 ± 16	bc	0.2 ± 0.02	abc	0.81 ± 0.02	abc	3 ± 0	def	187 ± 2	bcdef
VS16	PKLE17	U	394 ± 95	efg	320 ± 59	c	0.19 ± 0.05	abc	0.82 ± 0.05	abc	2 ± 0	ef	193 ± 4	abcde
VS16	CLMB18	U	337 ± 83	fg	286 ± 68	c	0.15 ± 0.02	bc	0.85 ± 0.02	abc	3 ± 1	ef	160 ± 9	cdefgh
VS16	KBSM20	U	403 ± 85	efg	308 ± 60	c	0.23 ± 0.01	ab	0.77 ± 0.01	bc	3 ± 1	ef	101 ± 8	ghi
DAC	KBSM16	U	373 ± 45	fg	321 ± 37	c	0.14 ± 0.02	bc	0.86 ± 0.02	ab	2 ± 0	ef	215 ± 3	abcd
DAC	CLMB16	U	364 ± 61	fg	309 ± 30	c	0.15 ± 0.06	bc	0.85 ± 0.06	abc	2 ± 0	f	154 ± 67	cdefgh
DAC	CLMB18	U	288 ± 131	g	229 ± 116	c	0.18 ± 0	abc	0.82 ± 0.01	abc	2 ± 1	f	151 ± 43	defgh
DAC	KBSM20	U	278 ± 39	g	206 ± 49	c	0.27 ± 0.13	a	0.73 ± 0.13	c	2 ± 1	f	68 ± 11	i
Total Average & SD			680 ± 282		556 ± 227		0.18 ± 0.04		0.82 ± 0.04		5 ± 2		170 ± 49	
MANOVA x Genotype*Environment			***[D]		***[D]		***[D]		***[D]		***[D]		***[D]	
Shapiro Wilks Test for Normality			Non-normal		Non-normal		Non-normal		Non-normal		Non-normal		Non-normal	

N = 3 to 6 clonal replicates per genotype at each environment except AP13 PKLE16 n = 2

Averages and standard deviation for each genotype environment

[T] = Tukey groups at alpha= 0.05

[D] = Dunn's test

Table 2.3 | Three-site internode anatomy significant variation in 2016 and 2017 data only.

	Cortical Cell Wall Thickness (µm)		Nearest VB Neighbor Cortex (µm)		Nearest VB Neighbor SCLR (µm)		Xylem Diameter Cortex (µm)		Phloem Area (µm^2)	
Genotype Differences for Given Site [c]										
KBSM	***	bc, c, a, a	***	a, b, b, c	***	b, a, b, b	***	a, b, b, c	***	a, b, b, c
CLMB	***	a, b, a, b	***	a, b, b, c	***	b, a, b, b	***	ab, ab, a, b	***	a, a, ab, c
PKLE	**	a, a, b, /	***	a, b, c, /	NS		***	a, a, b, /	***	a, b, b, c
Site Differences for Given Genotype [d]										
AP13	***	a, ab, ab	NS		NS		***	a, b, b	***	a, b, b
WBC	NS		*	a, b, ab	***	b, a, ab	*	b, ab, a	**	ab, a, b
VS16	***	b, a, a	***	c, b, a	NS		***	a, a, b	***	a, b, a
DAC	***	/, b, a	***	/, b, a	*	/, a, b	**	/, a, b	NS	

[c] MANOVA of four genotypes at each individual site

[d] MANOVA of each individual genotype across three sites

Groups listed in order: AP13, WBC, VS16, DAC; PKLE, CLMB, KBSM

Table 2.3 Continued | Three-site internode anatomy significant variation in 2016 and 2017 data only.

	Chlorenchyma Radial Thickness (µm)		Sclerenchyma Radial Thickness (µm)		Cell Wall per Sclerenchyma Fiber cell area		VB Fiber area / VB area	
Genotype Differences for Given Site [c]								
KBSM	***	a, b, c, c	***	a, c, b, d	**	bc, c, a, a	***	ab, a, bc, c
CLMB	***	a, c, c, b	*	a, b, ab, b	NS		**	a, a, ab, b
PKLE	*	a, a, b, /	**	a, ab, b, /	NS		**	a, a, b, /
Site Differences for Given Genotype [d]								
AP13	***	a, c, b	NS		*	a, a, a	NS	
WBC	***	a, c, b	***	a, c, b	NS		NS	
VS16	NS		***	a, b, a	NS		***	a, a, b
DAC	NS		**	/, a, b	NS		NS	

[c] MANOVA of four genotypes at each individual site

[d] MANOVA of each individual genotype across three sites

Groups listed in order: AP13, WBC, VS16, DAC; PKLE, CLMB, KBSM

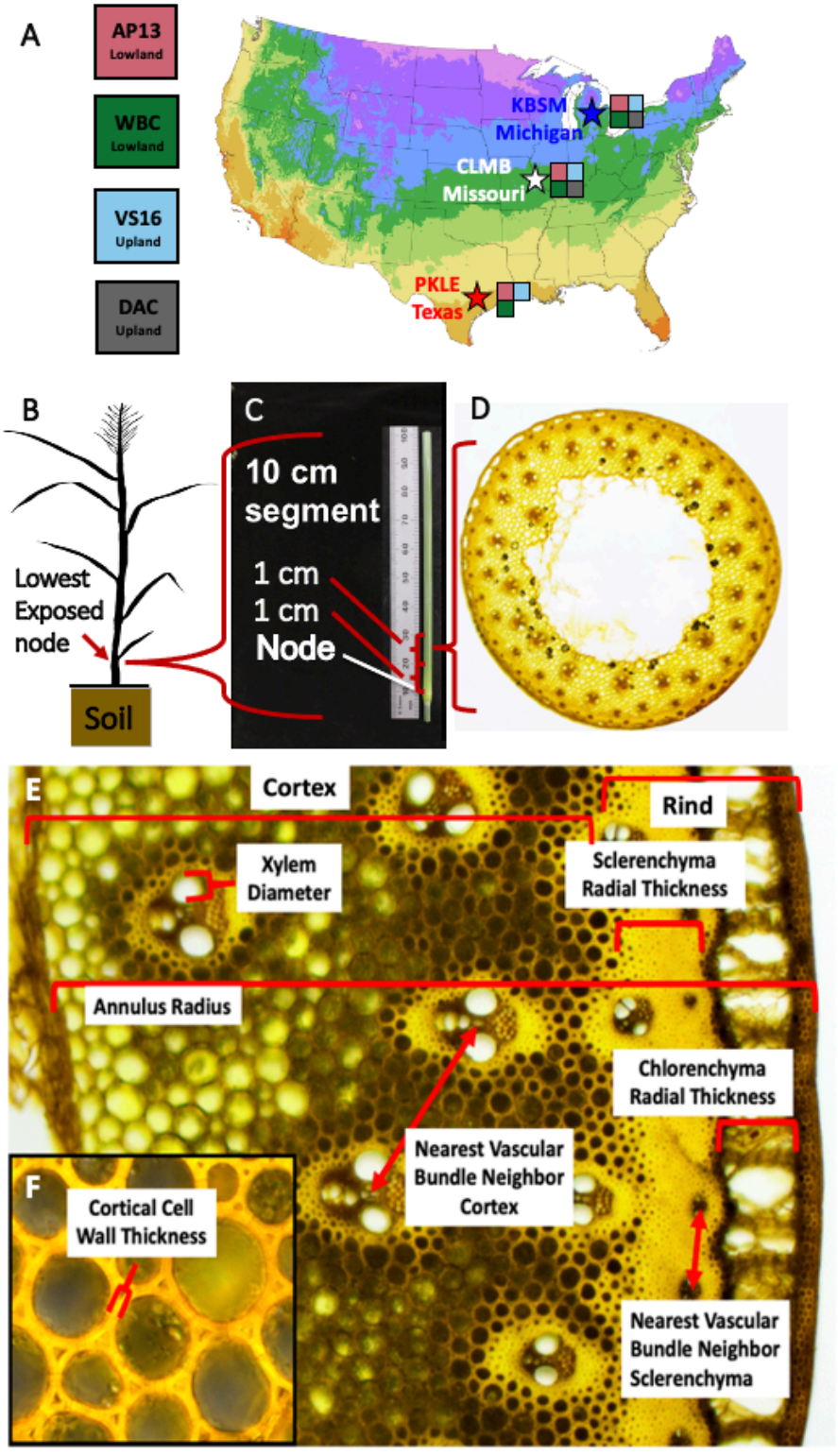
A
AP13
Lowland
WBC
Lowland
VS16
Upland
DAC
Upland
KBSM
Michigan
CLMB
Missouri
PKLE
Texas
B
Lowest
Exposed
node
Soil
C
10 cm
segment
1 cm
1 cm
Node
D
E
Cortex
Rind
Xylem
Diameter
Sclerenchyma
Radial Thickness
Annulus Radius
Chlorenchyma
Radial Thickness
Nearest Vascular
Bundle Neighbor
Cortex
Nearest Vascular
Bundle Neighbor
Sclerenchyma
F
Cortical Cell
Wall Thickness

Figure 2.1. Lowest exposed internode harvested at three sites for morphometric analysis of internode anatomy of four switchgrass genotypes. (A) Two upland (DAC and VS16) and two lowland (AP13 and WBC) switchgrass genotypes were clonally propagated and grown at three latitudes; Northern (KBSM) in Michigan, central (CLMB) in Missouri, and Southern (PKLE) in South Texas. (B,C) Ten cm stem segments were harvested at the lowest exposed node at end of season and preserved in 50% ethanol. (C,D) All cross sections were taken between 1 and 2 cm above the node. 22 traits were measured in total that include plant architecture and internode anatomy. Traits of interest are shown that include internode anatomy in terms of cell dimensions and cell type abundance, vascular related traits, and cell wall thickness of the cortex parenchyma and sclerenchyma cells. Additional traits in table 2.1.

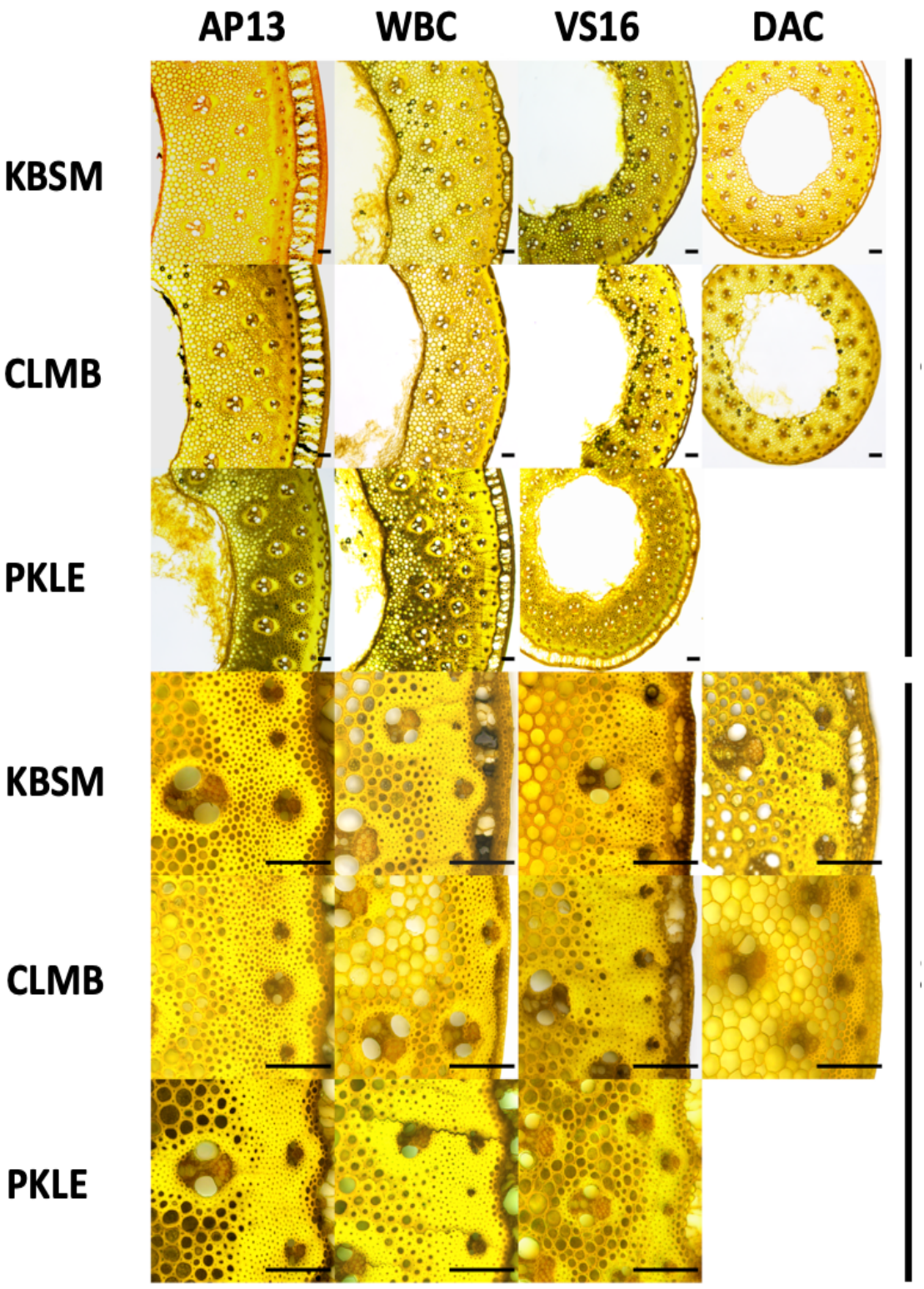
AP13
WBC
VS16
DAC
KBSM
CLMB
PKLE
KBSM
CLMB
PKLE

Figure 2.2. Internode anatomy of four genotypes show phenotypic plasticity and rank change across genotypes and sites. All genotypes harvested in 2016 at Northern (KBSM) and central (CLMB) sites, except AP13 (2016) WBC and VS16 (2017) and DAC dead at southern (PKLE). Cross sections reveal that the lowlands are larger in annulus radius (AP13 994 µm and WBC 817 µm) with 4x objective, but rank change occurs between lowlands across sites. Interestingly, cell wall thickness is largest in DAC KBSM (8 µm± 5) and WBC PKLE (8 µm ± 1), while sclerenchyma radial thickness largest in AP13 KBSM (126 µm ± 13) and smallest in WBC CLMB (40 µm ± 5) visible with the 20x objective. The rank change of traits among genotypes and across sites, and different genotypes showing the largest trait values suggests genotype x environment interactions are present in some but not all traits. Sections were stained with acriflavine hydrochloride to enhance contrast of cell walls. All scale bars are 100 µm.

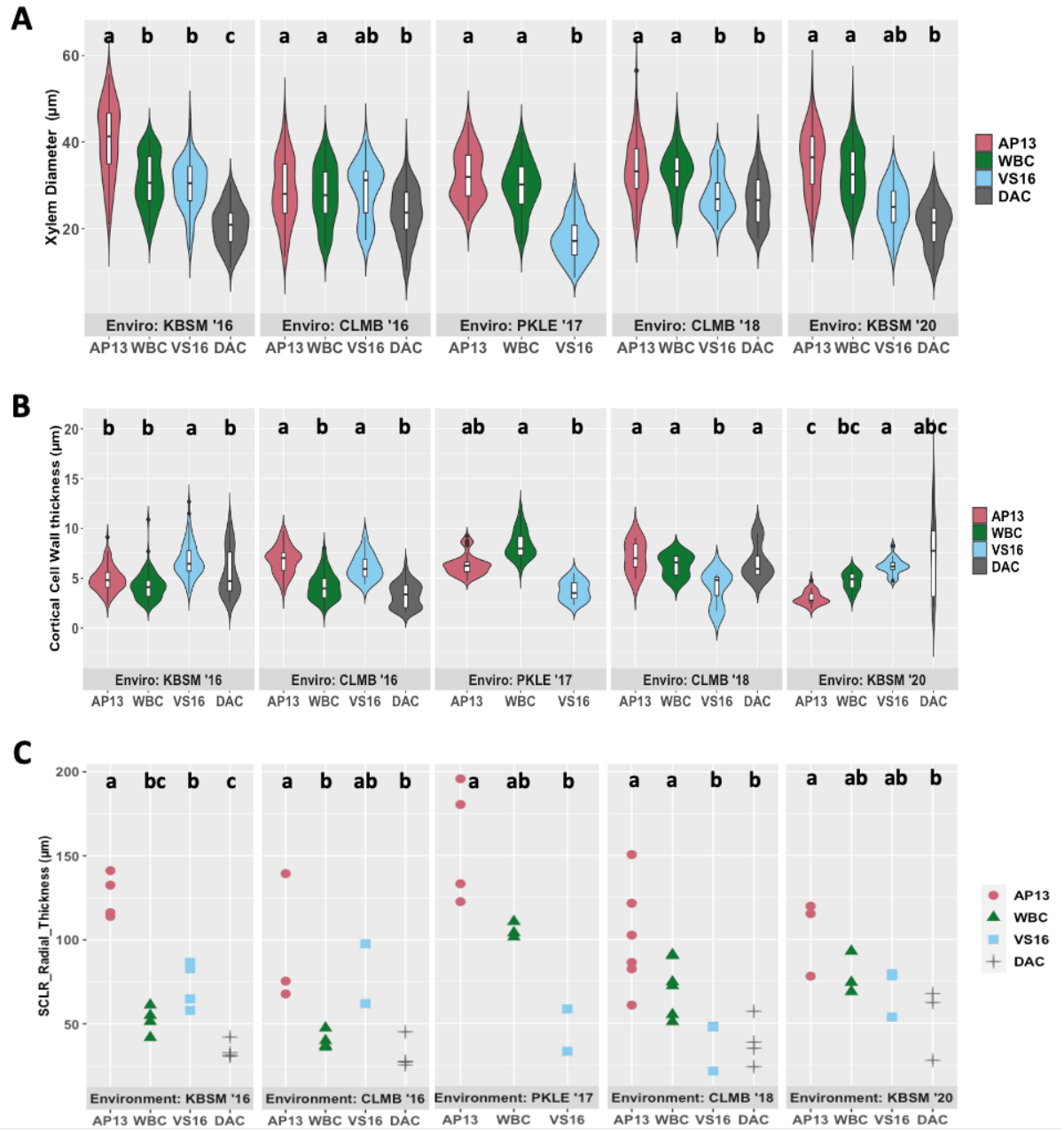

Figure 2.3. Anatomical variation of four genotypes across environments. (A) Xylem diameter shows consistent trend of ranks across sites with the lowlands largest, with VS16 in CLMB larger than WBC the one exception. (B) However, cortical cell wall thickness does not show a consistent ranking among genotypes and sites with each genotype ranking largest at least once. (C) SCLR radial thickness generally shows a consistent rank trend with AP13 always largest, though VS16 overtakes WBC in KBSM and CLMB '16. The shape of each violin reveals the distribution of values to be bimodal in xylem that represents the typical two size classes of vascular bundles most evident in AP13 PKLE '17 (B). Data consists of all cortical vascular bundle xylem diameters visible in cross section with no less than 25 xylem per section. Cortical cell walls were measured in ten cells per image, 3

images per individual, 2-4 individuals per genotype and site depending on plant survival. Averages of eight SCLR radial thickness measurements taken per genotype and site shown. Tukey groups at $p = 0.05$ applied after ANOVA within each site.

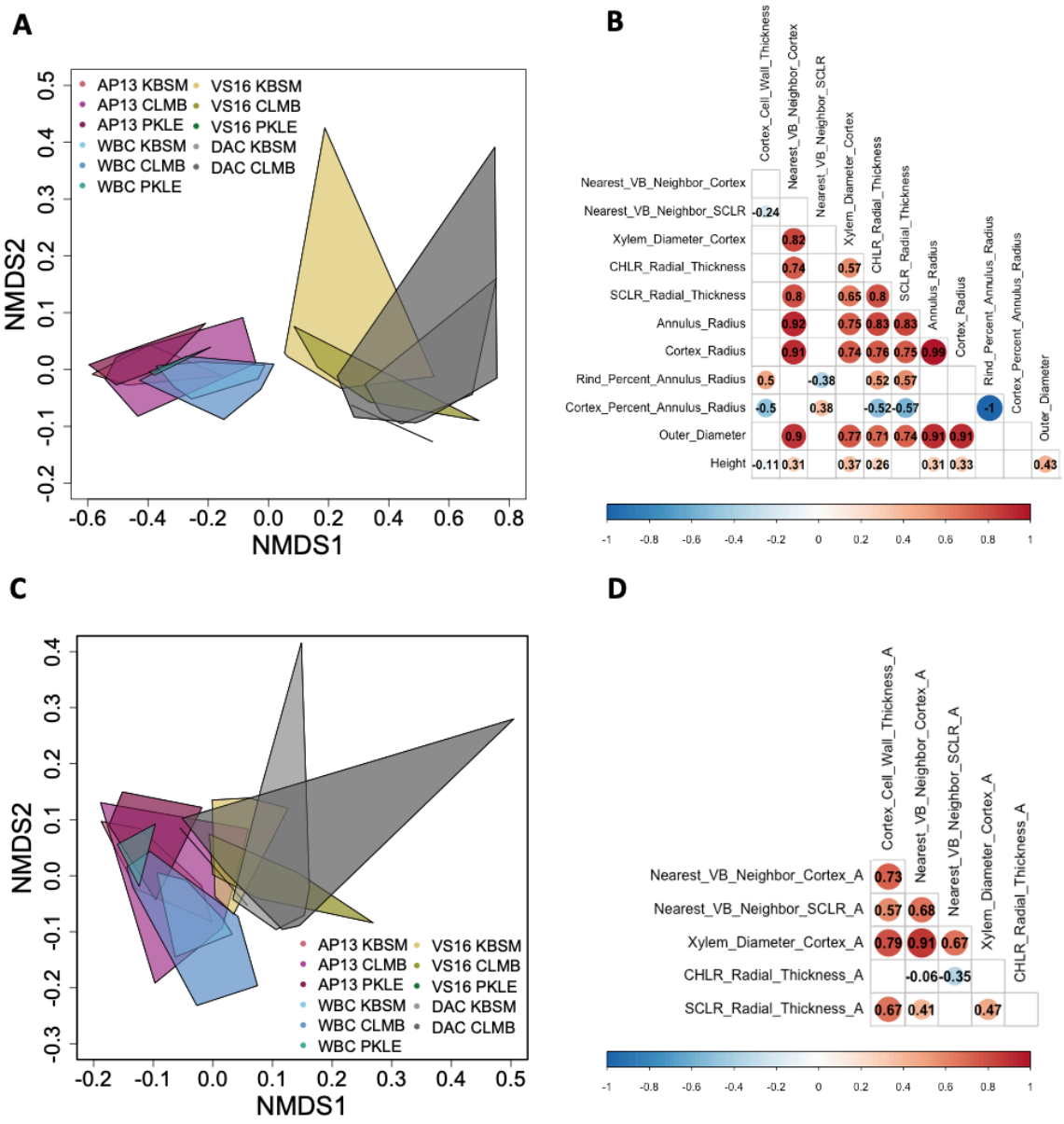

Figure 2.4. Internode anatomy phenes separate by ecotype in four genotypes across six environments with Non-Metric Multi-Dimensional Scaling (NMDS) and show numerous strong correlations. Ecotype dissimilarity remains after standardizing to annulus radius. Showing that significant variation exists in the other remaining traits that do not scale with Annulus radius. (A) Internode anatomy is dissimilar across ecotypes with substantial overlap of genotypes within ecotypes. (B) Many anatomical architecture traits are positively correlated, though most are minimally correlated with plant height. Cortical cell wall thickness shows weak correlations and only with rind and cortex percent anulus radius. (C) Scaled internode anatomy phenes to annulus radius show reduced but still distinct ecotype dissimilarity. (D) Positive correlations among traits, including cortical cell wall thickness, increase after standardizing to annulus radius (unique to each genotype replicate). This shows that cortical cell wall thickness lacks a broad relationship across genotypes and is actually specific to each genotype. Data shown was collected over six

environments with 3 sections analyzed from 2-6 individuals per genotype-environment. Refer to table 2.1 and Figures 2.1 and 2.2. Spearman rank correlations, only significant correlations shown (< 0.05.)

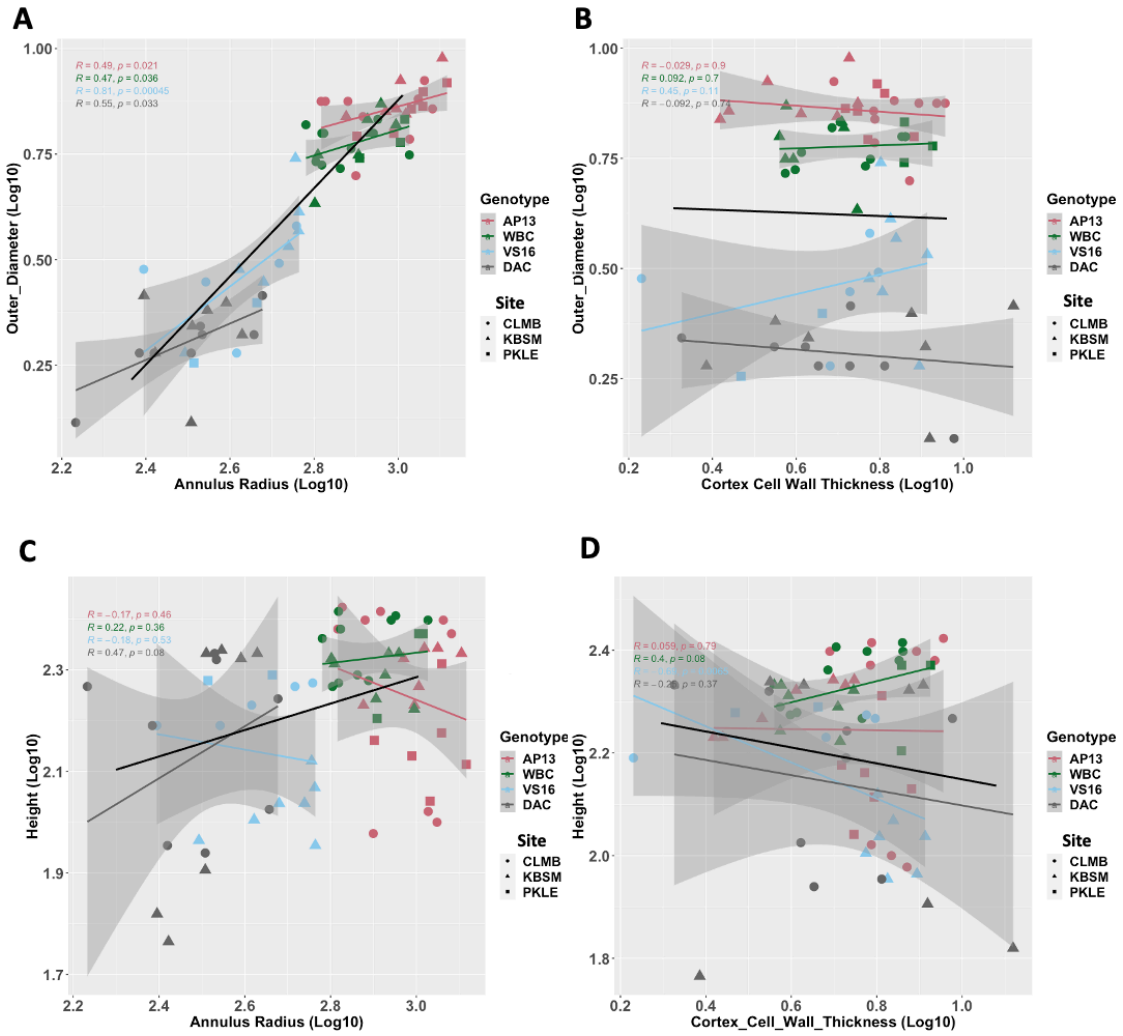

Figure 2.5. Allometry across sites and genotypes of internode anatomy phenes reveals different relationships between individual genotypes and combined data. The presence of multiple internode anatomy allometries across sites indicates phenotypic plasticity is a result of genotype x environment interactions observed as unique relationships within each genotypes. (A) Each color represents a single genotype with site denoted by shape. Single genotype slopes across sites show different allometric scaling observed as the slope of annulus radius and outer diameter. Lowlands are flatter than both uplands and the overall relationship for the combined genotypes appears to be allometric. The slope of the combined data indicates a potential for predictive power of annulus radius by outer diameter, though the individual genotypes vary from this scaling that reduces accuracy for single genotypes. (B) Annulus radius and height show positive and negative slopes for individual genotypes with an overall positive slope, indicating genotype specific anatomy phenes in response to site, presented as dissimilar allometry. (C) Cortical cell wall thickness and outer diameter show a flat slope indicating no scaling relationship across sites, while (D) shows similar variety in scaling allometries against height. A lack of allometry represents poor predictive power for cortical cell wall thickness by either outer diameter or height. All data was log10 transformed to control for magnitude effects.

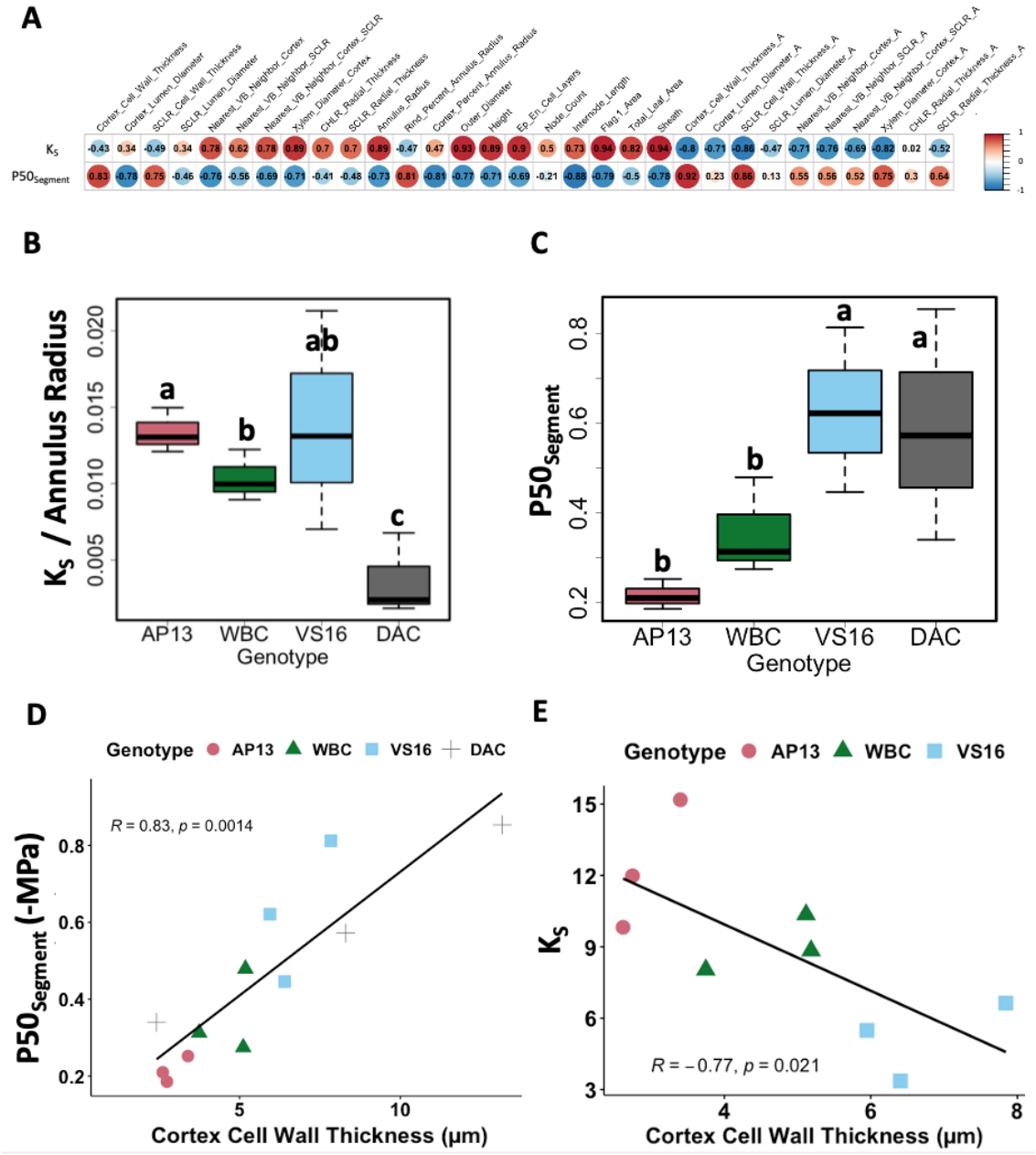

Figure 2.6. Internode anatomy correlates with maximum stem hydraulic conductivity (K_S) and resistance to hydraulic conductivity loss ($P50_{Segment}$). (A) Tiller size traits height, outer diameter, and annulus radius along with vascular traits xylem diameter of vascular bundles in the cortex and nearest neighbor distance to vascular bundles in the cortex are all highly significantly positively correlated with K_s. Fiber and cell wall traits are highly positively corelated with $P50_{Segment}$, (the pressure to induce 50% loss of conductivity in a 13 cm segment). Fiber traits include cortical cell wall thickness, sclerenchyma cell wall thickness, and rind % of annulus radius. (B)Though lowlands are largest in maximum stem hydraulic conductivity (Figure S2.7) , VS16 is statistically the same as lowlands and remains larger than DAC after scaling to annulus radius. (C)

Resistance to hydraulic conductivity loss in lower tiller segments varied significantly across four genotypes with the uplands (VS16 and DAC) more resistant than the lowlands (AP13 and WBC) at ($P<0.001$), the magnitude differences between genotypes and resistance are both mild. (D) Cortical cell wall thickness is positively correlated with resistance to hydraulic conductivity loss and is larger in the uplands. (E) Cortical cell wall thickness is negatively correlated with K_s with the uplands having significantly lower stem conductance than the lowlands. DAC removed from the plot due to very low conductance. Tukey groups at $p=0.05$ applied to B and C after ANOVA.

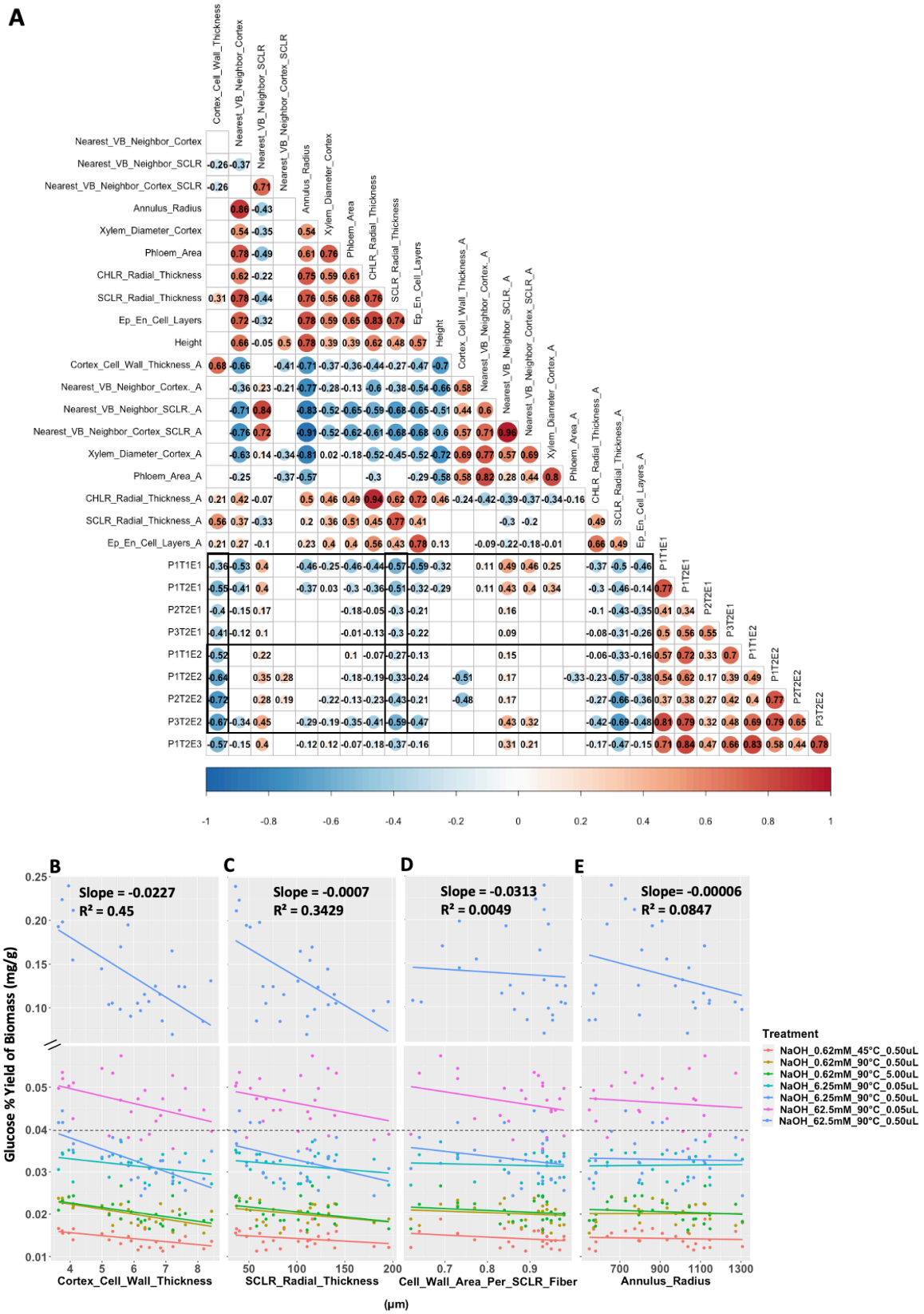
A
B
C
D
E
Slope = -0.0227
R² = 0.45
Slope = -0.0007
R² = 0.3429
Slope = -0.0313
R² = 0.0049
Slope= -0.00006
R² = 0.0847
Glucose % Yield of Biomass (mg/g)
Cortex_Cell_Wall_Thickness
SCLR_Radial_Thickness
Cell_Wall_Area_Per_SCLR_Fiber
Annulus_Radius
(µm)
Treatment
NaOH_0.62mM_45°C_0.50uL
NaOH_0.62mM_90°C_0.50uL
NaOH_0.62mM_90°C_5.00uL
NaOH_6.25mM_90°C_0.05uL
NaOH_6.25mM_90°C_0.50uL
NaOH_62.5mM_90°C_0.05uL
NaOH_62.5mM_90°C_0.50uL

Figure 2.7. Internode anatomy correlations with cell wall digestibility. (A) (B-E) Blue and pink treatments overlap. Small end of CWT blue overlaps with large CWT in pink. Similar yields are possible with less harsh (less expensive) treatment at 4 microns CWT as harsher treatment at 8 CWT. Similar trends observed in SCLR, and less but still present in CW per Fiber cell. Absent in annulus radius. (F-I) harshest treatment with much higher yield, shows the pattern that CWT and SCLR radial thickness both negatively correlate with yield, cell wall / fiber does not, and annulus radius does. A,B,E, and F support the hypothesis that numerous thick-walled cells reduce digestion yield efficiency mg/g. N= 26

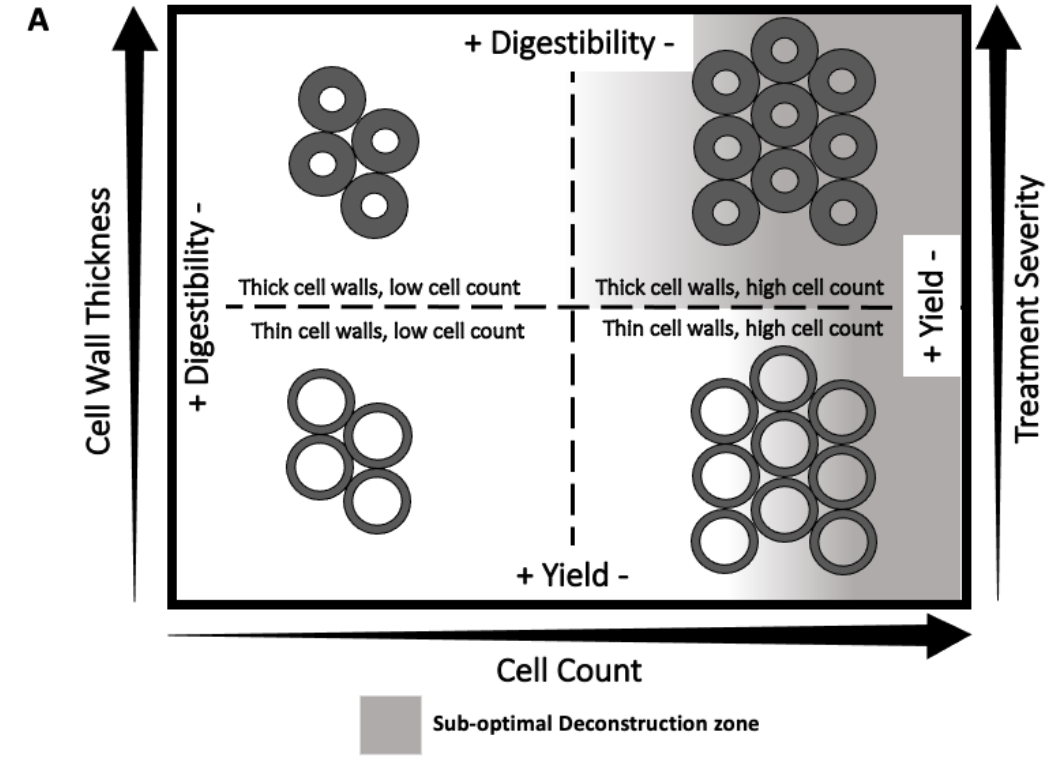
A
+ Digestibility -
+ Digestibility -
Cell Wall Thickness
Thick cell walls, low cell count
Thin cell walls, low cell count
Thick cell walls, high cell count
Thin cell walls, high cell count
+ Yield -
+ Yield -
Treatment Severity
Cell Count
Sub-optimal Deconstruction zone

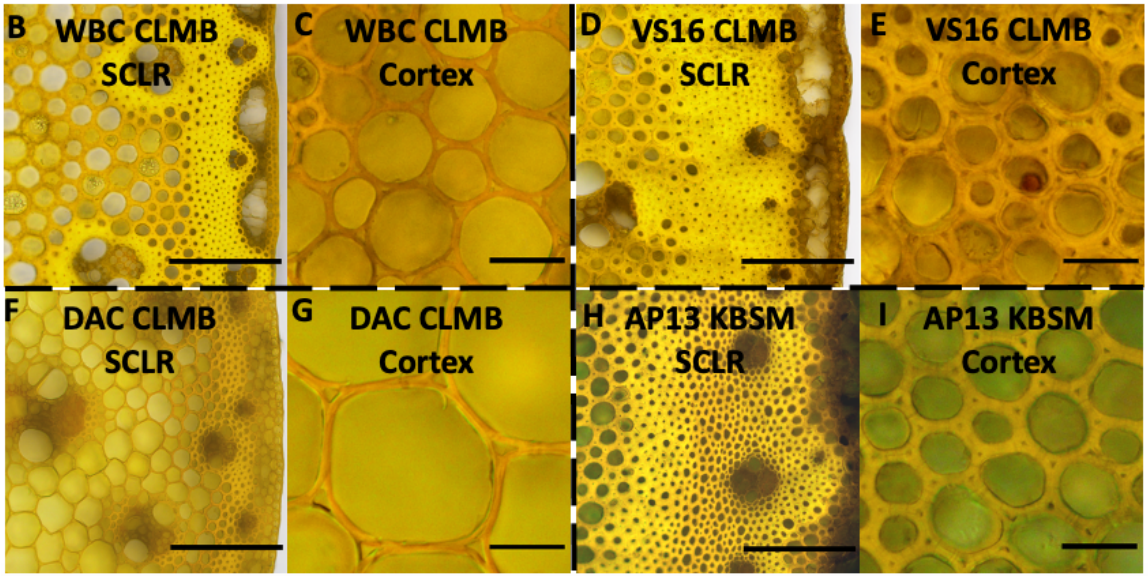
B WBC CLMB SCLR
C WBC CLMB Cortex
D VS16 CLMB SCLR
E VS16 CLMB Cortex
F DAC CLMB SCLR
G DAC CLMB Cortex
H AP13 KBSM SCLR
I AP13 KBSM Cortex

Figure 2.8. Model relating cell wall thickness and cell count with digestibility. Cortical cell wall thickness and sclerenchyma radial thickness traits are negatively correlated with glucose and pentose % yield from digestion across treatments, increasing this relationship with harsher digestion parameters(Figure 2.7, S2.15). (A) This model summarizes these relationships to show that thin walls and low cell count are the easiest samples to digest and produce the highest yield per treatment. (A – I) are organized to reflect the quadrants of the model in (A). Representative images of low cell count, (thin sclerenchyma radial thickness), and thicker cortical walls with are shown in (B and C). High cell count, (thick sclerenchyma radial thickness), and thicker cortical walls with are shown in (D and E). Low cell count, (thin sclerenchyma radial thickness), and thin cortical walls with are shown in (F and G). High cell count, (thick sclerenchyma radial thickness), and thinner cortical walls with are shown in (H and I). Considering this data together produces a guide for trade-offs in internode anatomy and digestibility. The thick walled and thick sclerenchyma radius plants may have more stored carbon in their thicker and more abundant cell walls, but it is not efficiently digested and therefore is not an attractive anatomy. Furthermore, thicker walls and thicker sclerenchyma radii reduce glucose and pentose % yields during digestion. Therefore, the optimal internode anatomy in terms of high efficiency is an anatomy comprised of thin cortical cells (4 μm) and thin sclerenchyma radial thickness. Ranks for favorable anatomy in terms of digestion efficiency is (F and G), followed by (B and C), then (H and I), and lastly (D and E).

2.20 References

Al-maskri, Ahmad, et al. (2014), 'Structural Features of Some Wheat (Triticum Spp.) Landraces/Cultivars Under Drought and Salt Stress', *Arid Land Research and Management,* 28 (3), 355-70.

Alder, NN, et al. (1997), 'Use of centrifugal force in the study of xylem cavitation', *Journal of experimental botany,* 48 (3), 665-74.

Arantes, Valdeir and Saddler, Jack N (2010), 'Access to cellulose limits the efficiency of enzymatic hydrolysis: the role of amorphogenesis', *Biotechnology for biofuels,* 3 (1), 1-11.

Aschan, Guido and Pfanz, Hardy (2003), 'Non-foliar photosynthesis – a strategy of additional carbon acquisition', *Flora - Morphology, Distribution, Functional Ecology of Plants,* 198 (2), 81-97.

Cao, Kun-Fang, et al. (2012), 'The maximum height of grasses is determined by roots', *Ecology Letters,* 15 (7), 666-72.

Casler, Michael D, et al. (2011), 'The switchgrass genome: tools and strategies', *The Plant Genome,* 4 (3), 273-82.

Casler, Michael D, et al. (2007), 'Latitudinal and longitudinal adaptation of switchgrass populations', *Crop Science,* 47 (6), 2249-60.

Cernusak, Lucas A. and Cheesman, Alexander W. (2015), 'The benefits of recycling: how photosynthetic bark can increase drought tolerance', *New Phytologist,* 208 (4), 995-97.

Chen, Weile, et al. (2021), 'The genetic basis of the root economics spectrum in a perennial grass', *Proceedings of the National Academy of Sciences,* 118 (47).

Chundawat, Shishir PS, et al. (2011), 'Multi-scale visualization and characterization of lignocellulosic plant cell wall deconstruction during thermochemical pretreatment', *Energy & Environmental Science,* 4 (3), 973-84.

Cochard, Hervé, Ridolfi, M, and Dreyer, Erwin (1996), 'Responses to water stress in an ABA-unresponsive hybrid poplar (Populus koreana× trichocarpa cv. Peace) II. Hydraulic properties and xylem embolism', *New Phytologist,* 134 (3), 455-61.

Davis, Stephen D, et al. (2002), 'Shoot dieback during prolonged drought in Ceanothus (Rhamnaceae) chaparral of California: a possible case of hydraulic failure', *American Journal of Botany,* 89 (5), 820-28.

DeMartini, Jaclyn D, et al. (2013), 'Investigating plant cell wall components that affect biomass recalcitrance in poplar and switchgrass', *Energy & Environmental Science,* 6 (3), 898-909.

Des Marais, David L, Hernandez, Kyle M, and Juenger, Thomas E (2013), 'Genotype-by-environment interaction and plasticity: exploring genomic responses of plants to the abiotic environment', *Annual Review of Ecology, Evolution, and Systematics,* 44, 5-29.

Ding, Shi-You, et al. (2012), 'How Does Plant Cell Wall Nanoscale Architecture Correlate with Enzymatic Digestibility?', *Science,* 338 (6110), 1055-60.

Donohoe, Bryon S and Resch, Michael G (2015), 'Mechanisms employed by cellulase systems to gain access through the complex architecture of lignocellulosic substrates', *Current opinion in chemical biology,* 29, 100-07.

Gleason, Sean M, et al. (2017), 'Embolized stems recover overnight in Zea mays: The role of soil water, root pressure, and nighttime transpiration', *Frontiers in Plant Science,* 8, 662.

Grabber, John H (2005), 'How do lignin composition, structure, and cross-linking affect degradability? A review of cell wall model studies'.

Hacke, Uwe G., et al. (2015), 'The standard centrifuge method accurately measures vulnerability curves of long-vesselled olive stems', *New Phytologist,* 205 (1), 116-27.

Hall, Mélanie, et al. (2011), 'Biological pretreatment of cellulose: Enhancing enzymatic hydrolysis rate using cellulose-binding domains from cellulases', *Bioresource technology,* 102 (3), 2910-15.

Hereford, Joe (2009), 'A quantitative survey of local adaptation and fitness trade-offs', *The American Naturalist,* 173 (5), 579-88.

Himmel, Michael E, et al. (2007), 'Biomass recalcitrance: engineering plants and enzymes for biofuels production', *science,* 315 (5813), 804-07.

HOLLOWAY-PHILLIPS, MEISHA-MARIKA and Brodribb, Timothy J (2011), 'Minimum hydraulic safety leads to maximum water-use efficiency in a forage grass', *Plant, cell & environment,* 34 (2), 302-13.

Jacobsen, Anna (2011), *Standard centrifuge method for the determination of xylem vulnerability to cavitation*.

Lens, Frederic, et al. (2016), 'Herbaceous angiosperms are not more vulnerable to drought-induced embolism than angiosperm trees', *Plant Physiology*.

Li, Guotian, et al. (2018), 'Overexpression of a rice BAHD acyltransferase gene in switchgrass (Panicum virgatum L.) enhances saccharification', *BMC biotechnology,* 18 (1), 1-10.

Lo Gullo, MA, et al. (2004), 'Hydraulic architecture of plants of Helianthus annuus L. cv. Margot: evidence for plant segmentation in herbs', *Journal of Experimental Botany,* 55 (402), 1549-56.

Lovell, John T, et al. (2016), 'Promises and challenges of eco-physiological genomics in the field: tests of drought responses in switchgrass', *Plant Physiology,* 172 (2), 734-48.

Lovell, John T., et al. (2021), 'Genomic mechanisms of climate adaptation in polyploid bioenergy switchgrass', *Nature,* 590 (7846), 438-44.

Lowry, David B (2012), 'Local adaptation in the model plant', *New Phytologist,* 194 (4), 888-90.

Lowry, David B, et al. (2014), 'Adaptations between ecotypes and along environmental gradients in Panicum virgatum', *The American Naturalist,* 183 (5), 682-92.

Lowry, David B, et al. (2015), 'QTLs for biomass and developmental traits in switchgrass (Panicum virgatum)', *BioEnergy research,* 8 (4), 1856-67.

Lowry, David B, et al. (2019), 'QTL× environment interactions underlie adaptive divergence in switchgrass across a large latitudinal gradient', *Proceedings of the National Academy of Sciences,* 116 (26), 12933-41.

Lynch, Jonathan P (2011), 'Root phenes for enhanced soil exploration and phosphorus acquisition: tools for future crops', *Plant physiology,* 156 (3), 1041-49.

Mascaro, Joseph, et al. (2013), 'Is logarithmic transformation necessary in allometry? Ten, one-hundred, one-thousand-times yes', *Biological Journal of the Linnean Society,* 111 (1), 230-33.

McCulloh, Katherine A., et al. (2019), 'A dynamic yet vulnerable pipeline: Integration and coordination of hydraulic traits across whole plants', *Plant, Cell & Environment,* 42 (10), 2789-807.

McCully, ME, Huang, CX, and Ling, LEC (1998), 'Daily embolism and refilling of xylem vessels in the roots of field-grown maize', *The New Phytologist,* 138 (2), 327-42.

Meikle, Peter J, et al. (1994), 'A (1→ 3, 1→ 4)-β-glucan-specific monoclonal antibody and its use in the quantitation and immunocytochemical location of (1→ 3, 1→ 4)-β-glucans', *The Plant Journal,* 5 (1), 1-9.

Milano, Elizabeth R, Lowry, David B, and Juenger, Thomas E (2016), 'The genetic basis of upland/lowland ecotype divergence in switchgrass (Panicum virgatum)', *G3: Genes, Genomes, Genetics,* 6 (11), 3561-70.

Mitra, Prajakta Pradhan and Loqué, Dominique (2014), 'Histochemical staining of Arabidopsis thaliana secondary cell wall elements', *Journal of visualized experiments: JoVE,* (87).

Neufeld, Howard S, et al. (1992), 'Genotypic variability in vulnerability of leaf xylem to cavitation in water-stressed and well-irrigated sugarcane', *Plant physiology,* 100 (2), 1020-28.

Nunes, Tiago DG, Zhang, Dan, and Raissig, Michael T (2020), 'Form, development and function of grass stomata', *The Plant Journal,* 101 (4), 780-99.

Price, David L. and Casler, Michael D. (2014), 'Predictive Relationships between Plant Morphological Traits and Biomass Yield in Switchgrass', *Crop Science,* 54 (2), 637-45.

Rao, Xiaolan, et al. (2019), 'Gene regulatory networks for lignin biosynthesis in switchgrass (Panicum virgatum)', *Plant biotechnology journal,* 17 (3), 580-93.

Saha, Malay C, Bhandhari, Hem S, and Bouton, Joseph H (2013), *Bioenergy Feedstocks: Breeding and Genetics* (John Wiley & Sons).

Sanderson, Matt A, et al. (2006), 'Switchgrass as a biofuels feedstock in the USA', *Canadian Journal of Plant Science,* 86 (Special Issue), 1315-25.

Sanford, Gregg R, et al. (2017), 'Biomass production a stronger driver of cellulosic ethanol yield than biomass quality', *Agronomy Journal,* 109 (5).

Sarath, Gautam, et al. (2011), 'Ethanol yields and cell wall properties in divergently bred switchgrass genotypes', *Bioresource technology,* 102 (20), 9579-85.

Schindelin, Johannes, et al. (2012), 'Fiji: an open-source platform for biological-image analysis', *Nature Methods,* 9, 676.

Schlichting, Carl D (1986), 'The evolution of phenotypic plasticity in plants', *Annual review of ecology and systematics,* 17 (1), 667-93.

Schneider, Hannah M, et al. (2021), 'Multiseriate cortical sclerenchyma enhance root penetration in compacted soils', *Proceedings of the National Academy of Sciences,* 118 (6).

Scoffoni, Christine, et al. (2017), 'Leaf vein xylem conduit diameter influences susceptibility to embolism and hydraulic decline', *New Phytologist,* 213 (3), 1076-92.

Serba, Desalegn D, et al. (2016), 'Cell wall composition and underlying QTL in an F 1 pseudo-testcross population of switchgrass', *BioEnergy research,* 9 (3), 836-50.

Shen, Hui, et al. (2009), 'A bioinformatic analysis of NAC genes for plant cell wall development in relation to lignocellulosic bioenergy production', *BioEnergy Research,* 2 (4), 217.

Stiller, Volker, Lafitte, H Renee, and Sperry, John S (2003), 'Hydraulic properties of rice and the response of gas exchange to water stress', *Plant Physiology,* 132 (3), 1698-706.

Taiz, Lincoln, et al. (2015), *Plant physiology and development* (Sinauer Associates Incorporated).

Trabucco, Gina M., et al. (2013), 'Functional characterization of cinnamyl alcohol dehydrogenase and caffeic acid O-methyltransferase in Brachypodium distachyon', *BMC Biotechnology,* 13 (1), 61.

Tu, Yi, et al. (2010), 'Functional analyses of caffeic acid O-methyltransferase and cinnamoyl-CoA-reductase genes from perennial ryegrass (Lolium perenne)', *The Plant Cell,* 22 (10), 3357-73.

Vega-Sanchez, Miguel, et al. (2013), 'Abundance of mixed linkage glucan in mature tissues and secondary cell walls of grasses', *Plant signaling & behavior,* 8 (2), e23143.

Vilagrosa, A, et al. (2003), 'Cavitation, stomatal conductance, and leaf dieback in seedlings of two co-occurring Mediterranean shrubs during an intense drought', *Journal of experimental botany,* 54 (390), 2015-24.

Weiner, Jacob (2004), 'Allocation, plasticity and allometry in plants', *Perspectives in Plant Ecology, Evolution and Systematics,* 6 (4), 207-15.

Wilson, JR and Mertens, DR (1995), 'Cell wall accessibility and cell structure limitations to microbial digestion of forage', *Crop Science,* 35 (1), 251-59.

Wullschleger, Stan D, et al. (2010), 'Biomass production in switchgrass across the United States: database description and determinants of yield', *Agronomy Journal,* 102 (4), 1158-68.

Chapter 3: Genetic Architecture and Candidate Gene Identification of Switchgrass Internode Anatomy Phenes

David J. Thomas[1], Jason Bonnette[2], Li Zhang[2], Alice S. McCaskill[1], Phuong M. Phi[1] , Felix Fritschi[3] , David Lowry[4],Thomas Juenger[2], Laura E. Bartley[5]

1- University of Oklahoma
2- University of Texas, Austin
3- University of Missouri, Columbia
4- Michigan State University
5- Washington State University

Publication Status: This chapter is in preparation for submission to New Phytologist

Authors Contributions: DT, LEB, and TJ conceived of and designed the study. DT helped with sample harvest, prepared samples, and conducted the analyses. DT and LEB wrote the manuscript. JB, FF, and TJ directed field collections. FF coordinated the harvest at CLMB and provided project insight. LZ advised on QTL analyses. AM and PP prepared, imaged, and analyzed internode samples, and commented on manuscript.

Acknowledgements

Field technicians in CLMB helped harvest plants. Collaborator datasets generated through the switchgrass common gardens were used to expand the analysis of the internode anatomy data described herein. Biomass yield and phenology traits measured by field technicians at the Columbia, MO site were incorporated into the correlation and Manhattan QTL plots. High school students Ash and Amiya prepared and imaged internode samples and provided protocol insight.

Funding sources

NSF grant (IOS 1444533)
DOE grant (DE-SC0014156, DE-SC0021126)

3.1 Abstract

Switchgrass (*Panicum virgatum* L.*)* is a perennial C4 bunch grass that is a promising feedstock for production of lignocellulosic biofuels. Characterizations of functional traits that modulate switchgrass biomass yields and those that optimize conversion efficiency are needed to improve the production of switchgrass biomass into transportation fuels. However, understanding of the genetic control for these traits in grasses is far from complete. Internode anatomy phenes of switchgrass may have implications for biomass yield, resistance to drought-induced xylem failure, biofuel conversion efficiency, and photosynthesis. Internode cross section analysis in an outbred, four-way F2 mapping population revealed numerous significant correlations among anatomy traits and mild correlations with end of season tiller height and biomass yield. Principal component analysis shows the extensive variability of the F0 and F1 generations with the variation of the first (41.9%) and second (13.4%) dimensions with the first primarily represented by internode size traits (cortical vascular bundle nearest neighbor distance, annulus radius, outer diameter). Quantitative trait loci (QTL) analysis and anatomical measurements to the F_2 population identified eight significant QTL (LOD alpha =0.1) for six traits: cortical cell wall thickness, cortex radius, chlorenchyma radius, annulus area, epidermis cell count, and cortex-to-rind ratio. Cell division, cell cycle regulation, secondary cell wall, and NAC family regulatory transcription factors were located within the significant QTL intervals. Phylogenetic reconstruction of NAC genes comprised of 304 switchgrass, 95 *Arabidopsis thaliana*, and 142 NACs in *Oryza sativa* revealed several grass expanded NAC subgroups and homologous genes of NAC located within QTL intervals. The identification of significant loci informs gene selection for functional

characterization to modify switchgrass cellular architecture toward improving biomass yield and conversion efficiency into biofuel.

3.2 Introduction

Lignocellulosic biofuels produced from plant biomass sources are a critical element of current and future renewable energy strategies (Carriquiry et al., 2011). Second generation biofuels produced from plant biomass derive their carbon from contemporary sources of atmospheric CO2 and represent a viable alternative to fossil fuels. Perennial grasses such as switchgrass, described as a high-potential energy crop fit for biofuel production (Wright, 2007), can provide relatively high lignocellulosic biomass yield across its distribution range (Wullschleger et al., 2010). Broad species adaptation from Canada to Mexico also provides genotypic and phenotypic diversity should be utilized to fit the needs of site-specific renewable energy strategies (Casler et al., 2007; Vogel et al., 2005). The morphological diversity of switchgrass in terms of anatomical variation among ecotypes and across growing environments suggests functional diversity driven by an underlying genetic diversity (Thomas et al., in prep.).

Numerous efforts to improve the viability of switchgrass as a biofuel feedstock have focused on biomass production as a primary breeding target (Sanderson et al., 2006; Schmer et al., 2008). As a fine scale feature of biomass, cell wall composition is known to vary among different cell types, primary vs. secondary cell walls, and secondary cell wall thickness (Vogel, 2008). Switchgrass conversion efficiency is largely a factor of tissue characteristics, which is directly impacted by internode anatomy (DeMartini et al., 2013). However, the relationship of anatomical variation present in switchgrass biomass with biomass conversion efficiency remains underrepresented in the literature. Recently, two quantitative trait locus (QTL) studies have explored biomass yield and the root economic spectrum in switchgrass (Chen et al., 2021; Lowry et al., 2019). Though multiple

significant QTL and connections were established in both studies, neither discuss or analyze the anatomy of internodes, especially in the context of biomass conversion efficiency or biomass quality. Recent evidence shows that internode anatomy is positively correlated with height, as well as establishes a connection between internode anatomy and glucose yield under a range of digestion treatment severity (Thomas et al., in prep). Positive Spearman correlations with height in four genotypes (lowlands AP13, WBC and uplands VS16,DAC) include outer diameter (0.43), cortex radius (0.33), as well as xylem diameter (0.37), while cortical cell wall thickness was found to negatively correlate (0.72) with glucose yield after biomass digestion (Thomas et al., in prep). These results indicate significant variation across genotypes and relationships between traits with biomass yield and deconstruction. Therefore, an investigation into the genetic basis for switchgrass internode anatomy variation is a crucial component to increasing our understanding of switchgrass biomass as a viable biofuel feedstock.

Because switchgrass is essentially undomesticated, rapid advancements in biomass quality and yield may be possible with emerging genomic resources and analyses. From a breeder's perspective, the main objective is to develop superior varieties that are suitable for economic production in commercial cropping systems (Brown & Caligari, 2008). High quality genomic resources are required to support the advance the pace of biomass improvement. The recent release of switchgrass genome version 5 and gene-trait associations described by (Lovell et al., 2021) provide a massive resource for breeders to further advance switchgrass for sustainable bioenergy production. Still, a genetic basis for switchgrass internode anatomy that is lacking in current literature will increase our understanding towards switchgrass biomass improvement.

Multiple anatomical traits within the internode play crucial roles in biomass production that may indirectly lead to differences in biomass quality for biofuel production. Microscopic analysis of internode cross-sections allows for measurement of numerous anatomical traits including internode annulus radius, cortex radius, and rind or cortex percent of annulus radius that may directly impact biomass yield and quality per plant. Cells with thick secondary cell walls represent a substantial carbon sink and, in most grasses, provide a dominant fraction of lignin, cellulose, and hemicellulose in biomass (Chen et al., 2002; Jung & Casler, 2006a, 2006b), their abundance and cell wall thickness ultimately influence biomass yield. Another aspect of the internode anatomy that influences biomass yield is photosynthesis and resistance to water stress. Stem photosynthesis is primarily located in the chlorenchyma which provides a source of non-foliar photosynthesis (Aschan & Pfanz, 2003) and is more abundant in wheat cultivars found to be most tolerant to drought conditions (Al-maskri et al., 2014). Additionally, there is some evidence that non-foliar photosynthesis is beneficial to survive leaf dieback due to severe drought effects (Cernusak & Cheesman, 2015). Furthermore, metaxylem diameter in vascular bundles dictates maximum conductance and vulnerability to embolism under water stress(Giordano et al., 1978; Lewis & Boose, 1995). Characterizing and establishing a genetic basis for these internode anatomy traits and the extent of their variation within a mapping population is an important step towards enhancing switchgrass biomass for biofuel production.

Understanding the genetic regulation of internode anatomy traits will lead to a better understanding of biomass conversion efficiency, echoing advancements made by applying this approach towards cell wall composition (Bouton, 2007). The organization of

cell types within a plant is a result of several processes within plant development and morphogenesis. Internode anatomy begins with meristematic tissues which are the site of cell division and cell differentiation, followed by cell elongation and secondary cell wall accumulation (Taiz et al., 2015). In turn, the CLAVATA3 (CLV3) peptide within the CLAVATA-WUSCHEL signaling pathway coordinates stem cell proliferation and differentiation (Somssich et al., 2016) Cell fate is determined either extrinsically or intrinsically according to molecular components that polarize in the mother cell prior to division (intrinsic), or through interactions with other neighboring cells (extrinsic) that cause divergence (Ten Hove & Heidstra, 2008). Grass stems elongate as a self-extruding cylinder from the shoot apical meristem (Harrison & Morris, 2018). Shoot apical meristems (SAM) produce leaf primordia and intercalary meristems in plants (Evans & Perez, 2004). As shoots produce new leaves and nodes very close to the SAM, the initial cell divisions that produce intercalary meristems occur just above the site of leaf initiation ((Sharman 1942, 1945; Sharman 1945; Kaufman 1959; Kaufman et al. 1965; Fisher and French 1976). In *Brachypodium distachyon,* BdERECTA is highly expressed in the nascent vascular bundles in shoot apex parenchyma near the SAM and is a negative regulator of vascular bundle number.(Sakai et al., 2021) Furthermore, BdERECTA was shown to be pleiotropic and has effects on hormone metabolism, lignin content, and mutants show a thicker annulus radius. It is possible that similar regulation is conserved in switchgrass and is an exciting prospect to explore in the future.

Plant cell division exhibits a plant cell specific structure that serves as a scaffold for a new cell wall during cell division called the phragmoplast. The orientation of the phragmoplast is tightly controlled with action of the preprophase band and determines the

plane of cell division to be either anticlinal or periclinal. Anticlinal division occurs when the phragmoplast forms perpendicular to the axis of the organ with periclinal division having a phragmoplast that form parallel to the axis. In rice, periclinal cell division were upregulated in rice *nal1* (Narrow leaf-1) which may interact with the action of the cortical preprophase band to produce mutants that have a mature phenotype of a thicker annulus radius but shorter overall height (Jiang et al., 2015). Periclinal cell division increase stem width with the two daughter cells horizontal to each other, while anticlinal division leads to daughter cells that are vertically stacked on each other. In this way, the dynamics that control the division plane produce the final abundance of cells in cross section.

The timing and location of proliferative cell divisions in coordination with expansion and differentiation produce the entire plant body (Rasmussen & Bellinger, 2018). Considering these aspects together produces the final organization, abundance, and proximity of the numerous cell types found within vegetative and reproductive plant structures. At a finer scale, secondary cell wall biosynthesis is regulated by several different factors that belong to several transcription factors families that include NACs (NAC (*NAM (NO APICAL MERISTEM), ATAF (ARABIDOPSIS THALIANA ACTIVATION FACTOR), and CUC2* (CUP-SHAPED COTYLEDON 2), growth regulation factors (GRF), and MYBs. Establishing a connection with these factors and switchgrass internode anatomy is imperative and relies largely on functional characterizations of genes and phylogenetic resources that identify homologs across species.

The NAC transcription factor family is comprised of proteins that encode one of the largest plant-specific transcription factors families with members involved in the regulation of vegetative growth, development, stress response signaling, and abscisic acid

and jasmonic acid signaling during biotic interactions (Yuan et al., 2019). The NAC protein family is defined by an N-terminal domain that mediates DNA binding (Olsen et al., 2005). A recent analysis of the Phytozome v1.1 genome of switchgrass identified 251 NACs in 19 subgroups (Yan et al., 2017). However, recent advancements in genomic resources warrant a phylogenetic reconstruction of the NAC transcription factors to explore sequence similarities across switchgrass, rice, and Arabidopsis in functional characterizations of this diverse family. The NAC family has a wide diversity of known and conserved functions and may provide key regulatory elements towards the enhancement of internode anatomy as a biofuel feedstock.

A subgroup of NAC transcription factors are top-level master switches specific for secondary cell wall biosynthesis (Rao & Dixon, 2018). Members of the master switch subgroup, secondary wall NACs (SWNs), bind to the secondary wall NAC binding element motif in target gene promoters involved in secondary cell wall thickening (Valdivia et al., 2013; Zhong et al., 2006; Zhong et al., 2011; Zhong et al., 2015). The SWN subgroup has orthologs across vascular plants, including in Arabidopsis, rice, and switchgrass (Zhong et al., 2011; Zhong et al., 2015). The SWN subgroup includes SND (SECONDARY WALL-ASSOCIATED NAC DOMAIN), NST (NAC SECONDARY WALL THICKENING PROMOTING FACTOR), VND (VASCULAR ASSOCIATED NAC DOMAIN PROTEIN), and VNI1 and VNI2 (VND-INTERACTING NAC). AtSND1 and AtNST1 redundantly regulate xylary fiber thickness by promoting SCW thickening in stem fibers; (Christiansen et al., 2011; Mitsuda et al., 2007; Rao & Dixon, 2018; Zhong et al., 2006; Zhong et al., 2007). A phylogenetic analysis of Arabidopsis and switchgrass SWNs showed that Arabidopsis SND1, NST1, and NST2 grouped with PvSWN1, PvSWN2A, and

PvSWN2B; AtVND7 with PvSWN3A and PvSWN3B; and AtVND1-6 group closely with PvSWN4-8 (Zhong et al., 2015).

Functional similarities are found in the Arabidopsis and grass transcription factors VND, VNI, and SND2 that regulate the secondary cell wall in vessels, fibers, and cortical cells. Arabidopsis thaliana genes AtVND6 and AtVND7 determine tracheary element differentiation by controlling both secondary wall thickening and programmed cell death in vessels (Ohashi-Ito et al., 2010; Yamaguchi et al., 2010). Overexpression in Arabidopsis of PvSWN4A, PvSWN5, or PvSWN7A showed ectopic deposition of secondary cell walls in cortical cells that attained a cell wall thickness up to 3-times thicker than that of the interfasicular fibers (Zhong et al., 2015). Rice NAC31, a member of the OsNAC7 subgroup that also includes rice and Arabidopsis VNDs, interacts with homeobox protein KNAT7 to regulate cell expansion and wall thickening (Wang et al., 2019). VND6 and VND7 are both negatively regulated by VNI2 (Yamaguchi et al., 2010). Overexpression of SND2 in Arabidopsis, an indirect target of SND1, produced fiber cell-specific increases in secondary cell wall thickness (Hussey et al., 2011). A yeast 1 -hybrid assay with Arabidopsis genes and promoters revealed 9 ANACs (Arabidopsis NACs) that bind to promoters of cell wall-associated genes (Taylor-Teeples et al., 2015). This study showed that 9 ANACs bind cell wall-associated gene promoters. One of these 9 ANACs, ANAC073/SND2, binds the promoter of ANAC030/VND7 and ANAC083/VNI2.

Here we identify regions on the chromosomes that are associated with internode anatomy traits that influence biomass quality and or yield. By utilizing a quantitative trait locus approach, we aimed to generate a list of candidate genes for further analysis towards biomass enhancement. Candidate genes of interest are those involved in secondary cell

wall regulation, cell cycle regulation, cell division regulation, stem development, and those that may contribute to enhancing internode anatomy and relative cell type abundance such as fiber cells and vascular bundles. Furthermore, the reconstruction of the NAC transcription factor family is provided in the context of elucidating homology of potential NAC candidate genes involved in the QTL analyses that may regulate the diversity of switchgrass internode anatomy we describe herein.

3.3 Results

3.4 Internode anatomy variation across F_2 mapping population at a single site

To characterize the variance of internode anatomy traits in the F2 population, we measured internode anatomy traits in over 400 individuals grown near Columbia, MO, described previously (Lowry, 2019). Twenty traits measured are described in Table 3.1 which includes the methods of measurement and if the traits values were represented as averages or are single measurements per individual plant. Measurement accuracy was favored over maximizing sample number which reduced measurement numbers of some cross sections measured in the mapping population.

Figure 3.1 shows representative measurements of the internode anatomy traits measured and labelled A - M. Internode anatomy traits are non-exclusively categorized by function and proposed impact on cell wall digestibility and hydraulic function. Internode architecture traits include measurements of the internode thickness and the radius of tissue types within the internode annulus (Figure 3.1, A-F). Fiber and cell wall associated traits include sclerenchyma cell file radius and radial cell count, as well as cortical cell wall thickness (Figure 3.1, C, D, J, and M). The third category of traits is vascular traits. Defined as traits associated with the vascular bundle, these include vascular bundle area traits and

distance between vascular bundles (Figure 3.1. G-L) . Additional traits outer and inner diameter, calculated traits: rind and cortex % of annulus radius, and vascular bundle fiber % area of vascular bundle are not shown in this Figure and are listed in Table 3.1.

Meaningful representation of trait variance in F2s is present for all traits and indicates a robust dataset for the detection of QTLs (Figure 3.2). Trait values across the F2 mapping population exceed the maximum, minimum, or both values for the grand parents of the cross except in only two traits shown in Figure 3.2. Data shown in the histograms are the 1.5x inner quartile range with outliers removed and thus are representative distributions. Conversely, a lack of variance after outliers removed would indicate poor allelic control over measured traits and low likelihood of QTL detection. Traits where the data exceeds F0 max and min are cortex radius (A), cortical cell wall thickness (B), chlorenchyma radius (C), and sclerenchyma radial cell count (E). Traits shown that exceed only the F0 minimum are metaxylem diameter (D) and annulus area (F). Additionally, the difference in distributions may also indicate different genetic regulation for these traits.

Table 3.2 provides internode anatomy trait summary statistics along with measurement counts. All traits except chlorenchyma radius are normally distributed as shown by minimal variance between mean and median across all other traits. Chlorenchyma radius is also the most variable (CV = 61.8) followed by sclerenchyma radius (CV = 29.9).

Principal components analysis of internode anatomy reveals the segregation of F0 genotypes from the F1 generation, distributed among the more variable F2 individuals. Principal components analysis of F2 internode anatomy shows that internode architecture traits dominate the first dimension (Figure 3.3 A). 41.9% of the overall variance is

explained by the first dimension when considering all generations together. Considering the three generations together reveals the wide variation among the F0s and the F1s in comparison to the F2s. Following the logic of isolating the F2 anatomical data for QTL analysis, the PCA were also run with the F0 and F1 excluded. This was done to understand the trends in the F2 data for relation to the QTL results and discussion of trait categorization. When isolating the F2s and analyzing them separately, the first dimension describes 45% of the variation and is represented mainly by variation of internode size traits and traits that highly correlate with internode size as seen in the loadings bar plot (Figure 3.3 B). The second component of the F2 PCA is mainly represented by variation in the sclerenchyma, cortical cell wall thickness, and traits associated with the sclerenchyma, explains 13.4% of the overall variance.

After scaling internode anatomy to annulus radius in the F2 population, vascular traits are responsible for the variance explained by the first dimension (Figure S3.1). The first dimension in both the three generation and isolated F2 PCAs explains 36% of the overall variance and is represented mainly by variation of vascular bundle traits as revealed by the loadings bar plot (Figure S3.2 B). The second dimension is mainly represented by variation in the cell type radii and sclerenchyma radial cell count which explains 20% of the overall variance. When considering F0, F1, and F2 together and in comparison to Figure 3.3 A show the wide variation is still present among F0s and F1s, though reduced slightly. This indicates strong variation of internode anatomy even after scaling to annulus radius.

Internode anatomy architecture traits are highly correlated and only mildly correlate with biomass yield and height at end of season (Figure 3.4). Internode architecture traits positively correlate with each other and show moderate correlation with tiller height and

biomass yield at end of season harvest. Fiber associated traits: cortical cell wall thickness, sclerenchyma (SCLR) radius, SCLR radial cell count, rind % annulus radius, and vascular bundle (VB) fiber area are positively correlated yet only SCLR traits show correlations above 0.20. Data was imputed using the MICE package in R. Imputed data was averaged from 5 independent runs using the cart method. Pearson correlations shown with only significant correlation coefficients displayed, all are significant at alpha = 0.05.

3.5 Quantitative trait loci (QTL) analysis of internode anatomy traits

Quantitative trait loci (QTL) analysis reveals regions of the chromosomes that may provide genetic basis for internode anatomy traits (Figure 3.5). For internode anatomy traits overall, we detected 8 significant ($P < 0.1$ with 1,000 permutations) and 13 suggestive ($0.1 < P < 0.25$ with 1,000 permutations) QTL. Confidence intervals (CIs) ranged from 4.56 to 74.66 centimorgans (cM) for all significant QTL, with an average interval of 20.20 cM. and average 851 genes within each interval (Table 3.3).. Though there are not common markers across the traits, the intervals overlap for many traits. 21 total QTL were found (7 Significant at alpha = 0.1, and 14 Suggestive at alpha = 0.25 in accordance to previously established parameters in a similar analysis (Chen et al., 2021). However, the rind and cortex percent of annulus radius are inverse of each other and map identically. Therefore, they are considered together as the rind : cortex proportion QTL that includes 1 significant and 1 suggestive QTL and accounted for in the total 21 QTL.

Significant peaks at 6N for annulus area and epidermis cell count suggest similar genetic basis, like chlorenchyma radius and the overall proportion of cortex and rind of the annulus radius at 5K region. Though the cortical cell wall thickness peak and associated interval between flanking markers is quite extensive, no other significant QTL for

internode anatomy overlap in this region on 2N (Figure 3.5 A). Significant and suggestive QTL displayed together reveal additional overlap among traits that provides support for shared genetic basis of control for these traits. This includes size coordinated traits: metaxylem diameter and annulus radius 4K and 6N, sclerenchyma radial cell count and rind-cortex proportion 5N; fiber and cell wall traits: vascular bundle fiber ratio and cortical cell wall thickness 3N; (Figure 3.5 B).

PCA component loadings of PCA coordinates with suggestive QTL shows internode architecture and vascular traits are dominant (Figure 3.3 B). The loadings show that 2nd dimension, which explains 13.4 % of the overall variance, is represented mainly by internode architecture trait and distance to nearest vascular bundles. The fourth dimension, which explains 3% of the overall variance, is represented primarily by the epidermis and endodermis cell count as well as the distance between vascular bundles. Suggestive anatomy QTL and Suggestive PCA peaks show overlap most predominately at 3N (Figure 3.5 C). PCA dimensions that are dominated by vascular bundle area and internode architecture traits when looking at the loadings overlap with peaks and QTLs of those same individual traits, substantiating each other.

Positively correlated fiber- and cell wall-associated traits show overlapping peaks that suggest a similar genetic basis for these similar traits (Figure 3.6 B). The significant QTL for cortical cell wall thickness has overlapping peaks from non-suggestive peaks at the 3N locus with SCLR radius (SCC = 0.41), SCLR radial cell count (SCC = 0.35), and VB fiber area (SCC = 0.34). The suggestive peak for rind % of annulus radius on 5N with SCLR radial cell count (SCC = 0.48), However, the SCLR radial cell count suggestive peak at 1N, and the significant rind : cortex proportion peak at 5K have no shared peaks

form other traits. Vascular associated traits show overlap with non-significant peaks across chromosome regions (Figure 3.6 C). Vascular bundle fiber area overlaps with vascular bundle area and metaxylem diameter, and phloem area at the 1N and 2N regions, which indicates vascular bundle size may be regulated by genes in these regions. The significant peak for epidermis cell count at 6N has a smaller, non-significant peak for metaxylem diameter which is contrary to the low correlation between these two traits (0.14). Conversely, a significant peak for epidermis cell count shows greater peak overlap with a sub-suggestive chlorenchyma radius peak at 8K, suggestion a shared genetic basis in these correlated (0.52) traits. Nearest vascular bundle in the cortex does have a solitary peak at 3K, yet overlaps with Vascular bundle fiber area, vascular bundle area, and phloem area at 4N and again with phloem area at 6K. The lack of an overlapping peak at 4N with metaxylem diameter suggests that the 4N region may not regulate the entire vascular bundle in concert.

Biomass and phenology QTL intervals overlap with those of internode anatomy to suggest common genetic basis (Figure 3.7). Biomass and phenology traits with LOD scores above 5 show highly represented regions on 2K, 2N,3K, 3N, 5N, 9K, and 9N (Figure 3.7 A). Biomass and phenology traits with LOD scores below 5 reveal additional significant QTL within 4K, 5K, 6N, 7N regions, and additional suggestive peaks that overlap with internode anatomy peaks (Figure 3.7 B). Internode anatomy significant and suggestive QTL show extensive interval and peak overlap with biomass and phenology traits (Figure 3.7 C). Shared markers were not found among anatomy, biomass and phenology QTL but overlapping intervals were found between flanking markers on 2K, 2N, 3N, 5N, 7K, 7N, 8K, 9K, and 9N regions. EM50 has suggestive peaks overlap on 7K, 7N, 8K, with

chlorenchyma radius, epidermis cell count, and metaxylem diameter in the cortex significant and suggestive peaks. Rind-to-cortex overlap with GR100 and Gr50 at 5N. Biomass and cortical cell wall thickness overlap at 3N. Cortex radius and EM50 at 9K and 9N. Height to average panicle a[ex at end of season before harvest (height), kg of biomass at end of season harvest (biomass), Date when first emergent panicle observed (EM1), Date when 50% of tillers had emergent panicles (EM50), Date when 50% of tillers had panicles in anthesis (FL50), Date of first emergent tillers observed (GR1), Date when 50% of crown had emergent tillers (GR50), Date when 100% of crown had emergent tillers (GR100). All dates logged as Julian days.

3.6 QTL Intervals contain numerous genes of interest involved in grass stem development and cell cycle regulation and NAC transcription factors

The intervals between flanking markers at each QTL contain hundreds of genes that can be scrutinized according to the function of the trait each interval pertains to. Many traits are directly influenced by cell division and cell cycle regulation including annulus area, cortex radius, SCLR radius, SCLR radial cell count, CHLR radius, epidermis and endodermis cell count, and even the rind : cortex proportion. Genes present in each interval of significant and suggestive QTLs are shown in Table 3.4. Many genes involved in secondary cell wall (SCW) regulation are found within the intervals for several of the traits that show cell wall thickness variation that may contribute to variations in cell wall composition and cell wall digestibility (Thomas et al., in prep). Included in the SCW regulatory genes are NAC transcription factors. Additional categories of genes include grass stem development related, expansin related and hormone related. Regions that include cell division protein kinases and cell division control proteins also contain hormone

response genes, functionally substantiating the genetic basis of these regions due to the established connection of cell division and plant hormones. The ubiquity of SCW genes across all traits provides an example of the prevalence of cell wall regulation across cell types.

3.7 Phylogenetic reconstruction of NAC transcription factor family in switchgrass, rice, and Arabidopsis

Compared to the recent analysis of switchgrass NACs (Yan et al., 2017), we observed an increase of total putative PvNACs from 251 to 304. Our number includes 11 truncated NACs that are missing one or more NAC sub-domains but still possess significant NAC identity with other NACs in the protein sequence alignment. Four of the 15 NAC subgroups described previously in Yan 2017 and Ooka 2003, contain known cell wall regulatory switchgrass NACs (Table 5). In addition, the ATAF subgroup contains two ANACs that bind the promoter of cell wall gene promoters (Taylor-Teeples et al., 2015). Among the cell wall-related NACs, subgroups OsNAC7, NAC2, and ONAC003 are significantly expanded in switchgrass compared to rice beyond what is generally attributable to the whole genome duplication in tetraploid switchgrass. Subgroups ANAC011 and ONAC022 also show significant expansion in switchgrass over rice but are not cell wall related (Table 5). Overall, the NACs described in the phylogenetic reconstruction provides a reference for future functional characterizations exploring NAC regulation of internode anatomy (Figure S3.2).

Fourteen NACs were identified within intervals of significant QTL and two within suggestive QTL intervals that includes 5 that are involved in secondary cell wall regulation (Table 6). Of the significant QTL, three are found in the epidermis and endodermis cell

count QTLs. The interval of the epidermis and endodermis QTL contains the secondary wall NAC in switchgrass (PvSWN2B) with close homologs OsSND1, OsNST1, OsNST2 and Arabidopsis NST1 and NST2. Additionally, PvSWN4A is found within the annulus area suggestive QTL interval in the 9K region with close homologs OsVND1, OsVND2, and Arabidopsis VND2 and CWPB9. Of the significant QTL, five NACs were found within the cortical cell wall thickness interval in the 2N region but are not characterized. Secondary cell wall homolog (SCWH13) described in Yan 2017 is found in the 5K CHLR radius QTL with close SND3 and cell wall promoter binding (CWPB6) homologs in rice and Arabidopsis, respectively. SCWH9 was found in the interval for the suggestive QTL of SCLR radial cell count though no close homologs were found in the phylogenetic reconstruction.

3.8 Discussion

This work describes internode anatomical analysis in switchgrass to identify quantitative trait loci and candidate genes to provide a genetic basis for the widespread variation we observe. Traits were selected based on function and level of internode description they provide. This analysis produced a list of QTLs that are significant according to the calculated values at alpha= 0.1, then there is a list of suggestive QTL that are between 0.1 and 0.25 significance threshold range. The third and final step of this project is to mine the intervals between neighboring markers that surround each QTL for genes of interest. This process produced a total list of over 17,872 genes within the total number of significant and suggestive QTL intervals, including extensive repeats where intervals overlap. Filtering by genes with functions of interest reduces this count to 697, and removing duplicates and triplicates reduces this number to 564 candidate genes.

candidate genes associated with these 20 traits that can be utilized to select genes for future studies, as well as to guide genetic marker assisted breeding efforts.

3.9 Internode Anatomy

Internode anatomy varies across F2s and reveals trends among anatomy, biomass yield, and plant phenology traits. Histograms show that the variance of F2s exceeds that of the F0s in many traits even when the outliers are removed. This means that through breeding, these internode anatomy traits of interest can be modified and outperform their parent counterparts. Furthermore, homo and hetero ecotype allelic combinations from the four grandparents produced the wide variation across the mapping population, which suggests that a genetic basis for these traits may be detected. Correlation plots of anatomy v. biomass, height, and other phenology traits show that anatomical traits are highly correlated with each other, but are only mildly associated with plant height, biomass yield, and various measures of phenology. In light of recent evidence, we can predict that the digestion of these individual plants will vary along by looking at several key traits identified to reduce digestibility. CWT, SCLR radius Thomas et al., in prep).

3.10 Quantitative Trait Locus (QTL) Mapping

Numerous overlapping QTL were located for internode anatomy traits across all nine chromosomes. Though this is not a functional characterization analysis and merely suggests connections of large chromosome regions with traits of interest, multiple QTLs of similar traits overlap and substantiate the relationship (Figure 3.5 and 3.6). Additionally, multiple regions contain significant QTL for biomass and flowering QTL that are similar but not identical to those described in (Lowry et al., 2019). Lowry et al. describes several significant biomass QTL identified by multiple site QTL analyses but are lacking at the

single CLMB site (Figure 3.7). These results suggests that QTL identified to significantly associate with biomass and or flowering traits across multiple sites are involved in multiple site response, or adverse environment response but are not identified to be involved in regulating biomass as a single site. Still, several fiber associated traits show peak similarity and suggest that a similar genetic basis may be present for these traits.

Suggestive QTL peaks overlap with numerous sub-suggestive peaks of correlated traits in same phenotypic or functional categories (Figure 3.6). Correlated traits show similar patterns of peak overlap (Figure 3.6 A). Significant and suggestive peaks overlap with peaks from highly correlated traits that do not reach the 0.25 alpha LOD score threshold. However, this indicates that not only are these traits highly correlated but suggests they may have a common genetic basis. Of the significant peaks for two traits with significant QTL, the peak for cortex radius on 2N has similar peaks underlying it from highly correlated traits: outer diameter (0.74), annulus radius (0.96), and inner diameter (0.67). An overlapping genetic basis for these traits is expected as these are all internode size traits. Cortex radius suggestive QTL also has similar, yet lower LOD score peaks on 9K with positively correlated (0.53) sclerenchyma radial thickness, and inner diameter (0.67). Additionally, several peaks are present that overlap with other non-significant loci, 1K: OD, ID,SCLR, and NVB Cortex; 4N: OD, ID,SCLR, annulus radius, and NVB Cortex; 5N: OD, Annulus radius, and ID: and a second peak on 9K with cortex radius, ID, and annulus radius. Considering the presence of multiple, low peaks at the same loci for multiple, positively correlated traits supports the notion that these regions of the chromosome may control these traits.

3.11 QTL interval genes of interest

Genes with regulatory functions that may influence internode anatomy including cell division and secondary cell wall biosynthesis are located within the intervals of seven internode anatomy QTL. Cell division protein kinases are located in SCLR radial cell count, CHLR radius, cortex radius, annulus area, and cortical cell wall thickness intervals and may contribute to the cell number and radius of these cell types. Grass stem development genes include several involved in cell elongation, lignin deposition, and internode patterning. Loss of function BRI1 mutants, a gene located in cortex radius QTL, showed disorganized internode cells and non-elongated internodes (Yamamuro et al., 2000). KNOX1, which regulates lignin deposition and composition in grasses (Townsley et al., 2013), is located within the interval of the 9K cortex radius QTL .KNOTTED1, involved in internode patterning in maize (Tsuda et al., 2017), is located in the 9N QTL interval for epidermis/endodermis cell count along with GA regulator (GASA) and fantastic four meristem regulators (FAF). TRM, involved in preprophase assembly (Motta & Schnittger, 2021) is located in the in CHLR radius significant QTL. Multiple cell cycle regulation genes, cyclin dependent kinases (CDK) and cell division kinases, were found in CHLR radius, metaxylem diameter, and epidermis/endodermis cell count QTL intervals. Genes related in hormone signaling include auxin response genes in CHLR radius, metaxylem diameter, SCLR radial cell count CHLR radius, and cortex radius. Furthermore, expansin genes were exclusively found in QTL intervals of cortex radius and annulus area traits that may be involved in the regulation of cell size and overall internode architecture. Further investigation into connecting genes contained within these intervals and the traits they associate with is needed to understand the potential to manipulate these traits.

3.12 QTL interval NACs and NAC family phylogenetic reconstruction

Over 17k genes are located within the intervals of the QTLs, many of which are transcription factors that belong to the multifunctional NAC family. Several NACs within the intervals are involved in SCW biosynthesis, but most lack annotation. To explore and identify the possible functions of these NACs through homologous gene identification, we reconstructed the NAC transcription factor family phylogeny with 541 total NAC genes in switchgrass, rice, and Arabidopsis. Our tree updated the membership of many NACs into subgroups and provides a resource for homologous gene identification across two grass species in reference to the highly studied Arabidopsis thaliana (Table 5).

Thirty-six NAC transcription factors were found within intervals of 17 QTLs for 12 internode anatomy traits and includes SCW NACs with close homologs in rice and Arabidopsis (Table 6 contains all NACs in the significant QTL intervals, and suggestive QTLs for annotated NACs). Chlorenchyma radius interval in 5K contains five NACs including a secondary cell wall homolog (SCWH13) that is similar to SCW regulatory elements found in yeast-1 hybrid assays (Taylor-Teeples et al., 2015). SCW13 is also homologous to OsSND3, a SCW regulator in rice, and CWPB6 in Arabidopsis, providing evidence that SCWH13 may be involved in SCW regulation in chlorenchyma. Furthermore, NAC TFs containing a transmembrane (TM) domain are located within the 5K Chlorenchyma radius QTL (TM10) with close homolog PvTM7, and within the 6N QTL interval for annulus radius (TM4) with close homolog PvTM3 (Yan et al., 2017). Transmembrane tethered NAC proteins are anchored to the cell membrane or endoplasmic reticulum with evidence in Arabidopsis to be involved abiotic stress response (Chen et al., 2008), and potentially, involved in the regulation of the chlorenchyma radius. PvSWN2B

is a secondary wall NAC that belongs to the master regulator NAC category and is found in the suggestive QTL interval of epidermis/ endodermis cell count in the 6N region. Close homologs to PvSWN2B are OsSND1, OsNST1\2 and Arabidopsis NST1 and NST2 that are all involved in various mechanisms of SCW biosynthesis regulation (Zhong et al., 2015). A PvSWN2-RNAi mutant line in switchgrass showed an increased S : G lignin ratio, and has visibly fewer SCLR radial cells, vascular bundle fiber cells, and less lignified cortical cells (Rao et al., 2019). Similarly, PvSWN4A is located within the suggestive QTL interval of annulus area on 9K with close homologs OsVND1, OsVND2, and Arabidopsis VND2 and CWPB9. PvSWN4A is involved in _regulation and may contribute to regulation of annulus area. SCWH9 was found in the 5N QTL interval for SCLR radial cell count and may be involved in the regulation of fiber cell wall thickening. Taken together, these connections provide a genetic basis for further elucidation through functional studies.

This effort provides some genetic basis for multiple internode anatomy traits and presents a phylogenetic reconstruction of 541 NAC transcription factor family genes. Though the presence of genes with functions of interest within intervals that in some cases include over a thousand genes does not indicate a direct connection, this analysis provides evidence for future work to establish a more direct connection between genes and internode anatomy phenotypes. Furthermore, the phylogenetic reconstruction of the NAC transcription factor family provides a reference for gene homology identification for functional gene characterizations among switchgrass, rice, and Arabidopsis. This phylogeny increases the accuracy of transferring known annotations of NACs from the highly studied Arabidopsis and model grass, Oryza sativa, into the prized biomass crop, switchgrass.

3.13 Materials and Methods

3.14 Experimental Planting Design

A description of the experimental planting has been presented previously (Lowry et al., 2019; Milano et al., 2016) The genetic mapping population was produced by crossing two uplands and two lowlands, VS16 and DAC, AP13 and WBC, respectively. The F1 hybrids were then intercrossed reciprocally to produce a four-way, outbred F2 mapping population. The F2 population was established in 2015 outside of Columbia, MO. All plant segments were harvested in 2018 in September.

3.15 Anatomical measurements

The hand sectioning method was used to take cross sections of each internode beginning at 1 cm above the node, taking sections as needed no further than 2 cm above the node. Acriflavine hydrochloride was used predominately on the sections as a general cell wall stain to enhance visibility of cell walls.

All anatomical trait measurements were carried out in FIJI image software (Schindelin et al., 2012). Distances between two points were measured using the line tool unless otherwise described below. Nearest neighbor distance of vascular bundles was determined in all visible vascular bundles that fit into either cortex or sclerenchyma categories defined by >50% vascular bundle area location within either tissue. This led to different total counts of vascular bundles measured but was never less than 25 per image. Phloem area was measured using the trace tool to draw around the perimeter of the phloem areas of each visible vascular bundle in the cortex only with no fewer than 25 phloem areas measured per image. Tiller height of all but the KBSM20 samples were obtained from shared database within the common gardens group. Outer internode diameters were

measured with digital calipers at the site of sectioning, 1 cm above the node. Tough tiller segments were sectioned with the "Rapid-Tome" hand-held microtome.

3.16 QTL analysis

Analysis conducted in R v 3.3.3 (R Development Core Team, 2022; RStudio Team (2020)), with the R/qtl2 package (Broman et al., 2019). R v 3.3.3 was used for QTL analyses as required for compatibility with certain packages. Between 181 and 412 samples from the F2 mapping population were used due to section quality (Table 2). LOD thresholds were calculated with 0.10 alpha for significant QTL and alpha = 0.25 for suggestive QTL. Peaks were defined as 1.5 drop and 1.5 peak drop to identify QTL markers from 4,380 total markers.

3.17 Candidate gene search

QTL marker intervals were mined for genes with functions of interest and cell wall associated candidate genes from a known list of curated cell wall related genes including an updated NAC list described herein using the Phytozome v13 phytomine regions tool.

3.18 Statistics

All statistics (excluding QTL analysis) were completed in R v 4.1.2 and R studio v 1.3.1093 (R Development Core Team, 2022; RStudio Team (2020)). Histograms were produced using the ggplot2 package in R.

Imputation of missing data for correlation plots was conducted with the MICE package in R. Data was produced using the "cart" algorithm with five iterations averaged and analyzed with the corplot package in R. Principal component analyses were run using the FactoMineR package in R. PCA coordinates were generated and ran for QTL.

3.19 NAC analysis

HMMER with the PFAM domains PFAM01849 and PFAM02365 was used to identify all putative members of the NAC family in switchgrass, which generated a list of 314 NAC domain containing proteins. A keyword search in the Phytozome Panicum virgatum genome v4.1 identified 12 additional putative NAC family members. The NCBI CDD tool was used to filter out proteins lacking NAC domains, leading to the removal of four sequences from the HMMER-generated list and all 12 genes from the Phytozome list. The entire coding sequences obtained from phytozome was used for sequence alignment, independent of the presence of subdomains (A-E), including, truncated NACs with fewer than 5 subdomains we retained, for a total of 310 switchgrass NACs. Putative rice NAC protein sequences were obtained from phytozome genome v7, adding 143 proteins to our analysis. Arabidopsis thaliana NACs identified on TAIR via keyword search produced 100 sequences. Based on the NCBI CDD tool, four Arabidopsis genes and one rice gene lack a NAC/NAM domain and were removed.

The protein sequence alignment was generated in Clustal X. Six additional PvNACs, and 1 AtNAC that shared no sequence similarity to one or more other sequences in the MegaX pairwise matrix were removed, though these are retained in Supplemental Table 1 and labeled “NAC Similar”. MegaX was used to generate a neighbor-joining bootstrap consensus tree using p-distance and 1000 bootstrap replicates. The tree containing 541 total NACs with 304 switchgrass NACs, 95 Arabidopsis thaliana NACs, and 142 rice NACs. Subfamilies containing cell wall-associated NACs were defined based on previously established NAC membership described in (Ooka et al., 2003), (Yan et al., 2017). PvSWN3A and PvSWN3B (Zhong et al., 2015) were not included in the switchgrass

genome v4.1 and are therefore excluded here. Additional notation includes cell wall promoter binding in Yeast 1 hybrid assay (CWPB) (Taylor-Teeples et al., 2015); transmembrane (TM), abiotic stress response and senescence (AbSS), and secondary cell wall homolog (SCWH) described in Yan2017 based on Panicum virgatum genome version 1.1. These designations are updated here by blasting transcript sequence provided in Yan 2017 against the early release Pv genome v4.1.

Table 3.1 | Internode anatomy trait descriptions

Trait	Short Name	Functional Importance	Data Type	Trait Measurement Method
Internode Architecture				
Internode diameter	*Outer Diameter*	Biomass yield	Single measurement per individual	Measured at 1 cm above the first node above soil line with digital calipers
Inner Diameter		Biomass yield	Single measurement per individual	Outer diameter – annulus radius
Internode annulus radius	*Annulus radius*	Biomass yield	Represented as an average per individual	Straight line distance drawn perpendicular to epidermis, drawn from epidermis to pith, N = 8 per section
Internode Annulus radius	*Annulus Radius*	Biomass yield		
Sclerenchyma radial thickness	*SCLR Radial Thickness*	Physical stress and water stress	Represented as an average per individual	Straight line distance drawn perpendicular to epidermis, drawn across maximum Chlorenchyma cavity. N = 10 per section
Sclerenchyma Radial Cell Count	*SCLR Cell Count*		Represented as an average per individual	Three measurements per individual.
Chlorenchyma radial thickness	*CHLR Radial Thickness*	Biomass yield	Represented as an average per individual	Straight line distance drawn perpendicular to epidermis, drawn across maximum Chlorenchyma cavity. N = 10 per section
Internode Annulus Area	*Annulus Area*	Biomass yield	Single measurement per individual	A= pi * (outer radius^2-inner radius^2)
Epidermis & hypodermis	*Epidermis*	Water stress and biotic stress	Single measurement per individual	Cell layer count from epidermis to chlorenchyma cavity
Rind radial thickness % of internode annulus radius	*Rind Percent Annulus Radius*	Cell wall digestibility	Single measurement per individual	(Chlorenchyma radial thickness + Sclerenchyma radial thickness) / Annulus radius
Cortex radial thickness % of internode annulus radius	*Cortex Percent Annulus Radius*	Cell wall digestibility	Single measurement per individual	(Annulus radius-(Chlorenchyma radial thickness + Sclerenchyma radial thickness)) / Annulus radius
Vascular Traits				
Meta Xylem diameter of vascular bundles in the cortex	*Xylem Diameter Cortex*	Biomass yield, water Stress	Represented as an average per individual	Horizontal width of metaxylem, bisected xylem not measured, cortex vascular bundles only. N = 25+ per section

Phloem area		Biomass yield	Represented as an average per individual	Phloem area traced per cortical vascular bundle, N = 15+ per section
Vascular Bundle Area	*VB area*	Biomass yield, water Stress	Represented as an average per individual	Vascular bundle area
Vascular Bundle Fiber Area	*VB Fiber Area*	Biomass yield, water Stress	Represented as an average per individual	Vascular bundle fiber area
Vascular bundle fiber % area of vascular bundle	*VB Fiber Ratio*	Biomass yield,	Represented as an average per individual	Area of vascular bundle fibers / Vascular bundle area (proto & meta xylem, proto & phloem) N =25+ / section See supp. #
Nearest cortical vascular bundle neighbor	*Nearest VB Neighbor Cortex*	Nutrient and moisture transport, water stress	Represented as an average per individual	All distances measured from center point of each vascular bundle surrounded by >50% cortical parenchyma. Nearest neighbor distance Averaged. See fig. 1E N = 50+ per section
Nearest sclerenchyma vascular bundle neighbor	*Nearest VB Neighbor SCLR*	Nutrient and moisture transport, water stress	Represented as an average per individual	Only vascular bundles <50% surrounded by sclerenchyma fibers measured as above.
Nearest vascular bundle neighbor in Cortex and SCLR	*Nearest VB Neighbor SCLR*	Nutrient and moisture transport, water stress	Represented as an average per individual	Only vascular bundles <50% surrounded by sclerenchyma fibers measured as above.
Cell Wall Trait				
Cortical parenchyma cell wall thickness	*Cortex Cell Wall Thickness*	Biomass yield, cell wall digestibility, water stress	Represented as an average per individual	Straight line measured from lumen to lumen, N =10 per section

Table 3.2 | F2 Internode anatomy Trait Summary

Trait	Count	Mean	Median	STD	Max	Min	Range	CV
Internode Architecture								
Outer Diameter (mm)	342	4.0	4.00	0.84	6.4	1.5	4.9	0.02
Inner Diameter (mm)	304	3.4	3.3	0.7	5.4	1.3	4.1	0.02
Annulus radius (µm)	369	580	567	149	1016	247	769	25.7
Cortex Radius (µm) * [S]	358	462	447	117	770	222	547	25.3
SCLR Radius (µm)	406	66	63	19	128	16	111	29.9
SCLR Radial Cell Count [S]	181	8.57	8.33	2.04	16.33	3.67	12.67	23.8
CHLR Radius (µm) * [S]	397	54	47	33	188	5	182	61.8
Annulus Area (mm^2) * [S]	301	13.4	12.6	5.6	29.8	1.4	28.3	2.4E-05
Epidermis Count * [S]	342	2.2	2.0	0.6	4	1	3	29.5
Rind Percent Annulus radius * [S]	356	0.20	0.20	0.04	0.31	0.10	0.21	22.5
Cortex Percent Annulus Radius * [S]	358	0.80	0.80	0.05	0.90	0.64	0.27	5.7
Vascular Traits								
Metaxylem Diameter in Cortex Vascular Bundles (µm) [S]	380	30	33	4.3	41	16	24	14.3
Phloem Area (µm^2)	402	990	963	289	1794	310	1484	29.2
Vascular Bundle Area (µm^2)	384	6563	6567	1804	13757	1900	11856	27.4
Vascular Bundle Fiber Area (µm^2)	384	13138	12664	3859	25762	3333	22428	29.3
Vascular Bundle Fiber Area Ratio	412	0.50	0.51	0.08	0.65	0.21	0.44	15.3
Nearest Vascular Bundle in Cortex (µm)	403	188	186	37	293	81	212	19.7
Nearest Vascular Bundle in SCLR (µm)	395	83	80	17	130	43	87	21.1
Nearest Vascular Bundle in Cortex and SCLR (µm)	394	107	106	16	152	65	87	15.7
Cell Wall Trait								
Cortical Cell Wall Thickness (µm) *	385	7.13	7.03	1.83	11.35	1.93	9.42	25.69

* - Significant QTL

[S] - Suggestive QTL

Table 3.3 | Significant and suggestive QTL for internode anatomy and principal components throughout the chromosomes

QTL	Trait	Chr	LOD Threshold Alpha	LOD	Marker	Flank_L	Flank_H	POS	CI_L	CI_H	Candidate Genes Count
1	**SCLR Radial Cell Count**	1N	0.25	3.96	Chr01N_56.371749	Chr01N_51.049036	Chr01N_58.044318	58.9976613	52.9344106	64.400757	144
2	**PCA Dim.2**	2N	0.25	3.98	Chr02N_5.318866	Chr02N_2.794744	Chr02N_7.183648	7.347471	1.539095	13.687367	340
3	**Cortex Radius**	2N	**0.1**	6.23	Chr02N_16.991047	Chr02N_11.695915	Chr02N_17.283214	31.0128096	22.8891435	33.042238	294
4	**PCA Dim.2**	3N	0.25	4.05	Chr03N_1.207954	Chr03N_1.207954	Chr03N_3.003724	0	0	4.562087	185
5	**Vascular Bundle Fiber Area**	3N	0.25	3.82	Chr03N_34.314679	Chr03N_8.279254	Chr03N_58.577986	70.2710110	40.0198111	53.215348	2223
6	**Metaxylem Diameter**	3N	0.25	4.05	Chr03N_1.68067	Chr03N_1.207954	Chr03N_3.887313	0.7930021	0	5.778302	233
7	**Cortical Cell Wall Thickness**	3N	**0.1**	5.24	Chr03N_46.274977	Chr03N_31.074841	Chr03N_53.302537	80.5563638	67.4162186	89.071247	1244
8	**PCA Dim.4**	3N	0.25	4.08	Chr03N_50.533228	Chr03N_31.074841	Chr03N_63.84169	85.709091	67.416219	110.921393	1391
9	**CHLR Radius**	5K	**0.1**	4.00	Chr05K_8.553115	Chr05K_5.719047	Chr05K_24.019903	18.9276641	8.6496575	43.439076	1432
10	**PCA Dim.2**	5K	0.25	3.96	Chr05K_10.083367	Chr05K_8.064928	Chr05K_23.685292	23.178392	17.072213	43.013927	1174
11	**Rind / Cortex % of Annulus Radius**	5K	**0.1**	5.58	Chr05K_14.62495	Chr05K_8.342839	Chr05K_19.754362	29.54882	18.1966995	37.10381	765
12	**SCLR Radial Cell Count**	5N	0.25	3.67	Chr05N_3.365713	Chr05N_1.464967	Chr05N_6.553711	5.526839	0	18.33957	340
13	**Rind / Cortex % of Annulus Radius**	5N	0.25	4.10	Chr05N_8.590537	Chr05N_1.464967	Chr05N_15.453667	23.5652842	0	4.562087	1021
14	**Phloem Area**	5N	0.25	3.77	Chr05N_12.438928	Chr05N_9.388549	Chr05N_14.132881	30.8577272	24.5721777	32.936016	327
15	**Epidermis Cell Count**	6N	**0.1**	4.81	Chr06N_4.034692	Chr06N_1.65653	Chr06N_11.794087	10.4500243	0.7969274	22.478973	368
16	**Annulus Area**	6N	**0.1**	4.33	Chr06N_6.439825	Chr06N_5.633389	Chr06N_12.721051	17.52235	13.9067542	23.36501	189
17	**CHLR Radius**	7K	**0.1**	4.73	Chr07K_51.347197	Chr07K_47.708677	Chr07K_51.663664	52.5354752	40.0198111	53.215348	331
18	**Epidermis Cell Count**	8K	**0.1**	4.23	Chr08K_45.778407	Chr08K_39.675907	Chr08K_53.831953	35.0135692	27.6899217	41.10029	355
19	**Cortex Radius**	9K	0.25	3.97	Chr09K_5.979988	Chr09K_2.164483	Chr09K_60.082683	18.1502291	9.7255147	84.392209	3117
20	**Annulus Area**	9K	0.25	4.03	Chr09K_54.154333	Chr09K_46.054576	Chr09K_60.736312	74.93338	62.12775	85.58636	740
21	**Epidermis Cell Count**	9N	0.25	4.04	Chr09N_17.839603	Chr09N_4.58776	Chr09N_23.547754	36.8175842	12.5609846	47.689391	1658

Table 3.4 | Candidate gene summary

Candidate gene classification							
	Grass Stem Development	**Cell Division**	**Cell Cycle**	**SCW**	**Hormone Related**	**Expansin**	**Meristem**
Significant QTL							
Cortex Radius				MYB, NAC, GT, GH			
Cortical Cell Wall Thickness		Cell Division Protein Kinase, Phragmoplast Orienting Kinesin		MYB, R2R3-MYB, NAC, GH, GT, Mitchell Clade	AUX/IAA,ARF2		
CHLR Radius	TRM	Cell Division Protein Kinase	Mitotic Phosphoprotein	R2R3-MYB, MYB, NAC, NAM, GH, GT, Mitchell Clade	Auxin responsive protein, Auxin inducible protein		
Epidermis Cell Count				NAC, GH, GT			
Epidermis Cell Count				R2R3-MYB, MYB, GT, Mitchell Clade			
Suggestive QTL							
Metaxylem Diameter			Mitotic Specific Cyclin B	R2R3-MYB, MYB, NAC, GT	G2/Mitotic specific cyclin B		
SCLR Radial Cell Count		Cell Division Protein Kinase		R2R3-MYB, MYB, NAC, GT	GH3 Auxin responsive promoter, AUX/IAA B3 DNA Binding domain		
CHLR Radius				R2R3-MYB, MYB, GH, GT			
Cortex Radius	BRI1, KNOX1	Cell Division Protein Kinase, Cell division control protein 7, CLE3		R2R3-MYB, MYB, NAC, GH, GT	Auxin responsive protein,	Expansin A18 related	Fantastic Four meristem regulator (FAF)
Annulus Area		Cell division control protein 7		MYB, NAC, GH, GT	Auxin Inducible, AUX/IAA B3 DNA Binding domain	Expansin A18 related	
Epidermis Cell Count	KNOTTED1	Cell Division Protein Kinase	Cell cycle arrest protein, Mitotic checkpoint protein,	R2R3-MYB, MYB, NAC, GH, GT	Auxin responsive protein, Auxin inducible protein		
Vascular Bundle Fiber Area		Phragmoplast Orienting Kinesin					

Table 3.5 | Subgroups of NACs

Subgroup	Subgroup Description	Known SCW regulators or Cell Wall Promoter Binding (cwpb) capability	Total NACs		
			At	Os	Pv
ATAF [a]		*cwpb*	4	3	6
NAC2[a, b]	Pv expanded	VNI1, *cwpb*	8	4	14
NAM [a]		*cwpb*	10	12	23
NAP[a]		VNI2	6	3	4
ONAC003[a, b]	Pv expanded	SND2, *cwpb*	4	6	20
OsNAC7[a,b]	Pv expanded	SWN, SND1, NST, VND, *cwpb*	13	9	22
ANAC011[b]	Pv expanded	*NA*	5	3	8
NAC1		*NA*	3	11	21
ONAC001[c]	Pv reduced	*NA*	0	9	13
ONAC022[b]	Pv expanded	*NA*	6	9	27
OsNAC3[d]	Grass-expanded	*NA*	0	3	6
OsNAC8[e]		*NA*	0	1	2
TERN		*NA*	2	4	8
TIP[c]	P.v. reduced	*NA*	3	2	2
AtNAC3[a,e]	At Only	*NA*	3	0	0

[a] SCW associated subgroups that contain at least 1 SCW regulator or cwpb
[b] Panicum virgatum expanded subgroups over expectations from WGD in P. virgatum.
[c] Panicum virgatum reduced subgroups compared to expectations with WGD.
[d] Grass expanded subgroups
[e] Subgroups that contain only Arabidopsis thaliana
At - Arabidopsis thaliana
Os - Oryza sativa
Pv – Panicum virgatum

SCWH indicates Secondary cell wall homologous genes that contain a motif present in ANAC073/SND2 (Yan et al., 2017) and found to belong to the same clade within the ONAC003 subfamily. Eleven switchgrass NACs contain a C-terminal trans membrane (TM) domain that anchors the protein to either the ER or plasma membrane, rendering it inactive until protease liberation (Yan et al., 2017). TM, Abiotic stress response (AbSS), Secondary cell wall homolog (SCWH), described in Yan 2017 based on Panicum virgatum genome version 1.1, Updated here by blasting transcript sequence provided in Yan 2017 against the early release Pv genome v4.1.

Table 3.6 | NAC genes found in internode anatomy QTL intervals

Internode Anatomy Trait	QTL marker	Accession	Sub-group	Function if known	Close Switchgrass homolog	Close Rice Homolog	Close Arabidopsis Homolog
Significant QTL							
Chlorenchyma Radius	Chr05K_8.553115	Pavir.5KG054400	ONAC003	SCWH13	/	LOC Os01g09550 OsSND3	AT4G29230 ANAC075 CWPB6
Chlorenchyma Radius	Chr05K_8.553115	Pavir.5KG148700	NAM	/	/	/	/
Chlorenchyma Radius	Chr05K_8.553115	Pavir.5KG160700	NAM	/	/	/	/
Chlorenchyma Radius	Chr05K_8.553115	Pavir.5KG151000	/	/	/	/	/
Chlorenchyma Radius	Chr05K_8.553115	Pavir.5KG170000	OsNAC8	TM10	Pavir.5NG169900 TM7	/	/
Cortex Radius	Chr03N_46.274977	Pavir.2NG104300	NAM	/	Pavir.2KG294400 SCWH11	/	/
Cortical Cell Wall Thickness	Chr02N_16.991047	Pavir.3NG212900	ONAC001	/	/	/	/
Cortical Cell Wall Thickness	Chr02N_16.991047	Pavir.3NG269000	ONAC022	/	/	/	/
Cortical Cell Wall Thickness	Chr02N_16.991047	Pavir.3NG254300	/	/	/	/	/
Cortical Cell Wall Thickness	Chr02N_16.991047	Pavir.3NG284800	NAC1	/	/	/	/
Cortical Cell Wall Thickness	Chr02N_16.991047	Pavir.3NG302500	/	/	/	/	/
Epidermis and Endodermis Cell Count	Chr06N_4.034692	Pavir.6NG015900	OsNAC7	PvSWN2B	Pavir.J130900 PvSWN2A, Pavir.J452700 PvSWN1	LOC Os08g02300 OsNST1|2, LOC Os06g04090 OsSND1	AT2G46770 ANAC043 NST1, AT3G61910 ANAC066 NST2
Epidermis and Endodermis Cell Count	Chr06N_4.034692	Pavir.6NG053500	/	/	/	/	/
Epidermis and Endodermis Cell Count	Chr08K_45.778407	Pavir.8KG251900	/	/	/	/	/
Annulus Radius	Chr06N_6.439825	Pavir.6NG060900	TIP	TM4	Pavir.6KG070800 TM3	/	/
Suggestive QTL							
Annulus Area	Chr09K_54.154333	Pavir.9KG307100	OsNAC7	PvSWN4A	Pavir.9NG493300 PvSWN4B, Pavir.9KG548300 PvSWN5	LOC Os03g03540 OsVND1, LOC Os10g38834 OsVND2	AT4G36160 ANAC076 VND2, AT5G66300 ANAC105 CWPB9
Sclerenchyma Radial Cell Count	Chr05N_3.365713	Pavir.5NG037700	ONAC003	SCWH9	Pavir.5KG054400 SCWH13	/	/

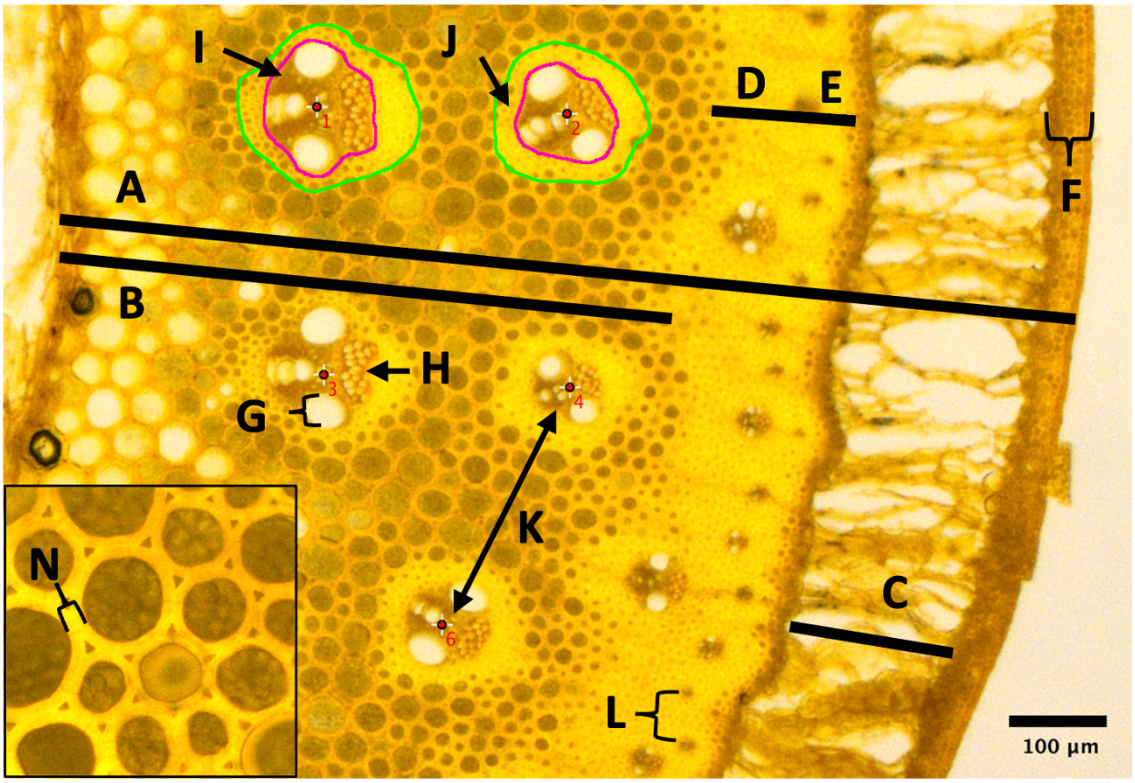

Figure 3.1. Internode anatomy traits measured in F2 switchgrass. Traits were selected based on impact on biomass quality and yield. Internode anatomy traits can be categorized by function and proposed impact on cell wall digestibility and hydraulic function. Internode architecture traits include annulus radius (A), Cortex radius (B), chlorenchyma radial width (C), sclerenchyma radial width (D), Sclerenchyma radial cell count (E), and epidermis and endodermis cell count (F). Vascular traits measured include metaxylem diameter of vascular bundles in the cortex (G), Phloem area per vascular bundle (H), Vascular bundle area circled in magenta (I), vascular bundle fiber area circled in green (J), nearest distance to neighboring vascular bundle in the cortex with numbered markers showing the points designated as the center of each vascular bundle (K), and nearest distance to neighboring vascular bundle in the sclerenchyma (L). The cell wall thickness between cortical cells was also measured (M). Additional traits not shown in this figure are listed in table 3.1.

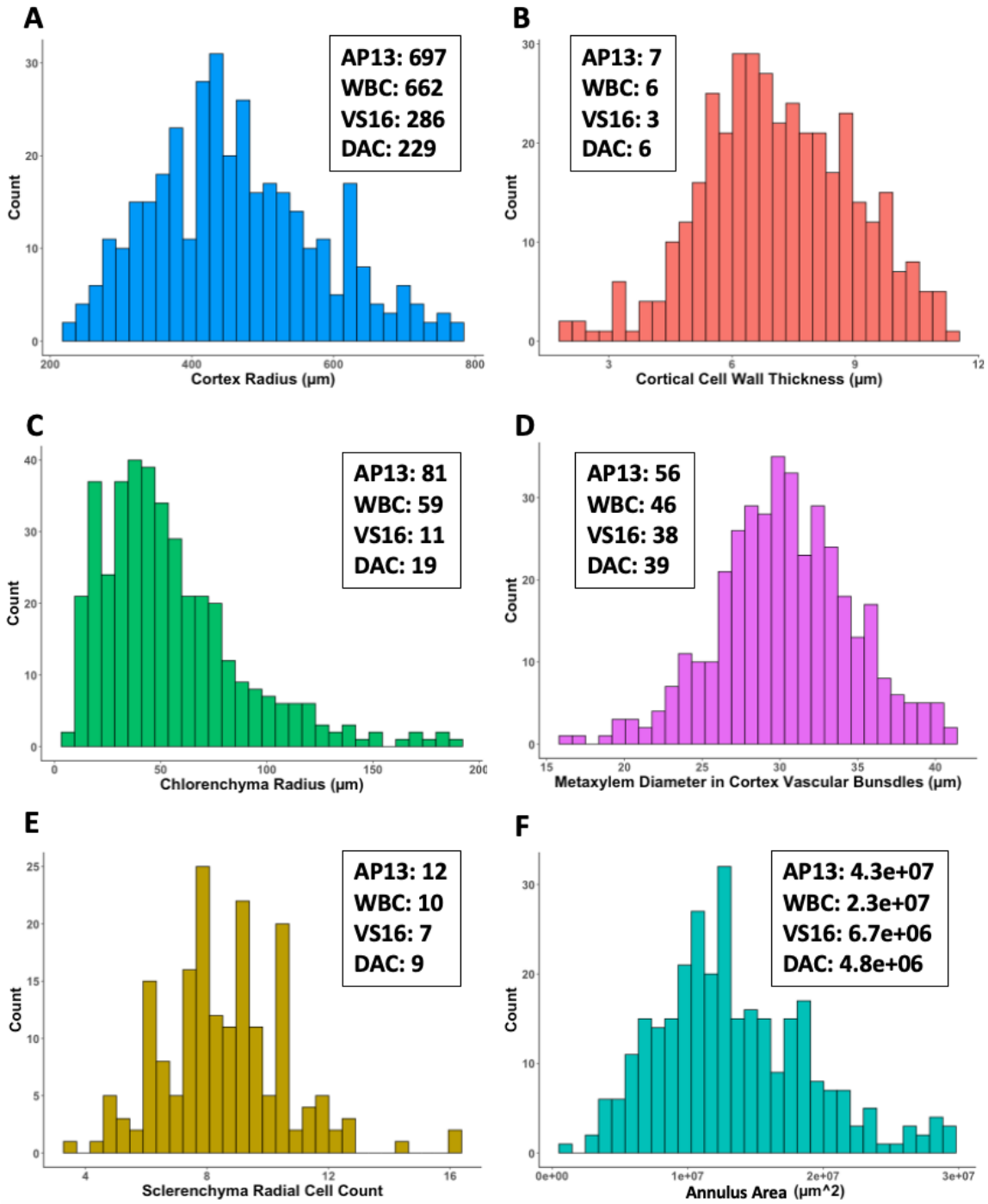

Figure 3.2. Meaningful representation of trait variance in F2s is present for all traits and indicates a robust dataset for the detection of QTLs. Trait values across the F2 mapping population exceed the maximum, minimum, or both values for the grand parents of the cross. Data shown in the histogram have had outliers removed by 1.5x inner quartile range and thus the data is representative of meaningful distributions. Conversely, a lack of variance after outliers removed would indicate poor allelic control over measured traits and low likelihood of QTL detection. Traits where the data exceeds F0 max and min are Cortex

radius (A), cortical cell wall thickness (B), chlorenchyma radius (C), and sclerenchyma radial cell count (E). Traits shown that exceed only the F0 minimum are metaxylem diameter (D) and annulus area (F). Additionally, the difference in distributions may also indicate different genetic regulation for these traits.

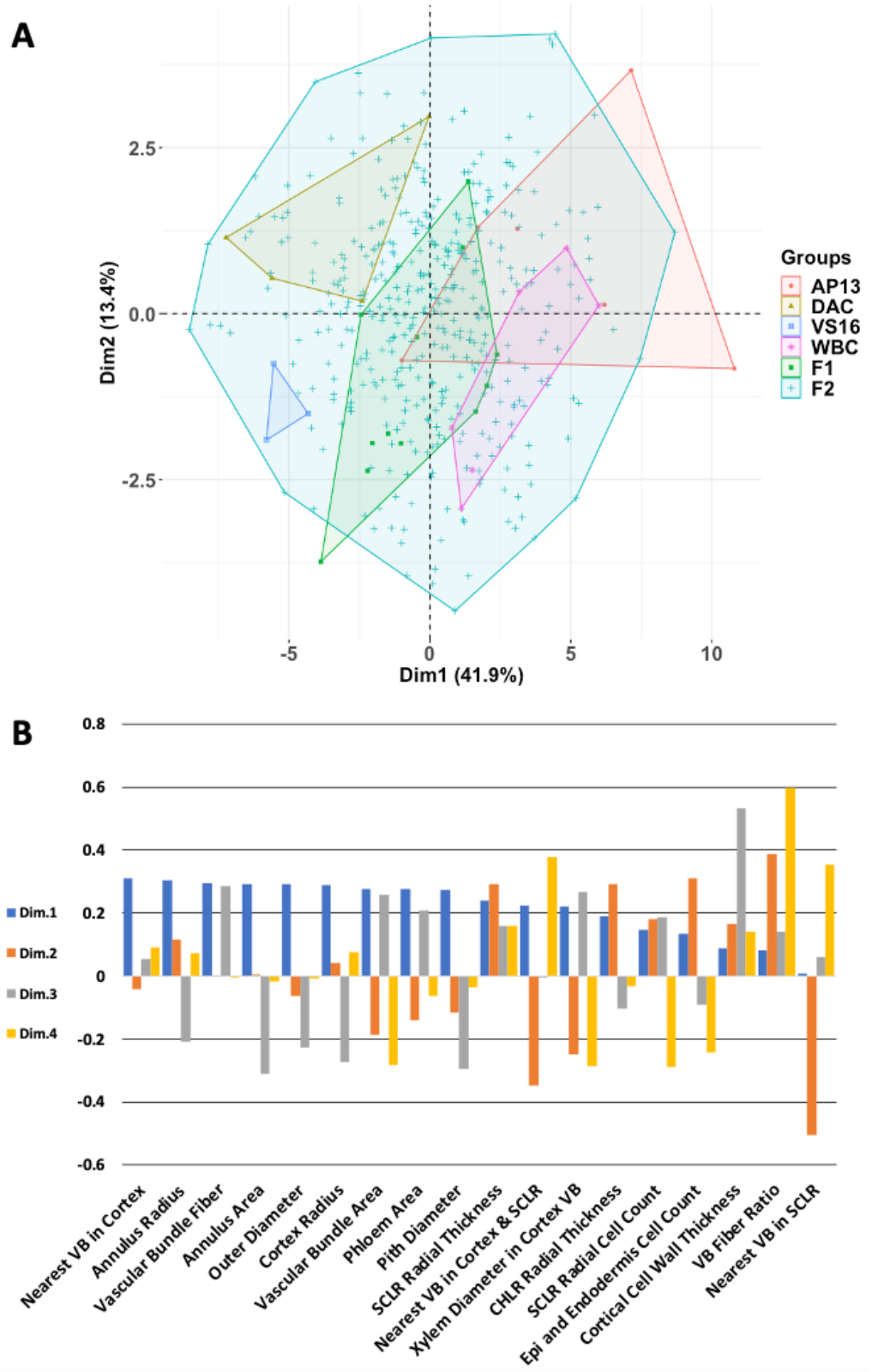
A
2.5
0.0
-2.5
Dim2 (13.4%)
-5
0
5
10
Dim1 (41.9%)
Groups
AP13
DAC
VS16
WBC
F1
F2
B
0.8
0.6
0.4
0.2
0
-0.2
-0.4
-0.6
Dim.1
Dim.2
Dim.3
Dim.4
Nearest VB in Cortex
Annulus Radius
Vascular Bundle Fiber
Annulus Area
Outer Diameter
Cortex Radius
Vascular Bundle Area
Phloem Area
Pith Diameter
SCLR Radial Thickness
Nearest VB in Cortex & SCLR
Xylem Diameter in Cortex VB
CHLR Radial Thickness
SCLR Radial Cell Count
Epi and Endodermis Cell Count
Cortical Cell Wall Thickness
VB Fiber Ratio
Nearest VB in SCLR

Figure 3.3. Principal components analysis of internode anatomy reveals the segregation of F0 genotypes and similarities with F2. PCA reveals the segregation of F0 genotypes from the F1 generation distributed among the more variable F2 individuals. The first component, which explains 41.9% of the overall variance, is represented mainly by variation of internode size traits and traits that highly correlate with internode size. The second component that is mainly represented by variation in the sclerenchyma, cortical cell wall thickness, and traits associated with the sclerenchyma, explain 13.4% of the overall variance. (A) PCA plot with individuals colored by generation, reveals the wide variation among the F0s and the F1s in comparison to the F2s. (B) PCA loadings of the F2 mapping population only PCA loadings show that internode size traits explain the highest amount of variation in the first dimension.

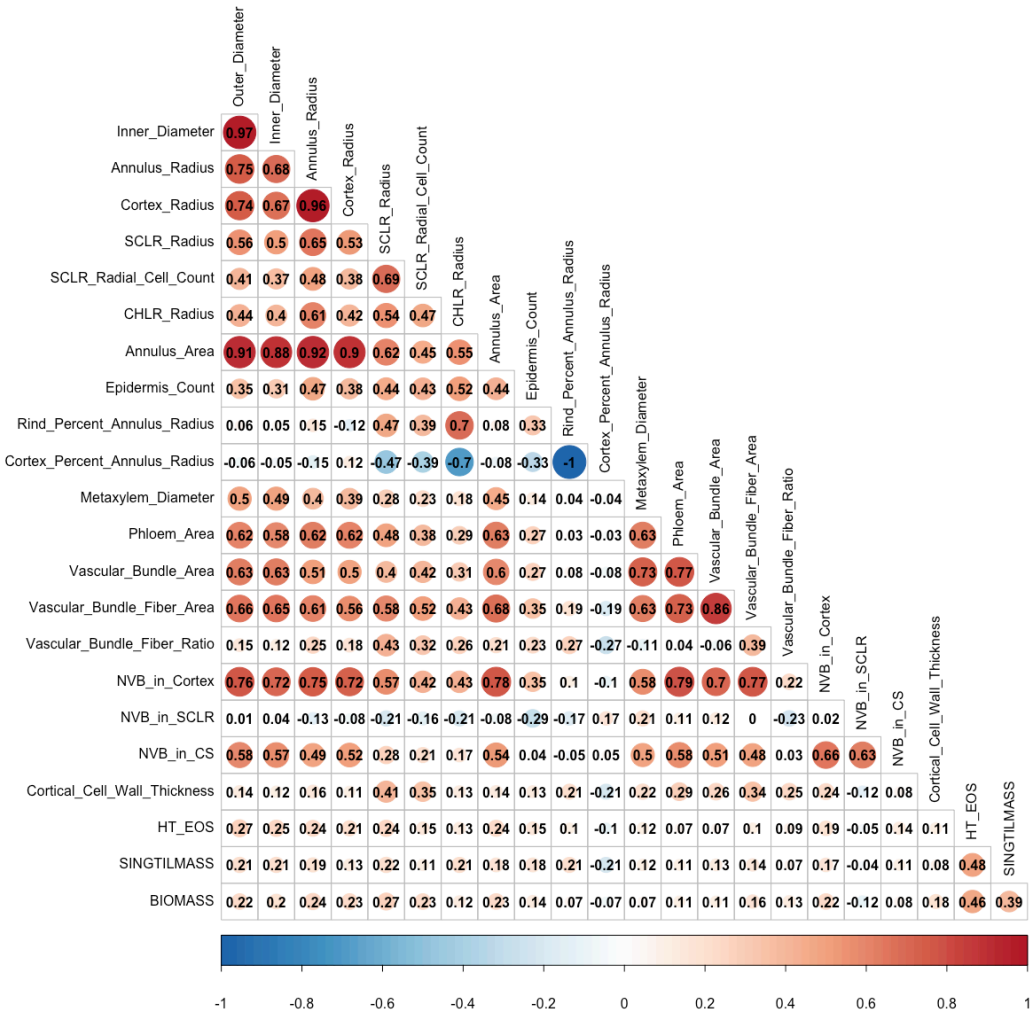

Figure 3.4. Internode anatomy architecture traits are highly correlated and only mildly correlate with biomass yield and height at end of season. Internode architecture traits positively correlate with each other and show moderate correlation with tiller height and biomass yield at end of season harvest. Fiber associated traits: cortical cell wall thickness, sclerenchyma (SCLR) radius, SCLR radial cell count, rind % annulus radius, and vascular bundle (VB) fiber area are positively correlated yet only SCLR traits show correlations above 0.20. Data as imputed using the MICE package in R. Imputed data was averaged from 5 independent runs of the algorithm. Pearson correlations shown with only significant correlation coefficients displayed, all are significant at alpha = 0.05.

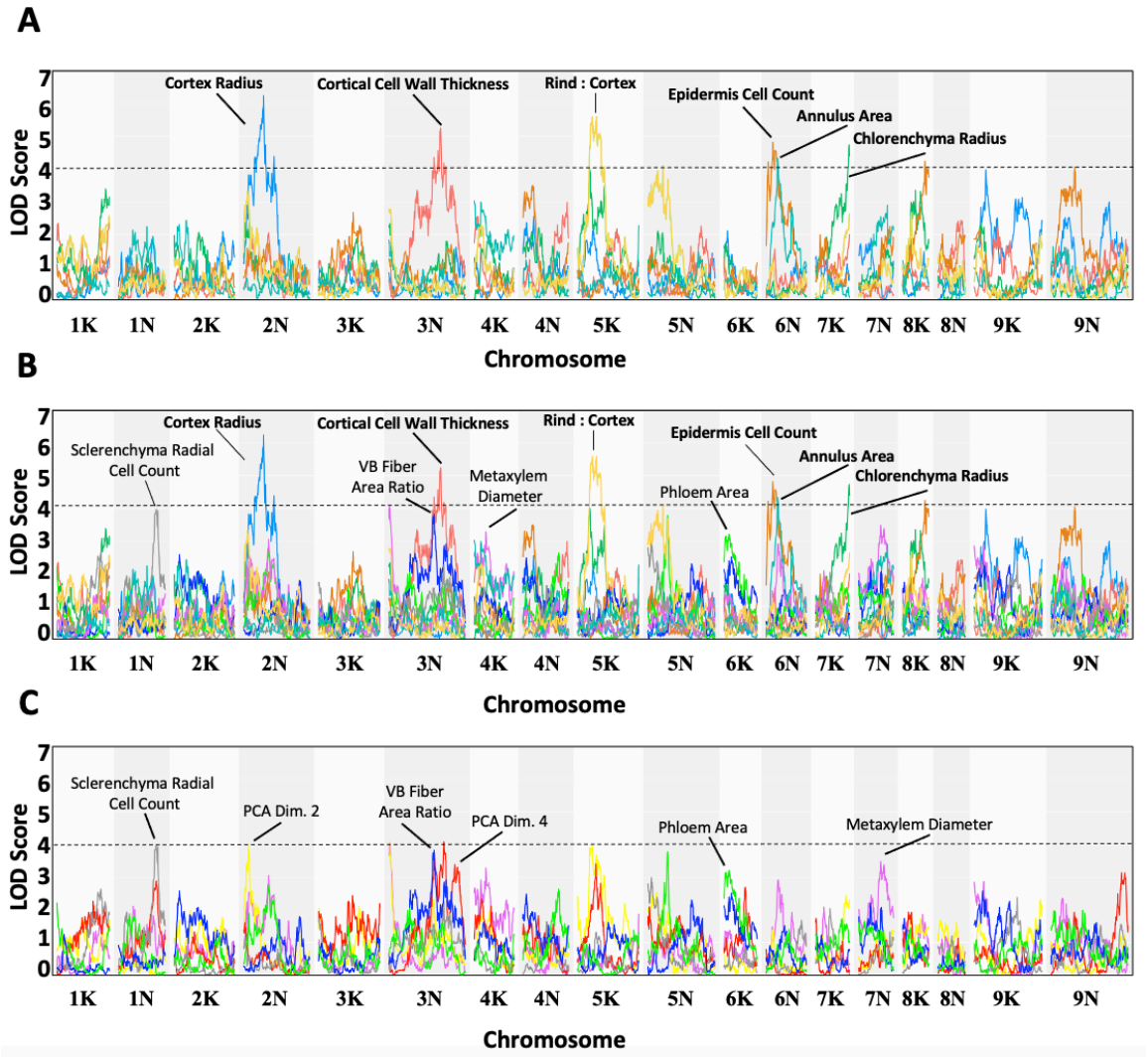

Figure 3.5. Quantitative trait loci (QTL) analysis reveals regions of the chromosomes that may provide the genetic basis for internode anatomy traits. (A) Eight significant QTL for six traits were found on 2N, 3N, 5K, 6N, 7K, 8K chromosome regions. Though the cortical cell wall thickness peak and associated interval between flanking markers is quite large, no other significant QTL for internode anatomy overlap in this region on 2N. Significant peaks at 6N for annulus area and epidermis cell count suggest similar genetic basis, similar to chlorenchyma radius and the overall proportion of cortex and rind of the annulus radius at 5K region. (B) Significant and suggestive QTL displayed together reveal additional overlap among traits that provides support for shared genetic basis of control for these traits. This includes size coordinated traits: metaxylem diameter and annulus radius 4K and 6N, sclerenchyma radial cell count and rind-cortex proportion 5N; fiber and cell wall traits: vascular bundle fiber ratio and cortical cell wall thickness 3N; (B). Suggestive anatomy QTL and Suggestive PCA (C). Significant and suggestive LOD score alpha = 0.1 and 0.25, respectively. Significant traits shown in Bold. Average LOD score significance threshold of 4 (SD = 0.12) is shown.

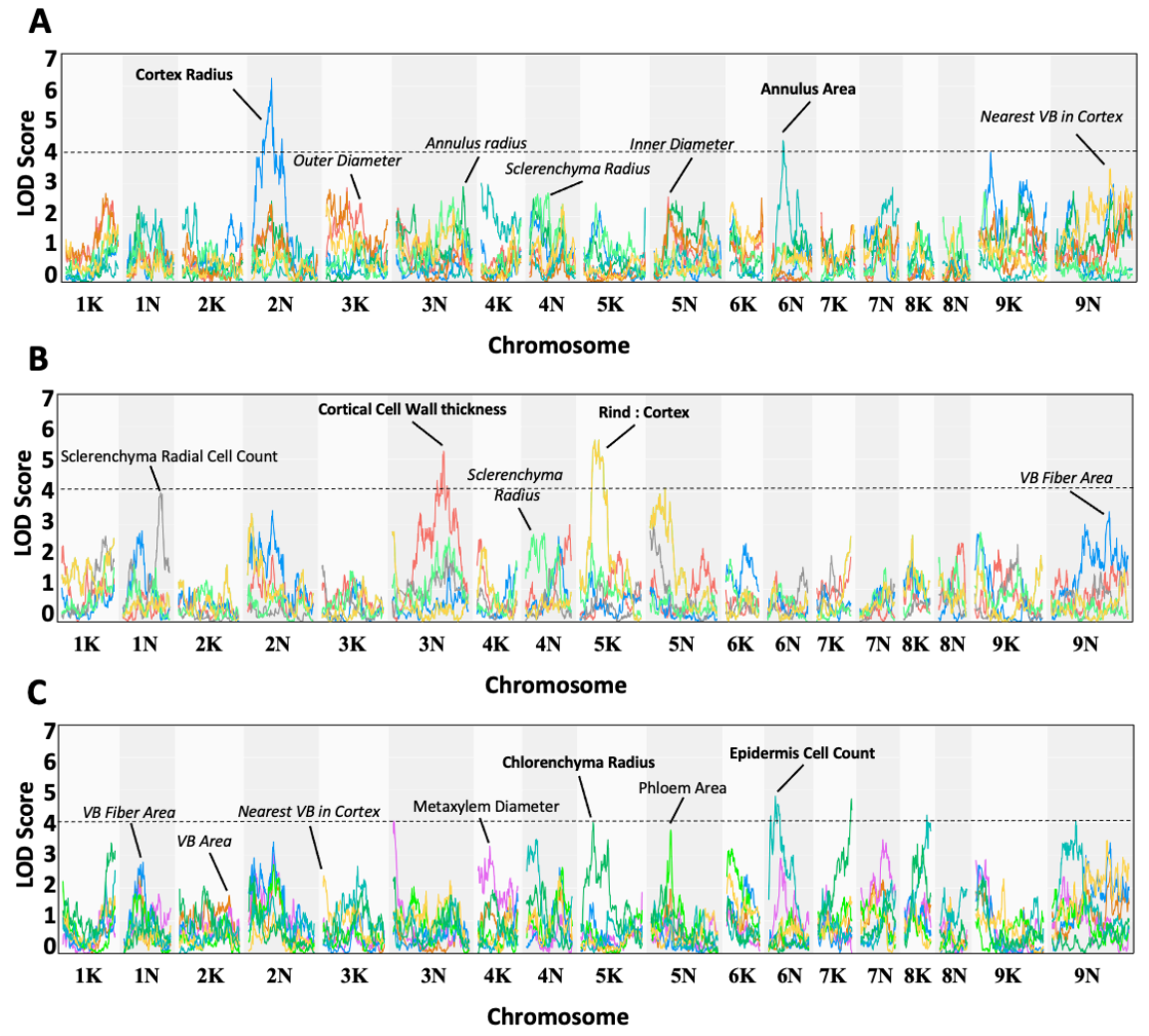

Figure 3.6. Suggestive QTL peaks overlap with numerous sub-suggestive peaks of correlated traits in same phenotypic or functional categories. (A) Correlated traits show similar patterns of peak overlap. Significant and suggestive peaks overlap with peaks from highly correlated traits that do not reach the 0.25 alpha LOD score threshold. However, this indicates that not only are these traits highly correlated but suggests they may have a common genetic basis. Of the significant peaks for two traits with significant QTL, the peak for cortex radius on 2N has similar peaks underlying it from highly correlated traits; outer diameter (0.74), annulus radius (0.96), and inner diameter (0.67). An overlapping genetic basis for these traits is expected as these are all internode size traits. Cortex radius suggestive QTL also has similar, yet lower LOD score peaks on 9K with positively correlated (0.53) sclerenchyma radial thickness, and inner diameter (0.67). Additionally, several peaks are present that overlap with other non-significant loci, 1K: OD, ID,SCLR, and NVB Cortex; 4N: OD, ID,SCLR, annulus radius, and NVB Cortex; 5N: OD, Annulus radius, and ID: and a second peak on 9K with cortex radius, ID, and annulus radius. Considering the presence of multiple, low peaks at the same loci for multiple, positively

correlated traits supports the notion that these regions of the chromosome may control these traits. (B) Positively correlated fiber associated traits show overlapping peaks that suggest a similar genetic basis for these similar traits. The significant QTL for cortical cell wall thickness has overlapping peaks from non-suggestive peaks at the 3N locus with SCLR radius (0.41), SCLR radial cell count (0.35), and VB fiber area (0.34). The suggestive peak for rind % of annulus radius on 5N with SCLR radial cell count (0.48), However, the SCLR radial cell count suggestive peak at 1N, and the significant rind : cortex proportion peak at 5K have no shared peaks form other traits. (C) Vascular associated traits show overlap with non-significant peaks across chromosome regions. Vascular bundle fiber area overlaps with vascular bundle area and metaxylem diameter, and phloem area at the 1N and 2N regions, which indicates vascular bundle size may be regulated by genes in these regions. The significant peak for epidermis cell count at 6N has a smaller, non-significant peak for metaxylem diameter which is contrary to the low correlation between these two traits (0.14). Conversely, a significant peak for epidermis cell count shows greater peak overlap with a sub-suggestive chlorenchyma radius peak at 8K, suggestion a shared genetic basis in these correlated (0.52) traits. Nearest vascular bundle in the cortex does have a solitary peak at 3K, yet overlaps with Vascular bundle fiber area, vascular bundle area, and phloem area at 4N and again with phloem area at 6K. The lack of an overlapping peak at 4N with metaxylem diameter suggests that the 4N region may not regulate the entire vascular bundle in concert. *Traits that do not have peaks above 0.25 LOD score significance threshold are shown in italics and referred to as sub-suggestive peaks.* Significant traits shown in Bold. Average LOD score significance threshold of 4 (SD = 0.12) is shown.

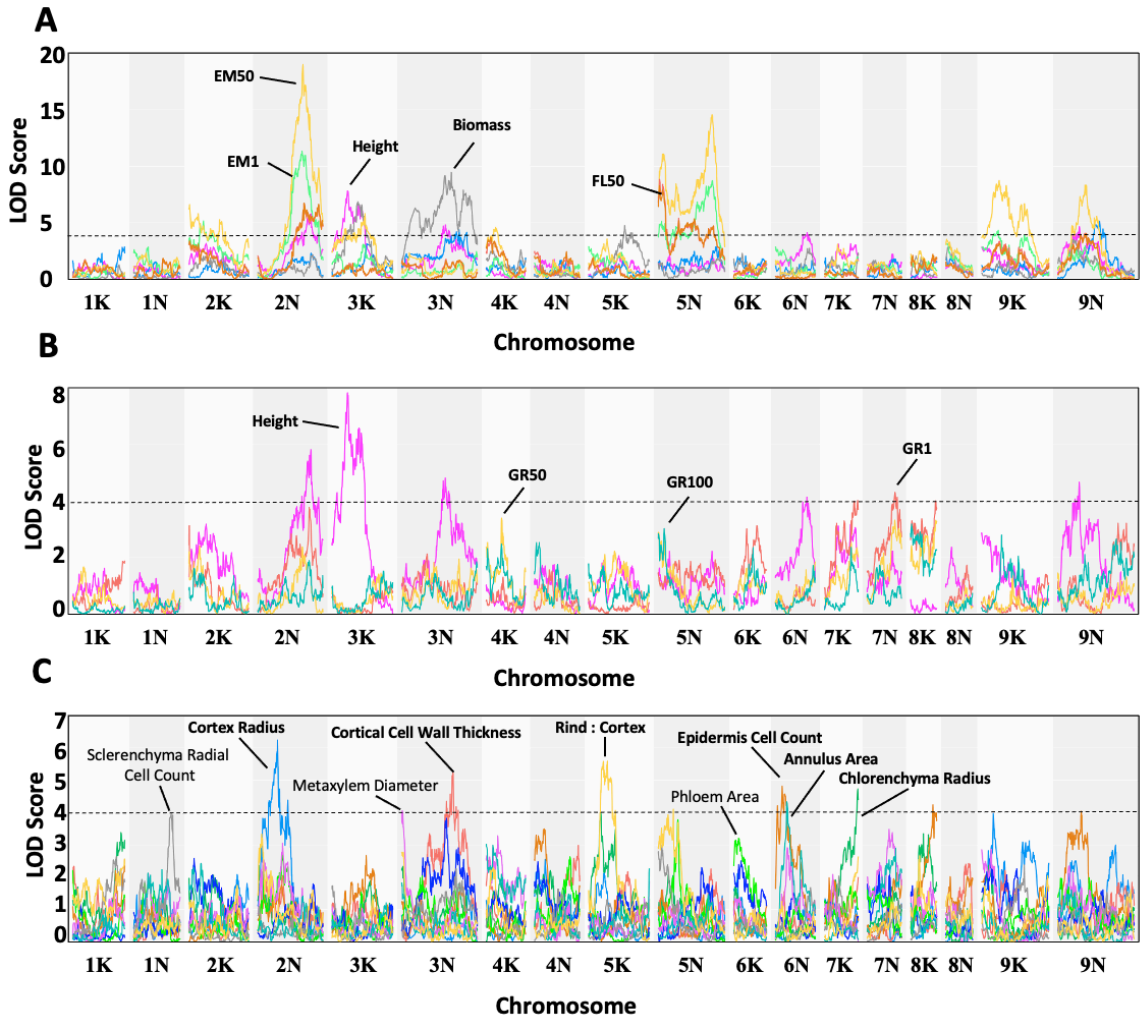

Figure 3.7. Biomass and phenology QTL overlap with internode anatomy to suggest common genetic basis. (A) Biomass and phenology traits with LOD scores above 5 show highly represented regions on 2K, 2N,3K, 3N, 5N, 9K, and 9N. (B) Biomass and phenology traits with LOD scores below 5 reveal additional significant QTL within 4K, 5K, 6N, 7N, and additional suggestive peaks that overlap with internode anatomy peaks. (C) Internode anatomy significant and suggestive QTL show extensive interval and peak overlap with biomass and phenology traits . Shared markers were not found among anatomy, biomass and phenology QTL but overlapping intervals were found between flanking markers on 2K, 2N, 3N, 5N, 7K, 7N, 8K, 9K, and 9N regions. EM50 has suggestive peaks overlap on 7K, 7N, 8K, with CHLR, EPI, and MXD significant and suggestive peaks. Rind : cortex overlap with GR100 and Gr50 at 5N. Biomass and CWT overlap at 3N. Cortex radius and EM50 at 9K and 9N. Height to average panicle apex at end of season before harvest (Height), kg of biomass at end of season harvest (Biomass), Date when first emergent panicle observed (EM1), Date when 50% of tillers had emergent panicles (EM50), Date when 50% of tillers had panicles in anthesis (FL50), Date of first emergent tillers observed (GR1), Date when 50% of crown had emergent tillers (GR50), Date when 100% of crown

had emergent tillers (GR100). All dates logged as Julian days. Significant and suggestive LOD score alpha = 0.1 and 0.25 respectively. Significant traits shown in Bold. Average LOD score significance threshold of 4 (SD = 0.12) is shown.

3.20 References

Al-maskri, Ahmad, et al. (2014), 'Structural Features of Some Wheat (Triticum Spp.) Landraces/Cultivars Under Drought and Salt Stress', *Arid Land Research and Management,* 28 (3), 355-70.

Aschan, Guido and Pfanz, Hardy (2003), 'Non-foliar photosynthesis – a strategy of additional carbon acquisition', *Flora - Morphology, Distribution, Functional Ecology of Plants,* 198 (2), 81-97.

Bouton, Joseph H (2007), 'Molecular breeding of switchgrass for use as a biofuel crop', *Current opinion in genetics & development,* 17 (6), 553-58.

Broman, Karl W, et al. (2019), 'R/qtl2: software for mapping quantitative trait loci with high-dimensional data and multiparent populations', *Genetics,* 211 (2), 495-502.

Brown, Jack and Caligari, Peter DS (2008), 'Breeding schemes', *An Introduction to Plant Breeding*, 34-59.

Carriquiry, Miguel A, Du, Xiaodong, and Timilsina, Govinda R (2011), 'Second generation biofuels: Economics and policies', *Energy policy,* 39 (7), 4222-34.

Casler, Michael D, et al. (2007), 'Latitudinal and longitudinal adaptation of switchgrass populations', *Crop Science,* 47 (6), 2249-60.

Cernusak, Lucas A. and Cheesman, Alexander W. (2015), 'The benefits of recycling: how photosynthetic bark can increase drought tolerance', *New Phytologist,* 208 (4), 995-97.

Chen, Lei, et al. (2002), 'Lignin Deposition and Associated Changes in Anatomy, Enzyme Activity, Gene Expression, and Ruminal Degradability in Stems of Tall Fescue at Different Developmental Stages', *Journal of Agricultural and Food Chemistry,* 50 (20), 5558-65.

Chen, Weile, et al. (2021), 'The genetic basis of the root economics spectrum in a perennial grass', *Proceedings of the National Academy of Sciences,* 118 (47).

Chen, Ya-Ni, Slabaugh, Erin, and Brandizzi, Federica (2008), 'Membrane-tethered transcription factors in Arabidopsis thaliana: novel regulators in stress response and development', *Current Opinion in Plant Biology,* 11 (6), 695-701.

Christiansen, Michael W, Holm, Preben B, and Gregersen, Per L (2011), 'Characterization of barley (Hordeum vulgare L.) NAC transcription factors suggests conserved functions compared to both monocots and dicots', *BMC research notes,* 4 (1), 302.

DeMartini, Jaclyn D, et al. (2013), 'Investigating plant cell wall components that affect biomass recalcitrance in poplar and switchgrass', *Energy & Environmental Science,* 6 (3), 898-909.

Giordano, R., et al. (1978), 'Flow in xylem vessels and Poiseuille's law', *Canadian Journal of Botany,* 56 (3), 333-38.

Hager, Achim (2003), 'Role of the plasma membrane H+-ATPase in auxin-induced elongation growth: historical and new aspects', *Journal of plant research,* 116 (6), 483-505.

Hussey, Steven G, et al. (2011), 'SND2, a NAC transcription factor gene, regulates genes involved in secondary cell wall development in Arabidopsis fibres and increases fibre cell area in Eucalyptus', *BMC plant biology,* 11 (1), 1-17.

Jung, HG and Casler, MD (2006a), 'Maize stem tissues: impact of development on cell wall degradability', *Crop Science,* 46 (4), 1801-09.
--- (2006b), 'Maize Stem Tissues: Cell Wall Concentration and Composition during Development [Erratum: 2009 Nov-Dec, v. 49, no. 6, p. 2412.]'.
Lewis, Ann M and Boose, Emery R (1995), 'Estimating volume flow rates through xylem conduits', *American journal of botany,* 82 (9), 1112-16.
Lovell, John T., et al. (2021), 'Genomic mechanisms of climate adaptation in polyploid bioenergy switchgrass', *Nature,* 590 (7846), 438-44.
Lowry, David B, et al. (2019), 'QTL× environment interactions underlie adaptive divergence in switchgrass across a large latitudinal gradient', *Proceedings of the National Academy of Sciences,* 116 (26), 12933-41.
Milano, Elizabeth R, Lowry, David B, and Juenger, Thomas E (2016), 'The genetic basis of upland/lowland ecotype divergence in switchgrass (Panicum virgatum)', *G3: Genes, Genomes, Genetics,* 6 (11), 3561-70.
Mitsuda, Nobutaka, et al. (2007), 'NAC transcription factors, NST1 and NST3, are key regulators of the formation of secondary walls in woody tissues of Arabidopsis', *The Plant Cell,* 19 (1), 270-80.
Motta, Mariana Romeiro and Schnittger, Arp (2021), 'A microtubule perspective on plant cell division', *Current Biology,* 31 (10), R547-R52.
Ohashi-Ito, Kyoko, Oda, Yoshihisa, and Fukuda, Hiroo (2010), 'Arabidopsis VASCULAR-RELATED NAC-DOMAIN6 directly regulates the genes that govern programmed cell death and secondary wall formation during xylem differentiation', *The Plant Cell,* 22 (10), 3461-73.
Olsen, Addie Nina, et al. (2005), 'NAC transcription factors: structurally distinct, functionally diverse', *Trends in plant science,* 10 (2), 79-87.
Ooka, Hisako, et al. (2003), 'Comprehensive Analysis of NAC Family Genes in Oryza sativa and Arabidopsis thaliana', *DNA Research,* 10 (6), 239-47.
.
Rao, Xiaolan and Dixon, Richard A (2018), 'Current models for transcriptional regulation of secondary cell wall biosynthesis in grasses', *Frontiers in plant science,* 9, 399.
Rao, Xiaolan, et al. (2019), 'Gene regulatory networks for lignin biosynthesis in switchgrass (Panicum virgatum)', *Plant biotechnology journal,* 17 (3), 580-93.
Rasmussen, Carolyn G and Bellinger, Marschal (2018), 'An overview of plant division-plane orientation', *New Phytologist,* 219 (2), 505-12.
Sanderson, Matt A, et al. (2006), 'Switchgrass as a biofuels feedstock in the USA', *Canadian Journal of Plant Science,* 86 (Special Issue), 1315-25.
Schindelin, Johannes, et al. (2012), 'Fiji: an open-source platform for biological-image analysis', *Nature Methods,* 9, 676.
Schmer, Marty R, et al. (2008), 'Net energy of cellulosic ethanol from switchgrass', *Proceedings of the National Academy of Sciences,* 105 (2), 464-69.
Somssich, Marc, et al. (2016), 'CLAVATA-WUSCHEL signaling in the shoot meristem', *Development,* 143 (18), 3238-48.
Taiz, Lincoln, et al. (2015), *Plant physiology and development* (Sinauer Associates Incorporated).
Taylor-Teeples, Mallory, et al. (2015), 'An Arabidopsis gene regulatory network for secondary cell wall synthesis', *Nature,* 517 (7536), 571-75.

Ten Hove, Colette A and Heidstra, Renze (2008), 'Who begets whom? Plant cell fate determination by asymmetric cell division', *Current opinion in plant biology,* 11 (1), 34-41.
Townsley, Brad, Sinha, Neelima, and Kang, Julie (2013), 'KNOX1 genes regulate lignin deposition and composition in monocots and dicots', *Frontiers in Plant Science,* 4.
Tsuda, Katsutoshi, et al. (2017), 'KNOTTED1 Cofactors, BLH12 and BLH14, Regulate Internode Patterning and Vein Anastomosis in Maize', *The Plant Cell,* 29 (5), 1105-18.
Valdivia, Elene R, et al. (2013), 'Regulation of secondary wall synthesis and cell death by NAC transcription factors in the monocot Brachypodium distachyon', *Journal of experimental botany,* 64 (5), 1333-43.
Vogel, John (2008), 'Unique aspects of the grass cell wall', *Current opinion in plant biology,* 11 (3), 301-07.
Vogel, Kenneth P, Schmer, Marty R, and Mitchell, Robert B (2005), 'Plant adaptation regions: ecological and climatic classification of plant materials', *Rangeland ecology & management,* 58 (3), 315-19.
Wang, Shaogan, et al. (2019), 'Rice homeobox protein KNAT7 integrates the pathways regulating cell expansion and wall stiffness', *Plant physiology,* 181 (2), 669-82.
Wright, Lynn (2007), 'Historical perspective on how and why switchgrass was selected as a "model" high-potential energy crop', *ORNL/TM-2007/109 Oak Ridge, TN: Bioenergy Resources and Engineering Systems*.
Wullschleger, Stan D, et al. (2010), 'Biomass production in switchgrass across the United States: Database description and determinants of yield', *Agronomy Journal,* 102 (4), 1158-68.
Yamaguchi, Masatoshi, et al. (2010), 'VASCULAR-RELATED NAC-DOMAIN6 and VASCULAR-RELATED NAC-DOMAIN7 effectively induce transdifferentiation into xylem vessel elements under control of an induction system', *Plant physiology,* 153 (3), 906-14.
Yamamuro, Chizuko, et al. (2000), 'Loss of function of a rice brassinosteroid insensitive1 homolog prevents internode elongation and bending of the lamina joint', *The Plant Cell,* 12 (9), 1591-605.
Yan, Haidong, et al. (2017), 'Genome-wide survey of switchgrass NACs family provides new insights into motif and structure arrangements and reveals stress-related and tissue-specific NACs', *Scientific reports,* 7 (1), 1-15.
Yuan, Xi, et al. (2019), 'NAC transcription factors in plant immunity', *Phytopathology Research,* 1 (1), 1-13.
Zhong, Ruiqin, Demura, Taku, and Ye, Zheng-Hua (2006), 'SND1, a NAC domain transcription factor, is a key regulator of secondary wall synthesis in fibers of Arabidopsis', *The Plant Cell,* 18 (11), 3158-70.
Zhong, Ruiqin, Richardson, Elizabeth A, and Ye, Zheng-Hua (2007), 'Two NAC domain transcription factors, SND1 and NST1, function redundantly in regulation of secondary wall synthesis in fibers of Arabidopsis', *Planta,* 225 (6), 1603-11.
Zhong, Ruiqin, et al. (2011), 'Transcriptional activation of secondary wall biosynthesis by rice and maize NAC and MYB transcription factors', *Plant and Cell Physiology,* 52 (10), 1856-71.

Zhong, Ruiqin, et al. (2015), 'Functional characterization of NAC and MYB transcription factors involved in regulation of biomass production in switchgrass (Panicum virgatum)', *PLoS One,* 10 (8), e0134611.

Chapter 4: Multi-site Milling Strategy Reveals Significant Variation in Biomass Composition of a Switchgrass *(Panicum virgatum)* Clone across 17 Degrees of Latitude

David J. Thomas[1], Jason Bonnette[2], Thomas Juenger[2], Laura E. Bartley[3]

1 - University of Oklahoma

2 - The University of Texas at Austin

3 - University of Washington

Author Contributions: JB, LB, TJ, and DT conceived of and designed the study. JB coordinated and conducted sample harvest. DT conducted analyses, DT and LB wrote the manuscript.

Acknowledgements

Steve Masterson scanned the biomass at the Wheat, Sorghum and Forage Research Unit at the University of Nebraska, Lincoln, NE

ORCID IDS:
Laura Bartley: 0000-0001-8610-7551,

Keywords:
Switchgrass. Biomass milling. Near Infrared Spectroscopy.

In Preparation for submission to Bioenergy Research

4.1 Abstract

Cell wall composition influences the efficiency of conversion of biomass into fuels and chemicals. To examine the influence of environment on composition of the bioenergy grass switchgrass (*Panicum virgatum* L.), we have designed a common garden experiment for growing clones of switchgrass genotypes at ten sites from North Dakota to southern Texas. Lowland Switchgrass WBC biomass composition varies significantly under varied environmental conditions across the 17 degrees of latitude. However, analyzing biomass at multiple sites presents the potential for inconsistent biomass processing across sites, which might confound determination of environmental and genotype by environment influences on composition. We conducted two experiments to determine if milling at different locations introduces false compositional differences prior to compositional prediction with near infrared spectroscopy (NIRS). Using both forage and bioenergy quality traits and combined Wiley and Cyclone mills, five biomass composition traits were significantly different ($p<0.05$) for an individual sample Wiley milled at eight sites. When Wiley milling alone was used at each location, two to six traits varied significantly for each sample ($p<0.05$). The variation in Klason lignin content when a single sample is Wiley milled at three sites is more than the variation observed due to environment of three plants across three sites($P<0.001$). Following a standard, but labor-intensive protocol, a second milling helps to reduce variation, yet does not remove it completely. Furthermore, significant differences in 29 out of 35 of traits were detected when comparing Wiley milled to Wiley and Cyclone milled biomass of the same sample. Based on this analysis we recommend a protocol that utilizes two, sequential millings and that unlinks a specific mill from a growth location, such as by

distributing the milling of material from each site across separate mills. We utilized this approach to find that all biomass composition traits of lowland Switchgrass WBC vary significantly in clones grown across a large latitudinal range. This approach can be used to examine environmental influences on composition toward the goal of maintaining cell wall composition across environments and optimizing biomass utilization.

4.2 Introduction

Switchgrass is a perennial crop with potential to serve as a source of renewable biomass for the production of lignocellulosic biofuels and biochemicals (Youngs & Somerville, 2012). Switchgrass has also been used as a feed for grazers, restoration of rangelands, and erosion control (Nageswara-Rao et al., 2012
; Perrin et al., 2008). The wide geographical range of switchgrass from Canada to Mexico and from the Rocky Mountains east to the Atlantic coast results in phenotypic variation driven by genetic factors and local environments. Understanding the interactions between environmental selective pressures and genotypic traits of switchgrass across its range can lead to selection of feedstocks with consistent biomass yield and cell wall content that in turn produce consistent biofuel yields.

Latitude of origin and local adaptation have previously been investigated as drivers of productivity and survival with significant differences in heading date, dry matter concentration, and biomass yields. Northern latitudes have shorter growing seasons and elicit earlier heading dates while southern latitudes have longer growing seasons and frequently remain above freezing year-round. The names of upland and lowland ecotypes reflect their origin, uplands were originally found in upland habitats, adapted to hardiness zones 3-7, while lowland ecotypes originated along flood plains of southern US adapted to hardiness zones 5 through 9 (Casler et al., 2011). Growing season length and growth habit differences between ecotypes moderate biomass yield in conjunction with environmental cues. These traits in turn have a direct influence on biofuel production. Multi-site field trials establish the opportunity to explore the influence of genotype x environment (G x E) interactions on biomass yield and composition. Novel allelic combinations clonally

propagated across a latitude gradient can reveal favorable traits that are not bound by typical source population survivorship constraints. (Hartman et al., 2011) (Lowry et al., 2014)

Near Infrared Spectroscopy (NIRS) is a rapid, reliable, non-destructive, and inexpensive method to streamline cell wall composition quantification, but which can be sensitive to biomass handling differences. Milling variability could lead to artifactual NIRS-predictions of compositional differences. Currently, Wiley and cyclone mills are the standard for biomass preparation, with the same model of Wiley mill located at each of the field sites. We have investigated the effect of using different mills on NIRS compositional predictions. Our results indicate significant variation introduced by different Wiley mills in several compositional traits that are comparable to actual compositional variation due to environment. Controlling for milling location revealed the effect of environment on the composition of a single genotype of switchgrass (WBC) grown at eight locations across 17 degrees of latitude. All traits were found to vary significantly across sites ($P<0.001$).

4.3 Materials & Methods

4.4 Milling analysis of single plant biomass

Field site locations in Texas involved in both milling test phases and the harvest of WBC clones are designated Tx1, Kingsville; Tx2, Austin; Tx3, Temple to be consistent with relevant publications (Lowry et al., 2019).

Milling test phase 1 consisted of two switchgrass (*Panicum virgatum*) lowland ecotype plants (genotype A and genotype B) that were harvested from Tx2. Each plant was sorted into 30 bundles. Three bundles of each plant were sent to each of 8 different sites (Table 1). An on-site Wiley mill with 2 mm screen was used at each site to mill the bundles.

Each site produced three technical replicates of Wiley milled samples for each genotype A and B. Technical replicates were each divided in half, with half being milled a second time with a single cyclone mill through a 1 mm screen. Both fractions were then analyzed with NIRS to make predictions of the composition of the samples.

Milling test phase 2 consisted of six different clones of the WBC (lowland ecotype) selected from the Tx2 site. Thirty to fifty uniform mature tillers were harvested from each plant at full maturity during senescence; leaf sheath and leaf blades were removed to minimize heterogeneity of biomass due to variable leaf fractions of total biomass. Tillers from each plant were divided into three groups and Wiley milled with 2 mm screen at the three Texas sites (Tx1, Tx2, and Tx3), and then half of each Wiley milled sample was Cyclone Milled with 1 mm at the central Tx2 site.

4.5 Three-site field-grown biomass of clonal propagates

Biomass was harvested as described in (Milano et al., 2016) from 10 WBC clones each from Tx1 and Tx2, and 15 WBC clones from Tx3. In brief, whole plants were tied upright as a bunch and harvested with a sickle bar mower. Biomass was then processed employing the multisite milling distribution scheme as described in the results section of this work. In short, representative tillers harvested from each individual plant are separated into four equal portions. One portion is milled on site with a Wiley mill through a 2 mm screen while the other three portions are distributed as intact tillers to three other field sites for Wiley milling. Wiley milling sites were selected randomly with Kingsville (Tx1) grown WBC sent to Brookings, ND; Temple, TX (Tx3); and Pickle, TX (Tx2) sites for Wiley milling. Pickle, TX (Tx2) grown WBC was sent to Kingsville, TX (Tx1); Brookings, ND; and Temple, TX (Tx3) for Wiley milling. Temple, TX (Tx3) grown WBC was Wiley

milled at Pickle, TX (Tx2); Lincoln, NE; and Overton, KS. After Wiley milling, the four divisions of each individual WBC plant were pooled and milled a second time with a single cyclone mill with a 1 mm screen, then scanned with NIRS to predict composition. Furthermore, Supplementary Table 4.2 shows the average and standard deviation of all 49 traits of WBC across all ten sites of the 17 degrees of latitude.

4.6 Biomass composition prediction with near infrared spectroscopy

Near Infrared Spectroscopy (NIRS) is described in (Vogel, Dien, et al., 2011). Briefly, milled biomass is placed in a shallow cup and scanned with a model 6500 near-infrared spectrometer (NIRSystems, Silver Springs, MD; now FOSS NIRSystems, Inc., Laurel, MD). Two sets of trait calibration equations are applied for the NIRS analysis. The forage traits (6) are also included in the bioenergy trait list but with updated calibration equations. All NIRS datasets include the six forage traits, those same traits with the bioenergy calibration equations, and 23 additional bioenergy traits to make 35 in total (Table 4.2). Traits analytes are described in Table S4.1. After phase 1 and 2 were completed, a 10-site WBC harvest was conducted with the redistribution scheme applied. Phase 2 and the 10-site WBC analysis (Table S1) include the same traits as phase one with an additional 14 derived traits to make 49 traits in total.

4.7 Statistics

Composition trait means from samples milled at different sites were compared using multiple analysis of variance (MANOVA). Analyses of variances (ANOVA) were conducted on data sets with adequate replicates ($n \geq 3$). Tukey HSD in the package agricolae (de Mendiburu & Yaseen, 2021), was applied to identify the sites producing

significantly different composition values. Calculations conducted in R Studio version 1.1.383, R v 3.3.3 (R Development Core Team, 2022; RStudio Team (2020)).

4.8 Results and Discussion

The general assumption is that using the same make and model of mill should produce milled biomass that will show insignificant variation above the expected variance within a homogenous single source material (Vogel, Dien, et al., 2011).To investigate if biomass milling introduces variation in NIRS composition prediction consistency we harvested above ground switchgrass biomass and milled with different Wiley mills. Two sets of biomass were generated that include half of the produced biomass of both lowland genotypes A and B in phase one, with genotypes not mixed. All of the biomass harvested from both genotypes in Austin (Tx2) were milled with eight different Wiley mills at eight different field sites and half was set aside and not milled a second time (set one). The second halves from each genotype were milled a second time with a single cyclone mill. Both sets were scanned with NIRS to compare predicted composition consistency across Wiley milled vs. Wiley and Cyclone milled. The results of phase one show that NIRS predicted composition of the tiller biomass from both A and B genotypes have five significantly variable traits (Table 4.1). While concerning, we note that the compositional variation that we detected among technical replicates is on average five-fold less ($P<0.001$) than real biological biomass composition variation reported previously (Vogel, Dien, et al., 2011). Global H (GH), a measure of prediction accuracy, is also significantly different in some cases but is not a compositional trait. No trends were observed in composition variation across sites, suggesting that the problem was not caused by errors or technical

difficulties from a single site. In direct enzymatic digestibility measures, we observed no differences among sites.

To test the possibility that compositional variation might be caused by heterogeneity in the material milled with the different Wiley mills, we designed a second phase with additional efforts to precut leaves and stems segments and combined to ensured biomass homogeneity prior to milling. This phase consists of six different WBC (lowland ecotype) plants that were selected from the Tx2 site, halved, milled, and scanned as in phase one. Though most traits were invariant, we detected significant differences ($P<0.05$) with MANOVA for three traits due to Wiley milling site, even after cyclone milling (Table 4.1) in comparison to WBC clones grown at different sites. Nitrogen, carbon, and Klason lignin, varied significantly when different Wiley mills were used (Table 4.1, $P<0.05$).

The use of different Wiley mills to prepare biomass for scanning with NIRS introduces greater variability of composition prediction than actual biological variation in some compositional traits. (4.1 A) Biomass of a single plant of genotype WBC was harvested for the milling pilot and processed identically except for the first milling step where three different Wiley mills were used at Kingsville, Pickle, and Temple. The use of different mills results in significant variation in compositional predictions with NIRS that in some cases exceeds biological variation (4.1 A vs. 4.1 B) or is consistent across different mills compared to a variable trait in WBC clones (4.1 C vs 4.1 D). Milling pilot data from 2016 biomass harvest where three separate samples of clonally propagated WBC grown at three different sites represent environmentally influenced biological variation for comparison. 2016 Harvest biomass was processed according to the randomized

distribution milling described in the text. Significance determined with MANOVA ($p<0.001$) and Tukey HSD test to assign groups.

The common practice of biomass processing for NIRS analysis begins by Wiley milling through a 2 mm screen followed by a second milling with a Cyclone mill through a 1 mm screen. A report predicting wheat grain composition with NIRS shows that kernel surface texture and topography influence the spectra and suggest that scanning finely ground kernels produces more accurate predictions than intact kernels (Knight et al., 1996). Therefore, the current standard of milling biomass a second time through a smaller screen should produce the most accurate predictions of biomass composition. We evaluated whether Wiley milling alone would be sufficient as a possible time saving measure (Supplementary Table 4.2). Our results show that milling only with a Wiley mill through a 2 mm screen leads to variable NIRS composition predictions of identical biomass. The first milling test phase results show that the NIRS predicted composition values of single plant biomass milled only once with a Wiley mill (2 mm screen) are significantly different ($P < 0.05$) in an average of 29 out of 35 (82%) traits. Phase two results are less variable with 22 of 49 (44%) traits significantly different ($P < 0.05$), (Table 4.2). Therefore, Wiley milling alone was found to be insufficient for consistent predictions and would also be disadvantageous when comparing data set among researchers. After the quality check that identified variation due to Wiley mill used, we decided to investigate the genotype x environment influence on biomass composition along a large latitude gradient covering 17 degrees of latitude in the United States.

Ten common garden field sites described in Lowry et al. (2019) were established to investigate genotype by environment interactions and explore trait plasticity across 17

degrees of latitude from Texas to South Dakota. We predicted the biomass composition of WBC clones at each site harvested in 2016. All 49 biomass traits vary significantly ($P < 0.001$) in across the ten sites except Klason lignin, which was still significantly different but less so ($P < 0.05$) Table S4.2. The most significant variation ($P < 2.2$ e-16) is observed in the following traits, forage traits: IVDMD, NDF, ADF ($P<2.99$e-16); bioenergy traits: IVDMD, N, ASH, C, RHA, FUC, FETH, SUC, GLCS, and PENT. This biomass composition diversity we observed along the latitude gradient sets the stage to utilize this variability on a site-by-site basis for optimized biomass production to utilize favorable variability introduced by local growing conditions.

In summary, we found that traits predicted by NIRS varied significantly when multiple Wiley mills were used prior to spectroscopy. In some cases, the observed "technical" variation is more than real biological variation from other sets of switchgrass (Figure 4.1 A, $P<0.001$). Based on this analysis we are implementing a randomized distributed milling plan for switchgrass samples collected at each site. Mill site will be used as a covariate in gene X environment mapping to ensure that it does not bias results.

Table 4.1 | NIRS predicted composition in multiple milling treatments

Phase[a]	1	1	2	Complete[b]
Mill Type	Wiley + Cyclone	Wiley + Cyclone	Wiley + Cyclone	Wiley + Cyclone
Genotype	A	B	WBC stems	WBC
Milling Sites	7	8	3	10
Forage				
GH	2.4 (0.6)**	2.4 (0.38)**	ns	1.7 (0.5)***
ASHall	52 (3.6)**	ns	ns	43 (6)***
Bioenergy[c]				
GH	ns	10 (1.9)*	ns	6.4 (1.3)***
IVDMD	ns	ns	ns	355 (37)***
N	ns	ns	2.5 (0.42)*	7 (1.3)***
ASH	81 (6.8)*	ns	ns	89 (11)***
C	ns	ns	450 (4.6)*	433 (7.4)***
KL	ns	300 (17)*	370 (23)*	319 (39)***
RHA	ns	0.37 (0.11)**	ns	1 (0.2)***
XYL	200 (3.4)**	ns	ns	186 (8.6)***
GLC	ns	300 (6.1)*	ns	290 (7.9)***
FEST	ns	1.8 (0.15)*	ns	1 (0.3)***
FETH	0.15 (0.12)*	ns	ns	0.2 (0.5)***
FRU	ns	5 (1.8)	ns	5 (2.3)***
STA	5.5 (1.4)*	ns	ns	16 (6.5)***
Total significantly different traits	5	5	3	All

[a] Phase 1 and 2 biomass harvested from single location

[b] Biomass harvested from field grown clones

[c] Vogel et al. 2011

Reported significance refers to averages: '***' p<0.001, '**' p<0.01 , '*' p<0.05

Significant differences of biomass compositional traits predicted with NIRS. Different Wiley mills were used to mill biomass from individual plants, A and B, in phase 1. Phase 2 includes six WBC clones grown at ten sites and milled with three different Wiley mills. Data shown is the average and standard deviation in parentheses for each trait of listed genotypes. Significance determined by MANOVA. Only traits with significant differences shown, data for all traits is in Table S4.2. All Wiley mills fit with 2 mm screen, Cyclone mills with 1 mm screen. “ns” indicates comparison is not significant. All traits (mg/g) except CAL, (cal/g). Values in red are produced with previous calibration equations, all others produced with the updated calibrations.

Table 4.2 | NIRS predicted composition compared between Wiley and Wiley with Cyclone mills

Phase[a]	1	1	2
Genotype	A	B	WBC
Mill Type	Wiley only vs. Wiley + Cyclone	Wiley only vs. Wiley + Cyclone	Wiley only vs. Wiley + Cyclone
Milling Sites	7	8	3
Forage			
GH	**	*	**
IVDMD	***	*	ns
NDF	**	*	ns
ADF	*	***	ns
N	ns	*	ns
ASHall	***	***	***
Bioenergy[c]			
GH	***	**	ns
IVDMD	***	*	**
NDF	**	**	**
ADF.1	**	**	ns
ADL.1	***	ns	ns
N.1	**	**	**
DM	**	**	ns
FAT	**	*	***
ASH.1	***	*	*
C	*	ns	***
KL	***	***	***
UA	**	**	ns
RHA	***	**	***
FUC	*	**	ns
ARA	**	***	***
MAN	***	**	***
GAL	*	*	*
GLC	**	**	ns
PCA	***	***	*
FEST	**	***	**
FETH	**	**	***
SUC	**	***	*
GLCS	**	*	ns
STA	*	ns	*
ETOH	***	**	ns
PENT	*	ns	ns

HEX	ns	ns	**
SUG	ns	ns	*
CWEP	ns	ns	*
CAL	***	***	***

[a] Phase 1 and 2 biomass harvested from single location
[b] Biomass harvested from field grown clones
[c] Vogel et al. 2011
Reported significance refers to averages: '***' p<0.001, '**' p<0.01 , '*' p<0.05
Significant differences of NIRS predictions of biomass milled only with a Wiley mill (2 mm screen) vs. predictions of the same biomass after being milled a second time with a Cyclone mill (1 mm screen). Maximum significance of all the sites within each pilot is reported. Significance determined with Student's T test. All Wiley mills fit with 2 mm screen, Cyclone mills with 1 mm screen. "ns" indicates comparison is not significant. All traits (mg/g) except CAL, (cal/g).

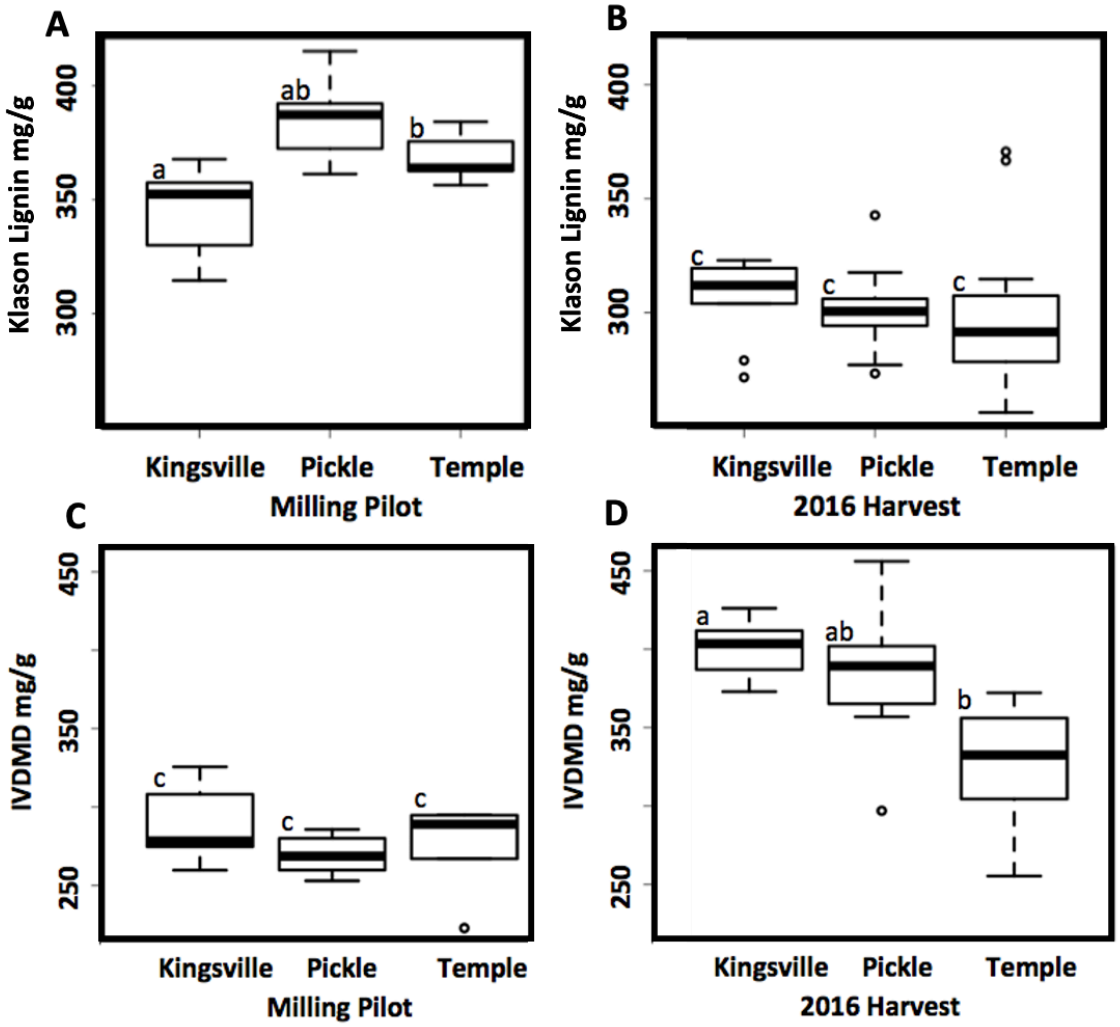

Figure 4.1. Single plant Klason lignin variation due to different Wiley mills exceeds clonal propagate variation when grown across same milling site. The use of different Wiley mills to prepare biomass for scanning with NIRS introduces greater variability of composition prediction than actual biological variation in some compositional traits. (A) Biomass of a single plant of genotype WBC was harvested for the milling pilot and processed identically except for the first milling step where three different Wiley mills were used at Kingsville, Pickle, and Temple. The use of different mills results in significant variation in compositional predictions with NIRS that in some cases exceeds biological variation (A vs. B) or is consistent across different mills compared to a variable trait in WBC clones (C vs D). Milling pilot data from 2016 biomass harvest where three separate samples of clonally propagated WBC grown at three different sites represent environmentally influenced biological variation for comparison. 2016 Harvest biomass was processed according to the randomized distribution milling described in the text. Significance determined with MANOVA ($p<0.001$) and Tukey HSD test to assign groups.

4.9 References

.
Casler, Michael D, et al. (2011), 'The switchgrass genome: tools and strategies', *The Plant Genome,* 4 (3), 273-82.
Hartman, Jeffrey C, et al. (2011), 'Potential ecological impacts of switchgrass (Panicum virgatum L.) biofuel cultivation in the Central Great Plains, USA', *biomass and bioenergy,* 35 (8), 3415-21.
Knight, James B, et al. (1996), 'Experimental study of granular convection', *Physical Review E,* 54 (5), 5726.
Lowry, David B, et al. (2014), 'Adaptations between ecotypes and along environmental gradients in Panicum virgatum', *The American Naturalist,* 183 (5), 682-92.
Lowry, David B, et al. (2019), 'QTL× environment interactions underlie adaptive divergence in switchgrass across a large latitudinal gradient', *Proceedings of the National Academy of Sciences,* 116 (26), 12933-41.
Milano, Elizabeth R, Lowry, David B, and Juenger, Thomas E (2016), 'The genetic basis of upland/lowland ecotype divergence in switchgrass (Panicum virgatum)', *G3: Genes, Genomes, Genetics,* 6 (11), 3561-70.
Nageswara-Rao, Madhugiri, Stewart, C Neal, and Kwit, Charles (2012
), 'Genetic diversity and structure of natural and agronomic switchgrass (Panicum virgatum L.) populations', *Genetic resources and crop evolution,* 60 (3), 1057-68.
Perrin, Richard, et al. (2008), 'Farm-scale production cost of switchgrass for biomass', *BioEnergy Research,* 1 (1), 91-97.
.
Vogel, Kenneth P, et al. (2010), 'Quantifying actual and theoretical ethanol yields for switchgrass strains using NIRS analyses', *BioEnergy Research,* 4 (2), 96-110.
--- (2011), 'Quantifying actual and theoretical ethanol yields for switchgrass strains using NIRS analyses', *BioEnergy Research,* 4 (2), 96-110.
Youngs, Heather and Somerville, Chris (2012), 'Development of feedstocks for cellulosic biofuels', *F1000 biology reports,* 4.

Chapter 5: 3D-Printed Handheld Microtome for High Quality and Rapid Plant Sectioning: A Time and Cost Improvement Over Hand Sectioning and Traditional Microtomes.

David J. Thomas[1], Laura E. Bartley[2]

1- University of Oklahoma

2- University of Washington

Publication Status: This chapter is in preparation to be submitted for publication in BMC Plant Methods.

Authors Contributions: DT designed the Rapid-Tome. DT and LEB wrote the manuscript.

Acknowledgements

Bobby Reed at the Innovation @ the EDGE at the OU Bizzell Memorial Library for making this project possible due to the numerous print iterations I went through until the final design was reached.

Keywords: Plant Sectioning, Microscopy, Plant Anatomy, 3D-Printing

5.1 Abstract

Microscopic analysis of plant anatomy is a common procedure in plant biology that requires high quality sections. Decent quality sections can be achieved with hand sectioning of certain specimens, though is typically limited to mostly soft-tissue, or freshly harvested samples. Described herein is a hand sectioning method that is effective with field grown herbaceous stems but is sub-optimal for plant samples that have undergone secondary growth (wood production) or cell wall reinforcement (lignification). To section woody and lignified stems, benchtop microtomes can produce extremely thin sections (<100 microns) and have been commonplace in labs for many decades. However, these instruments often require a lengthy process of resin or wax imbedding to achieve the quality of section required for analysis, are time consuming to set up, possess a steep learning curve, and in many cases are prohibitively expensive. The progression of additive manufacturing technology and the decreasing cost of such machines makes 3D printing an effective alternative to create new low-cost microtomes. Here I present a novel microtome design that can be printed in less than 12 hours on any high-quality 3D printer common at most major university maker spaces. The "Rapid-tome" is specifically designed to effectively section hollow materials such as switchgrass (*Panicum virgatum*) and can handle a woody 5 mm thick branch of *Juniper virginiana*. This microtome features rapid sample change, rapid sample advancement, rapid blade change, and rapid sectioning. Additionally, assembly of the Rapid-Tome can be done in under a minute and only requires five non-printed metal parts found at any hardware store.

5.2 Introduction

Plant anatomy is a wondrous micro verse to explore that is rich with information about botanical form and function. The numerous cell types and the complex cellular structures contained within plants are easily visible under a microscope, even at low magnification. The variable characteristics across cell types such as cell wall thickness increase the strength of the cells as well as the energy required to section those tissues. Section integrity is the most impactful variable towards obtaining high-quality images, and therefore, high accuracy measurements at the image analysis stage (Chen et al., 2016). Section thickness is a major constraint for microanalysis with a transmitted light microscope.

Plant anatomy provides a great deal on insight about plants in terms of development and function, but high-quality sections are needed that require reliable and accessible tools to produce those sections. Individual cell traits, i.e. dimensions or cell wall thickness, can provide insight into the functional performance of different cell types easily measured in sectioned plant tissues. To accurately measure these traits, sections that are flat, consistent thickness, and thin enough to place on a microscope slide are required. The tools to produce these high-quality sections must be accurate and accessible to ensure that accurate analyses of plant anatomy can be achieved.

Several factors that primarily determine section quality are the characteristics of the plant material being sectioned, the tool used to section. The hardness and thickness of the material, i.e. a thin leaf or young root compared to a lignified grass stem or woody twig, determine the best approach for sectioning and the degree of difficulty of obtaining thin, high quality sections. Heterogeneous plant parts include extremely rigid, sclerenchymatic

cells of vascular bundles and interfasicular fibers that occur together with softer cell with less cell wall accumulation (Barbosa et al., 2010). Sample preparation can take several days for microscopic analysis due to sample preparation requirements (Soukup & Tylová, 2019). Soft tissues such as young roots can be hand sectioned or gently embedded in 3% agarose and easily sectioned through with a vibratome. Hand sectioning and vibratome sectioning can both be done the same day as sampling. Conversely, tough stems are harder to section thinly and require great control over the advancement of the sample and blade advancement. Embedding materials commonly used for plant materials includes paraffin wax (Takahashi et al., 2010), and HistoResin which is commonly used for botanical studies but is limited to rather small block and inhibits the analysis of large plant sections (Bancroft & Gamble, 2008; Kiernan, 1999; Shimotsuma & Schoefl, 1992). Resin embedded samples can be tightly clamped into place and sectioned with a benchtop microtome. A major drawback with this process is that embedding in resin or wax requires the samples to be dehydrated first. The dehydration process greatly influences the success of resin infiltration, which determines the quality of the sections obtained. Thick samples and those with highly dense and numerous cells take longer to completely dehydrate as well as infiltrate with resin. Determining the required length of dehydration with ethanol and time to achieve resin infiltration can often require pilot investigations and multiple trials. Additionally, the duration of these steps may in fact be on the order of days, or even weeks. In these ways, the sample type determines, the sectioning tool best suited for the job, if embedding is required embedding medium, and the duration of sample preparation.

There are several options for producing plant sections that range in cost and learning curves required (Table 5.1). Hand sectioning with only a razor blade requires the

least amount of investment but does come with disadvantages, while benchtop microtomes can be several thousand dollars and can require extensive sample preparation. Hand sectioning is perhaps the easiest approach but doesn't handle tough tissues like abundant fibers or woody stems very well, which reduces section quality. There is also a steep learning curve and the consistency in section thickness is extremely variable and can vary widely among researchers. Still, hand sectioning is a very valuable method for early investigations and softer tissues. Benchtop microtomes typically require sample embedding and the hardness of the embedding material depends on the many factors from tissue hardness to the thickness of section desired or required by different types of microscopy. Our purposes are focused on light microscopy and so our discussion is limited to preparation for such analyses.

5.3 Results

The most common approach to sectioning fresh tissue in classrooms and the laboratory setting is to use hand sectioning. Interestingly, currently available literature on hand sectioning methods is lacking and in need of an update. Here we present a detailed hand sectioned method that is highly effective with fresh and soft tissues. However, when sectioning harder samples that are highly lignified or woody, the hand sectioning method is not applicable. To solve this, we present a novel hand-held microtome that can produce high-quality sections even in the hands of a novice.

The hand sectioning method is described in detail in Figures 5.1 and 5.2. Figure S5.1 shows the approach to section hollow stems if it collapses. These figures depict sectioning a switchgrass internode. Figure 5.3 shows the quality of section that this described hand sectioning method can produce (A and B). Both images are less than a

single cell thick (< 100 μm) and exceed the quality required to accurately measure anatomical traits as desired. However, tougher sections that contain more lignin in the sclerenchyma fibers prove difficult to hand section and often break apart and structural integrity is lost (Figure 5.3 C). Furthermore, the tough material in the sclerenchyma is often marked with chatter marks from the blade making inconsistent contact (Figure 5.3 D, black arrowheads), and in some cases will cause the tissue to break (Figure 5.3 D, white arrowhead).

After several rounds of prototypes and design iterations, the final models were completed and printed for testing (Figure S5.2 and S5.3). Figure 5.4 displays the assembly process and is discussed further in the results. An additional method for achieving longitudinal sections is shown in Figure S5.4 that utilizes a carrot to hold the sample in place while sectioning with the Rapid-Tome. The critical points of the design are the blade clamp and angle of the stage that holds the blade in a flexed and rigid position. Because of the flexed position, the cutting edge of the blade is held flat and produces sections with consistent thickness every time. This is especially important in tougher samples and when compared to hand sectioning. The blade must be held in a rigid and flexed fashion so that the blade does not travel upward into the z axis that results in thicker sections and a cover slip that does not make consistent contact with the section. Also, wedge-shaped sections present an inconsistent focal plane and prevent large field of view to be in focus at low magnification.

When hand sectioning tougher samples such as large and fibrous switchgrass internodes or woody branches of eastern red cedar, control of the blade is difficult to maintain which results in poor section quality and inconsistent section thickness. Because

the blade is clamped, flexed, and held in place by the sled, the researcher has more control over blade advancement and can proceed slowly and safely. Additionally, the sled and blade clamp keep the researchers fingers away from the sharp razor and completely prevents the possibility of injury even if the sample slips and the blade quickly advances. To demonstrate the utility of the Rapid-Tome, a variety of sample types were sectioned including switchgrass internodes and roots (Figures 5.5 and S5.5, respectively), and small branches from Eastern Red Cedar (*Juniperus virginiana)* and American Sycamore (*Plantanus occidentalis)* (Figures. 5.6 and S5.6, respectively).

5.4 Discussion

Several recent studies utilized 3D-printing to enhance plant tissue sectioning methods. Other analyses have recently explored the use of 3D-printing to increase the throughput of plant tissue sectioning (Atkinson & Wells, 2017). Atkinson et al. created a 3D-printed embedding mold to embed plant roots in agarose for sectioning but is not applicable for harder tissues. Another group created a 3d -printed sectioning tool to simply produce sections of plant material but has not sample advancement mechanism to control section thickness (Giannini, 2017) .

I set out to design a microtome that accomplishes 5 main goals: 1) section hollow stems without crushing 2) Quick sample change out, 3) portability, 4) use disposable razor blades, and 5) utilize low cost and sharable design of 3D printing. The hand sectioning method is described in detail in Figures 5.1 and 5.2. Figure 5.3 shows the approach to section hollow stems if it collapses. Though the hand sectioning method works well with softer samples and fresh tissues, the novel microtome produces sections that are high quality across several different bases for comparison. My goal is to produce sections that

are very thin with consistent thickness and cut edge quality. The sample can be swapped out with ease and is held in place by the thumb of the researcher. The blade advances at an angle so that the hollow grass stems are not crushed. The blade can quickly and easily be replaced when dulled. Furthermore, utilizing 3D printing and easily available nuts and bolts requires only an email to share the print files. The parts are printed and then assembled with machine screws.

This microtome is both low-cost and low stress. There is also the added safety concern of hand sectioning that comes from handling sharp razor blades very close to the researcher's own fingertips. The Rapid-Tome, if used properly with attached blade guard, completely removes the danger of cutting oneself. A major benefit of the simple design and ability to download it increases the accessibility to using such a tool. A prominent aspect of the rationale behind the design of this microtome is that it is low-cost and easy to use. That means that even primary schools in districts with smaller budgets can purchase a printed microtome and easily produce sections far superior to risky hand sectioning that requires hours of practice. The cost to make one of these microtomes, including the additional parts that are metal and must be purchased, is still less than $20. The low cost allows for more young people to explore the incredible micro verse that awaits them. Furthermore, the portability of this microtome is compatible with field sampling to section on site with no need to carry large sampling materials and equipment.

The sectioning materials that can be cut with the hand section method are also limited by toughness and hardness. The hand sectioning method described herein is an improvement over available information and protocols. Achieving sections of woody stems up to 5 mm in diameter are easily accomplished with the Rapid-Tome. Accomplishing

quality hand sections of woody tissue is not so easily achieved. Yet with the Rapid-Tome performs very well to section harder tissues, produce sections of consistent high quality, and can be used to target specific sample features like lateral roots.

5.5 Methods

5.6 Plant material and collection

Switchgrass internodes were collected from field grown plants in 2018 from Columbia , Missouri. Additional switchgrass samples for root sectioning and imaging were harvested from greenhouse grown plants under stable, well-watered conditions. Juniper and sycamore were harvested from the University of Oklahoma campus in Norman, Oklahoma.

5.7 Hand Sectioning Method for Hollow-Stemmed Grasses

This document describes sectioning fresh and or hydrated plant samples. There are several key points to consider when hand section plant materials: Always use new blades that are rust free and have been stored in a dry place. When sectioning, balance your arms by resting your elbows on table surface or against your body. Keep your hands together and take five or more sections without separating your hands. Every time you separate your hands, you have to reset and dial it back in. Do not use a chopping motion. Slice the stem by utilizing the length of the blade. Catch sections with a water droplet resting on top of the blade. Take approximately 2x the number of sections you need. Samples will not section well if allowed to partially dry out and will likely bend or collapse while attempting to section them. If partially dried, rehydrate in distilled water or 50% ethanol and distilled water overnight. Following these rules will produce the best possible sections for the material. Below is a more detailed description of this approach.

It is important to balance your hands by resting your elbows on a table surface or forearms against the table's edge, or against your body. Always use a fresh razorblade. We use PTFE coated single edge blades made by GEM, available from Electron Microscopy Supply (item #71970). It makes a big difference which blades are used; others may work but these are superior. The silica content in grass stems dulls the cutting edge rather quickly. If the blade doesn't cut well, use a fresh blade. I typically use a new blade for each new stem or after cutting about 10-20 sections. It is also possible to reorient the blade in your hands to use a different part of the blade when switching to a new sample or if sectioning is poor. It is also important to make an initial cut a few mm away from the exact place you want to get sections from, then section your way to it. The initial cut must be perpendicular to the length of the stem and can be made with the stem lying horizontal on a lab bench or cutting mat. I use a different blade to make the first cut that I use for multiple stems (can also use hand shears as in Figure 5.1 E), but always use a fresh new blade for each stem to cut the thin sections. It is important to hold the stem firmly vertical and make a horizontal cutting motion to ensure a flat section is taken. If the stem is not vertical or the blade is not held horizontal the section will likely be wedge shaped which interferes with consistent focus in the field of view when imaging. This is not as much of an issue with small diameter stems or if cell dimension measurements are not desired. Oblique or wedge-shaped sections will exaggerate the cell lumen area if the blade is not perpendicular to the length of the stem.

It is important to use the length of the blade rather than a chopping motion to prevent the hollow stem from collapsing. When sectioning a 3 mm diameter stem, approximately 1cm of the cutting edge of the blade is used, to utilize the blade length. This

sectioning approach is similar to slicing bread rather than chopping carrots. The bread will compress and smash if a chopping motion is attempted, similar to a hollow stem that will likely collapse. However, if the length of the blade is used and a slicing motion is applied, the bread will keep its shape and can be cleanly sliced, much like the stem. The first section will be too thick and will be discarded. This is also when corrections to the angle of the first cut can be made by making sure that subsequent cuts are perpendicular to the length of the stem.

5.8 Holding the blade

The blade is held in your dominant hand between the middle finger and thumb with the blade facing toward you and the length of the blade parallel to the blade holding thumb (Figure 5.1 A and B). The blade is held firmly and horizontally by the dominant hand with the broadside of the blade pressed firmly downward against the index fingertip holding the stem. The primary movement of the blade comes from the tip of the index finger holding the stem, bending back and forth to advance the blade horizontally to cut the section (Figure 5.1 C and D; 5.2 C and D).

5.9 Holding the stem

If possible, the length of the stem to be sectioned from can cut to length to help with holding the stem steady. The length will be different depending on the size of the sectioner's hands. The length can be from the tip of the index finger to the base of the thumb (Figure 5.1 E). This way the opposite end of the stem can rest against the palm while being held by the tips of the thumb and index finger with the index finger slightly above the tip of the thumb (Figure 5.1 F and G).

5.10 Hand sectioning

When sectioning, the blade moves forward through the stem with the movement of the index fingertip. The dominant hand index finger holding the blade also applies enough pressure to slightly rotate the blade (~15º) with the pivot point between the dominant hand thumb and middle finger (Figure 5.2 A and B). The key is to make multiple sections (5-10) without separating your hands from each other. This is to keep the vertical separation of the blade and the cutting surface in as consistent proximity as possible. Holding the blade so that it is resting on top of the cut surface, slightly apply downward pressure (held in balance against opposing pressure of the index fingertip that is holding the stem) and pull the blade backwards so the cutting edge just barely drops off the side of the stem. The downward pressure should be just slightly more than the upward pressure so that the blade height moves down just a tiny bit after reaching the edge of the stem's cut surface. This is to zero in on the level at which the last section was taken and to orient where to cut the next section. This is a key movement to get very thin sections (< 100 μm) and takes practice.

To expose more stem to section without taking your hands apart, advance the stem upwards very slightly by bending backwards the thumb that holds the stem in between bending the index fingertip back and forth (Figure 5.2 E and F). The first cut or two just get the cutting surface of the stem situated in the right place relative to your hands. The best sections will be the ~3rd or later. Move the stem upwards ever so slightly by rocking your thumb slightly backwards after each cut. Plan to cut about twice the number of sections that are needed.

It is important to keep the sample wet and hydrated during sectioning, touch the end that is being sectioned to water after the initial cut and after ~10 sections are taken. Dip the cutting edge of the blade into water so a few ul are resting on the cutting edge where the sections will be. The water droplet helps lubricate the cut and catch the sections. The wet sections will also more readily stick to the blade if they miss the water droplet. Once 5-10 sections are taken without separating your hands, collect the sections with forceps or dunking the blade into water to "wash" them off into a shallow vessel or petri dish.

5.11 The Rapid-Tome 3D-printed hand-held microtome

5.12 Assembly instructions

Remove all supports and brims, etc. Install advancement screw: place one of the nuts over the screw about 5 mm, (Figure 5.4 A), and slide into the opening at the base of the handle. With a screwdriver, turn the screw until the end reaches the other side of the hexagonal seat on the bottom of the handle (Figure 5.4 B). Place a nut into the base of the handle and turn the screw into it. If the nut is not flush with the base of the handle, (Figure 5.4 C), back the screw out of it, lift the nut out carefully and rotate 180 degrees and put back into the seat for the nut. This rotates the bite point for the screw within the nut so that the nut should be held flush with the bottom of the handle (Figure 5.4 D). The screw should not have any play or rattle around. In other words, the two nuts should both be firm against and sandwiching the bas of the handle. This is crucial to insure proper control on slider and sample advancement during sectioning.

After advancing the screw 1 cm through the bottom of the handle, attached the drawer knob and firmly tighten the screw all the way into the knob. Place a slider into the

slider groove (Figure 5.4 E). Note: multiple sliders can be stacked according to the length of the sample segment or if a shorter advancement screw is used. Alternatively, if longitudinal sections are desired, stack the longitudinal section slider on top of the slider (Figure 5.4 F). Line up the pegs on the top of the handle with the holes on the underside of the stage, thread the screw into the opening through the stage, place nut over the screw on the back of the handle and tighten down firmly (Figure 5.4 G). Install the ½ inch washer by simply pressing into place. Alternatively, if the washer does not stay put, use a small amount of JB weld epoxy (Figure 5.4 I), to hold it in place. Apply the weather stripping to the blade clamp (Figure 5.4 K).

Insert the printed nut into the slot on the back of the sled, (Figure 5.4 L). Place the printed washer over the screw and thread it through the blade clamp. Place a razor blade into the sled ensuring the notches in the blade fit around the tabs in the sides of the blade bed (Figure 5.4 L). Attached the blade clamp and tighten down as far as possible with the printed screw, (approx. 2.5 turns) (Figure 5.4 M). Install the blade guard by placing the tip of the guard into the slot beneath the Rapid-Tome label, then press the squared column into the opening on the top of the sled (Figure 5.4 N, H, J).

When ready to section, remove the blade guard by pulling the squared grip indention. Place the blade guard into the holster, slight bending is required to ensure it stays in place. Insert the tip first, then press the squared column downward into place. Slide the sled onto the stage nearly halfway. The blade may need to be gently pushed from beneath to clear the front edge of the washer the first time the blade is used.

5.13 Sectioning

5.14 Cross sectioning of cylindrical samples:

Cut the sample to length before using the Rapid-Tome. This can be done with shears or a razor blade on bench top. For right-handed people: Place the segment into the groove and firmly hold with your left-hand thumb against the back of the handle. Turn the advancement knob with your right hand to make the top of the segment just above the surface of the washer. Note: the sample must be firmly against the back of the handle groove. Woody twigs that are not completely straight will need to be rotated until firmly against the back wall that is required for a clean cut. If this is not followed, the section will not fully cut from the sample segment and the sample will likely split. To help with this for grasses, 2 wraps of stretched parafilm help to prevent splitting as well as crushing. With right hand, place your thumb on the front of the sled and your forefinger on the back of the stage. The left-hand forefinger is used to push the sled back to the start position.

Make the first cut by sliding the sled forward by pressing your thumb and forefinger together. Remove section with tweezers and immediately place into water. If using the optional section catcher, flick sections into the catcher with a small paintbrush or forceps. Catcher should contain some drops of water to prevent samples from drying out.

Turn the advancement knob 180 degrees. The amount rotated can be adjusted according to your sample and desired section thickness. Advance the sled again toward your sample. Note: do not move the sample in any way in between sections, other than by the advancement screw. If the blade is dulled or bends and catches on the washer as can happen with tough samples, keep hold of the sample in the handle with your left hand, using only your right hand to unscrew the blade clamp and replace with a new blade.

5.15 Longitudinal sectioning of cylindrical samples:

The longitudinal slider must be installed as described above. The sample must be trimmed to 1 cm in length. Place the sample with the v groove on the slider. Take sections as above with the following exceptions. The downward angle of the blade holds the sample in place as it cuts. However, blunt tip forceps to press downward on the sample to keep it in place are useful. An alternative approach to achieve longitudinal sections is to use a carrot to quickly support the tissue (Figure S5.4). This approach is an adaptation of a tried-and-true approach that utilizes the structural integrity and cutability of the widely available root vegetable. For this approach, a hole is first cut through the carrot perpendicular to its long axis with a drill bit that matches the diameter of the plant tissue or is slightly smaller (Figure S5.4 A and B). The stem segment in this example is the soft tissue of an Alocasia sp. which has been pushed through the cut hole of the carrot, which is then trimmed to fit through the opening in the stage of the Rapid-Tome (Figure S5.4 C and D). Figure S5.4 E shows a partially sectioned carrot with stem segment intact and the "grip" that the carrot has that secures the alocasia stem in place while sectioning. A thin longitudinal section with visible vascular bundle fibers between the dark epidermis (Figure S5.4 F).

5.16 Important sectioning tips:

Hold the sample in place and take 5 – 10 sections at a time without removing your hands or resituating the sample (other than vertical advancement). This is to help get the best sections possible. Apply spray on PTFE dry coating lubrication to the contact points on the left and right edges of the stage (Figure 5.4 G), and within the C-shaped grooves of the sled (Figure 5.4 O).

5.17 Staining

Acriflavine hydrochloride was used in Figure 5.3. Crystal violet was used on the Juniper sections Toluidine blue O was used for the switchgrass roots in Figure S5.5.

5.18 Image collection

All microscopy completed on a Nikon Eclipse Ni microscope and a Nikon Ds-Qi1Mc camera. Scale bar applied in FIJI (Schindelin et al., 2012).

5.19 Printing instructions with PLA filament

Print all parts in provided orientation for optimal quality. The recommend setting for the filament extruder resolution to be high detail. We had great success with 0.14 mm layers on a TAZ 6 Lulzbot. On a Snapmaker 2.0 the dimensions were precise with a layer height of 0.24 mm. These are simply the default printer setting for “high detail” and “normal fast print”, respectively. The exact settings required will vary from printer to printer. The default “high quality” setting for any printer should be adequate, though may not be needed.

To test the quality capable at each setting for a printer, start by printing the nut and blade clamp screw. These parts require the highest accuracy and will serve as an accuracy test. The setting at which these parts can accurately be printed and tightly fit together is the max detail needed. Furthermore, these parts are relatively small and can be printed in just a few hours or less. Infill for the “stage” and “blade clamp” are ~30%. All other parts should be printed no less than 15% infill. Add brims to all parts, though a raft would be effective as well if desired but adds a bit more print time. Make sure to add supports to all overhangs with at least 20% infill.

Table 5.1 | Microtome Comparison

Method	Section quality and accuracy [a]	Benchtop required?	Additional Materials	Sample preparation	Learning curve	Portable	Shareability	Cost	Weight
Hand sectioning									
Chopping on bench	• Medium • Poor	Yes	Razor blades	None	< 15 minutes	No	protocol by email	$	/
Dave's Hand sectioning method	• High • High	No	• Razor blades • Parafilm	None	Medium - high	Semi	protocol by email	$	/
Microtomes									
Hand microtomes	• High • High	Depends on model		Cut to size to fit clamps	Medium	Semi	In person only	$$	
Benchtop microtomes	• High • High	Yes	• Embedding materials and equipment • May require electricity	Requires multiple days to embed material	Medium - high	No	In person only	$$$$	~30 lbs
Vibratome	• High • Medium	Yes	• Embedding materials and equipment • Electrical outlet	Requires hours - days to embed material	Medium - high	No	In person only	$$$$	~30 lbs
Rapid-Tome	• High • High	No	• Access to 3D-printer • Razor blades • Nuts and bolts • Teflon dry lube • Adhesive foam strip	None	< 15 minutes	Field capable	3D print files and protocol by email	$	< 1 lb

a- Accuracy is defined as the ability to target and produce sections of a specific region if interest

Table 5.2 | Metal parts list for Rapid-Tome

Part	# Required	Description
Bolt (A)	1	Machine screw #8-32 x 1.5 inch
Nut (A)	1	Nut #8-32
Advancement Screw	1	Machine screw #8-32 x 4 inch
Advancement nut	2	Nut #8-32
Drawer pull knob	1	Large diameter and flat, must fit #8-32 machine screw
Washer	1	Stainless steel ½ inch flat washer.
Self adhesive High density weather strip	1 x .25 inch strip	Cut to size from: Duck Brand Foam Weatherstrip Seal for Small Gaps (found at Walmart), must be dense foam
Razor blades	Box of 100	Single Edge, GEM "PTFE" Coated #71970 https://www.emsdiasum.com/microscopy/products/preparation/blades.aspx#71970
Blaster Advanced Dry Lube with Teflon	1 can	Widely available. Model # 16-TDL

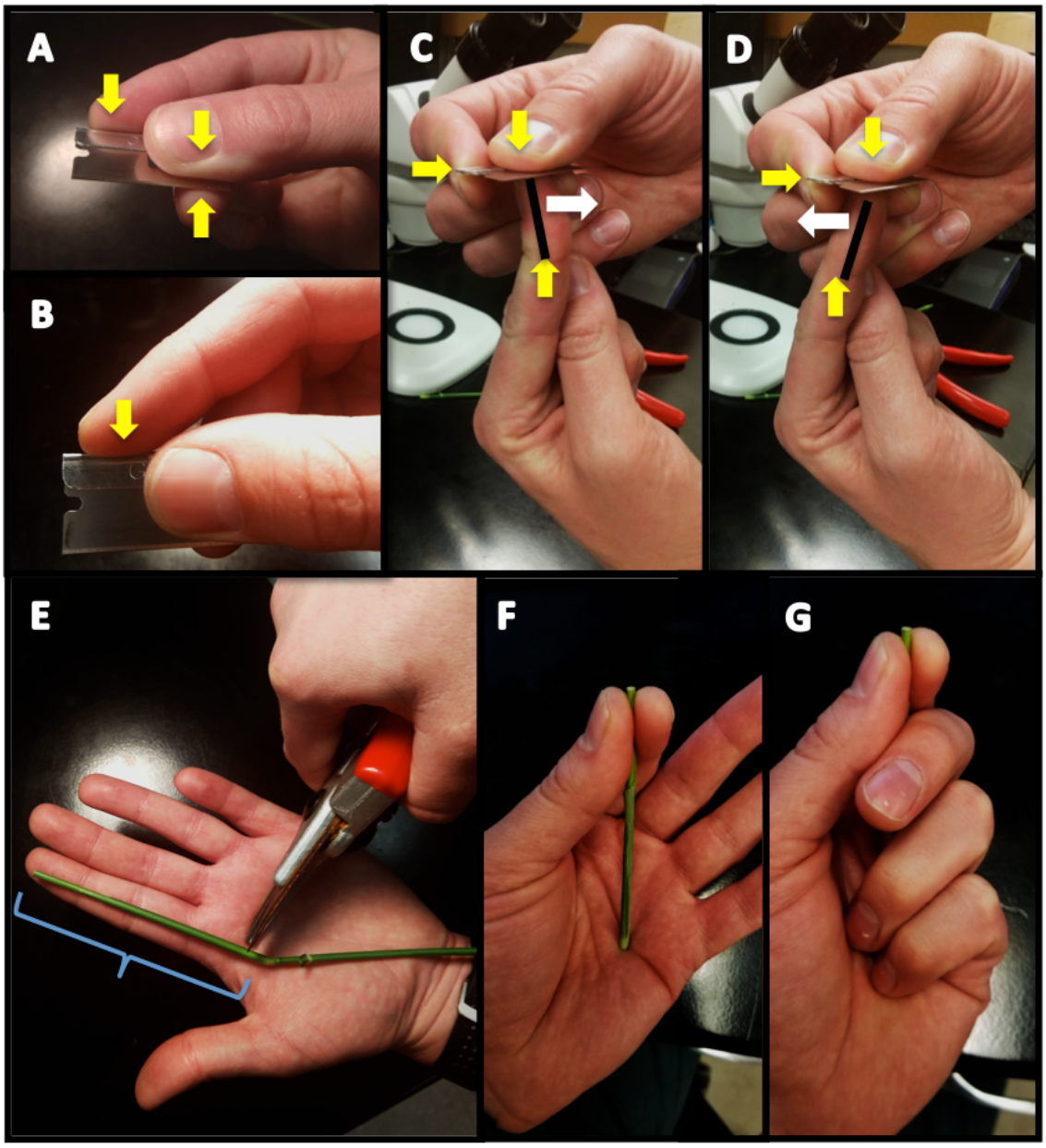

Figure 5.1. How to hold the blade and the stem. (A and B) Yellow arrows represent static pressure applied by fingers to hold the blade firmly in place. (C and D) White arrows represent finger movements. Black bars (C and D) represent the orientation of the finger before and after pivoting. (E) cut the stem segment to length to match the size of the sectioner's hand as shown. (F) the stem is held between the thumb and forefinger and pressed into the palm gently to further stabilize in the non-dominant hand. (G) shows the closed fingers around the stem.

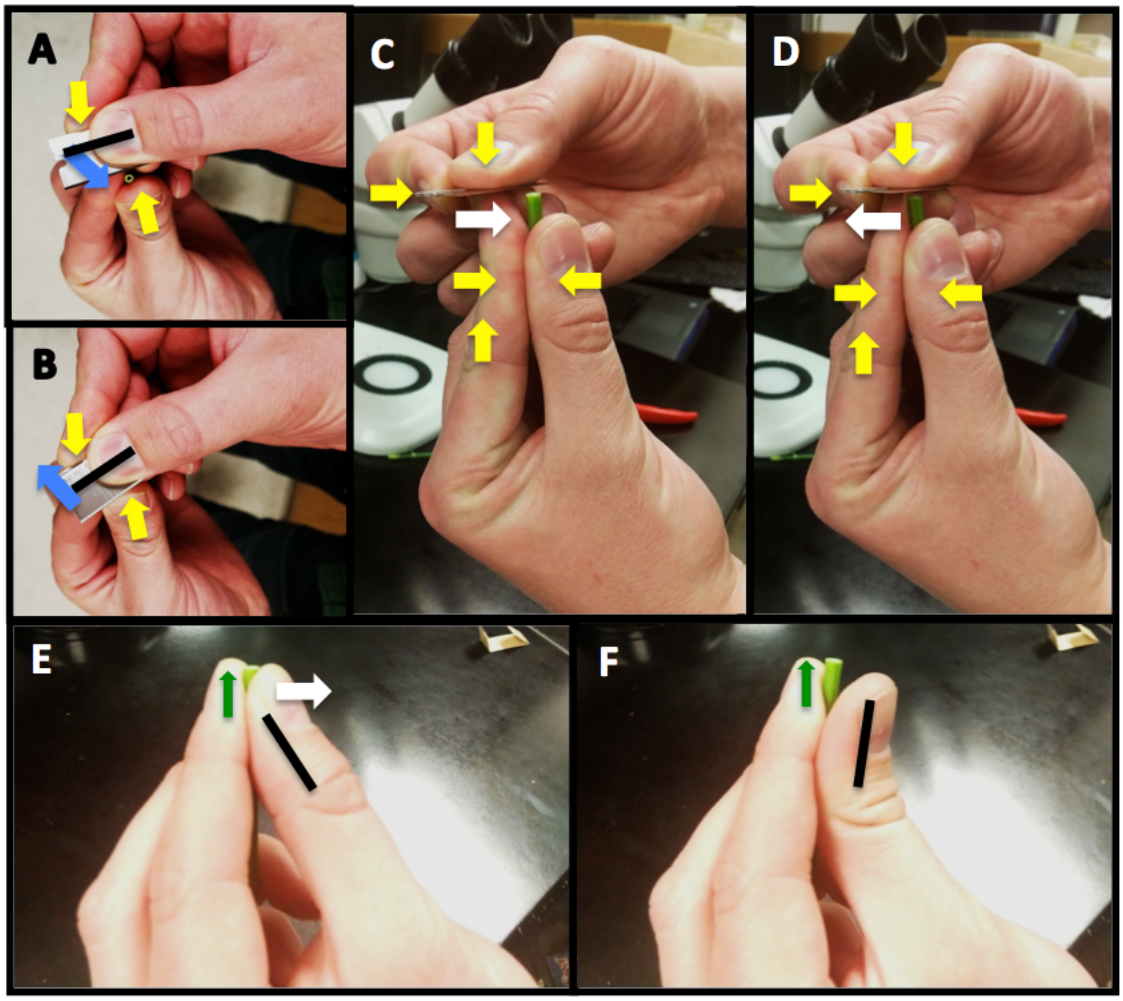

Figure 5.2. Sectioning the stem with the hand sectioning method. Yellow arrows represent static pressure applied by fingers to hold the blade and stem firmly in place. White arrows represent finger movements. (A) Blue arrow represents blade movement. Green arrow (E and F) represents stem movement upwards. Black bars (E and F) represent the orientation of the finger or blade before and after pivoting (A, B, E, F).

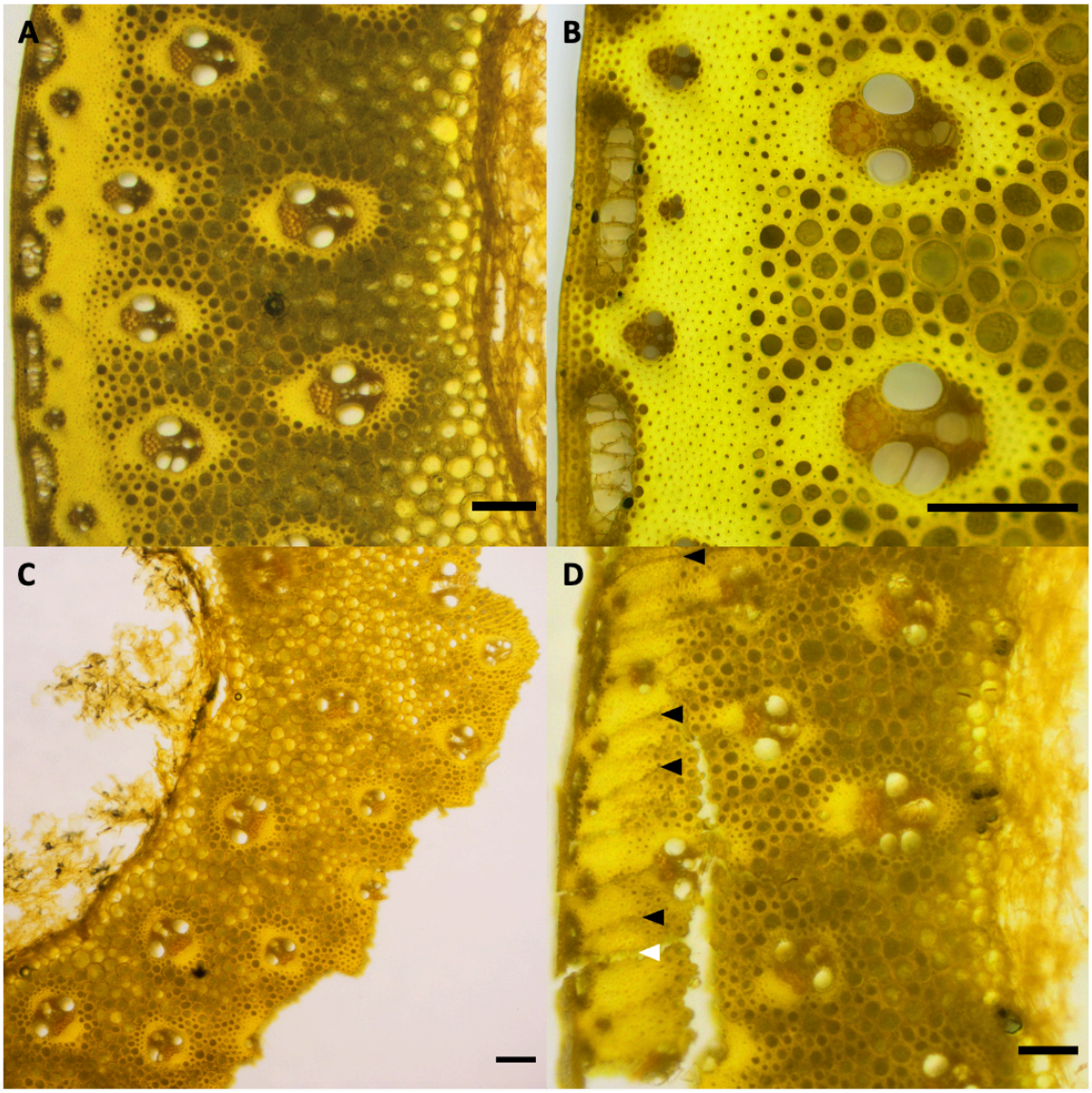

Figure 5.3. The hardness of the plant material reduces the quality of sections possible with the hand sectioning method. Adequate quality for image analysis is shown in (A & B), with individual cells distinguishable in B. (C and D) Tougher samples are not able to be sectioned well with the hand sectioning method and often produce cut artifacts where the sample is pulled apart when the tough sclerenchyma contacts the blade. Furthermore, blade chatter marked with arrowhead in (D) will interfere with image analysis, produces uneven section thickness that causes uneven focal planes, and in some cases causes a full break in the sample (white arrowhead). All scale bars are 100 microns. Samples are switchgrass internode cross sections stained with acriflavine hydrochloride.

Figure 5.4. Assembly of the Rapid-Tome. (A-D) The advancement bolt is installed first. (E-G) The slider is placed within the grooves of the handle before the stage is attached. Optional longitudinal slider (white) is shown in (F) that can be stacked on top of a slider. (H-J) The washer and blade guard are attached. The blade clamp (K) is crucial and holds the blade in place (L-N). Sliding the sled into place over the stage against the inclined washer flexes the blade and ensures a flat cut is made. All plastic parts are 3-D printed with PLA.

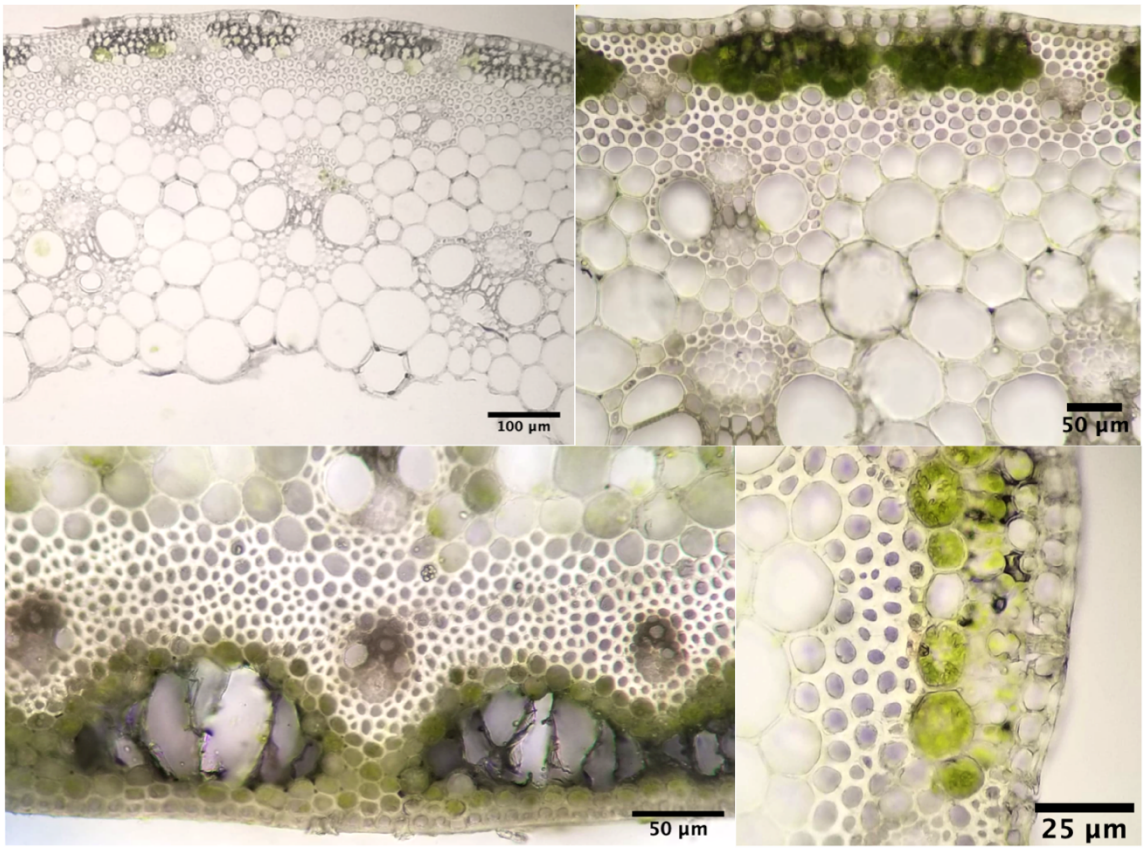

Figure 5.5. Fresh switchgrass internode samples sectioned with the Rapid-Tome are extremely thin. Thin-walled cortical cells, vascular bundles, and sclerenchyma fibers are easily sectioned and are in excellent condition for analysis. Sections are unstained with scale bars as labelled.

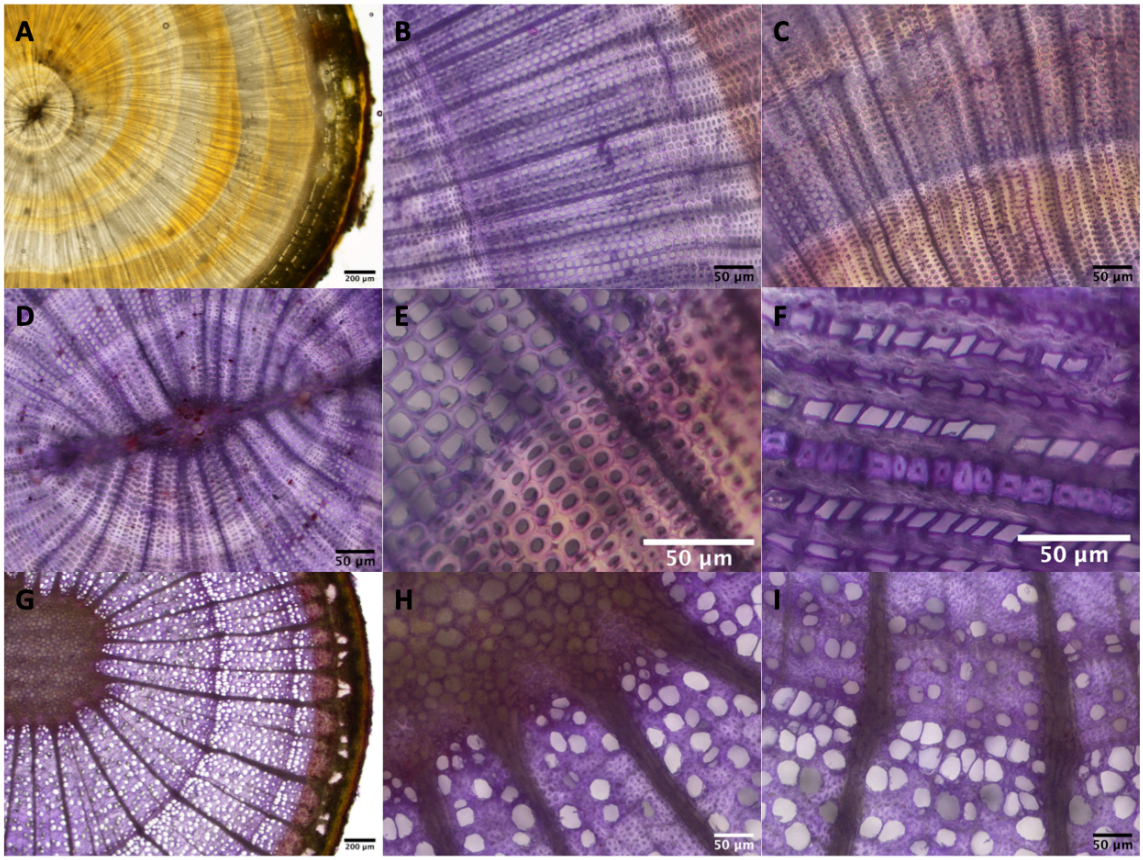

Figure 5.6. Sectioning of woody Eastern Red Cedar and Sycamore twigs show the versatility of the Rapid-Tome. (A) Eastern Red Cedar (ERC) with approximately 5 years of woody growth was sectioned to adequate section thickness for transmitted light illumination. (B-F) Higher magnification of ERC reveals the quality of the sections to reveal cell wall characteristics of single cells. (G-I) The softer wood of the Sycamore twig with approximately 2+ years of growth also sectioned well to reveal individual cell characteristics. Samples cut from tree and sectioned fresh the day of harvest. Image A is raw color, images B-I were stained with crystal violet. Scale bars as labelled.

5.20 References

Atkinson, Jonathan A. and Wells, Darren M. (2017), 'An Updated Protocol for High Throughput Plant Tissue Sectioning', *Frontiers in Plant Science,* 8.

Bancroft, John D and Gamble, Marilyn (2008), 'Theory and practice of histological techniques. Churchill Livingstone', *London, England*.

Barbosa, Antonio CF, et al. (2010), 'A new method to obtain good anatomical slides of heterogeneous plant parts', *IAWA journal,* 31 (4), 373-83.

Chen, Tien-Kuan, et al. (2016), 'Hybrid-Cut: an improved sectioning method for recalcitrant plant tissue samples', *JoVE (Journal of Visualized Experiments),* (117), e54754.

Giannini, John 'The OPN Microtome: An Inexpensive, Open Source Hand-Held Mini Microtome', <https://pages.stolaf.edu/wp-content/uploads/sites/803/2017/04/Giannini_OPN_Microtome_Manual_20170415.pdf>, accessed.

Kiernan, John Alan (1999), 'Histological and histochemical methods: theory and practice', *Shock,* 12 (6), 479.

Schindelin, Johannes, et al. (2012), 'Fiji: an open-source platform for biological-image analysis', *Nature Methods,* 9, 676.

Shimotsuma, Masataka and Schoefl, Gutta I (1992), 'A method for embedding thin membranes in historesin', *Biotechnic & histochemistry,* 67 (6), 377-79.

Soukup, Aleš and Tylová, Edita (2019), 'Essential methods of plant sample preparation for light microscopy', *Plant cell morphogenesis* (Springer), 1-26.

Takahashi, Hirokazu, et al. (2010), 'A method for obtaining high quality RNA from paraffin sections of plant tissues by laser microdissection', *Journal of plant research,* 123 (6), 807-13.

Chapter 6: Perspectives and Future directions

Conversion of switchgrass into biofuels is a process that includes multiple aspects of both biomass yield and biomass quality. Biomass yield is an important factor in terms of production, described as tons of biomass produced per acre or hectare. The focus of biomass quality is typically set in terms of how biomass and cell wall composition influences biomass digestibility, as well as the efficiency of this process. Here we present evidence that shows the importance of integrating internode anatomy traits as key components of biomass quality towards increasing biofuel conversion efficiency. This work increases our understanding of the biomass features that impact biomass quality and is of great significance for the improvement of biofuel production-relevant traits in switchgrass biomass.

In Chapter 2, we reported that switchgrass ecotypes exhibit significantly variable internode anatomy among clones of four genotypes within and across six environments. Trends among the internode anatomy traits reveal that cortical cell wall thickness uniquely deviates from the large lowlands trend and displays rank change among genotypes and across environments. Cortical cell wall thickness was identified to significantly correlate with biomass digestion efficiency, and positively correlates with mild resistance to loss of conductivity. In Chapter 3, we identified eight significant quantitative trait loci (QTL) for six internode anatomy traits and multiple candidate genes involved in grass internode architecture. A QTL was identified for cortical cell wall thickness, providing a genetic basis for potential future optimization of this impactful and variable trait. In addition to cell division regulation, hormone responsive genes, and cell wall biosynthesis transcription factors, transcription factors belonging to the multifunctional NAC family were identified

within the QTL intervals. The phylogenetic reconstruction of NAC factors revealed expanded switchgrass subgroups, homologous NAC genes in rice and Arabidopsis, and provides a reference for future studies and breeding efforts. In Chapter 4 we identified variable cell wall composition of the lowland genotype, WBC, across 17 degrees of latitude. Additionally, we established the need to control for milling site as a variable factor in the analysis of biomass with near infrared spectroscopy (NIRS) across sites. In Chapter 5, we designed a novel handheld microtome that is 3D-printed and greatly expands the opportunity for high-quality sections for microanalysis. Additionally, we provide a detailed hand-sectioning method description for sectioning hollow pith stem segments. In all, this work significantly expands our understanding of switchgrass internode anatomy variation in the context biofuel production-relevant traits.

This work presents several new avenues for future research to build upon. The isolation of cortical cell wall thickness and its multifunctional capacity presents evidence for expanding the evaluation of this trait plasticity and impacts on biomass digestibility. Another aspect of this work that brings to light new questions is the study of hydraulic conductivity and resistance to hydraulic conductivity loss in switchgrass segments. Furthermore, there is evidence that loss of conductivity is regained through positive root pressure. Additional investigations are needed to elucidate these mechanisms further.

6.1 Mild Embolism Resistance may be explained by plant segmentation theory

The segregation of ecotype resistance to conductivity loss, shown in Figures 2.6 and S2.7, is an indication that local adaptation differences among genotypes is present and impacts P50, though the differences are small and embolism resistance is mild. The key takeaway is that variation does exist among genotypes and correlates with numerous

anatomical traits consistent with published literature (xylem diameter and leaf area), as well as herein, Figure 2.6 A. Still, plant productivity and survival are likely not heavily influenced by such mild embolism resistance. Instead, there is a different explanation that describes the mild resistance to be a water saving *strategy* shared among other herbaceous plants: hydraulic segmentation theory.

6.2 Hydraulic segmentation theory

Plant segmentation theory suggests leaf die-back and sacrificial death of plant regions that are disposable in terms of whole plant survival that would effectively be a last resort to protect intercalary and apical meristems (Cochard et al., 1996; Davis et al., 2002; Lo Gullo et al., 2004; Vilagrosa et al., 2003). This depends on the growth habit of the plant, which can be potentially very effective in perennials that annually die back to the ground for winter dormancy. But in this case, the die back only lasts until the soil moisture status can support the return of vegetative growth. In ryegrass, it only takes approximately 21 days to regrow the maximum three leaves it typically supports (Holloway-Phillips & Brodribb, 2011). One study also found daily embolism in the roots of Maize even in wet soil, suggesting that the impact of stem emboli may be larger if roots embolize and soil moisture content is too low to facilitate root refilling (McCully et al., 1998). However, alternative strategies may be present in maize as it is an annual, compared to perennial grasses such as switchgrass that have root systems that persist below ground. Interestingly, in *Arundo donax*, produces independent clonal units of the same branching order that differ in their vulnerability to vessel cavitation (Shtein et al., 2021). However, the vertical segmentation within a single culm or tiller is not described. This presents a knowledge gap where future works can elucidate daily embolism cycles in grasses and differences among

grass genera, as well as intraspecific differences that may exist. Grasses may have an alternative mechanism here where large vessels fail last, opposite to traditionally held observations and beliefs (Ocheltree et al., 2016) The lowlands with larger diameter metaxylem and longer tillers have lower resistance to hydraulic conductivity loss (Figure 2.6). For this approach to function, there must be a source of banked water that facilitates turgor pressure maintenance and continued photosynthetic rates. The status of tiller hydraulic capacitance may play a role to maintain hydration status that is affected by multiple internode anatomy traits shown to vary herein.

Additionally, vascular anatomy mutant phenotypes have been observed in *Brachypodium distachyon* that share similarity with several observed switchgrass phenotypes (Figure 6.1). In *Brachypodium distachyon,* BdERECTA is highly expressed in the nascent vascular bundles in shoot apex parenchyma near the SAM and VASC, the progeny of a mutagenized line of BdERECTA, produces highly amphivasal vascular bundles.(Sakai et al., 2021) Amphivasal, or vascular bundles with xylem surrounding the phloem, are also observed in the C3922 F_2 individual from VWAD lineage and grown in Columbia, Missouri. Figure 6.1 A displays the typical vascular bundle with two metaxylem situated on either side of protoxylem and a basal area of phloem. However, Figure 6.1 B-F shows a drastic departure from the typical switchgrass vascular bundle with multiplied metaxylem or protoxylem surrounding the phloem. Additionally, Switchgrass genotype DVR3 (Figure 6.1 G and H) show a different phenotype where metaxylem consistently remain in typical arrangement but are highly multiplied in 100% of the large cortical vascular bundles. The implications are that the largest metaxylem cell diameters are diminished along with their multiplication, thus rendering them more resistant to embolism

than the larger diameter vessels typically present in comparable sized genotypes in terms of annulus radius and outer diameter. The mechanisms that regulate vascular bundle identify in switchgrass likely play a role in the DVR3 phenotype are require further investigation. If this phenotype can be regulated, the implications may be highly impactful.

6.3 Hydraulic capacitance

Though hydraulic capacitance was not directly measured in our study, its definition of water storage capacity for introduction into the transpiration stream affords us to make assumptions based on anatomical architecture traits that are associated with water storage. The abundance, dimensions, and distribution of water storing parenchyma cells and the proximity of vascular bundles to each other provide insight about plasticity of water storage capacity among genotypes. Vascular bundles are further apart in AP13 which also has thinner cortical cell walls, both translate to higher stem capacitance. The thickness of the cell wall also directly impacts the amount of water the cells are capable of storing, and thicker walls mean more area of the cell is not free for water storage (McCulloh et al., 2019). Another source of above ground water storage is the leaf sheath that surrounds much of the length of the internode in many grasses, including switchgrass. The larger the distance between vascular bundles, the greater the conductance and milder P50, which is explained by the observed positive correlation of average xylem diameter and distance between cortical vascular bundles (SCC = 0.82). Sheath radial thickness also highly positively correlates with Ks (SCC = 0.94) and negatively with P50 (SCC = -0.78). Leaf sheath area in cross section reveals multiple large cavities in the lowlands, as well as wide range in radial thickness. Sheath radius is negatively correlated with 50% loss of segment hydraulic conductivity, and therefore are larger in the lowlands that have poor resistance

to conductivity loss. Combining the water storage area in the stem with that of the leaf sheath provides further evidence of hydraulic capacitance nearest to the site of maximum photosynthetic activity, the leaf blade. The hypothesis to test is that each leaf, sheath, and its adjacent node as well as some amount if internode operate semi-independently to maintain turgor and carbon capture until water storage is depleted, ultimately causing stomatal closure. Conversely, the opposite may occur where the segments maintain carbon capture until overnight root pressure repairs the emboli and capacitance is restored for the cycle to repeat again the next day. To test this hypothesis, multiple segments are removed predawn and mid-day as shown in Figure 6.2, allowed to equilibrate, and then measured with a pressure probe to identify the water potential status of each segment. The theory goes that each leaf-node-internode segment will have a decreasing water potential in acropetal fashion.

6.4 Alternate methods to detect embolism resistance produce different results

Multiple methods exist for measuring hydraulic conductivity in plants and for the detection of vessel embolism. There is some debate about the accuracy of the centrifuge method and is discussed extensively in (Bouche et al., 2015; Hacke et al., 2015). A traditional method to induce hydraulic failure using a custom-built rotor is under some scrutiny due to the lack of consistent agreement with newer methods(Venturas et al., 2019). Some of the observed variation is likely due to the variation in sampling procedures and how distant from an intact plant the sample being evaluated is. Samples from the same plant has been observed to produce different P50 with the optical method. The sampled leaves that were attached to a long branch had more than double the P50 than a sample from the same species comparing only a detached leaf, with a leaf attached to a short stem

in the middle found in *Quercus sylvatica*, with similar patterns in *Prunus avium* and to lesser extent *Carpinus betulus*, (Guan 2021). The 13 cm segments measured here in Chapter 2 represent a distant resemblance of the intact plant, though still compare like samples to identify variability and performance in these samples with this method. It would be interesting to see what results are produced with different methods that can measure P50 of intact plants.

The main feature up for debate that may cause variable P50 results across methods is the impact of "open vessels" on the reliability of using the rotor to induce emboli. Open vessels are those that traverse from one cut end to the other of a stem segment without an intervessel pit membrane or end wall, essentially a hollow tube through the entirely of the plant segment. The current understanding is that open vessels drain at low RPM and then seed air to neighboring vessels, causing artificial early losses in conductivity. The presence of embolism in the open vessel is only impactful on the other vessels if the embolism travels through the membrane into other vessels at the nodal plexus. So the degree to which the open vessel emboli spread to neighboring vessels relies on the connectedness of the open vessel in the node.

Emboli occur in the center of the stem segment in the rotor and then the water column break is free to supposedly "drain" out unimpeded. However, even if the open vessel empties out entirely, the force of the centrifuge pushes the emboli away from the neighboring vessels simply due to the nature of the branching in the nodal plexus. Since switchgrass and maize have an atactostele vascular bundle arrangement, an embolism anywhere along the vessel length within the internode renders the entire vessel unfunctional. This differs from ring- or diffuse-porous woody stems with numerous

neighboring vessels through which conductivity can be re-routed around and restored to some extent. But in grasses, the presence or absence of the ability to prevent propagation of an emboli (end-wall or not) from one vessel to the subsequent vessel in a solitary conduit is less a point of concern due to the separation of vascular bundles. The vessels branch and split facing upwards like a capital Y. The location of the node in the tiler segments described in chapter 2.The basal portion of the segment is shorter than the apex end, placing the node off center from the axis of rotation, with the base of the Y at the outer length of the segment. If multiple emboli occur in the open vessel in the center of the segment (in the left arm of the Y) and are pushed outwards by the weight of the water column, the embolism is pushed out and down, away from the intact branch vessel (the right arm of the Y). The updated rotor design includes hydration reservoirs firmly pressed against the cut ends of the plant that holds water at the cut ends of the segment (Jacobsen, 2011) . The emboli may occur in the open vessels, but the idea is that the water doesn't simply drain out after that. The vessels are still hydrated and are not *completely* filled with air. The water *can* drain from the open vessels until it reaches the same height as the water in the reservoirs, which is ~ 1 - 2 cm. Therefore, I propose a new design to modify the existing rotor that prevents the water from simply draining out of the open vessel due to the force generated by the centrifuge.

A new rotor design to induce hydraulic conductivity loss in plant stem segments relies on the physics in a U-tube manometer to keep the embolized vessels from completely draining and, in theory, prevents the open vessel artifact. The emboli can still take place since their occurrence does not rely on the *flowing* of the water out through the cut ends of the segment. The segment is contained within a tube, submerged in water (Figure 6.3.

When spinning, the water level in the tube (surrounding the stem segment), only travels a few cm at most from the axis of rotation, and that is as far as the water can drain out of the segment. This allows for the emboli to occur at the center of the rotor but prevents the emboli from being pushed into neighboring vessels by a draining water column.

The main argument for the open vessel artifact is that the conductivity is reduced by the spreading of the air-filled open vessel to neighboring vessels, reducing conductivity artifactually. However, the embolism that occurs within the open vessel at the center of the segment would still in fact be due to low pressure. This would be limited to the center of the segment where the opposing relative centrifugal force (RCF) is highest. if there is a way to prevent water from simply draining out of the vessel, the open vessel artifact would essentially be prevented. Using centrifugal force, a balance in water pressures can theoretically be achieved with the new design shown in Figure 6.3. The level of the water held by the end cubes balances the water inside the segment and prevents vessel held water from draining out of the stem while leaving a gap in the center of the stem segment to allow for pressure induced emboli to occur. P1 and P2 pressures are generated by the relative centrifugal force (RCF) acting on the surface of the water in the cube, and on the surface of the water within the vessels *only after embolism occurs*. Water trough is only filled up halfway. The center piece that the segment rests on top of has low sides that are half the height of the cubes, shown in dotted lines in (Figure 6.3 A), with the edges of the open ends of the cubes also shown as vertical dotted lines. The stem segment is clamped into the stem holder with the top piece (*t)* with attached compression foam. (Figure 6.3 B) when stationary, the water level keeps the segment submerged. (Figure 6.3 C) When rotating, the water is held in the cubes that house the cut ends of the stem segment by relative centrifugal

force. Internal pressure build is according to the rotation speed of the rotor and emboli may occur at the center of the segment where the opposing force of draining water is in opposite direction is greatest (emboli = white bubbles). (Figure 6.3 D) (*i*) the initial condition at low RPM, the level of the water within the vessels of the stem segment is continuous. Shortly after an embolism occurs, the water level within the segment vessel is higher than the water outside of the segment. The RCF is applied to both the water in the vessels (P_1) and the water outside of the segment (P_2), pushing them to equilibrium ($P_1 = P_2$) at the final position (*f*). The water level outside of the segment is held in place by the RCF and prevents the vessel held water within the stem segment from passing this point and. This prevents the open vessel from completely draining and removes the opportunity for the air-filled vessel to lead to air seeding artifacts and artificial loss of conductivity. Figure 6.3 E depicts the four-piece segments holder design, and Figure 6.3 F shows the assembly of the segment holder into the rotor. This design is purely theoretical and is untested.

6.5 Root pressure refilling

The mild resistance to embolism in switchgrass described here may be interpreted as diurnal embolism and positive root pressure mediated refilling, a common phenomenon in herbaceous plants (Holloway-Phillips et al. 2011). This idea posits that embolism occurs during times of peak transpiration due to plant exposure to sunlight, warm temperatures, and wind. When evaporative demand subsides, positive root pressure in the roots has been shown in several grasses to mediate xylem refilling and the repair of cavitation. For example, rice (Stiller et al., 2003), and sugarcane (Neufeld et al., 1992) show that over 60% of hydraulic conductivity may be lost during peak transpiration that can be restored by overnight root pressure (Holloway-Phillips & Brodribb, 2011). Furthermore, the

maximum tiller height of bamboo (more than 30m tall) is observed to be determined by positive root pressure, that is, height is closely predicted by maximum root pressure to repair hydraulic dysfunction that occurred during diurnal gas exchange (Cao et al., 2012). In maize, mid-day leaf water potential of -1.98 MPa resulted in 68% loss of stem-specific conductivity that reduced to 24% overnight after returning the Ψ_{soil} to ~0 MPa (Gleason et al., 2017). This indicates recovery of stem-specific conductance overnight from positive root pressure during low rate of transpiration. Ryegrass was identified to be drought–insensitive with xylem highly susceptible to water stress-induced hydraulic dysfunction coupled with water spending stomatal behavior. This is described by Holloway-Phillips 2011 to maximize short-term carbon gain by allowing hydraulic conductivity to decline. This strategy makes the leaves functional for gas exchange and carbon capture while protecting vital plant parts such as nodes, stems for desiccation (Cochard et al., 1996) . Furthermore, Cochard et al. describes heavily droughted plants that experience leaf mortality and 90 % loss of conductivity (PLC), the remaining conductivity is likely enough to supply water to the apex. A similar phenomenon is likely to occur diurnally where PLC is above 50, but enough to maintain water status in the vital tiller regions of the apical and intercalary meristems. Further support of the decoupling of stomatal closure and stem embolism was found in wheat where xylem cavitation, collapse, or changing leaf conductance did not drive stomatal closure (Corso et al., 2020). Two-fold lower mid-day leaf water potentials observed in switchgrass under both well-watered and water limited conditions (~ -2 MPa and -2.8 MPa, respectively) compared to pre-dawn leaf water potentials indicate switchgrass is anisohydric, showing a decreased water potential under drought conditions (Lovell et al., 2016; Sade et al., 2012). This approach is described to be

risky in the fact that stomatal closure is insensitive to stem and soil water status, which maintain transpiration even under water limited conditions. This leads to increased tension in the soil to atmosphere water continuum within vascular bundles in the plant and causes stem cavitation. Lens et al. 2016 describes the decoupling of stomatal closure and stem embolism results in plants operating at a negative hydraulic safety margin, which translates to hydraulic failure at mild internal negative pressure by design. This is in contrast to the strategy employed by most trees that operate under a positive hydraulic safety margin to avoid cavitation (Lens et al., 2016). Therefore, the occurrence of xylem cavitation in grasses is not only commonplace, but not detrimental to water assimilation. In theory, soil water availability could be manipulated (provided nocturnally to facilitate generation of positive root pressure) to improve water use efficiency and biomass production (Holloway-Phillips & Brodribb, 2011). This idea proposes that field management practices in terms of irrigation can play a large role in producing positive root pressure vs. genetic variation conferring variable root pressure capabilities under.

An additional factor to consider with positive root pressure refilling is that it is likely a phenological mechanism. During times of tiller elongation and turgor driven growth, multiple internodes are lengthening during the early months of the growing season. After vegetative growth has concluded and floral transition has occurred and the panicle has completely emerged, turgor driven growth is effectively zero. The root generated pressure may subside at this point in the plants perennial cycle and be less detectable. Therefore, in order to test the hypothesis of variable root pressure among the ecotypes for xylem embolism repair, early and mid-season sampling must be done to properly capture this phenomenon. Figure 6.4 depicts the set-up of root pressure measurements taken

overnight that identified a positive pressure of 20.84 kPa and over 15 cm of tubing filled with water. This kind of approach can be taken both in greenhouse grown plants as shown here, as well as in the field.

6.6 RNA sequencing analysis of segmented internode at multiple sites

One of the biggest questions that builds on the internode anatomical variation described in both chapter 2 and 3, is to identify differentially expressed genes in the young shoots of various switchgrass genotypes. What we describe in these studies is the results, the final phenotypes at the end of season growth. The action is earlier in the growing season when the "decisions" taking place and the differential architecture is being made. The way to explore this is to capture tissues of newly emerged meristems at the time of first emergence in Spring.

An attractive goal is to identify internode anatomy and cell wall biosynthesis regulatory genes that are expressed differently that produce the variable internode phenotypes we observe in chapters 2 and 3. Although great improvements in the understanding of cell wall biosynthesis have been accomplished, much of this work has been carried out in the eudicot, *Arabidopsis,* which has similar cell wall polymer composition to grasses, yet grasses contain many unique aspects to their cell walls not present in *Arabidopsis* (Vogel, 2008). Therefore, understanding of cell wall biosynthesis and its regulation in grasses is playing catch-up to Arabidopsis in many cases (Handakumbura & Hazen, 2012). An additional level of specificity we are looking to get is to identify in which cell type of the internode genes that control internode anatomy are expressed. The internode acropetally matures with significant secondary cell wall accumulation in the upper portion of each internode (Mamedes-Rodrigues et al., 2018).

However, not all internodes are actively growing with the uppermost internodes growing the most. Understanding the zone of the internode where key transcription factor and cell wall biosynthesis genes are expressed will reveal the transcriptomic landscape gradient of internode maturation.

Harvest for evaluating differential gene expression in switchgrass tillers is straight forward. Elongating tillers with three or four nodes (stage E3 or E4) could be harvested from the four F_0 genotypes and 50 F_2 individuals. The F_0 internodes will be subdivided into four parts due to that fact that different segments that are undergoing cell division, elongation, and secondary cell wall accumulation will have unique gene expression profiles as observed in rice (Lin et al., 2017). The uppermost internode should be harvested when the intercalary meristem located just above each node is active and when abundant (Lin et al., 2017) cell division, cell elongation, and secondary cell wall formation are present. Developmentally staged harvest of vegetative growth is key for this analysis to avoid differential expression artifacts introduced by floral transition and reallocation of photosynthate from vegetative growth to reproductive structures (Moore et al., 1991).

Many genes involved in cell wall biosynthesis and regulation, cell cycle, hormone production and transport, light perception, floral transition, are all anticipated to both be differentially expressed, but also absent in some cases when comparing across the latitude gradient as well as within the internode gradient as cells mature and lignify. The MYB family of proteins includes both positive and negative regulators of secondary cell wall formation and thus expression level predictions depend on the type of regulation (Zhao & Bartley, 2014). Additionally, regulators previously identified in other grasses such as are anticipated to vary that include the global repressor of secondary wall biosynthesis,

WRKY, a higher order cell wall biosynthesis activator: secondary wall associated NAC domain protein 1 (SND1). Additionally, cell wall positive master regulators of the group secondary wall NACS are anticipated to vary (Handakumbura & Hazen, 2012). These projections are based on the anatomical variation observed in chapter 2 and 3 that are most likely due to differential regulation by cell wall transcription factors regulatory genes. Furthermore, a recent report found that the blue light receptor CRY1 in Arabidopsis influenced secondary cell wall accumulation by negatively regulating several factors listed above (Zhang et al., 2018). Furthermore, light quality was found to influence cellulose synthase activity in the grass *Brachypodium distachyon,* providing a cell wall biosynthesis gene family in which to anticipate differential expression.

6.7 Methods for evaluating transgene expression in functional characterizations

One currently applied approach for evaluating transcription factor regulation of downstream genes of interest is to utilize protoplast transfection assays (Mazarei et al., 2008). However, this process is carried out in cells that have had their cell walls enzymatically stripped and are single cells floating in a stabilizing solution. Although this system may work well for many purposes, the desired exploration of the crosstalk between multiple cells and cell types is impossible. Furthermore, the highly modified state of the cell introduces a molecular condition unlike any observed in higher plants of the world. Therefore, a system that can deliver DNA to intact tissues is of great interest when investigating transcription factors that may be produced in one cell that influence neighboring cells. This scenario is likely taking place in the intercalary meristem of grasses where cell division, elongation, and primary and secondary cell wall accumulation is taking place in close vicinity.

6.8 Alternative transformation application of carbon nanotube mediated transient expression of transgenes in the developing switchgrass internode

Carbon nanotube (CNT) mediated DNA delivery for infiltration and transient gene expression into intact cells was recently described (Demirer et al., 2019). Their CNT-DNA delivery system is possible in part because of passing through the cell wall size exclusion limit (Schwab et al., 2016) of 5-20 nm by the combined dimensions of nanotubes 3nm diameter and a 12kb plasmid diameter, of approximately 15nm when electrostatically grafted to each other. This phenomenon allows for DNA to be delivered to intact cells with cell walls in complete tissues and organs for expression studies.

The goal of this approach is to investigate ectopic expression or candidate genes identified in chapter 3. This effort would test hypotheses about the functional impact of transcription factor regulation of internode anatomical architecture genes. Rapid identification of the downstream effects of transgene expression is the goal of the carbon nanotube-mediated DNA delivery system. Expression of cell wall regulators in in the cells of intact tissues during developmental stage of rapid vegetative growth can give a much more accurate transcriptomic snapshot than can be achieved with protoplast isolated from very young seedlings, as is the norm. This approach can test the hypotheses that genes identified in chapter 3 either regulate genes that lead to or directly produce their correlated cell wall and or internode anatomy traits.

The experimental approach is to use carbon nanotubes to deliver the DNA into switchgrass, which has been selected because it holds promise to be a rapid method to investigate the effects of an entire list of gene function and address the issue of transgene incorporation into the genome. An exciting first step is to verify the viability of CNT

infiltration of intact tissues of switchgrass. This effort would focus on establishing a CNT-DNA infiltration system in switchgrass for transient expression of a transgene within intact switchgrass internodes and leaves. Efforts involve the detection of successful transient expression of intact tissues that are actively undergoing cell wall accumulation.

Understanding the complex nature of cross regulatory effects and interactions of multiple TFs and molecular processes with cell wall biosynthesis under a more natural molecular environment is uniquely possible with the CNT delivery method. This study effort would be supported by the hypothesis that studies on cell wall biosynthesis regulatory factors with CNT delivery system can give a more accurate depiction of cell wall biosynthesis gene-gene interactions and regulatory functions than studies that produce results influenced by the extremely altered cellular state of protoplasts. After optimization for switchgrass, the CNT mediated transformation method can be utilized to explore the isolated transcriptional effects of transiently expressing cell wall biosynthesis regulators identified in chapter 3. Transforming grasses is not as routine as with some other model plants. Transformation of embryonic grass callus cells has been greatly improved by utilizing tissue culture micropropagation techniques but still requires several months to go from transformation to a viable transgenic plant line .

We produced preliminary results with initial infiltration efforts at targeted switchgrass leaf and internode tissues for transformation with a Ubi1:GUS reporter construct (Figure 6.5). However, endogenous GUS activity is present in switchgrass and additional parameters are needed to prevent this activity and preserve transgene GUS activity, which requires optimization for compatibility with transgene expression and the particular switchgrass tissues. Yellow fluorescent protein (YFP) has an excitation and

emission profile that is within an inactive spectral range of switchgrass autofluorescence. For this reason, a second reporter construct utilizing the same highly active maize Ubi1 promoter driving the YFP gene should also be incorporated into future efforts of infiltration success detection. Furthermore, mixing the two reporter vectors that each separately contain Ubi1:GUS and Ubi1:YFP constructs into a single infiltration buffer provides the opportunity of three verification options by either light or fluorescence microscopy as well as transcript detection with qPCR.

To accomplish delivery of the CNT:DNA conjugation to the internal tissues of the intercalary meristem the CNT:DNA mixture is injected with a 34-gauge syringe needle into the intercalary meristem itself. This gauge needle was chosen as it is the second smallest on the market though doesn't clog as easily as the 36g needle. Limiting the amount of cellular damage to accomplish infiltration is crucial to reduce wound response and transcriptional artifacts. Additional parameters to reduce wounding are to treat target infiltration samples with an MMG buffer. The MMG solution is a buffer used in protoplast assays optimized for switchgrass, (Mazarei et al., 2008). 150 ng of CNT per 100 µl with a 1:1 CNT:DNA concentration has proven to be marginally successful if at all. To address this, total concentrations of 300 ng and 600 ng per 100 µl of CNT should be applied at ratios with DNA of 6:1, 3:1, 1:1, 1:3, and 1:6. Plasmid vectors containing the GUS reporter gene as well as plasmid vectors with YFP, both driven by the maize Ubi1 promoter should be used to detect infiltration success within intercalary meristems of 1-month post emergence tillers. Methods of verification should include the imaging of serial sections of the targeted transformed area with fluorescence microscopy. Additionally, qPCR can be used to detect YFP transcripts to validate fluorescence image observations.

6.9 Apply CNT delivery to transiently express cell wall biosynthesis genes in mature tissues of switchgrass.

The goal of this effort would be to isolate the downstream effects of overexpressing a cell wall biosynthesis master regulator transcription factor under a more natural molecular atmosphere where cell wall biosynthesis "business as usual" is taking place, with the goal of visualizing interactions taking place downstream due to the complex nature of cross regulatory effects of other TFs and molecular processes underway as the cell packs on secondary cell wall.

Ongoing cloning efforts will be vital in providing vectors for infiltration and investigation of the function of each gene of interest identified in chapter 3, as well as identified in the literature. Experimental methods should include multiplexing where plasmids containing reporter genes and genes of interests are delivered to targets cells with carbon nanotube scaffolds. An appropriate destination vector containing the UBI promoter and YFP or GUS reporter gene should be incorporated into the cloning pipeline.

This effort would primarily focus on the expression of transgenes in mature cells of an intact switchgrass tiller and leaf. The developers of this general method describe it to be useful for rapid screening of large numbers of genes of interest. This study would be directed at evaluating the downstream expression response of overexpressing a TF identified both from previous Bartley lab researchers and novel identified differentially expressed genes produced from the efforts of chapter 3. Verification and analysis methods with qPCR should be expanded from transgene(s) to also include putative downstream genes affected by the transgene. Though the expected results depend on the putative or known function of the transgene, the prospect of increased expression of cell wall

biosynthesis regulatory and or biosynthesis genes if the transgene is a positive regulator, and the opposite effect if the transgene is a transcription repressor is significant to explore.

This work describes internode anatomy plasticity as it occurs among four characteristic genotypes across 17 degrees of latitude in the U.S. The independent variation in cortical cell wall thickness from other traits shows there is potential to match genotype to specific environment to optimize internode anatomy for biomass conversion efficiency into biofuels. This work concludes that biomass production and conversion efficiency must include measures of internode anatomy, in addition to total biomass composition, when conducting evaluations toward increasing biofuel production efficiency. The genetic basis established here for 6 traits to the level of QTL interval provides a candidate gene list for further evaluation and trait optimization. The genetic basis and candidate genes for each of the internode traits provide guidance for selective breeding of favorable anatomy phenotypes. Additionally, this work provides a foundation to pursue these internode traits as targets for genetic engineering in switchgrass as well as other bioenergy crops.

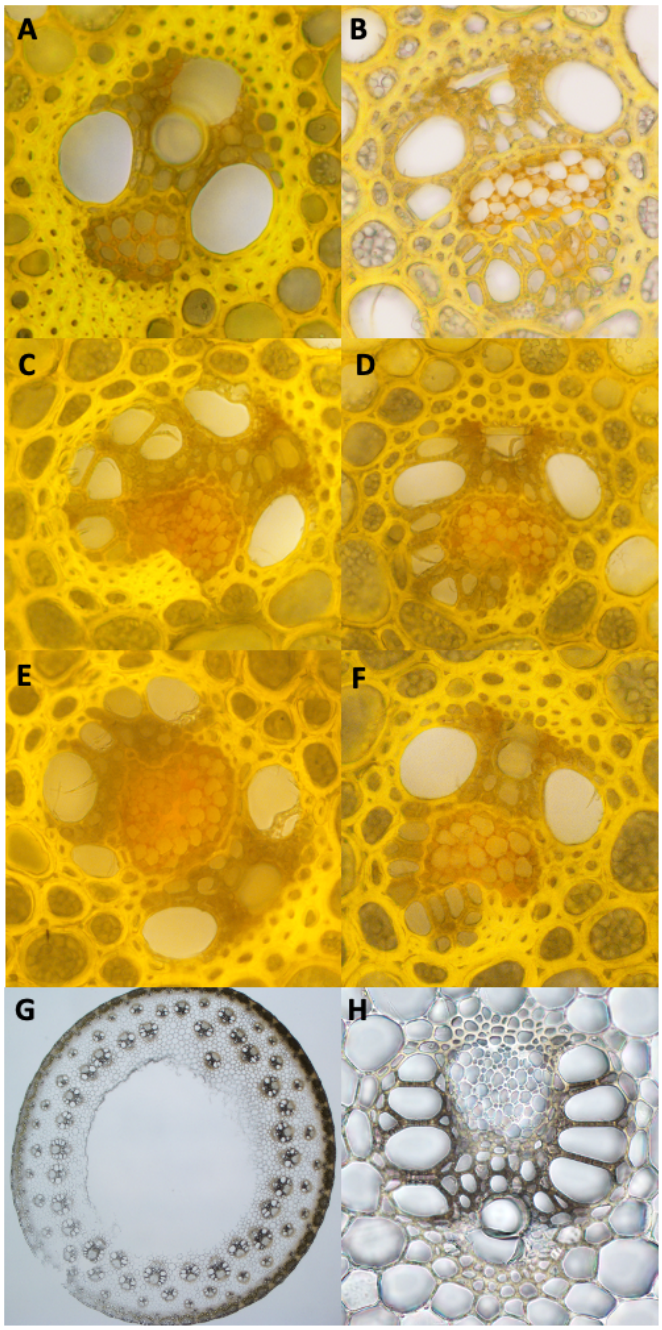

Figure 6.1. Abnormal vascular bundle phenotypes with multiplied metaxylem. (A) A typical switchgrass vascular bundle with two metaxylem. (B-E) C3922 a VWAD F2 from the four-way cross shows extensive abnormal cortical vascular bundles with extra metaxylem surrounding the phloem (amphivasal). (G and H) is DVR3 and shows a different but very consistent metaxylem phenotype. The metaxylem does not surround the phloem but is multiplied in 100% of the large cortical vascular bundles (G). These abnormalities have implications with water relations and resistance to water-limited stress. Additionally, the amphivasal phenotype is described in *Brachypodium distachyon* to have pleiotropic effects to include lignin and cell wall sugar content reduced as well as hormone metabolism alterations.

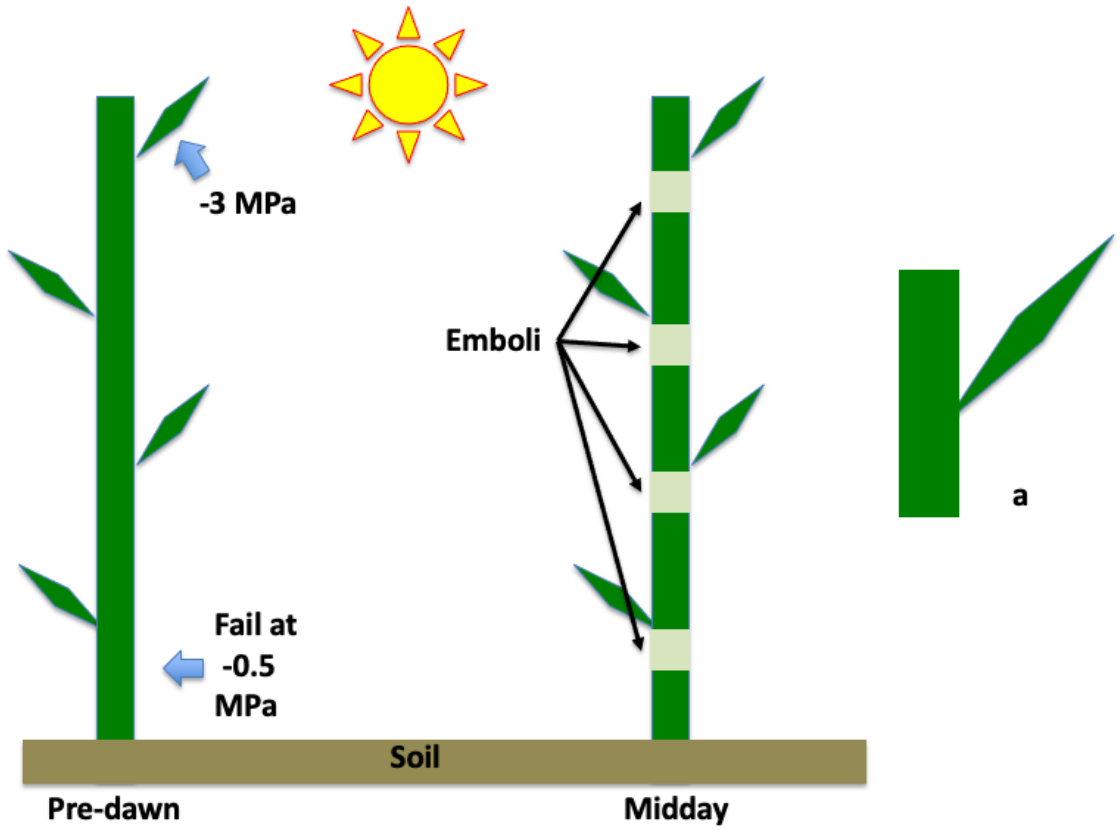

Figure 6.2 Example of potential approach to investigate the presence of hydraulic segmentation among leave-node-internode segments (a). The hypothesis is that each segment may operate semi-independently in terms of hydraulics during times of high evaporative demand and multiple vessel embolisms throughout the tiller length. The maintenance of turgor and water status within each segment relies on banked water in terms of hydraulic capacitance within the internode and leaf sheath.

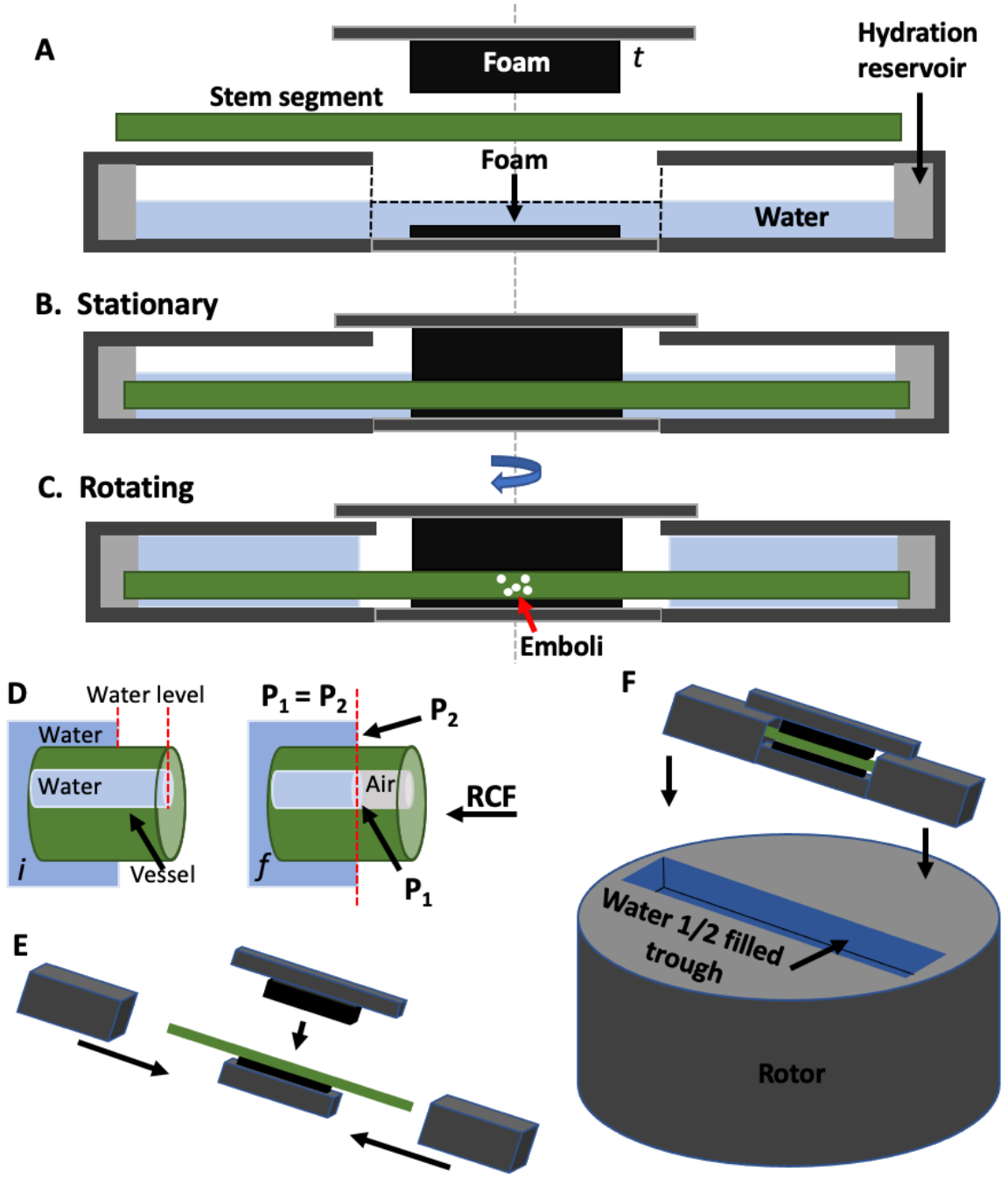

Figure 6.3 Rotor and stem segment holder design prevents open vessel artifacts. The level of the water held by the end cubes balances the water inside the segment and prevents vessel held water from draining out of the stem while leaving a gap in the center of the stem segment to allow for pressure induced emboli to occur. P1 and P2 pressures are generated by the relative centrifugal force (RCF) acting on the surface of the water in the cube, and on the surface of the water within the vessels *only after embolism occurs*. Water trough is only filled up halfway. The center piece that the segment rests on top of has low sides that are half the height of the cubes, shown in dotted lines in (A), with the edges of the open ends of the cubes also shown as vertical dotted lines. The stem segment is clamped into the stem holder with the top piece (*t*) with attached compression foam. (B) when

stationary, the water level keeps the segment submerged. (C) When rotating, the water is held in the cubes that house the cut ends of the stem segment by relative centrifugal force. Internal pressure build is according to the rotation speed of the rotor and emboli may occur at the center of the segment where the opposing force of draining water is in opposite direction is greatest (emboli = white bubbles). (D) (*i*) the initial condition at low RPM, the level of the water within the vessels of the stem segment is continuous. Shortly after an embolism occurs, the water level within the segment vessel is higher than the water outside of the segment. The RCF is applied to both the water in the vessels (P_1) and the water outside of the segment (P_2), pushing them to equilibrium ($P_1 = P_2$) at the final position (*f*). The water level outside of the segment is held in place by the RCF and prevents the vessel held water within the stem segment from passing this point and. This prevents the open vessel from completely draining and removes the opportunity for the air-filled vessel to lead to air seeding artifacts and artificial loss of conductivity. .(E) depicts the four-piece segments holder design, and (F) shows the assembly of the segment holder into the rotor. This design is purely theoretical and is untested.

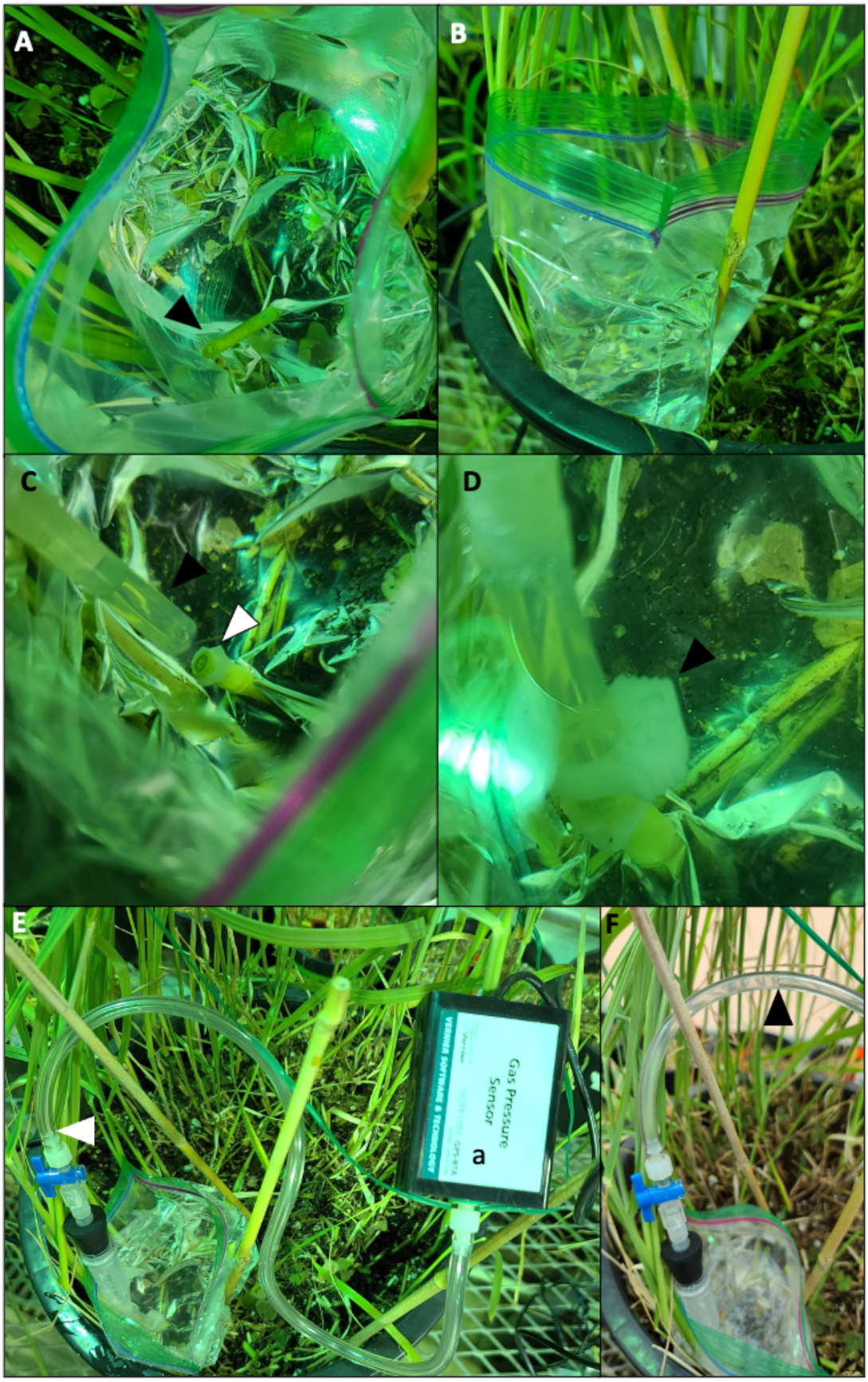
A
B
C
D
E
F
Gas Pressure
Sensor
a

Figure 6.4 Pilot set up to measure overnight root pressure. The set up includes an initial cut of the internode at a slant 10 cm above the ground surface at a severe angle (A, black arrowhead). Prop up the bag with bamboo stakes to prevent water flowing out (B). The angle is to make the tiller sharp to easily cut through the plastic bag that is full of water. This must be done quickly after the cut is made to prevent air bubbles form entering the internode. With the cut end of the tiller under water, another 3 cm are cut to remove any bubbles introduced from the first cut. The Vermier gas pressure sensor (E, a) should be attached to a tube with a side vent valve and a cork at the end that fits into a standard 15 ml tube. Here we use a 5 ml tube that has the same diameter, filled to the top with water. The bottom tip of the tube is removed with a razor blade according to the diameter of the tubing used that has an inner diameter of the tiller (C, black arrowhead). The tubing is sealed to the 5 ml tube with several wraps of parafilm. Apply a heaping amount of Loctite gel (or petroleum jelly) to the entire outside of the tiller under water, take care not to get any on the cut end (C, white arrowhead). Slide the tubing over the end of the tiller. Secure the tube with a locking plastic clamp (D). Open the vent to release any pressure from the set up. Twist to the open position to allow water to flow upward, read as pressure build up by the sensor. The initial set up is done at time of low transpiration, after the sun is down. Starting water level is just above the valve (white arrowhead) (E). The pressure build up after 8 hours overnight is seen here as the increase in water level, noted by the black arrowhead and corresponds to 20.84 kPa (F). This approach can be taken in the greenhouse setting as shown, as well as in the field.

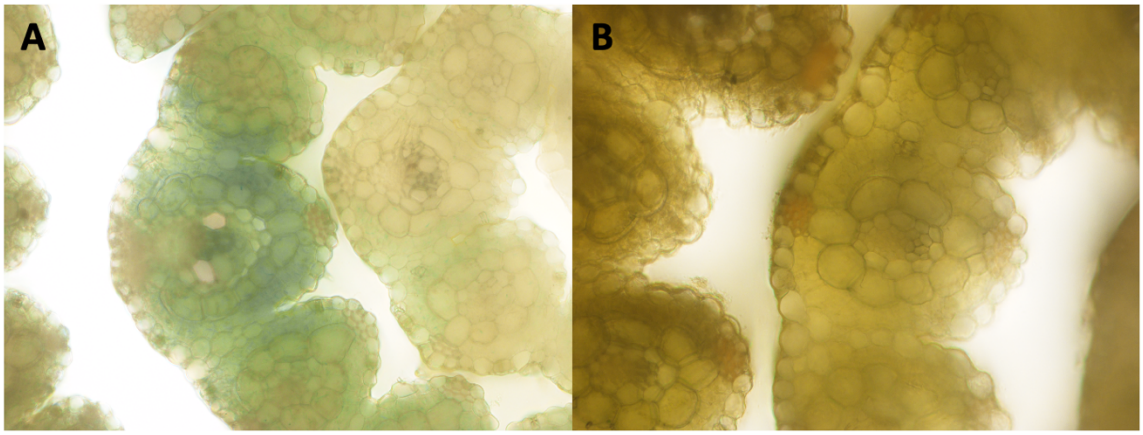

Figure 6.5 CNT mediated transient GUS expression. (A) GUS activity indicated by presence of blue in the leaf of switchgrass after surface incision and application of CNT :: UBI:GUS solution. (B) GUS activity absent in control plant treated with CNT :: no vector. Further replication is required to verify these results.

6.10 References

Al-maskri, A., Hameed, M., Ashraf, M., Khan, M. M., Fatima, S., Nawaz, T., & Batool, R. (2014). Structural Features of Some Wheat (Triticum Spp.) Landraces/Cultivars Under Drought and Salt Stress. *Arid Land Research and Management*, *28*(3), 355-370. https://doi.org/10.1080/15324982.2013.841306

Alder, N., Pockman, W., Sperry, J., & Nuismer, S. (1997). Use of centrifugal force in the study of xylem cavitation. *Journal of Experimental Botany*, *48*(3), 665-674.

Arantes, V., & Saddler, J. N. (2010). Access to cellulose limits the efficiency of enzymatic hydrolysis: the role of amorphogenesis. *Biotechnology for biofuels*, *3*(1), 1-11.

Aschan, G., & Pfanz, H. (2003). Non-foliar photosynthesis – a strategy of additional carbon acquisition. *Flora - Morphology, Distribution, Functional Ecology of Plants*, *198*(2), 81-97. https://doi.org/https://doi.org/10.1078/0367-2530-00080

Atkinson, J. A., & Wells, D. M. (2017). An Updated Protocol for High Throughput Plant Tissue Sectioning [Methods]. *Frontiers in Plant Science*, *8*. https://doi.org/10.3389/fpls.2017.01721

Bancroft, J. D., & Gamble, M. (2008). Theory and practice of histological techniques. Churchill Livingstone. *London, England*.

Barbosa, A. C., Pace, M. R., Witovisk, L., & Angyalossy, V. (2010). A new method to obtain good anatomical slides of heterogeneous plant parts. *IAWA journal*, *31*(4), 373-383.

Bartley, L. E., Peck, M. L., Kim, S.-R., Ebert, B., Manisseri, C., Chiniquy, D. M., Sykes, R., Gao, L., Rautengarten, C., & Vega-Sánchez, M. E. (2013). Overexpression of a BAHD acyltransferase, OsAt10, alters rice cell wall hydroxycinnamic acid content and saccharification. *Plant Physiology*, *161*(4), 1615-1633.

Bhandari, H., Saha, M., Mascia, P., Fasoula, V., & Bouton, J. (2010). Variation among half-sib families and heritability for biomass yield and other traits in lowland switchgrass (Panicum virgatum L.). *Crop Science*, *50*(6), 2355-2363.

Blackman, C. J., Brodribb, T. J., & Jordan, G. J. (2010). Leaf hydraulic vulnerability is related to conduit dimensions and drought resistance across a diverse range of woody angiosperms. *New Phytologist*, *188*(4), 1113-1123.

Bouche, P. S., Jansen, S., Cochard, H., Burlett, R., Capdeville, G., & Delzon, S. (2015). Embolism resistance of conifer roots can be accurately measured with the flow-centrifuge method. *Journal of Plant Hydraulics*, *2*, e002.

Bouton, J. H. (2007). Molecular breeding of switchgrass for use as a biofuel crop. *Current opinion in genetics & development*, *17*(6), 553-558.

Broman, K. W., Gatti, D. M., Simecek, P., Furlotte, N. A., Prins, P., Sen, Ś., Yandell, B. S., & Churchill, G. A. (2019). R/qtl2: software for mapping quantitative trait loci with high-dimensional data and multiparent populations. *Genetics*, *211*(2), 495-502.

Brown, C., Griggs, T., Keene, T., Marra, M., & Skousen, J. (2016). Switchgrass biofuel production on reclaimed surface mines: I. Soil quality and dry matter yield. *BioEnergy Research*, *9*(1), 31-39.
Brown, J., & Caligari, P. D. (2008). Breeding schemes. *An Introduction to Plant Breeding*, 34-59.
Cao, K. F., Yang, S. J., Zhang, Y. J., & Brodribb, T. J. (2012). The maximum height of grasses is determined by roots. *Ecology letters*, *15*(7), 666-672.
Caporaso, N., Whitworth, M. B., & Fisk, I. D. (2018). Near-Infrared spectroscopy and hyperspectral imaging for non-destructive quality assessment of cereal grains. *Applied Spectroscopy Reviews*, *53*(8), 667-687. https://doi.org/10.1080/05704928.2018.1425214
Carriquiry, M. A., Du, X., & Timilsina, G. R. (2011). Second generation biofuels: Economics and policies. *Energy policy*, *39*(7), 4222-4234.
Casler, M. D. (2010). Changes in mean and genetic variance during two cycles of within-family selection in switchgrass. *BioEnergy Research*, *3*(1), 47-54.
Casler, M. D., Tobias, C. M., Kaeppler, S. M., Buell, C. R., Wang, Z.-Y., Cao, P., Schmutz, J., & Ronald, P. (2011). The switchgrass genome: tools and strategies. *The Plant Genome*, *4*(3), 273-282.
Casler, M. D., Vogel, K. P., Taliaferro, C., Ehlke, N., Berdahl, J., Brummer, E., Kallenbach, R. L., West, C., & Mitchell, R. (2007). Latitudinal and longitudinal adaptation of switchgrass populations. *Crop Science*, *47*(6), 2249-2260.
Cernusak, L. A., & Cheesman, A. W. (2015). The benefits of recycling: how photosynthetic bark can increase drought tolerance. *New Phytologist*, *208*(4), 995-997. https://doi.org/10.1111/nph.13723
Chen, F., & Dixon, R. A. (2007). Lignin modification improves fermentable sugar yields for biofuel production. *Nature biotechnology*, *25*(7), 759.
Chen, L., Auh, C., Chen, F., Cheng, X., Aljoe, H., Dixon, R. A., & Wang, Z. (2002). Lignin Deposition and Associated Changes in Anatomy, Enzyme Activity, Gene Expression, and Ruminal Degradability in Stems of Tall Fescue at Different Developmental Stages. *Journal of Agricultural and Food Chemistry*, *50*(20), 5558-5565. https://doi.org/10.1021/jf020516x
Chen, T.-K., Yang, H.-T., Fang, S.-C., Lien, Y.-C., Yang, T.-T., & Ko, S.-S. (2016). Hybrid-Cut: an improved sectioning method for recalcitrant plant tissue samples. *JoVE (Journal of Visualized Experiments)*(117), e54754.
Chen, W., Wu, Y., Fritschi, F. B., & Juenger, T. E. (2021). The genetic basis of the root economics spectrum in a perennial grass. *Proceedings of the National Academy of Sciences*, *118*(47).
Chen, X., Equi, R., Baxter, H., Berk, K., Han, J., Agarwal, S., & Zale, J. (2010). A high-throughput transient gene expression system for switchgrass (Panicum virgatum L.) seedlings. *Biotechnology for biofuels*, *3*(1), 9.
Chen, Y.-N., Slabaugh, E., & Brandizzi, F. (2008). Membrane-tethered transcription factors in Arabidopsis thaliana: novel regulators in stress response and development. *Current Opinion in Plant Biology*, *11*(6), 695-701. https://doi.org/https://doi.org/10.1016/j.pbi.2008.10.005
Christiansen, M. W., Holm, P. B., & Gregersen, P. L. (2011). Characterization of barley (Hordeum vulgare L.) NAC transcription factors suggests conserved

functions compared to both monocots and dicots. *BMC research notes*, *4*(1), 302.
Chundawat, S. P., Donohoe, B. S., da Costa Sousa, L., Elder, T., Agarwal, U. P., Lu, F., Ralph, J., Himmel, M. E., Balan, V., & Dale, B. E. (2011). Multi-scale visualization and characterization of lignocellulosic plant cell wall deconstruction during thermochemical pretreatment. *Energy & Environmental Science*, *4*(3), 973-984.
Clarke, K. R. (1993). Non-parametric multivariate analyses of changes in community structure. *Australian journal of ecology*, *18*(1), 117-143.
Cochard, H., Ridolfi, M., & Dreyer, E. (1996). Responses to water stress in an ABA-unresponsive hybrid poplar (Populus koreana× trichocarpa cv. Peace) II. Hydraulic properties and xylem embolism. *New Phytologist*, *134*(3), 455-461.
Corso, D., Delzon, S., Lamarque, L. J., Cochard, H., Torres-Ruiz, J. M., King, A., & Brodribb, T. (2020). Neither xylem collapse, cavitation, or changing leaf conductance drive stomatal closure in wheat. *Plant, cell & environment*, *43*(4), 854-865.
Davis, S. D., Ewers, F. W., Sperry, J. S., Portwood, K. A., Crocker, M. C., & Adams, G. C. (2002). Shoot dieback during prolonged drought in Ceanothus (Rhamnaceae) chaparral of California: a possible case of hydraulic failure. *American Journal of Botany*, *89*(5), 820-828.
de Mendiburu, F., & Yaseen, M. (2021). Agricolae: statistical procedures for agricultural research. 2020. *Google Scholar There is no corresponding record for this reference*.
DeMartini, J. D., Pattathil, S., Miller, J. S., Li, H., Hahn, M. G., & Wyman, C. E. (2013). Investigating plant cell wall components that affect biomass recalcitrance in poplar and switchgrass. *Energy & Environmental Science*, *6*(3), 898-909.
Demirer, G. S., Zhang, H., Matos, J. L., Goh, N. S., Cunningham, F. J., Sung, Y., Chang, R., Aditham, A. J., Chio, L., & Cho, M.-J. (2019). High aspect ratio nanomaterials enable delivery of functional genetic material without DNA integration in mature plants. *Nature nanotechnology*, *14*(5), 456.
Des Marais, D. L., Hernandez, K. M., & Juenger, T. E. (2013). Genotype-by-environment interaction and plasticity: exploring genomic responses of plants to the abiotic environment. *Annual Review of Ecology, Evolution, and Systematics*, *44*, 5-29.
Dexter, E., Rollwagen-Bollens, G., & Bollens, S. M. (2018). The trouble with stress: A flexible method for the evaluation of nonmetric multidimensional scaling. *Limnology and Oceanography: Methods*, *16*(7), 434-443.
Ding, S.-Y., Liu, Y.-S., Zeng, Y., Himmel, M. E., Baker, J. O., & Bayer, E. A. (2012). How Does Plant Cell Wall Nanoscale Architecture Correlate with Enzymatic Digestibility? *Science*, *338*(6110), 1055-1060. https://doi.org/10.1126/science.1227491
Dixon, H. H., & Joly, J. (1895). XII. On the ascent of sap. *Philosophical Transactions of the Royal Society of London.(B.)*(186), 563-576.
Donohoe, B. S., & Resch, M. G. (2015). Mechanisms employed by cellulase systems to gain access through the complex architecture of lignocellulosic substrates. *Current opinion in chemical biology*, *29*, 100-107.

Esau, K. (1960). Anatomy of seed plants. *Soil Science*, *90*(2), 149.
Evans, L. S., & Perez, R. K. (2004). Diversity of cell lengths in intercalary meristem regions of grasses: location of the proliferative cell population. *Canadian Journal of Botany*, *82*(1), 115-122.
Fu, C., Mielenz, J. R., Xiao, X., Ge, Y., Hamilton, C. Y., Rodriguez, M., Jr., Chen, F., Foston, M., Ragauskas, A., Bouton, J., Dixon, R. A., & Wang, Z. Y. (2011). Genetic manipulation of lignin reduces recalcitrance and improves ethanol production from switchgrass [Research Support, U.S. Gov't, Non-P.H.S.]. *Proc Natl Acad Sci U S A*, *108*(9), 3803-3808. https://doi.org/10.1073/pnas.1100310108
Fukushima, R. S., & Hatfield, R. D. (2004). Comparison of the acetyl bromide spectrophotometric method with other analytical lignin methods for determining lignin concentration in forage samples. *Journal of Agricultural and Food Chemistry*, *52*(12), 3713-3720.
Giannini, J. (2017). *The OPN Microtome: An Inexpensive, Open Source Hand-Held Mini Microtome*. https://pages.stolaf.edu/wp-content/uploads/sites/803/2017/04/Giannini_OPN_Microtome_Manual_20170415.pdf
Giordano, R., Salleo, A., Salleo, S., & Wanderlingh, F. (1978). Flow in xylem vessels and Poiseuille's law. *Canadian Journal of Botany*, *56*(3), 333-338. https://doi.org/10.1139/b78-039
Gleason, S. M., Wiggans, D. R., Bliss, C. A., Young, J. S., Cooper, M., Willi, K. R., & Comas, L. H. (2017). Embolized stems recover overnight in Zea mays: The role of soil water, root pressure, and nighttime transpiration. *Frontiers in Plant Science*, *8*, 662.
Grabber, J. H. (2005). How do lignin composition, structure, and cross-linking affect degradability? A review of cell wall model studies.
Gu, Y., & Wylie, B. K. (2018). Mapping cropland waterway buffers for switchgrass development in the eastern Great Plains, USA. *GCB Bioenergy*, *10*(6), 415-424.
Hacke, U. G., Venturas, M. D., MacKinnon, E. D., Jacobsen, A. L., Sperry, J. S., & Pratt, R. B. (2015). The standard centrifuge method accurately measures vulnerability curves of long-vesselled olive stems. *New Phytologist*, *205*(1), 116-127. https://doi.org/https://doi.org/10.1111/nph.13017
Hall, M., Bansal, P., Lee, J. H., Realff, M. J., & Bommarius, A. S. (2011). Biological pretreatment of cellulose: Enhancing enzymatic hydrolysis rate using cellulose-binding domains from cellulases. *Bioresource technology*, *102*(3), 2910-2915.
Handakumbura, P. P., & Hazen, S. P. (2012). Transcriptional regulation of grass secondary cell wall biosynthesis: playing catch-up with Arabidopsis thaliana. *Frontiers in Plant Science*, *3*, 74.
Harrison, C. J., & Morris, J. L. (2018). The origin and early evolution of vascular plant shoots and leaves. *Philosophical Transactions of the Royal Society B: Biological Sciences*, *373*(1739), 20160496.
Hartman, J. C., Nippert, J. B., Orozco, R. A., & Springer, C. J. (2011). Potential ecological impacts of switchgrass (Panicum virgatum L.) biofuel cultivation in the Central Great Plains, USA. *Biomass and Bioenergy*, *35*(8), 3415-3421.

He, Y., Mouthier, T. M. B., Kabel, M. A., Dijkstra, J., Hendriks, W. H., Struik, P. C., & Cone, J. W. (2018). Lignin composition is more important than content for maize stem cell wall degradation. *Journal of the Science of Food and Agriculture*, *98*(1), 384-390. https://doi.org/10.1002/jsfa.8630

Hereford, J. (2009). A quantitative survey of local adaptation and fitness trade-offs. *The American Naturalist*, *173*(5), 579-588.

Himmel, M. E., Ding, S.-Y., Johnson, D. K., Adney, W. S., Nimlos, M. R., Brady, J. W., & Foust, T. D. (2007). Biomass recalcitrance: engineering plants and enzymes for biofuels production. *Science*, *315*(5813), 804-807.

Holloway-Phillips, M.-M., & Brodribb, T. J. (2011). Minimum hydraulic safety leads to maximum water-use efficiency in a forage grass. *Plant, cell & environment*, *34*(2), 302-313.

Hu, Z., & Ragauskas, A. J. (2011). Hydrothermal pretreatment of switchgrass. *Industrial & Engineering Chemistry Research*, *50*(8), 4225-4230.

Hu, Z., & Wen, Z. (2008). Enhancing enzymatic digestibility of switchgrass by microwave-assisted alkali pretreatment. *Biochemical Engineering Journal*, *38*(3), 369-378. https://doi.org/https://doi.org/10.1016/j.bej.2007.08.001

Hussey, S. G., Mizrachi, E., Spokevicius, A. V., Bossinger, G., Berger, D. K., & Myburg, A. A. (2011). SND2, a NAC transcription factor gene, regulates genes involved in secondary cell wall development in Arabidopsis fibres and increases fibre cell area in Eucalyptus. *BMC plant biology*, *11*(1), 1-17.

Jacobsen, A. (2011). *Standard centrifuge method for the determination of xylem vulnerability to cavitation*. https://doi.org/10.13140/RG.2.2.14164.30089

Jiang, D., Fang, J., Lou, L., Zhao, J., Yuan, S., Yin, L., Sun, W., Peng, L., Guo, B., & Li, X. (2015). Characterization of a null allelic mutant of the rice NAL1 gene reveals its role in regulating cell division. *PLoS One*, *10*(2), e0118169.

Jung, H., & Casler, M. (2006a). Maize Stem Tissues: Cell Wall Concentration and Composition during Development [Erratum: 2009 Nov-Dec, v. 49, no. 6, p. 2412.].

Jung, H., & Casler, M. (2006b). Maize stem tissues: impact of development on cell wall degradability. *Crop Science*, *46*(4), 1801-1809.

Kawecki, T. J., & Ebert, D. (2004). Conceptual issues in local adaptation. *Ecology letters*, *7*(12), 1225-1241.

Kearsey, M., & Farquhar, A. (1998). QTL analysis in plants; where are we now? *Heredity*, *80*(2), 137-142.

Kiernan, J. A. (1999). Histological and histochemical methods: theory and practice. *Shock*, *12*(6), 479.

Knight, J. B., Ehrichs, E. E., Kuperman, V. Y., Flint, J. K., Jaeger, H. M., & Nagel, S. R. (1996). Experimental study of granular convection. *Physical Review E*, *54*(5), 5726.

Knox, J. P. (1997). The use of antibodies to study the architecture and developmental regulation of plant cell walls. In *International review of cytology* (Vol. 171, pp. 79-120). Elsevier.

Kruskal, J. B. (1964a). Multidimensional scaling by optimizing goodness of fit to a nonmetric hypothesis. *Psychometrika*, *29*(1), 1-27. https://doi.org/10.1007/BF02289565

Kruskal, J. B. (1964b). Nonmetric multidimensional scaling: A numerical method. *Psychometrika*, *29*(2), 115-129. https://doi.org/10.1007/BF02289694

Lens, F., Picon-Cochard, C., Delmas, C. E., Signarbieux, C., Buttler, A., Cochard, H., Jansen, S., Chauvin, T., Chacon Doria, L., del Arco, M., & Delzon, S. (2016). Herbaceous angiosperms are not more vulnerable to drought-induced embolism than angiosperm trees. *Plant Physiology*. https://doi.org/10.1104/pp.16.00829

Lewis, A. M., & Boose, E. R. (1995). Estimating volume flow rates through xylem conduits. *American Journal of Botany*, *82*(9), 1112-1116.

Li, G., Jones, K. C., Eudes, A., Pidatala, V. R., Sun, J., Xu, F., Zhang, C., Wei, T., Jain, R., & Birdseye, D. (2018). Overexpression of a rice BAHD acyltransferase gene in switchgrass (Panicum virgatum L.) enhances saccharification. *BMC biotechnology*, *18*(1), 54.

Lin, F., Williams, B. J., Thangella, P. A., Ladak, A., Schepmoes, A. A., Olivos, H. J., Zhao, K., Callister, S. J., & Bartley, L. E. (2017). Proteomics coupled with metabolite and cell wall profiling reveal metabolic processes of a developing rice stem internode. *Frontiers in Plant Science*, *8*, 1134.

Lo Gullo, M., Castro Noval, L., Salleo, S., & Nardini, A. (2004). Hydraulic architecture of plants of Helianthus annuus L. cv. Margot: evidence for plant segmentation in herbs. *Journal of Experimental Botany*, *55*(402), 1549-1556.

Loow, Y.-L., Wu, T. Y., Jahim, J. M., Mohammad, A. W., & Teoh, W. H. (2016). Typical conversion of lignocellulosic biomass into reducing sugars using dilute acid hydrolysis and alkaline pretreatment. *Cellulose*, *23*(3), 1491-1520.

Lovell, J. T., MacQueen, A. H., Mamidi, S., Bonnette, J., Jenkins, J., Napier, J. D., Sreedasyam, A., Healey, A., Session, A., Shu, S., Barry, K., Bonos, S., Boston, L., Daum, C., Deshpande, S., Ewing, A., Grabowski, P. P., Haque, T., Harrison, M., Jiang, J., Kudrna, D., Lipzen, A., Pendergast, T. H., Plott, C., Qi, P., Saski, C. A., Shakirov, E. V., Sims, D., Sharma, M., Sharma, R., Stewart, A., Singan, V. R., Tang, Y., Thibivillier, S., Webber, J., Weng, X., Williams, M., Wu, G. A., Yoshinaga, Y., Zane, M., Zhang, L., Zhang, J., Behrman, K. D., Boe, A. R., Fay, P. A., Fritschi, F. B., Jastrow, J. D., Lloyd-Reilley, J., Martínez-Reyna, J. M., Matamala, R., Mitchell, R. B., Rouquette, F. M., Ronald, P., Saha, M., Tobias, C. M., Udvardi, M., Wing, R. A., Wu, Y., Bartley, L. E., Casler, M., Devos, K. M., Lowry, D. B., Rokhsar, D. S., Grimwood, J., Juenger, T. E., & Schmutz, J. (2021). Genomic mechanisms of climate adaptation in polyploid bioenergy switchgrass. *Nature*, *590*(7846), 438-444. https://doi.org/10.1038/s41586-020-03127-1

Lovell, J. T., Shakirov, E. V., Schwartz, S., Lowry, D. B., Aspinwall, M. J., Taylor, S. H., Bonnette, J., Palacio-Mejia, J. D., Hawkes, C. V., & Fay, P. A. (2016). Promises and challenges of eco-physiological genomics in the field: tests of drought responses in switchgrass. *Plant Physiology*, *172*(2), 734-748.

Lowry, D. B. (2012). Local adaptation in the model plant. *New Phytologist*, *194*(4), 888-890.

Lowry, D. B., Behrman, K. D., Grabowski, P., Morris, G. P., Kiniry, J. R., & Juenger, T. E. (2014). Adaptations between ecotypes and along environmental gradients in Panicum virgatum. *The American Naturalist*, *183*(5), 682-692.

Lowry, D. B., Lovell, J. T., Zhang, L., Bonnette, J., Fay, P. A., Mitchell, R. B., Lloyd-Reilley, J., Boe, A. R., Wu, Y., & Rouquette, F. M. (2019). QTL× environment interactions underlie adaptive divergence in switchgrass across a large latitudinal gradient. *Proceedings of the National Academy of Sciences*, *116*(26), 12933-12941.

Lowry, D. B., Taylor, S. H., Bonnette, J., Aspinwall, M. J., Asmus, A. L., Keitt, T. H., Tobias, C. M., & Juenger, T. E. (2015). QTLs for biomass and developmental traits in switchgrass (Panicum virgatum). *BioEnergy Research*, *8*(4), 1856-1867.

Lynch, J. P. (2011). Root phenes for enhanced soil exploration and phosphorus acquisition: tools for future crops. *Plant Physiology*, *156*(3), 1041-1049.

Mamedes-Rodrigues, T. C., Batista, D. S., Napoleão, T. A., Cruz, A. C. F., Fortini, E. A., Nogueira, F. T. S., Romanel, E., & Otoni, W. C. (2018). Lignin and cellulose synthesis and antioxidative defense mechanisms are affected by light quality in Brachypodium distachyon [journal article]. *Plant Cell, Tissue and Organ Culture (PCTOC)*, *133*(1), 1-14. https://doi.org/10.1007/s11240-017-1356-7

Mannan, S., Paul Knox, J., & Basu, S. (2017). Correlations between axial stiffness and microstructure of a species of bamboo. *Royal Society open science*, *4*(1), 160412.

Mascaro, J., Litton, C. M., Hughes, R. F., Uowolo, A., & Schnitzer, S. A. (2013). Is logarithmic transformation necessary in allometry? Ten, one-hundred, one-thousand-times yes. *Biological Journal of the Linnean Society*, *111*(1), 230-233. https://doi.org/10.1111/bij.12177

Mazarei, M., Al-Ahmad, H., Rudis, M. R., & Stewart Jr, C. N. (2008). Protoplast isolation and transient gene expression in switchgrass, Panicum virgatum L. *Biotechnology Journal: Healthcare Nutrition Technology*, *3*(3), 354-359.

McCulloh, K. A., Domec, J.-C., Johnson, D. M., Smith, D. D., & Meinzer, F. C. (2019). A dynamic yet vulnerable pipeline: Integration and coordination of hydraulic traits across whole plants. *Plant, cell & environment*, *42*(10), 2789-2807. https://doi.org/https://doi.org/10.1111/pce.13607

McCully, M., Huang, C., & Ling, L. (1998). Daily embolism and refilling of xylem vessels in the roots of field-grown maize. *The New Phytologist*, *138*(2), 327-342.

Meikle, P. J., Hoogenraad, N. J., Bonig, I., Clarke, A. E., & Stone, B. A. (1994). A (1→ 3, 1→ 4)-β-glucan-specific monoclonal antibody and its use in the quantitation and immunocytochemical location of (1→ 3, 1→ 4)-β-glucans. *The Plant Journal*, *5*(1), 1-9.

Milano, E. R., Lowry, D. B., & Juenger, T. E. (2016). The genetic basis of upland/lowland ecotype divergence in switchgrass (Panicum virgatum). *G3: Genes, Genomes, Genetics*, *6*(11), 3561-3570.

Mitra, P. P., & Loqué, D. (2014). Histochemical staining of Arabidopsis thaliana secondary cell wall elements. *Journal of visualized experiments: JoVE*(87).

Mitsuda, N., Iwase, A., Yamamoto, H., Yoshida, M., Seki, M., Shinozaki, K., & Ohme-Takagi, M. (2007). NAC transcription factors, NST1 and NST3, are key regulators of the formation of secondary walls in woody tissues of Arabidopsis. *The Plant Cell*, *19*(1), 270-280.

Moore, K., Moser, L. E., Vogel, K. P., Waller, S. S., Johnson, B., & Pedersen, J. F. (1991). Describing and quantifying growth stages of perennial forage grasses. *Agronomy Journal*, *83*(6), 1073-1077.

Motta, M. R., & Schnittger, A. (2021). A microtubule perspective on plant cell division. *Current Biology*, *31*(10), R547-R552. https://doi.org/https://doi.org/10.1016/j.cub.2021.03.087

Nageswara-Rao, M., Stewart, C. N., & Kwit, C. (2012
). Genetic diversity and structure of natural and agronomic switchgrass (Panicum virgatum L.) populations. *Genetic resources and crop evolution*, *60*(3), 1057-1068.

Nageswara-Rao, M., Stewart, C. N., & Kwit, C. (2013). Genetic diversity and structure of natural and agronomic switchgrass (Panicum virgatum L.) populations. *Genetic resources and crop evolution*, *60*(3), 1057-1068.

Neufeld, H. S., Grantz, D. A., Meinzer, F. C., Goldstein, G., Crisosto, G. M., & Crisosto, C. (1992). Genotypic variability in vulnerability of leaf xylem to cavitation in water-stressed and well-irrigated sugarcane. *Plant Physiology*, *100*(2), 1020-1028.

Nunes, T. D., Zhang, D., & Raissig, M. T. (2020). Form, development and function of grass stomata. *The Plant Journal*, *101*(4), 780-799.

Ocheltree, T. W., Nippert, J. B., & Prasad, P. V. V. (2016). A safety vs efficiency trade-off identified in the hydraulic pathway of grass leaves is decoupled from photosynthesis, stomatal conductance and precipitation. *New Phytologist*, *210*(1), 97-107. https://doi.org/10.1111/nph.13781

Ohashi-Ito, K., Oda, Y., & Fukuda, H. (2010). Arabidopsis VASCULAR-RELATED NAC-DOMAIN6 directly regulates the genes that govern programmed cell death and secondary wall formation during xylem differentiation. *The Plant Cell*, *22*(10), 3461-3473.

Olsen, A. N., Ernst, H. A., Leggio, L. L., & Skriver, K. (2005). NAC transcription factors: structurally distinct, functionally diverse. *Trends in Plant Science*, *10*(2), 79-87.

Ong, R. G., Higbee, A., Bottoms, S., Dickinson, Q., Xie, D., Smith, S. A., Serate, J., Pohlmann, E., Jones, A. D., & Coon, J. J. (2016). Inhibition of microbial biofuel production in drought-stressed switchgrass hydrolysate. *Biotechnology for biofuels*, *9*(1), 1-14.

Ooka, H., Satoh, K., Doi, K., Nagata, T., Otomo, Y., Murakami, K., Matsubara, K., Osato, N., Kawai, J., Carninci, P., Hayashizaki, Y., Suzuki, K., Kojima, K., Takahara, Y., Yamamoto, K., & Kikuchi, S. (2003). Comprehensive Analysis of NAC Family Genes in Oryza sativa and Arabidopsis thaliana. *DNA Research*, *10*(6), 239-247. https://doi.org/10.1093/dnares/10.6.239

Perrin, R., Vogel, K., Schmer, M., & Mitchell, R. (2008). Farm-scale production cost of switchgrass for biomass. *BioEnergy Research*, *1*(1), 91-97.

Pickard, W. F. (1981). The ascent of sap in plants. *Progress in biophysics and molecular biology*, *37*, 181-229.

Price, D. L., & Casler, M. D. (2014). Predictive Relationships between Plant Morphological Traits and Biomass Yield in Switchgrass. *Crop Science*, *54*(2), 637-645. https://doi.org/10.2135/cropsci2013.04.0272

R Development Core Team. (2022). R: A language and environment for statistical computing. R Foundation for Statistical Computing, Vienna, Austria. URL https://www.R-project.org/. In.
Rao, X., Chen, X., Shen, H., Ma, Q., Li, G., Tang, Y., Pena, M., York, W., Frazier, T. P., & Lenaghan, S. (2019). Gene regulatory networks for lignin biosynthesis in switchgrass (Panicum virgatum). *Plant biotechnology journal*, *17*(3), 580-593.
Rao, X., & Dixon, R. A. (2018). Current models for transcriptional regulation of secondary cell wall biosynthesis in grasses. *Frontiers in Plant Science*, *9*, 399.
Rasmussen, C. G., & Bellinger, M. (2018). An overview of plant division-plane orientation. *New Phytologist*, *219*(2), 505-512.
Reichmann, L. G., Collins, H. P., Jin, V. L., Johnson, M.-V. V., Kiniry, J. R., Mitchell, R. B., Polley, H. W., & Fay, P. A. (2018). Inter-Annual Precipitation Variability Decreases Switchgrass Productivity from Arid to Mesic Environments. *BioEnergy Research*, *11*(3), 614-622.
RStudio Team (2020). RStudio: Integrated Development for R. RStudio, PBC, Boston, MA URL http://www.rstudio.com/. In.
Sade, N., Gebremedhin, A., & Moshelion, M. (2012). Risk-taking plants: anisohydric behavior as a stress-resistance trait. *Plant signaling & behavior*, *7*(7), 767-770. https://doi.org/10.4161/psb.20505
Sagyndyk, K., Aidossova, S., & Prasad, M. (2007). Grasses tolerant to radionuclides growing in kazakhstan nuclear test sites exhibit structural and ultrastructural changes-implications for phytoremedaition and involved risks. *Terrestrial and Aquatic Ecotoxicology*, *1*, 70-77.
Saha, M. C., Bhandhari, H. S., & Bouton, J. H. (2013). *Bioenergy Feedstocks: Breeding and Genetics*. John Wiley & Sons.
Saha, S., & Ramachandran, S. (2013). Genetic improvement of plants for enhanced bio-ethanol production. *Recent Pat DNA Gene Seq.*, *7*. https://doi.org/10.2174/1872215611307010006
Sakai, K., Citerne, S., Antelme, S., Le Bris, P., Daniel, S., Bouder, A., D'Orlando, A., Cartwright, A., Tellier, F., Pateyron, S., Delannoy, E., Laudencia-Chingcuanco, D., Mouille, G., Palauqui, J. C., Vogel, J., & Sibout, R. (2021). BdERECTA controls vasculature patterning and phloem-xylem organization in Brachypodium distachyon. *BMC plant biology*, *21*(1), 196. https://doi.org/10.1186/s12870-021-02970-2
Sanderson, M. A., Adler, P. R., Boateng, A. A., Casler, M. D., & Sarath, G. (2006). Switchgrass as a biofuels feedstock in the USA. *Canadian Journal of Plant Science*, *86*(Special Issue), 1315-1325.
Sanford, G. R., Oates, L. G., Roley, S. S., Duncan, D. S., Jackson, R. D., Robertson, G. P., & Thelen, K. D. (2017). Biomass production a stronger driver of cellulosic ethanol yield than biomass quality. *Agronomy Journal*, *109*(5).
Sarath, G., Dien, B., Saathoff, A. J., Vogel, K. P., Mitchell, R. B., & Chen, H. (2011). Ethanol yields and cell wall properties in divergently bred switchgrass genotypes. *Bioresource technology*, *102*(20), 9579-9585.
Scagline-Mellor, S., Griggs, T., Skousen, J., Wolfrum, E., & Holásková, I. (2018). Switchgrass and Giant Miscanthus Biomass and Theoretical Ethanol Production from Reclaimed Mine Lands. *BioEnergy Research*, 1-12.

Schindelin, J., Arganda-Carreras, I., Frise, E., Kaynig, V., Longair, M., Pietzsch, T., Preibisch, S., Rueden, C., Saalfeld, S., Schmid, B., Tinevez, J.-Y., White, D. J., Hartenstein, V., Eliceiri, K., Tomancak, P., & Cardona, A. (2012). Fiji: an open-source platform for biological-image analysis [Perspective]. *Nature Methods*, *9*, 676. https://doi.org/10.1038/nmeth.2019
https://www.nature.com/articles/nmeth.2019#supplementary-information
Schlichting, C. D. (1986). The evolution of phenotypic plasticity in plants. *Annual review of ecology and systematics*, *17*(1), 667-693.
Schmer, M. R., Vogel, K. P., Mitchell, R. B., & Perrin, R. K. (2008). Net energy of cellulosic ethanol from switchgrass. *Proceedings of the National Academy of Sciences*, *105*(2), 464-469.
Schneider, H. M., Strock, C. F., Hanlon, M. T., Vanhees, D. J., Perkins, A. C., Ajmera, I. B., Sidhu, J. S., Mooney, S. J., Brown, K. M., & Lynch, J. P. (2021). Multiseriate cortical sclerenchyma enhance root penetration in compacted soils. *Proceedings of the National Academy of Sciences*, *118*(6).
Schwab, F., Zhai, G., Kern, M., Turner, A., Schnoor, J. L., & Wiesner, M. R. (2016). Barriers, pathways and processes for uptake, translocation and accumulation of nanomaterials in plants – Critical review. *Nanotoxicology*, *10*(3), 257-278. https://doi.org/10.3109/17435390.2015.1048326
Scoffoni, C., Albuquerque, C., Brodersen, C. R., Townes, S. V., John, G. P., Cochard, H., Buckley, T. N., McElrone, A. J., & Sack, L. (2017). Leaf vein xylem conduit diameter influences susceptibility to embolism and hydraulic decline. *New Phytologist*, *213*(3), 1076-1092.
Serba, D. D., Daverdin, G., Bouton, J. H., Devos, K. M., Brummer, E. C., & Saha, M. C. (2015). Quantitative trait loci (QTL) underlying biomass yield and plant height in switchgrass. *BioEnergy Research*, *8*(1), 307-324.
Serba, D. D., Sykes, R. W., Gjersing, E. L., Decker, S. R., Daverdin, G., Devos, K. M., Brummer, E. C., & Saha, M. C. (2016). Cell wall composition and underlying QTL in an F 1 pseudo-testcross population of switchgrass. *BioEnergy Research*, *9*(3), 836-850.
Shen, H., Yin, Y., Chen, F., Xu, Y., & Dixon, R. A. (2009). A bioinformatic analysis of NAC genes for plant cell wall development in relation to lignocellulosic bioenergy production. *BioEnergy Research*, *2*(4), 217.
Shimotsuma, M., & Schoefl, G. I. (1992). A method for embedding thin membranes in historesin. *Biotechnic & histochemistry*, *67*(6), 377-379.
Shtein, I., Baruchim, P., & Lev-Yadun, S. (2021). Division of labour among culms in the clonal reed Arundo donax (Poaceae) is underlain by their pre-determined hydraulic structure. *Botanical Journal of the Linnean Society*, *195*(3), 348-356.
Somleva, M., Tomaszewski, Z., & Conger, B. (2002). Agrobacterium-mediated genetic transformation of switchgrass. *Crop Science*, *42*(6), 2080-2087.
Somssich, M., Je, B. I., Simon, R., & Jackson, D. (2016). CLAVATA-WUSCHEL signaling in the shoot meristem. *Development*, *143*(18), 3238-3248.
Soukup, A., & Tylová, E. (2019). Essential methods of plant sample preparation for light microscopy. In *Plant cell morphogenesis* (pp. 1-26). Springer.

Stiller, V., Lafitte, H. R., & Sperry, J. S. (2003). Hydraulic properties of rice and the response of gas exchange to water stress. *Plant Physiology*, *132*(3), 1698-1706.

Taiz, L., Zeiger, E., Møller, I. M., & Murphy, A. (2015). *Plant physiology and development*. Sinauer Associates Incorporated.

Takahashi, H., Kamakura, H., Sato, Y., Shiono, K., Abiko, T., Tsutsumi, N., Nagamura, Y., Nishizawa, N. K., & Nakazono, M. (2010). A method for obtaining high quality RNA from paraffin sections of plant tissues by laser microdissection. *Journal of plant research*, *123*(6), 807-813.

Taylor-Teeples, M., Lin, L., De Lucas, M., Turco, G., Toal, T., Gaudinier, A., Young, N., Trabucco, G., Veling, M., & Lamothe, R. (2015). An Arabidopsis gene regulatory network for secondary cell wall synthesis. *Nature*, *517*(7536), 571-575.

Ten Hove, C. A., & Heidstra, R. (2008). Who begets whom? Plant cell fate determination by asymmetric cell division. *Current Opinion in Plant Biology*, *11*(1), 34-41.

Townsley, B., Sinha, N., & Kang, J. (2013). KNOX1 genes regulate lignin deposition and composition in monocots and dicots [Original Research]. *Frontiers in Plant Science*, *4*. https://doi.org/10.3389/fpls.2013.00121

Trabucco, G. M., Matos, D. A., Lee, S. J., Saathoff, A. J., Priest, H. D., Mockler, T. C., Sarath, G., & Hazen, S. P. (2013). Functional characterization of cinnamyl alcohol dehydrogenase and caffeic acid O-methyltransferase in Brachypodium distachyon. *BMC biotechnology*, *13*(1), 61. https://doi.org/10.1186/1472-6750-13-61

Tsuda, K., Abraham-Juarez, M.-J., Maeno, A., Dong, Z., Aromdee, D., Meeley, R., Shiroishi, T., Nonomura, K.-i., & Hake, S. (2017). KNOTTED1 Cofactors, BLH12 and BLH14, Regulate Internode Patterning and Vein Anastomosis in Maize. *The Plant Cell*, *29*(5), 1105-1118. https://doi.org/10.1105/tpc.16.00967

Tu, Y., Rochfort, S., Liu, Z., Ran, Y., Griffith, M., Badenhorst, P., Louie, G. V., Bowman, M. E., Smith, K. F., & Noel, J. P. (2010). Functional analyses of caffeic acid O-methyltransferase and cinnamoyl-CoA-reductase genes from perennial ryegrass (Lolium perenne). *The Plant Cell*, *22*(10), 3357-3373.

Valdivia, E. R., Herrera, M. T., Gianzo, C., Fidalgo, J., Revilla, G., Zarra, I., & Sampedro, J. (2013). Regulation of secondary wall synthesis and cell death by NAC transcription factors in the monocot Brachypodium distachyon. *Journal of Experimental Botany*, *64*(5), 1333-1343.

Vega-Sanchez, M., Verhertbruggen, Y., Scheller, H. V., & Ronald, P. (2013). Abundance of mixed linkage glucan in mature tissues and secondary cell walls of grasses. *Plant signaling & behavior*, *8*(2), e23143.

Venturas, M. D., Pratt, R. B., Jacobsen, A. L., Castro, V., Fickle, J. C., & Hacke, U. G. (2019). Direct comparison of four methods to construct xylem vulnerability curves: differences among techniques are linked to vessel network characteristics. *Plant, cell & environment*.

Venturas, M. D., Sperry, J. S., & Hacke, U. G. (2017). Plant xylem hydraulics: What we understand, current research, and future challenges. *Journal of Integrative Plant Biology*, *59*(6), 356-389. https://doi.org/10.1111/jipb.12534

Vermaas, J. V., Petridis, L., Qi, X., Schulz, R., Lindner, B., & Smith, J. C. (2015). Mechanism of lignin inhibition of enzymatic biomass deconstruction. *Biotechnology for biofuels*, *8*(1), 217.
Vilagrosa, A., Bellot, J., Vallejo, V., & Gil-Pelegrín, E. (2003). Cavitation, stomatal conductance, and leaf dieback in seedlings of two co-occurring Mediterranean shrubs during an intense drought. *Journal of Experimental Botany*, *54*(390), 2015-2024.
Vogel, J. (2008). Unique aspects of the grass cell wall. *Current Opinion in Plant Biology*, *11*(3), 301-307. https://doi.org/https://doi.org/10.1016/j.pbi.2008.03.002
Vogel, K. P., Dien, B. S., Jung, H. G., Casler, M. D., Masterson, S. D., & Mitchell, R. B. (2011). Quantifying actual and theoretical ethanol yields for switchgrass strains using NIRS analyses. *BioEnergy Research*, *4*(2), 96-110.
Vogel, K. P., Sarath, G., Saathoff, A. J., & Mitchell, R. B. (2011). Switchgrass.
Vogel, K. P., Schmer, M. R., & Mitchell, R. B. (2005). Plant adaptation regions: ecological and climatic classification of plant materials. *Rangeland ecology & management*, *58*(3), 315-319.
Volaire, F., Lens, F., Cochard, H., Xu, H., Chacon-Doria, L., Bristiel, P., Balachowski, J., Rowe, N., Violle, C., & Picon-Cochard, C. (2018). Embolism and mechanical resistances play a key role in dehydration tolerance of a perennial grass Dactylis glomerata L. *Annals of Botany*, *122*(2), 325-336. https://doi.org/10.1093/aob/mcy073
Wang, S., Yang, H., Mei, J., Liu, X., Wen, Z., Zhang, L., Xu, Z., Zhang, B., & Zhou, Y. (2019). Rice homeobox protein KNAT7 integrates the pathways regulating cell expansion and wall stiffness. *Plant Physiology*, *181*(2), 669-682.
Weiner, J. (2004). Allocation, plasticity and allometry in plants. *Perspectives in Plant Ecology, Evolution and Systematics*, *6*(4), 207-215.
Wilson, J., & Mertens, D. (1995). Cell wall accessibility and cell structure limitations to microbial digestion of forage. *Crop Science*, *35*(1), 251-259.
Wright, L. (2007). Historical perspective on how and why switchgrass was selected as a "model" high-potential energy crop. *ORNL/TM-2007/109 Oak Ridge, TN: Bioenergy Resources and Engineering Systems*.
Wullschleger, S. D., Davis, E. B., Borsuk, M. E., Gunderson, C. A., & Lynd, L. (2010). Biomass production in switchgrass across the United States: database description and determinants of yield. *Agronomy Journal*, *102*(4), 1158-1168.
Xu, J., Cheng, J. J., Sharma-Shivappa, R. R., & Burns, J. C. (2010). Sodium Hydroxide Pretreatment of Switchgrass for Ethanol Production. *Energy & Fuels*, *24*(3), 2113-2119. https://doi.org/10.1021/ef9014718
Yamaguchi, M., Goué, N., Igarashi, H., Ohtani, M., Nakano, Y., Mortimer, J. C., Nishikubo, N., Kubo, M., Katayama, Y., & Kakegawa, K. (2010). VASCULAR-RELATED NAC-DOMAIN6 and VASCULAR-RELATED NAC-DOMAIN7 effectively induce transdifferentiation into xylem vessel elements under control of an induction system. *Plant Physiology*, *153*(3), 906-914.
Yamamuro, C., Ihara, Y., Wu, X., Noguchi, T., Fujioka, S., Takatsuto, S., Ashikari, M., Kitano, H., & Matsuoka, M. (2000). Loss of function of a rice brassinosteroid

insensitive1 homolog prevents internode elongation and bending of the lamina joint. *The Plant Cell*, *12*(9), 1591-1605.
Yan, H., Zhang, A., Ye, Y., Xu, B., Chen, J., He, X., Wang, C., Zhou, S., Zhang, X., & Peng, Y. (2017). Genome-wide survey of switchgrass NACs family provides new insights into motif and structure arrangements and reveals stress-related and tissue-specific NACs. *Scientific reports*, *7*(1), 1-15.
Yin, P., Meng, F., Liu, Q., An, R., Cai, J., & Du, G. (2019). A comparison of two centrifuge techniques for constructing vulnerability curves: insight into the 'open-vessel' artifact. *Physiologia Plantarum*, *165*(4), 701-710. https://doi.org/https://doi.org/10.1111/ppl.12738
Youngs, H., & Somerville, C. (2012). Development of feedstocks for cellulosic biofuels. *F1000 biology reports*, *4*.
Yuan, X., Wang, H., Cai, J., Li, D., & Song, F. (2019). NAC transcription factors in plant immunity. *Phytopathology Research*, *1*(1), 1-13.
Zhang, Q., Xie, Z., Zhang, R., Xu, P., Liu, H., Yang, H.-Q., Doblin, M. S., Bacic, A., & Li, L. (2018). Blue light regulates secondary cell wall thickening via MYC2/MYC4 activation of the NST1-directed transcriptional network in Arabidopsis. *The Plant Cell*. https://doi.org/10.1105/tpc.18.00315
Zhao, K., & Bartley, L. E. (2014). Comparative genomic analysis of the R2R3 MYB secondary cell wall regulators of Arabidopsis, poplar, rice, maize, and switchgrass. *BMC plant biology*, *14*(1), 135.
Zhong, R., Demura, T., & Ye, Z.-H. (2006). SND1, a NAC domain transcription factor, is a key regulator of secondary wall synthesis in fibers of Arabidopsis. *The Plant Cell*, *18*(11), 3158-3170.
Zhong, R., Lee, C., McCarthy, R. L., Reeves, C. K., Jones, E. G., & Ye, Z.-H. (2011). Transcriptional activation of secondary wall biosynthesis by rice and maize NAC and MYB transcription factors. *Plant and Cell Physiology*, *52*(10), 1856-1871.
Zhong, R., Richardson, E. A., & Ye, Z.-H. (2007). Two NAC domain transcription factors, SND1 and NST1, function redundantly in regulation of secondary wall synthesis in fibers of Arabidopsis. *Planta*, *225*(6), 1603-1611.
Zhong, R., Yuan, Y., Spiekerman, J. J., Guley, J. T., Egbosiuba, J. C., & Ye, Z.-H. (2015). Functional characterization of NAC and MYB transcription factors involved in regulation of biomass production in switchgrass (Panicum virgatum). *PLoS One*, *10*(8), e0134611.
Zuo, C., Blow, M., Sreedasyam, A., Kuo, R. C., Ramamoorthy, G. K., Torres-Jerez, I., Li, G., Wang, M., Dilworth, D., & Barry, K. (2018). Revealing the transcriptomic complexity of switchgrass by PacBio long-read sequencing. *Biotechnology for biofuels*, *11*(1), 170.

Appendix A: Supplementary Tables

Table S2.1. Traits, Genotypes, and Environments

Plant Architecture

Trait	Genotype	Environment
Height	AP13	KBSM20, KBSM16, CLMB18, CLMB16, PKLE17, PKLE16
	WBC	KBSM20, KBSM16, CLMB18, CLMB16, PKLE17, PKLE16
	VS16	KBSM20, KBSM16, CLMB18, CLMB16, PKLE17, PKLE16
	DAC	KBSM20, KBSM16, CLMB18, CLMB16
Internode Diameter *(Outer Diameter)*	AP13	KBSM20, KBSM16, CLMB18, CLMB16, PKLE17, PKLE16
	WBC	KBSM20, KBSM16, CLMB18, CLMB16, PKLE17, PKLE16
	VS16	KBSM20, KBSM16, CLMB18, CLMB16, PKLE17, PKLE16
	DAC	KBSM20, KBSM16, CLMB18, CLMB16
Internode Length	AP13	KBSM20
	WBC	KBSM20
	VS16	KBSM20
	DAC	KBSM20
Node Count per Tiller *(Node Count)*	AP13	KBSM20
	WBC	KBSM20
	VS16	KBSM20
	DAC	KBSM20
Flag Leaf -1 Area	AP13	KBSM20
	WBC	KBSM20
	VS16	KBSM20
	DAC	KBSM20
Total Leaf Area	AP13	KBSM20
	WBC	KBSM20
	VS16	KBSM20
	DAC	KBSM20
Sheath Thickness at Midvein *(Sheath)*	AP13	KBSM20
	WBC	KBSM20
	VS16	KBSM20
	DAC	KBSM20

Internode Anatomy

Internode Annulus Radius	AP13	KBSM20, KBSM16, CLMB18, CLMB16, PKLE17, PKLE16
	WBC	KBSM20, KBSM16, CLMB18, CLMB16, PKLE17, PKLE16
	VS16	KBSM20, KBSM16, CLMB18, CLMB16, PKLE17, PKLE16
	DAC	KBSM20, KBSM16, CLMB18, CLMB16

Cortical Cell File Radius *(Cortex Radius)*	AP13	KBSM20, KBSM16, CLMB18, CLMB16, PKLE17, PKLE16
	WBC	KBSM20, KBSM16, CLMB18, CLMB16, PKLE17, PKLE16
	VS16	KBSM20, KBSM16, CLMB18, CLMB16, PKLE17, PKLE16
	DAC	KBSM20, KBSM16, CLMB18, CLMB16
Chlorenchyma Radial Thickness *(CHLR Radial Thickness)*	AP13	KBSM20, KBSM16, CLMB18, CLMB16, PKLE17, PKLE16
	WBC	KBSM20, KBSM16, CLMB18, CLMB16, PKLE17, PKLE16
	VS16	KBSM20, KBSM16, CLMB18, CLMB16, PKLE17, PKLE16
	DAC	KBSM20, KBSM16, CLMB18, CLMB16
Sclerenchyma Radial Thickness *(SCLR Radial Thickness)*	AP13	KBSM20, KBSM16, CLMB18, CLMB16, PKLE17, PKLE16
	WBC	KBSM20, KBSM16, CLMB18, CLMB16, PKLE17, PKLE16
	VS16	KBSM20, KBSM16, CLMB18, CLMB16, PKLE17, PKLE16
	DAC	KBSM20, KBSM16, CLMB18, CLMB16
Vascular Bundle Fiber Area Percent of Vascular Bundle Area	AP13	KBSM20, KBSM16, CLMB18, CLMB16, PKLE17, PKLE16
	WBC	KBSM20, KBSM16, CLMB18, CLMB16, PKLE17, PKLE16
	VS16	KBSM20, KBSM16, CLMB18, CLMB16, PKLE17, PKLE16
	DAC	KBSM20, KBSM16, CLMB18, CLMB16
Xylem Diameters of Cortical Vascular Bundles *(Xylem Diameter Cortex)*	AP13	KBSM20, KBSM16, CLMB18, CLMB16, PKLE17, PKLE16
	WBC	KBSM20, KBSM16, CLMB18, CLMB16, PKLE17, PKLE16
	VS16	KBSM20, KBSM16, CLMB18, CLMB16, PKLE17, PKLE16
	DAC	KBSM20, KBSM16, CLMB18, CLMB16
Phloem Area per Vascular Bundle	AP13	KBSM16, CLMB18, CLMB16, PKLE17, PKLE16
	WBC	KBSM16, CLMB18, CLMB16, PKLE17, PKLE16
	VS16	KBSM16, CLMB18, CLMB16, PKLE17, PKLE16
	DAC	KBSM16, CLMB18, CLMB16
Cortical Parenchyma Cell Wall Thickness *(Cortex Cell Wall Thickness)*	AP13	KBSM20, KBSM16, CLMB18, CLMB16, PKLE17, PKLE16
	WBC	KBSM20, KBSM16, CLMB18, CLMB16, PKLE17, PKLE16
	VS16	KBSM20, KBSM16, CLMB18, CLMB16, PKLE17, PKLE16
	DAC	KBSM20, KBSM16, CLMB18, CLMB16
Sclerenchyma Cell Wall Thickness	AP13	KBSM20

(SCLR Cell Wall Thickness)		
	WBC	KBSM20
	VS16	KBSM20
	DAC	KBSM20
Cell Wall Area per Lignified Fiber	AP13	KBSM16, CLMB16, PKLE17, PKLE16
	WBC	KBSM16, CLMB16, PKLE17, PKLE16
	VS16	KBSM16, CLMB16, PKLE17, PKLE16
	DAC	KBSM16, CLMB16, PKLE17, PKLE16
Epidermis and Hypodermis Cell Count	AP13	KBSM20, KBSM16, CLMB18, CLMB16, PKLE17, PKLE16
	WBC	KBSM20, KBSM16, CLMB18, CLMB16, PKLE17, PKLE16
	VS16	KBSM20, KBSM16, CLMB18, CLMB16, PKLE17, PKLE16
	DAC	KBSM20, KBSM16, CLMB18, CLMB16
Nearest Cortical Vascular Bundle Neighbor *(Nearest VB Neighbor Cortex)*	AP13	KBSM20, KBSM16, CLMB18, CLMB16, PKLE17, PKLE16
	WBC	KBSM20, KBSM16, CLMB18, CLMB16, PKLE17, PKLE16
	VS16	KBSM20, KBSM16, CLMB18, CLMB16, PKLE17, PKLE16
	DAC	KBSM20, KBSM16, CLMB18, CLMB16
Nearest Sclerenchyma Vascular Bundle Neighbor *(Nearest VB Neighbor SCLR)*	AP13	KBSM20, KBSM16, CLMB18, CLMB16, PKLE17, PKLE16
	WBC	KBSM20, KBSM16, CLMB18, CLMB16, PKLE17, PKLE16
	VS16	KBSM20, KBSM16, CLMB18, CLMB16, PKLE17, PKLE16
	DAC	KBSM20, KBSM16, CLMB18, CLMB16
Rind Radial Thickness percent of Internode Annulus Radius *(Rind Percent Annulus Radius)*	AP13	KBSM20, KBSM16, CLMB18, CLMB16, PKLE17, PKLE16
	WBC	KBSM20, KBSM16, CLMB18, CLMB16, PKLE17, PKLE16
	VS16	KBSM20, KBSM16, CLMB18, CLMB16, PKLE17, PKLE16
	DAC	KBSM20, KBSM16, CLMB18, CLMB16
Cortex Radial Thickness percent of Internode Annulus Radius *(Cortex Percent Annulus Radius)*	AP13	KBSM20, KBSM16, CLMB18, CLMB16, PKLE17, PKLE16
	WBC	KBSM20, KBSM16, CLMB18, CLMB16, PKLE17, PKLE16
	VS16	KBSM20, KBSM16, CLMB18, CLMB16, PKLE17, PKLE16
	DAC	KBSM20, KBSM16, CLMB18, CLMB16
Cortex Lumen Diameter	AP13	KBSM20
	WBC	KBSM20
	VS16	KBSM20

	DAC	KBSM20
Sclerenchyma Lumen Diameter	AP13	KBSM20
	WBC	KBSM20
	VS16	KBSM20
	DAC	KBSM20
Hydraulic Conductivity		
Pressure to Induce 50% Loss of Hydraulic Conductivity of Internode-Node Segment *(P50)*	AP13	KBSM20
	WBC	KBSM20
	VS16	KBSM20
	DAC	KBSM20
Stem Specific Conductance *(Ks)*	AP13	KBSM20
	WBC	KBSM20
	VS16	KBSM20
	DAC	KBSM20

Table S2.2. Deconstruction Treatment Conditions

Pre-treatment	Code
0.62 mM NaOH	P1
6.25 mM NaOH	P2
62.5 mM NaOH	P3
Temperature °C for 3 hours	
45	T1
90	T2
Enzyme Concentration	
0.05 uL	E1
0.50 uL	E2
5.00 uL	E3

Table S4.1 | NIRS analyte descriptions

Analyte	Definition
GH	Global H
IVDMD	In vitro dry matter digestibility
NDF	Neutral detergent fiber
ADF	Acid detergent fiber
ADL	Acid detergent lignin
N	Nitrogen
DM	Dry matter
FAT	Fat
ASH	Minerals (total ash)
C	Carbon
KL	Klason Lignin
UA	Uronic acids
RHA	Rhamnose
FUC	Fucose
ARA	Arabinose
XYL	Xylose
MAN	Mannose
GAL	Galactose
GLC	Glucose
PCA	*p*-Coumarate esters
FEST	Esterified ferulates
FETH	Etherified ferulates
CWC	Cell wall concentration
AXMG	ARA + XYL + Man + GAL
AX	ARA +XYL
SUC	Sucrose
GLCS	Soluble glucose
FRU	Fructose
SC	Total soluble carbohydrates
STA	Starch
ETOH	Ethanol/g dry forage
PENT	Pentose sugars released/g dry forage
HEX	Total hexoses
SUG	Total sugars
PPEN	Pentose proportion of total carbohydrates (%)
HEXE	Theoretical ethanol from hexoses (excluding starch)
PENTP	Pentoses extraction efficiency (%)
HEXEP	Hexose ethanol extraction efficiency (%)
CWE	Cell wall ethanol
CWEP	Theoretical ethanol conversion efficiency from cell wall hexosans (%)
NSC	Non-structural carbohydrates (starch + SC)
PSOL	Proportion of hexoses that are non-structural or soluble (%)

NSCE	Estimated ethanol from non-structural carbohydrates
CAL	Calories

All descriptions reproduced from Vogel et al. 2011
All analytes presented as mg /g except where noted

Table S4.2 | Expanded Table 4.1. Biomass compositional traits predicted with NIRS

Phase[a]	1	1	2	Complete[b]
Mill Type	Wiley + Cyclone	Wiley + Cyclone	Wiley + Cyclone	Wiley + Cyclone
Genotype	Plant A	Plant B	WBC	WBC
Milling Sites	7	8	3	10
Forage				
GH	2.4 (0.6)**	2.4 (0.38)**	8.1 (2.8)	1.7 (0.5)***
IVDMD	490 (26)	420 (25)	300 (27)	400 (66)***
NDF	770 (12)	790 (13)	790 (27)	780 (28)***
ADF	440 (17)	460 (15)	560 (16)	500 (33)***
ADL	67 (5.6)	71 (4.7)	120 (4.8)	85 (8)***
Nitrogen	7.2 (0.95)	4.8 (0.63)	0.5 (0.35)	4.9 (1.8)***
ASHall	52 (3.6)**	53 (4.7)	30 (4.4)	43 (6)***
Bioenergy[c]				
GH	7.8 (1.4)	10 (1.9)*	25 (8.2)	6.4 (1.3)***
IVDMD	420 (22)	380 (23)	280 (23)	355 (37)***
NDF	770 (15)	790 (12)	870 (17)	792 (17)***
ADF	420 (14)	430 (13)	520 (18)	443 (18)***
ADL	58 (3.9)	63 (4.1)	97 (3)	76 (8)***
N	7 (0.85)	4.9 (0.58)	2.5 (0.42)*	7 (1.3)***
DM	910 (1.4)	920 (1.8)	930 (2)	915 (2.9)***
FAT	13 (1)	13 (0.81)	15 (0.89)	12 (2.2)***
ASH	81 (6.8)*	82 (5)	73 (13)	89 (11)***
C	440 (1.8)	450 (2.7)	450 (4.6)*	433 (7.4)***
KL	290 (13)	300 (17)*	370 (23)*	319 (39)***
UA	16 (0.27)	15 (0.33)	14 (0.3)	16 (0.5)***
RHA	0.34 (0.089)	0.37 (0.11)**	0.62 (0.12)	1 (0.2)***
FUC	0.19 (0.026)	0.22 (0.024)	0.43 (0.022)	0.26 (0.03)***
ARA	30 (0.93)	30 (0.82)	21 (1.2)	27 (1.8)***
XYL	200 (3.4)**	210 (3.7)	200 (9.8)	186 (8.6)***
MAN	7.3 (0.66)	6.2 (0.5)	8.4 (0.7)	7 (1.1)***

GAL	8 (0.56)	8 (0.57)	2.5 (0.7)	11 (33)**
GLC	300 (6.3)	300 (6.1)*	290 (10)	290 (7.9)***
PCA	8 (0.42)	7.4 (0.37)	7.8 (0.67)	6 (0.8)***
FEST	2.1 (0.14)	1.8 (0.15)*	0.84 (0.34)	1 (0.3)***
FETH	0.15 (0.12)*	0.27 (0.18)	1.7 (0.25)	0.2 (0.5)***
CWC	ND	ND	930 (23)	815 (36)***
AXMG	ND	ND	240 (8.7)	229 (8.3)***
AX	ND	ND	250 (7)	224 (7.8)***
SUC	37 (2.5)	36 (2.7)	19 (8.7)	17 (6.6)***
GLCS	11 (0.88)	13 (1.2)	21 (4.2)	10 (3.3)***
FRU	6.3 (1.4)	5 (1.8)*	1.1 (1.2)	5 (2.3)***
SC	ND	ND	62 (15)	38 (9.3)***
STA	5.5 (1.4)*	7 (1.6)	19 (3.7)	16 (6.5)***
ETOH	83 (4.2)	79 (3.1)	61 (8.2)	69 (8.5)***
PENT	180 (4.6)	200 (4)	190 (6.9)	181 (8.7)***
HEX	ND	ND	420 (13)	369 (16)***
SUG	ND	ND	660 (8.1)	645 (14.8)***
PPEN	ND	ND	0.38 (0.012)	0.42 (0.01)***
HEXE	ND	ND	220 (5.6)	190 (6.3)***
PENTP	ND	ND	78 (2.2)	77 (1.8)***
HEXEP	ND	ND	34 (4.7)	39 (4.3)***
CWE	ND	ND	49 (3.6)	51 (6)***
CWEP	ND	ND	9.4 (1.9)	29 (4.4)***
NSC	ND	ND	65 (18)	38 (12)***
PSOL	ND	ND	0.13 (0.04)	0.12 (0.03)***
NSCE	ND	ND	35 (8.3)	20 (6)***
CAL	4200 (9.2)	4100 (12)	4200 (15)	4100 (16)***
Total significantly different analytes	5	5	3	All

[a] Phase 1 and 2 biomass harvested from single location
[b] Biomass harvested from field grown clones
[c] Vogel et al. 2011
Reported significance refers to averages: '***' p<0.001 , '**' p<0.01 , '*' p<0.05
Different Wiley mills were used to mill biomass from individual plants, A and B, in phase 1. Phase 2 includes six WBC clones grown at single sites and milled with three different Wiley mills. Data shown is the average and standard deviation in parentheses for each trait of listed genotypes. Significance determined by MANOVA. All Wiley mills fit with 2 mm screen, Cyclone mills with 1 mm screen. Significantly variable traits are displayed in Table 4.1. “ns” indicates comparison is not significant. All traits (mg/g) except CAL, (cal/g). Values in red are produced with previous calibration equations, all others produced with the updated calibrations.

Table S4.3 | Full table of all trait values after only Wiley milling

Phase[a]	1	1	2
Mill Type	Wiley	Wiley	Wiley
Genotype	A	B	WBC
Milling Sites	7	8	3
Forage			
GH	2.5 (0.38)***	2.8 (0.48)**	7.8 (2.3)
IVDMD	450 (30)	380 (23)	250 (18)
NDF	800 (11)	810 (13)	790 (26)
ADF	450 (20)	480 (16)	560 (17)
ADL	69 (6.1)	74 (5.2)	120 (5.1)
Nitrogen	7.5 (1.2)	4.3 (0.8)	()
ASHall	23 (5.1)**	20 (5.1)**	12 (4.9)
Bioenergy[b]			
GH	6.3 (0.67)**	8.9 (1.4)	22 (5.6)
IVDMD	430 (27)	370 (26)	240 (20)
NDF	790 (16)	830 (17)	910 (18)
ADF	430 (17)	450 (14)	540 (15)
ADL	60 (4.8)	66 (3.9)	99 (3.1)
N	7.5 (1.1)	5 (0.53)	2.9 (0.6)
DM	920 (2)	920 (2)	930 (2)
FAT	10 (1.1)	12 (0.89)	19 (1.9)*
ASH	70 (7.7)**	74 (6.8)*	88 (18)
C	440 (2.6)	440 (2.5)	450 (3.9)
KL	240 (13)	250 (16)	340 (21)
UA	16 (0.3)	15 (0.32)	14 (0.18)
RHA	0.74 (0.13)	0.81 (0.11)	0.88 (0.1)
FUC	0.21 (0.027)	0.26 (0.023)	0.43 (0.019)
ARA	27 (1.1)	27 (1.2)	19 (0.94)
XYL	200 (4.7)	210 (4.5)**	200 (9.2)
MAN	8.9 (0.76)***	8.6 (0.87)	11 (0.56)
GAL	7.7 (0.79)	7.2 (0.88)	1.7 (0.83)
GLC	310 (7.3)	310 (5.3)	300 (11)
PCA	8.6 (0.56)	8.5 (0.47)	8.5 (0.69)
FEST	2.4 (0.16)***	2.2 (0.14)	1.3 (0.26)
FETH	0.4 (0.25)	0.37 (0.21)*	1.3 (0.35)**
CWC	ND	ND	970 (36)
AXMG	ND	ND	240 (8.5)
AX	ND	ND	250 (9.3)
SUC	30 (3.7)	24 (4.4)	11 (4.6)

GLCS	9.8 (1.4)**	12 (1.5)	20 (4.5)
FRU	6.1 (1.5)	4.2 (1.9)	1.3 (1.6)
SC	ND	ND	62 (17)
STA	4.6 (1.6)	6.4 (1.7)*	14 (4)
ETOH	88 (4.3)	85 (3.6)	62 (8.2)
PENT	180 (3.4)	200 (4.9)	190 (7.3)
HEX	ND	ND	440 (13)
SUG	ND	ND	650 (8)
PPEN	ND	ND	0.37 (0.011)
HEXE	ND	ND	220 (5.8)
PENTP	ND	ND	77 (2.1)
HEXEP	ND	ND	32 (5)
CWE	ND	ND	51 (4)
CWEP	ND	ND	7.8 (2)
NSC	ND	ND	65 (18)
PSOL	ND	ND	0.14 (0.043)
NSCE	ND	ND	32 (8.6)
CAL	4200 (11)*	4200 (17)	4200 (15)

[a] Phase 1 and 2 biomass harvested from single location

[b] Vogel et al. 2011

Reported significance refers to averages: '***' $p<0.001$, '**' $p<0.01$, '*' $p<0.05$

Appendix B: Supplementary Figures

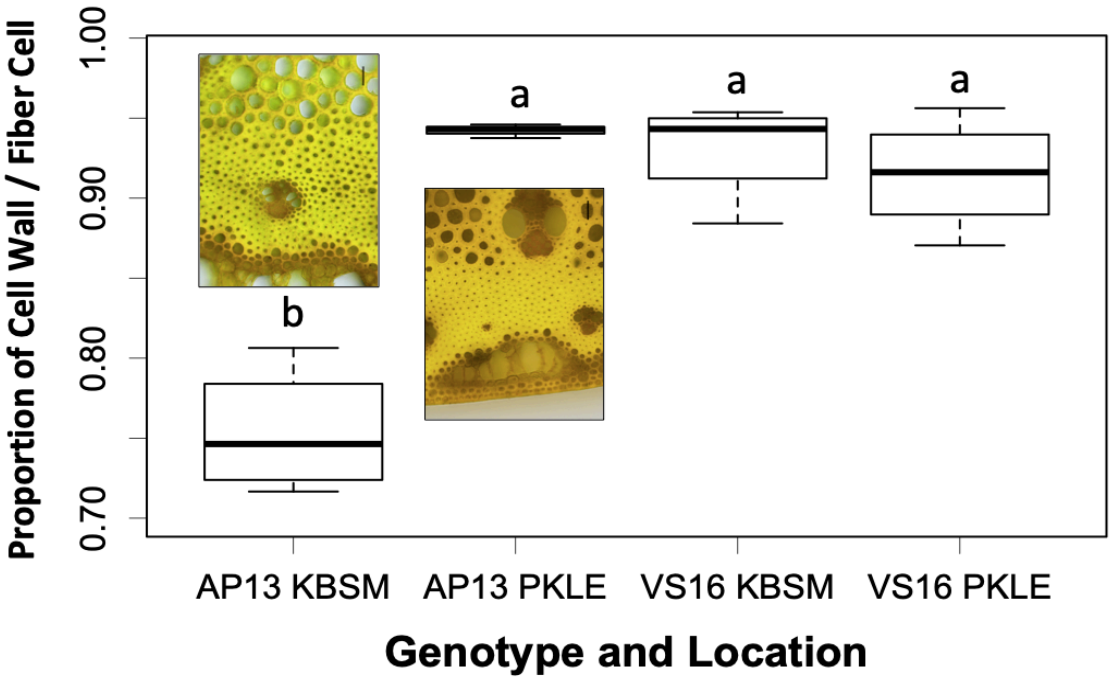

Figure S2.1. Average proportion of cell wall per sclerenchyma fiber cell is significantly reduced in AP13 grown at KBSM (0.75) compared to the PKLE site (0.95) while VS16 remains consistent across sites. Measurements taken only on 2016/2017 collection, 3 sections per each of 3 individual plant per genotype per site. Measured as cell wall area of entire cell area, see figure S2.4 for method description. Scale bars 25 µm.

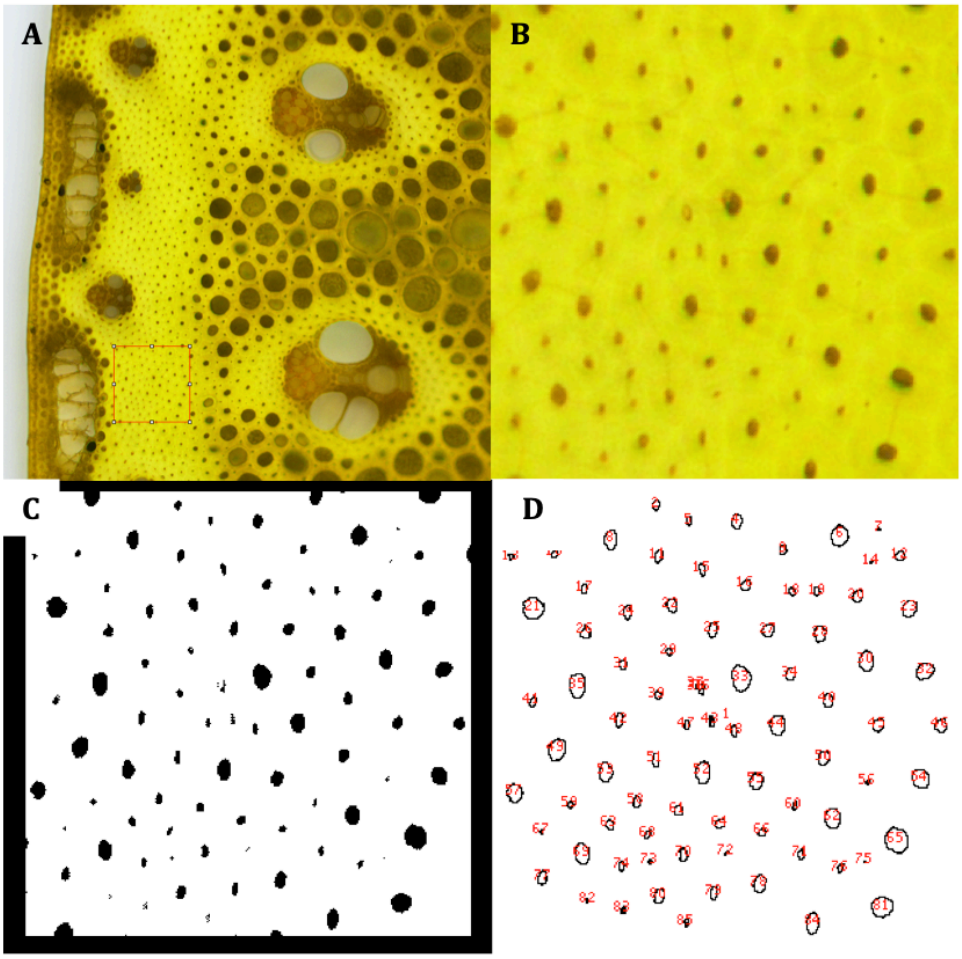

Figure S2.2. Cell wall area detection with FIJI for the cell wall per fiber cell area measurements. (A) A square is drawn in the sclerenchyma that captures representative cells and is cut from the larger image. (B and C) Contrast is optimized, and the cut image made binary. (D) The function "analyze particles" is run to identify cell count and measure each cell lumen area. A manual inspection of the image is required to confirm only true lumens are identified and to rule out the inclusion of cell corners, pit canals, or otherwise misidentified lumens contained in the image. The cell lumen area is subtracted from the total image area to produce the total cell wall area. Cell wall area per cell is calculated by dividing the cell wall area by the cell count. All measurements taken in FIJI, calculations conducted in Excel.

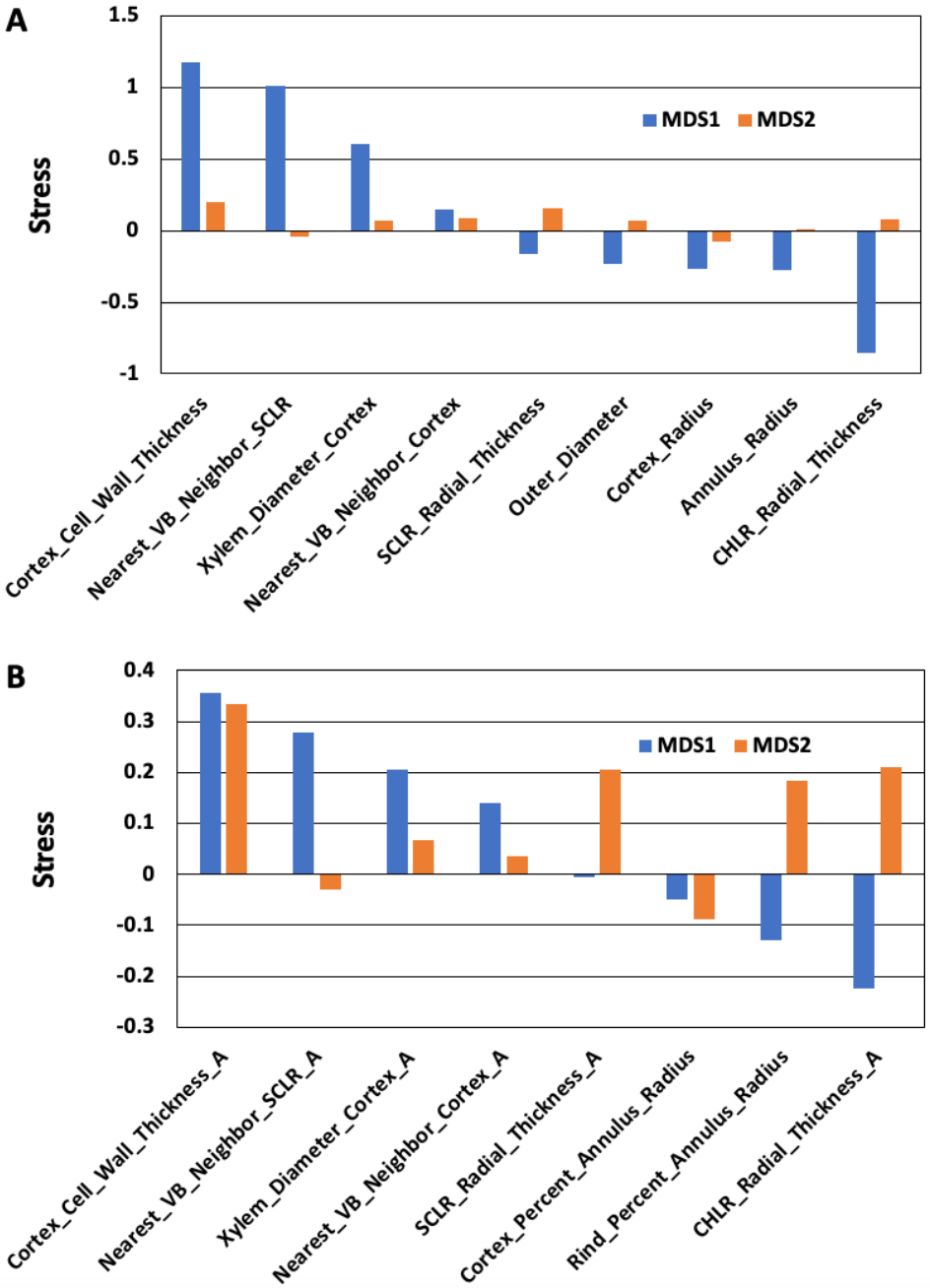

Figure S2.3. Internode anatomy includes traits with both high and low stress, indicating a lack of trait ranking preservation. Stress, a quantitative measure of ordination fit, has a cutoff at 0.2 above which the ordination becomes unranked for traits exceeding this threshold. (A) NMDS stress shows four traits with stress that exceeds +/- 0.2 which suggests these traits do not rank with the traits that have stress levels below the 0.2 threshold. (B) In an attempt to reduce high stress, the traits were scaled to their respective annulus radii. The stress is reduced after scaling though cortical cell wall thickness, nearest vascular bundle neighbor in the sclerenchyma chlorenchyma radial thickness and xylem diameter of cortex vascular bundles all raise above the 0.3 threshold. These results further indicate a lack of consistent trait rankings.

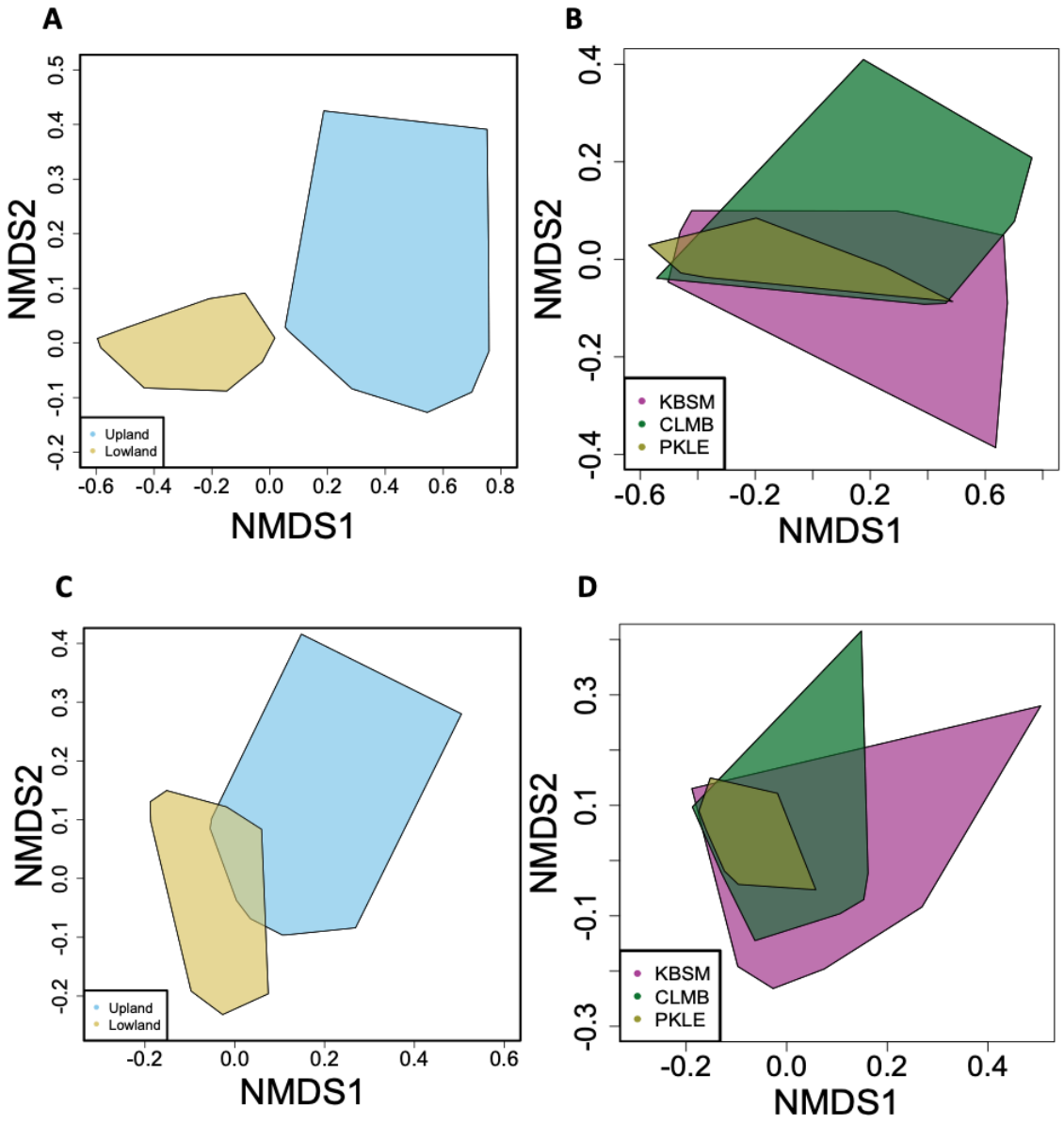

Figure S2.4. Internode anatomy phenes are similar across sites without sorting by genotype, though scaling to annulus radius reveals increasing dissimilarity by latitude in NMDS. (A) Three sites show significant overlap in raw data in unscaled data when AP13, WBC, VS16, and DAC data is combined. (B) Scaled data to annulus radius shows that the southern site is most similar, followed by CLMB, and KBSM. Data is from six environments described in Table 2.1.

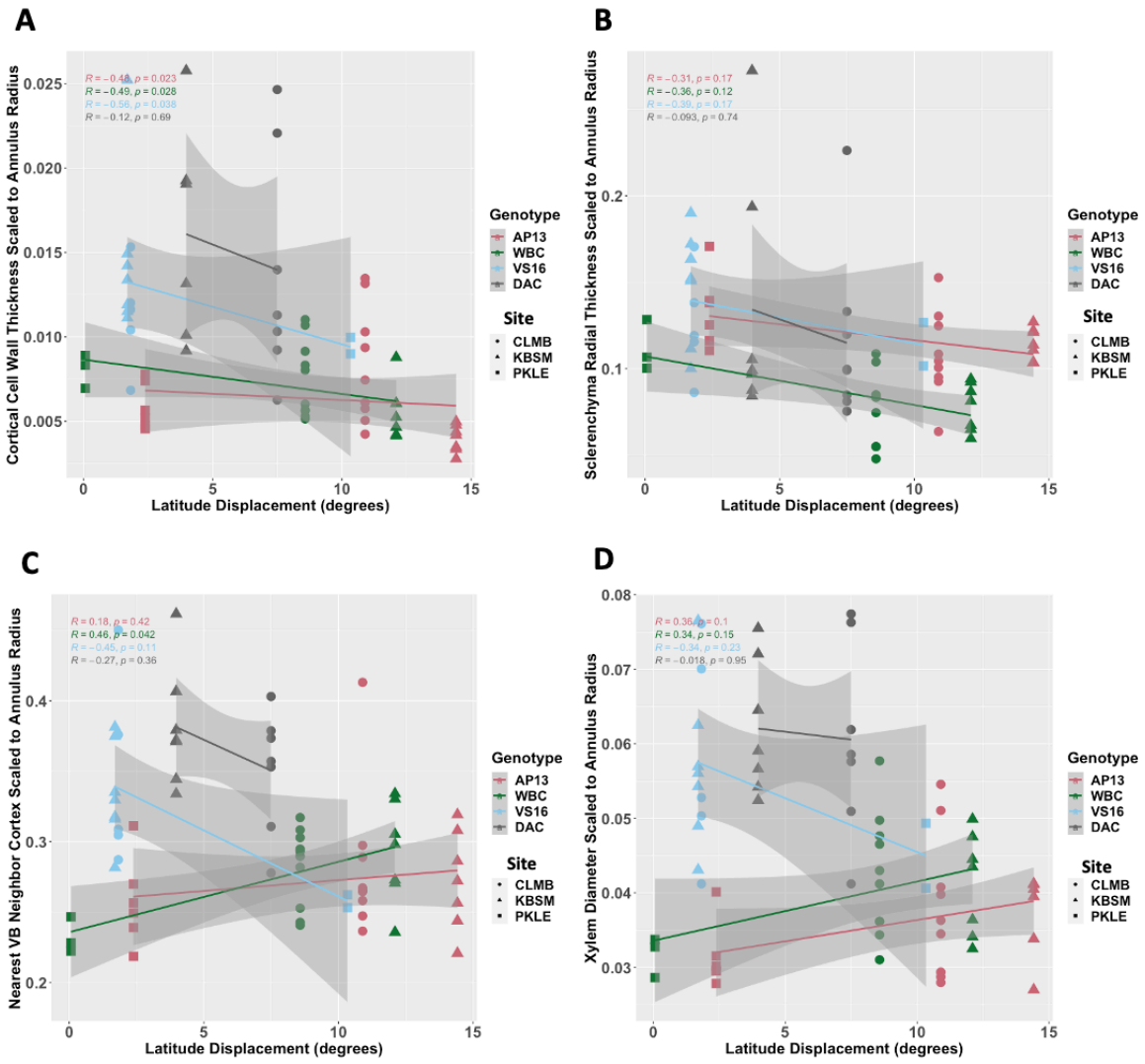

Figure S2.5. Vascular bundle distance and xylem diameter decrease in uplands and increase in lowlands with latitude displacement across three sites. (A) All four genotypes, uplands displaced southward, and lowlands displaced northward, show a decrease in average cortical cell wall thickness when grown further from latitude of origin. (B) Similarly, Sclerenchyma radial thickness show the same negative trend with latitude displacement. (C and D) However, not all traits show this pattern with nearest neighbor vascular bundle distance in the cortex and xylem diameter exhibiting an increase in both traits for lowlands, and a decrease for uplands with latitude displacement. This suggests that atypical environmental conditions have a similar global influence that reduces cortical cell wall thickening, and differently in among ecotypes. 1.5x IQR applied to remove outliers.

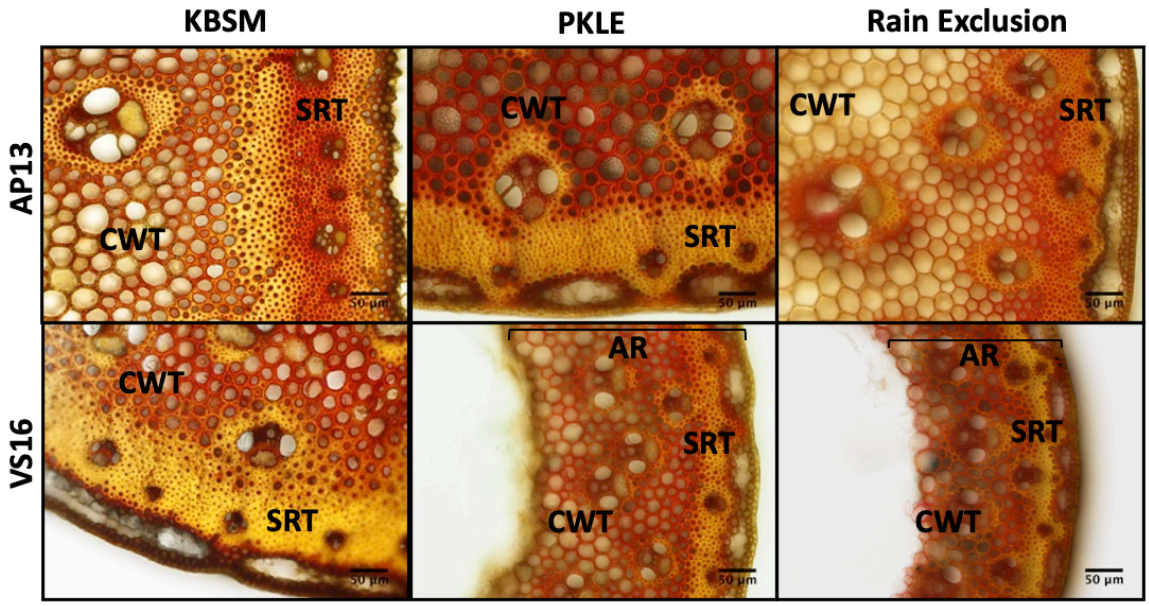

Figure S2.6. Two genotypes show internode anatomy phenotypic variation across sites and a diminished stature when grown under rain exclusion. Significant differences in cortical cell wall thickness (CWT), sclerenchyma radial thickness (SRT), and annulus radius (AR) are clear between AP13 and VS16. The Maule reaction stains s-rich lignin red and g-rich lignin gold that reveals compositional differences across cell types and between genotypes. Images taken with 20x objective. See Figure S17.

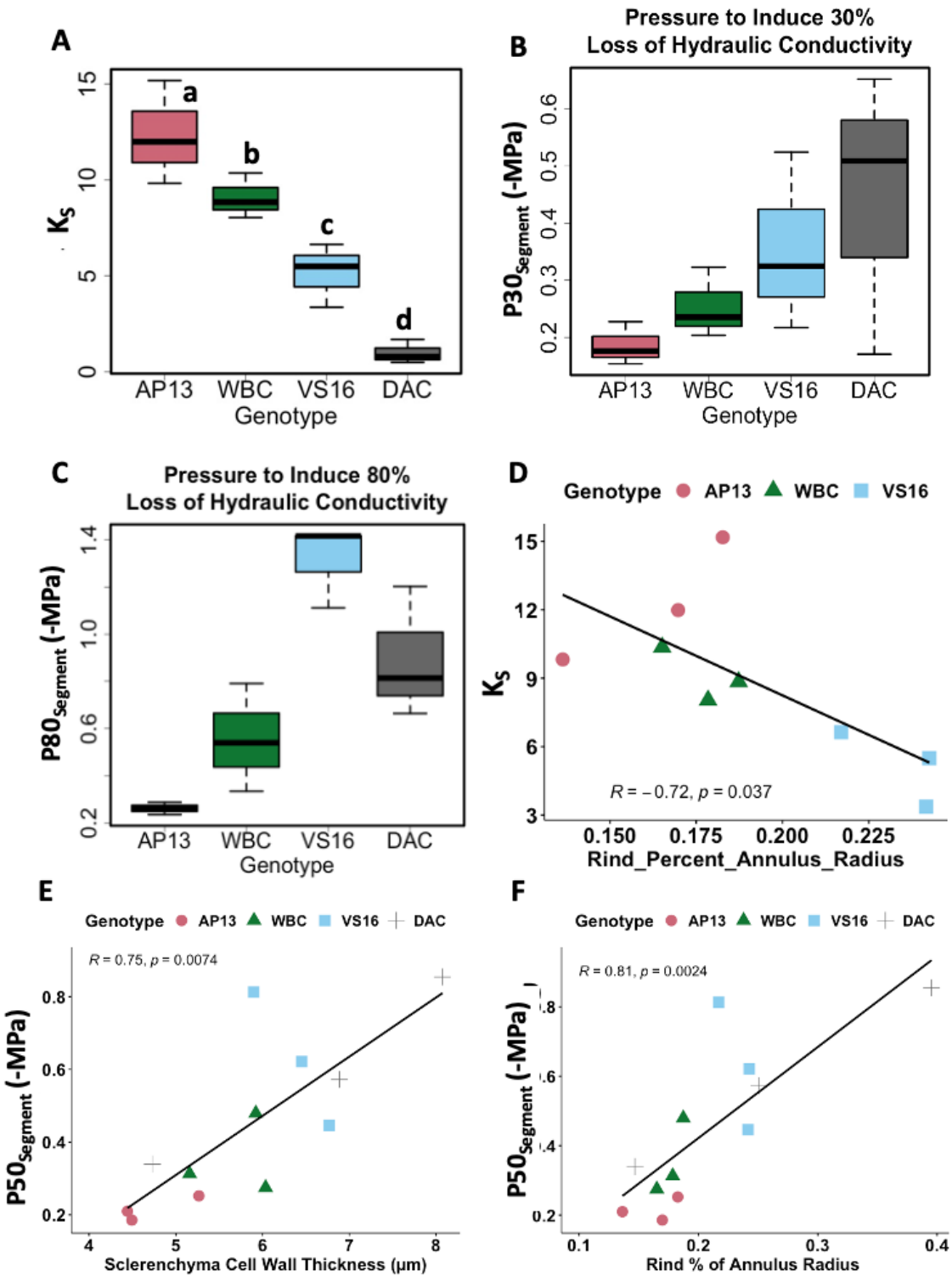

Figure S2.7. Maximum stem hydraulic conductivity (K_S) and resistance to hydraulic conductivity loss ($P50_{Segment}$). (A) raw hydraulic conductivity. (B) $P30_{Segment}$. (C) $P80_{Segment}$. (D) Rind % negatively correlated with K_S. (E) SCLR positively correlated and (F) rind % annulus radius are both negatively correlated with $P50_{Segment}$.

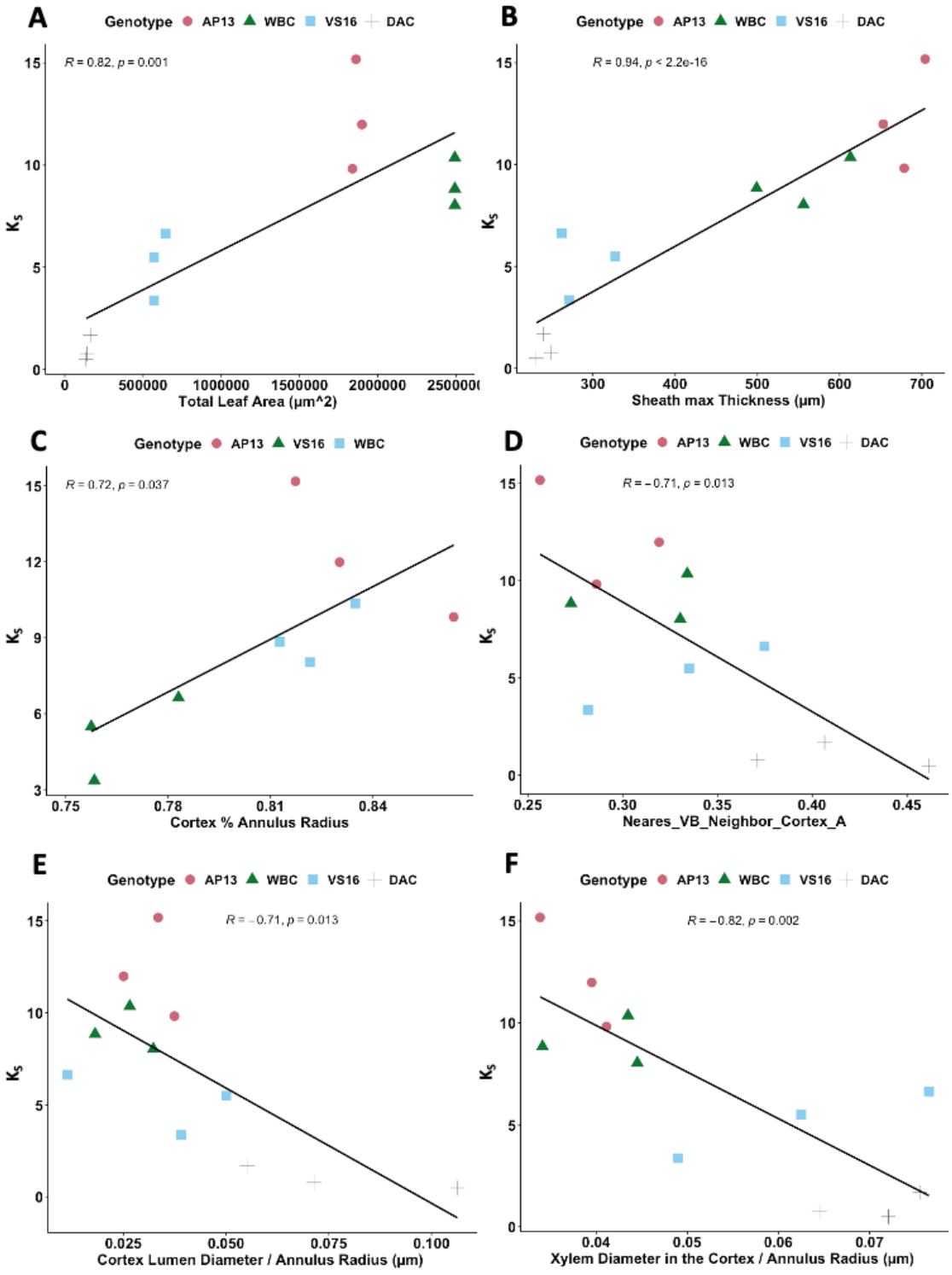

Figure S2.8 Several significant relationships with K_s vs. leaf traits and annulus radius scaled internode anatomy. (A) Total leaf area (SCC = 0.82) vs. Ks shows that lowlands are larger than the uplands in both features. (B) Sheath maximum thickness is also largest in the lowlands and shows a highly significant positive correlation (SCC = 0.94), with AP13 the largest. Considering traits that influence stem water storage capacity (capacitance) in relation to K_s is best to do so with scaled data to annulus radius. This way

we can compare the differences in proportion of tissues and cells relative to genotype differences, etc, rather than raw values. (C) Cortex % of the annulus radius is not significant with all four genotypes (data not shown in figure) but is significant with DAC removed (SCC = 0.72). (D) The distance between vascular bundles in the cortex scaled to annulus radius is negatively correlated with K_s (SCC = -0.71) and is largest in DAC, while the other genotypes all overlap. (E) Cortex cell lumen diameter scaled to annulus radius is also negatively correlated (SCC = -0.71), with DAC again having the largest proportion of cortex lumen diameter / annulus radius. (F) Lastly, xylem diameter in cortex vascular bundles scaled to annulus radius negatively correlates with K_s (SCC = -0.82).

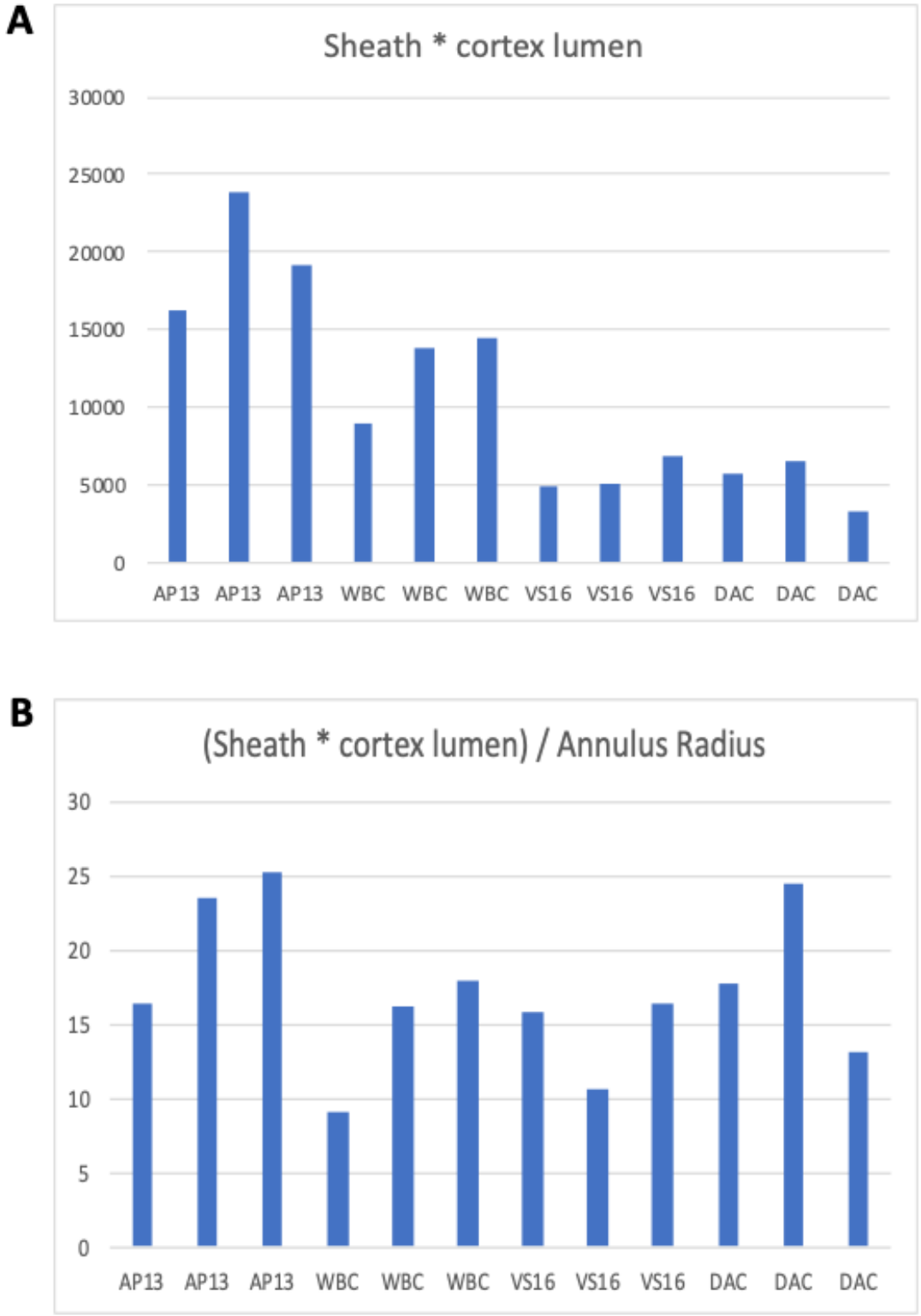

Figure S2.9 Capacitance related traits (A) Raw capacitance related trait values are higher in lowlands and significantly different from uplands ($p < 0.001$). (B) Differences are no longer significant when the features are scaled to annulus radius with genotypes practically indistinguishable from each other.

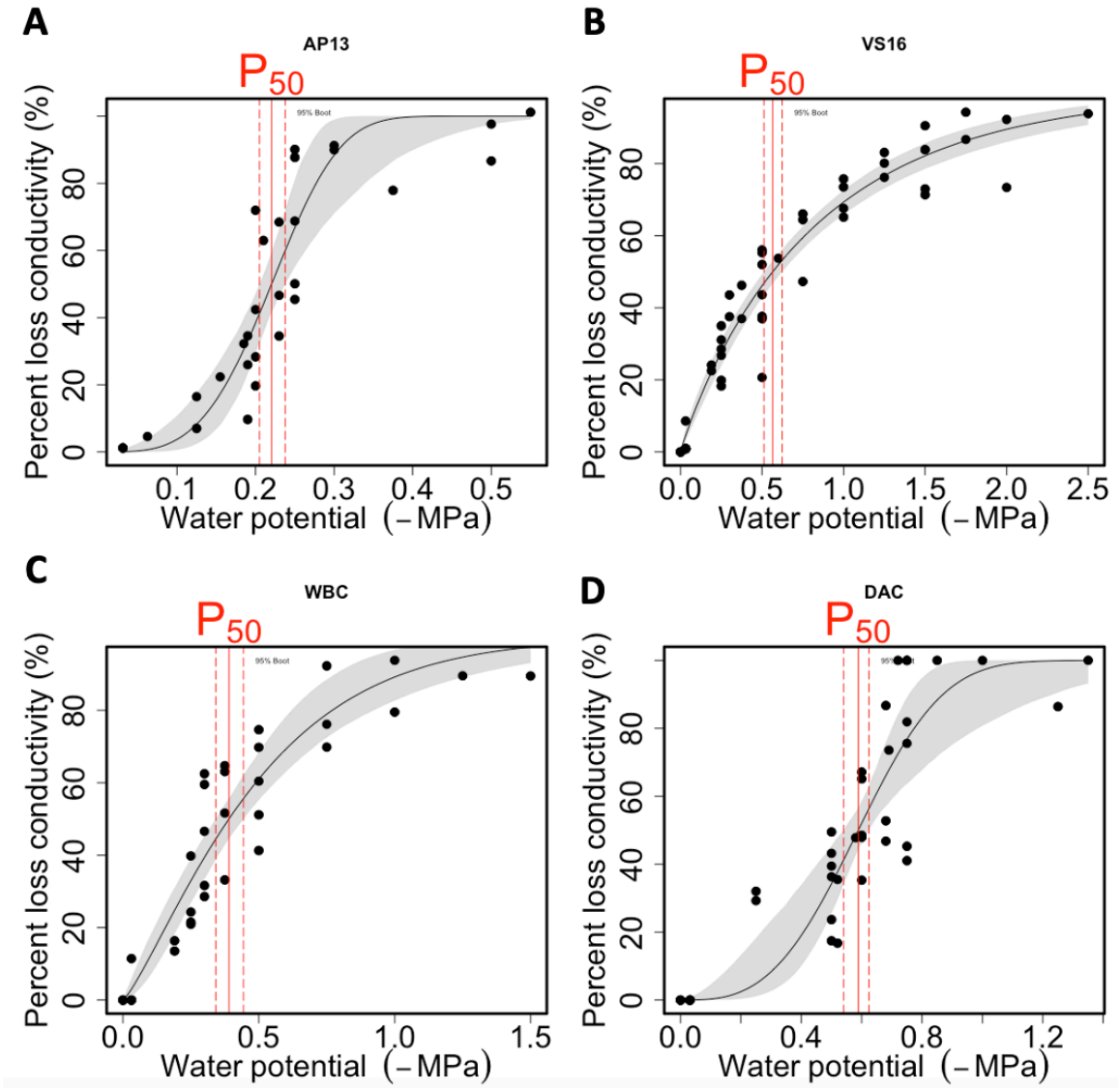

Figure S2.10. **Percent loss of conductivity curves reveal mild resistance overall**. Though resistance to loss of conductivity is mild, pressures to induce 50 PLC in all four genotypes are statistically different (P<0.001) by ecotype; AP13 (-0.21 MPa), WBC (-0.30 MPa), DAC (-0.57 MPa), and VS16 (-0.62 MPa). VS16 showed the highest resistance to conductivity loss by requiring -1.9 MPa to induce 90% loss of conductivity, compared to DAC (-1.0 MPA), AP13 (-0.29 MPA), and WBC (-0.72 MPa). Curves generated with the standard centrifuge technique and hydraulic conductivity apparatus used to measure conductivity with ConductR in R studio. vulnerability curves are produced from multiple stems segments per genotype taken to 90% loss of conductivity or greater. Segments per genotype are 5 or more; 5 segments each for AP13 and WBC, 6 for VS16, and 7 for DAC.

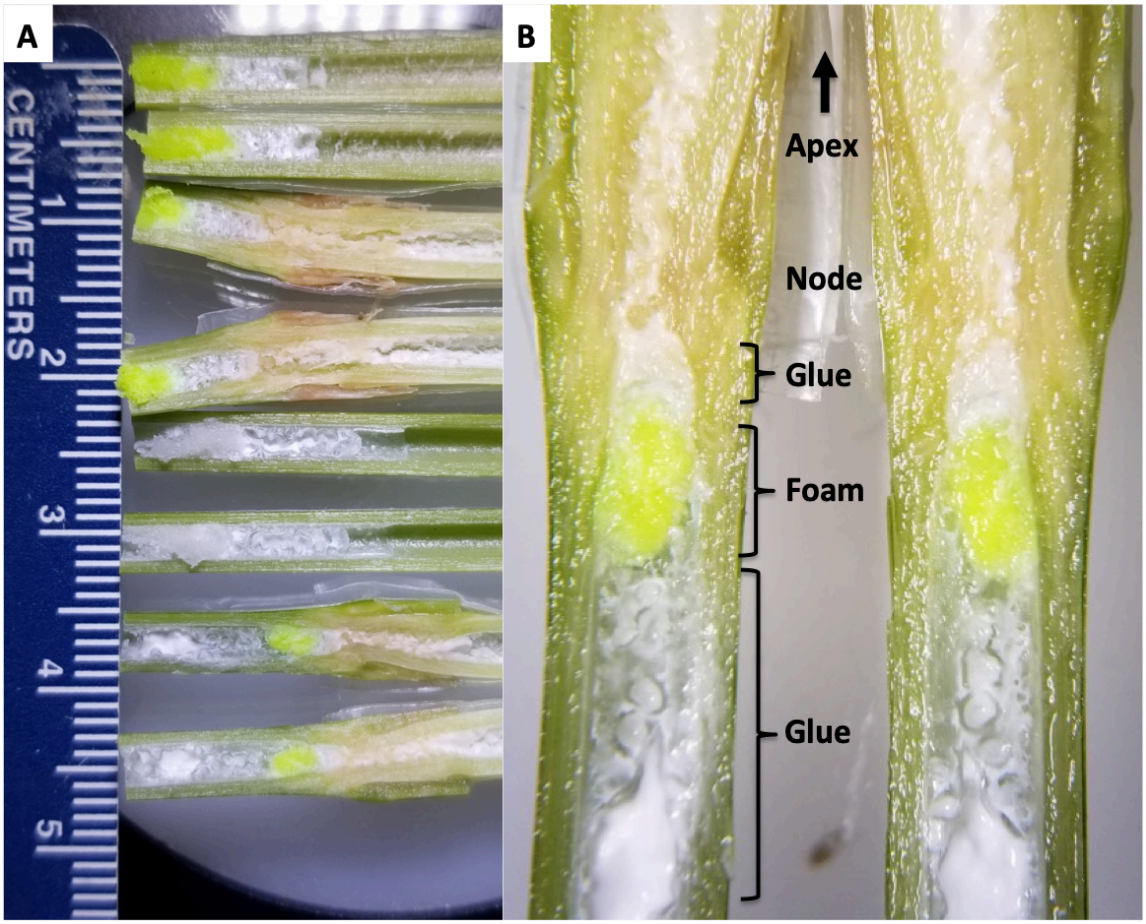

Figure S2.11. Sealing of the hollow pith present in switchgrass accomplished with polyvinyl foam and cyanoacrylate glue. The hollow pith must be sealed in order to accurately measure conductivity through a 130mm stem segment of switchgrass. Furthermore, the method of embolism induction by centrifugation requires a sealing method that is resistant to dislodging under centrifugal force. The node serves as an adequate point to apply cyanoacrylate gel glue with a micro-tip applicator from the cut end of the stem segment. A 1-3 mm thick rectangle of cut polyvinyl foam is next inserted with fine point forceps, which is pressed in as deep as possible with minimal pressure to prevent crushing the inner cortical parenchyma or rupturing the segment. A second application of cyanoacrylate follows the foam to effectively sandwich the foam between the glue to ensure the foam absorbs it, swells to its span within the pith, and then sets rather than soaking up water and remaining malleable. (A) shows the various approaches. (B) shows the final approach applied in all stem segments described. Test conductivity measurements were taken to confirm the seal.

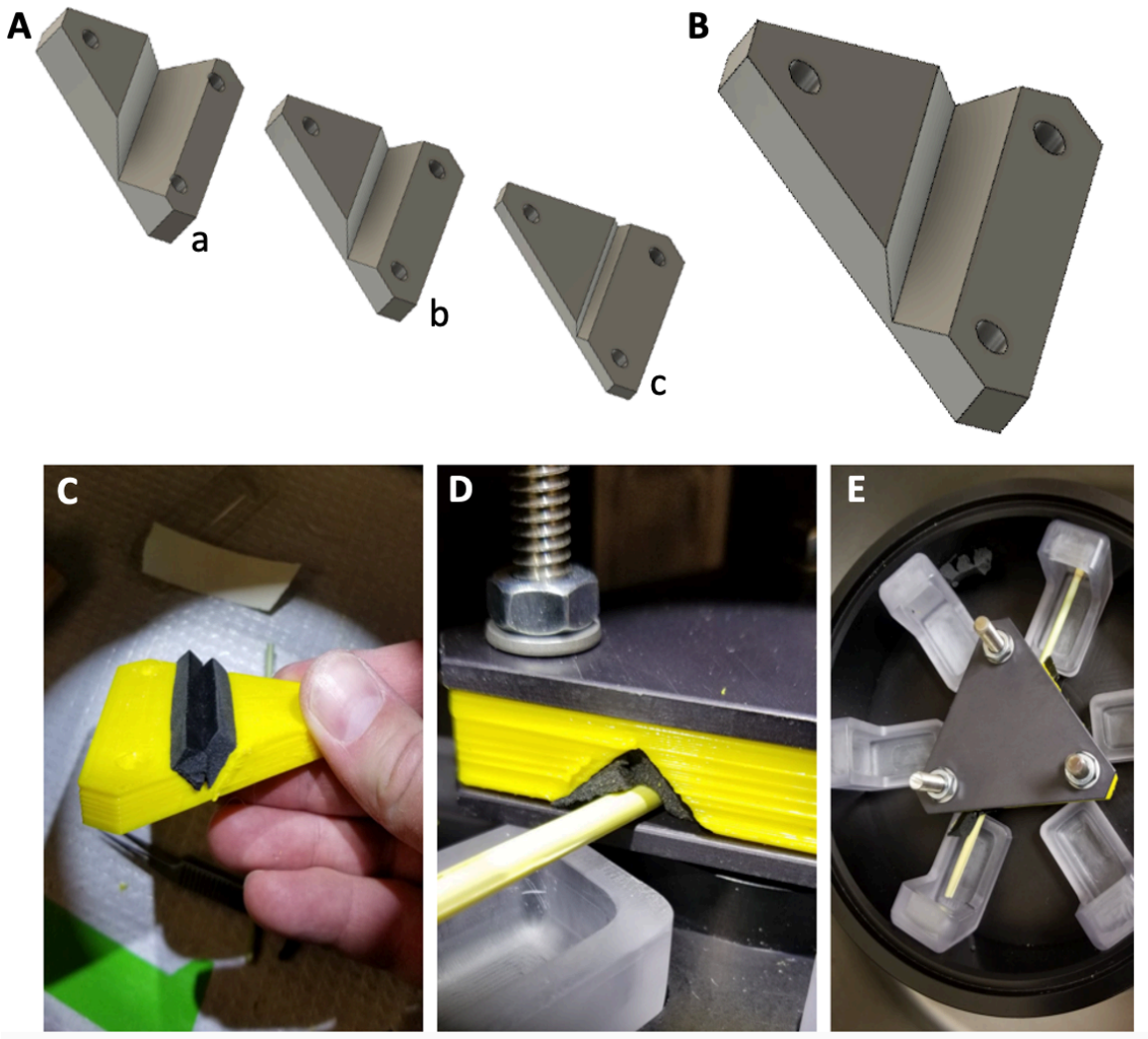

Figure S2.12. 3D printed hollow stem insert for embolism induction rotor. The hollow stem segments of switchgrass crushes with the established method of clamping the stems between the metal plates (Jacobsen 2018). The insert comes in three thicknesses, think (Aa), medium (Ab) and thin (Ac) to accommodate a variety of stem diameters, (B) enlarged image of the most common insert used for switchgrass described herein. (C) Adhesive backed foam affixed in the central groove holds the segment in place to prevent lateral shifts during centrifugation. The foam also accepts and supports variable diameter segments such as the presence of a node that is approximately 1-4 mm larger in diameter than the rest of the segment. (D and E) This simple insert design ensures a secure stem segment during this phase. The presence of the inserts also supports the above stem segment so that the following configurations can be stacked : three small inserts, two medium inserts, 1 small and 1 medium inserts, or 1 small and 1 large to run multiple stems at once. Inserts printed on a Lulzbot Taz 6 3D printer. Inserts were printed at 0.25 mm layer height with 100% infill and maintained integrity after 25 test centrifugation at 20,000 rpm and 200+ spins at 500-15,000 rpm.

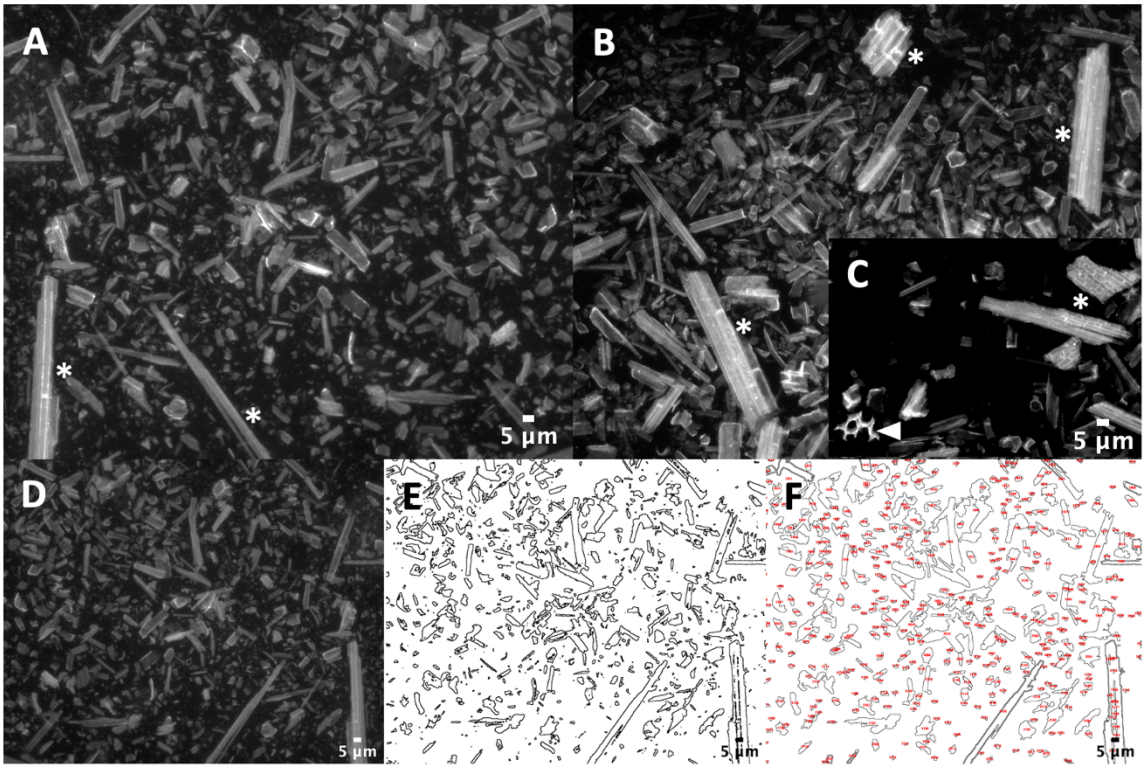

Figure S2.13 Milled and cryo-ball-ground internode biomass retains aggregates of fibers while cortical cells are taken to smaller particle sizes. Particle size likely influences digestion efficiency with sizing ranging <1 µm to <20 µm in width, shards are commonly >50 µm in length. (A) Particles of AP13 internode grown at PKLE site in Texas with multiple thick-walled fiber shards visible (*). (B) WBC particles from PKLE also contain multiple shards of fiber cells (*), and (C) contains a single cortical cell with attached walls from neighboring cells (white arrow), scale bar also applies to (B). (D-F) show the stages of images analysis for particle size analysis to compare differences among genotypes to explore a direct connection with digestibility efficiency. (D) the raw image, (E) shows particle outlines, (F) particle counting for individual particle counts by weight of biomass suspended in 60 ul of distilled water. A-D are autofluorescent images with GFP filter cube. All scale bars 5 microns as labelled.

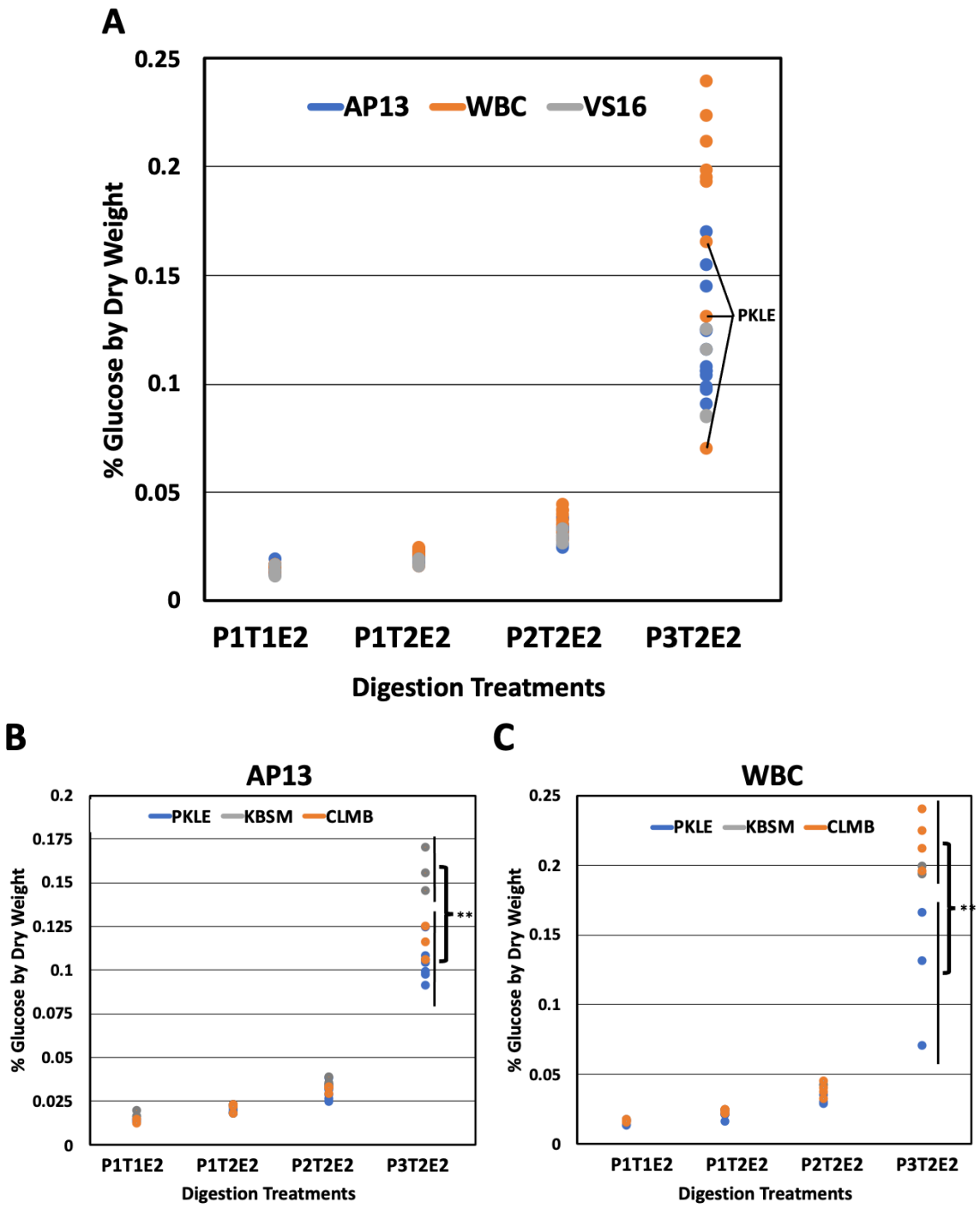

Figure S2.14 Percent glucose yield by dry weight segregates by genotype under severe digestion treatment. (A) Comparing across genotypes and digestion treatments, WBC and AP13 have significantly higher glucose yield ($P < 0.001$). (B) Looking within genotypes across sites shows that AP13 has higher glucose yield at KBSM ($p < 0.01$) compared to CLMB and PKLE (Figure S2.14 B). (C) WBC has higher glucose yield at CLMB ($p < 0.01$) than PKLE and KBSM.

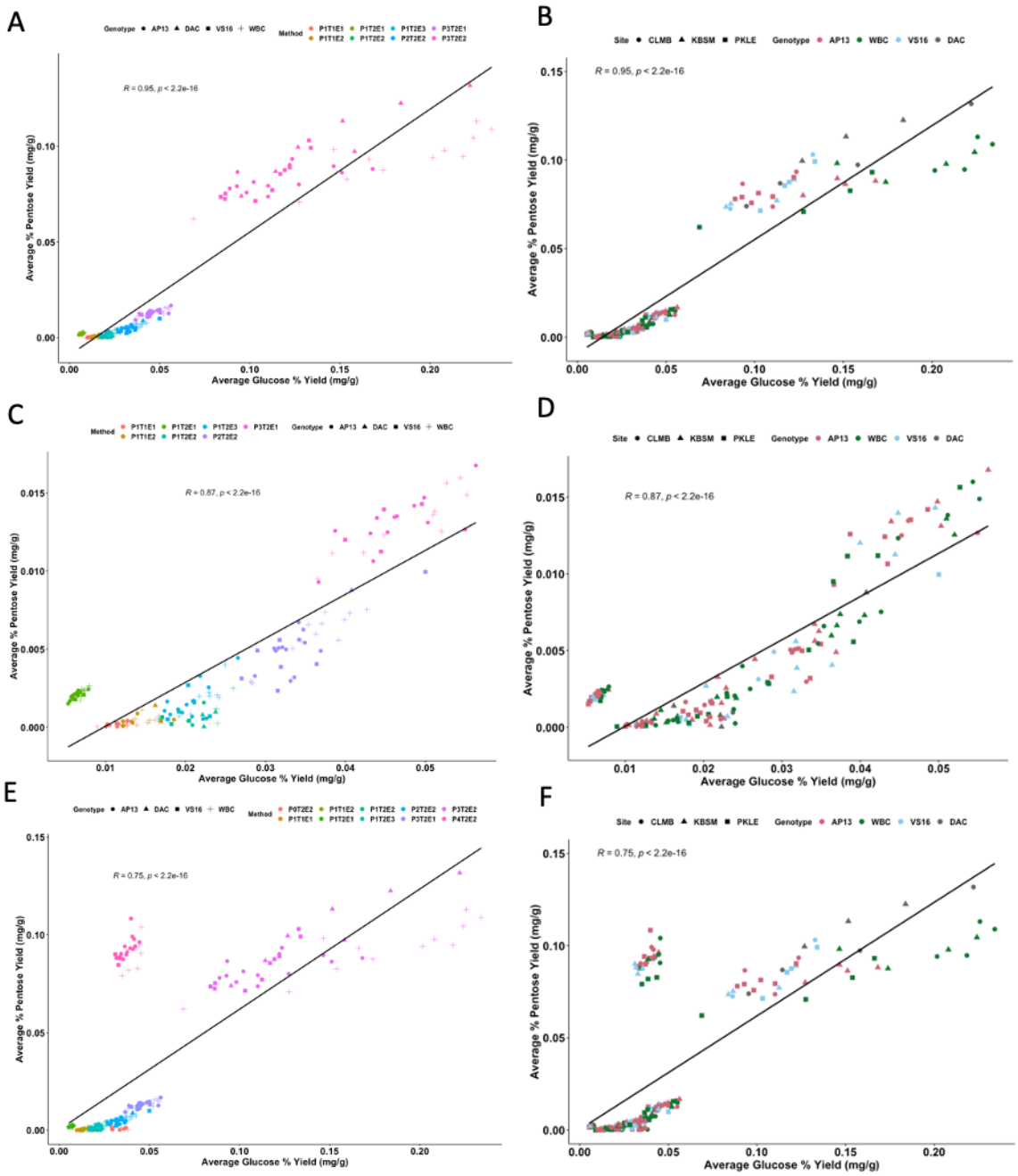

Figure S2.15. Glucose and pentose % yield by biomass dry weight are positively correlated across samples and digestion treatments. (A) All NaOH Treatments by genotype and (B) by genotype and site. (C) All digestion NaOH digestion treatments except P3T2E2 by genotype and (D) by genotype and site. (E) All treatments including water pretreatment (no acid or base) and sulfuric acid digestion treatment by genotype and (F) by genotype and site.

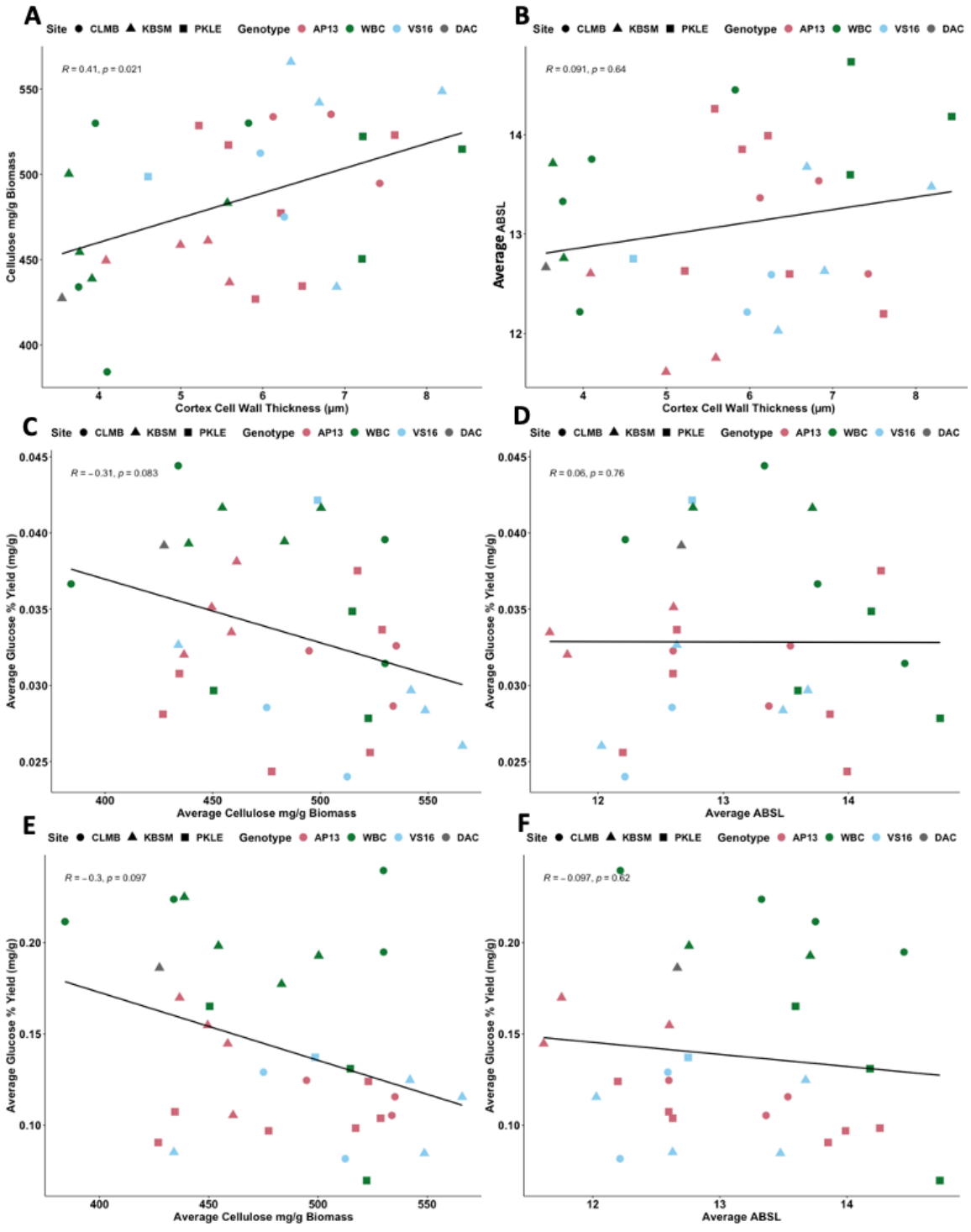

Figure S2.16 Acetyl bromide soluble lignin (ABSL) and cellulose content in three site biomass show an overall lack of significant relationships with cortical cell wall thickness (CWT) and digestibility. (A) CWT is significantly positively correlated with cellulose content (p = 0.021). (B) CWT is moderately positively correlated with ABSL though is not significant. (C) Average cellulose mg/g of biomass is negatively correlated

though not significantly with glucose % yield mg/g. (D) Average ABSL shows no relationship with average glucose yield % mg/g after P2T2E2 digestion parameters. (E) Average cellulose mg/g biomass is negatively correlated with glucose yield % mg/g after harsher P3T2E2. (F) Average ABSL shows moderately negative relationship with average glucose yield % mg/g after P3T2E2 digestion parameters though is not significant1.5 x inner quartile range cutoff applied to remove outliers, removing only three low outliers in ABSL.

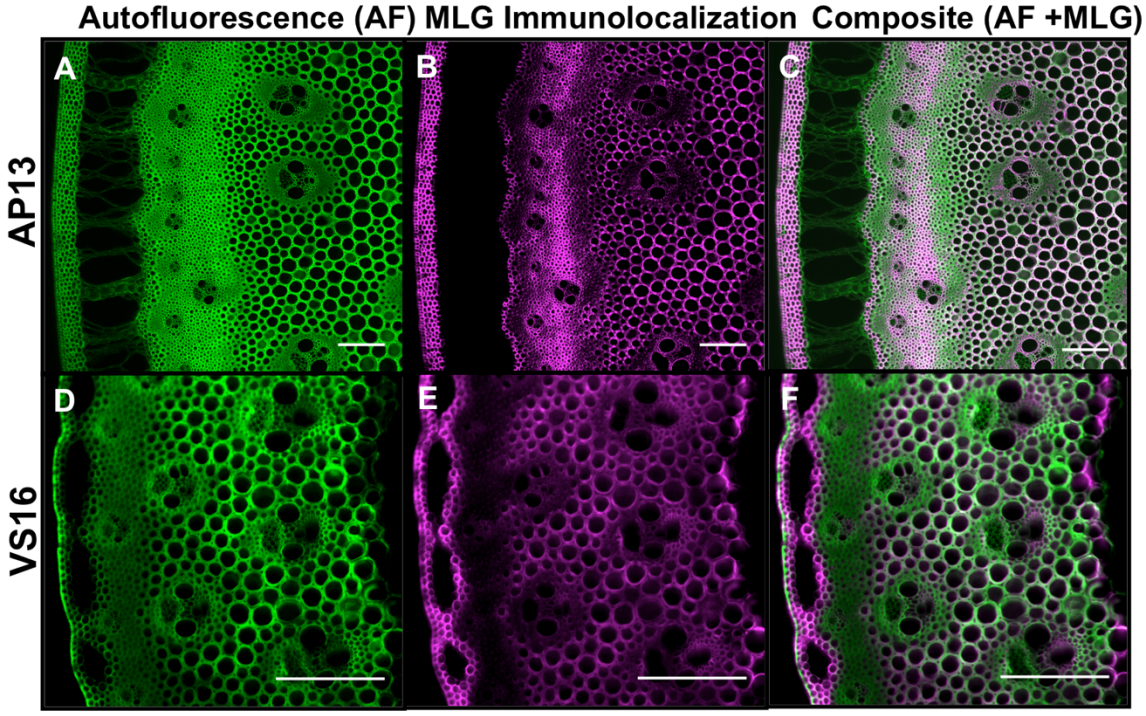

Figure S2.17. Immunolocalization of mixed linkage glucans (MLG) with indirect antibody detection in switchgrass. AP13 exhibits MLG content in sclerenchyma and that is absent in the upland genotype, VS16. MLGs are described as low recalcitrant glucose polymers that are valuable in terms of biomass conversion into biofuels. (A and D) Autofluorescence. B and E) Alexafluor 647 conjugated to secondary antibody. (C and F)Composite autofluorescence and label. Scale bar = 100 microns.

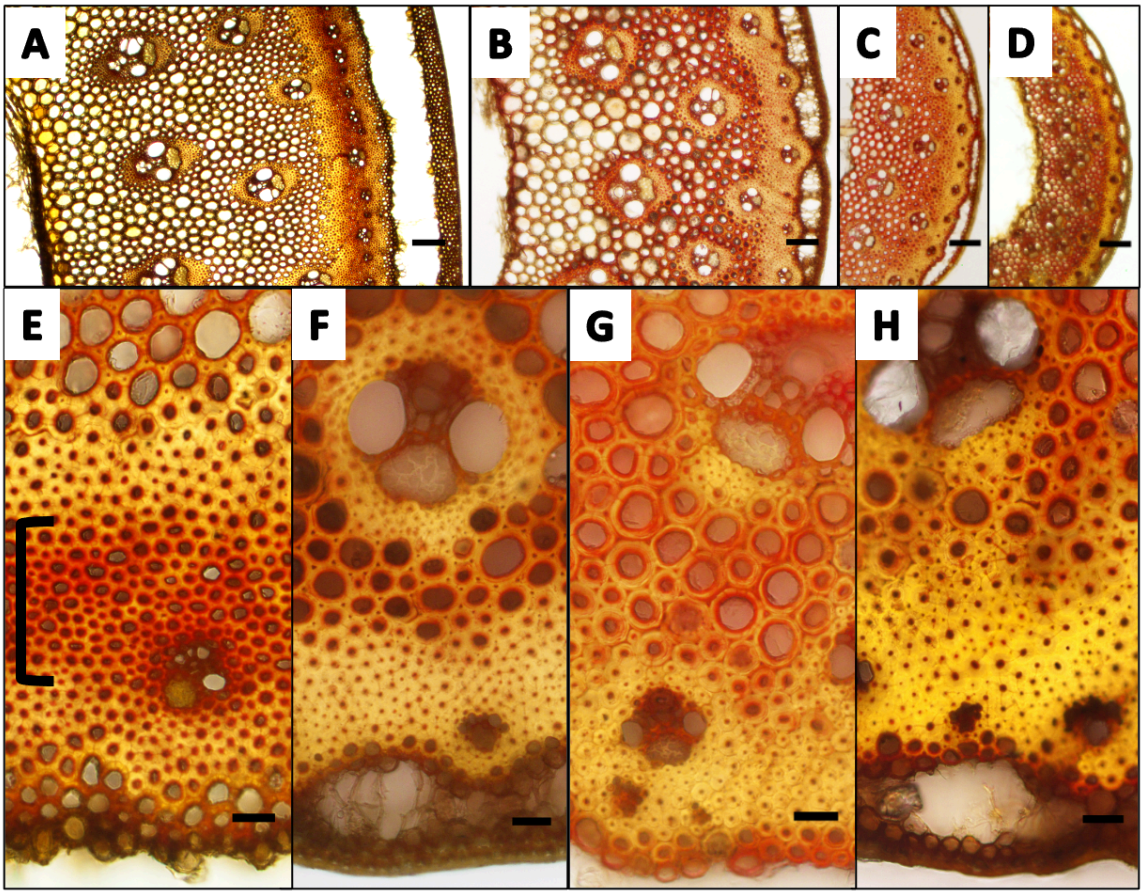

Figure S2.18. Cell wall lignin composition and cellular architecture vary significantly across switchgrass genotypes grown in common location. The Maule reaction stains S-rich lignin red and G-rich lignin golden brown, unique differences in lignin composition can be seen in sclerenchyma of AP13 (A,E) and the cortex of WBC (B,F). Additionally, sclerenchyma cell count, size, and cell wall thickness; vascular bundle fiber cell count; as well as other cellular architecture traits vary significantly among all four genotypes. sclerenchyma abundance and cell wall traits influence digestion efficiency and physiological performance. Sections are 1 cm above the 1st basal node. VS16 (C,G) DAC (D,H) Scale bar = 100 microns (A-D) and 20 microns (E-H).

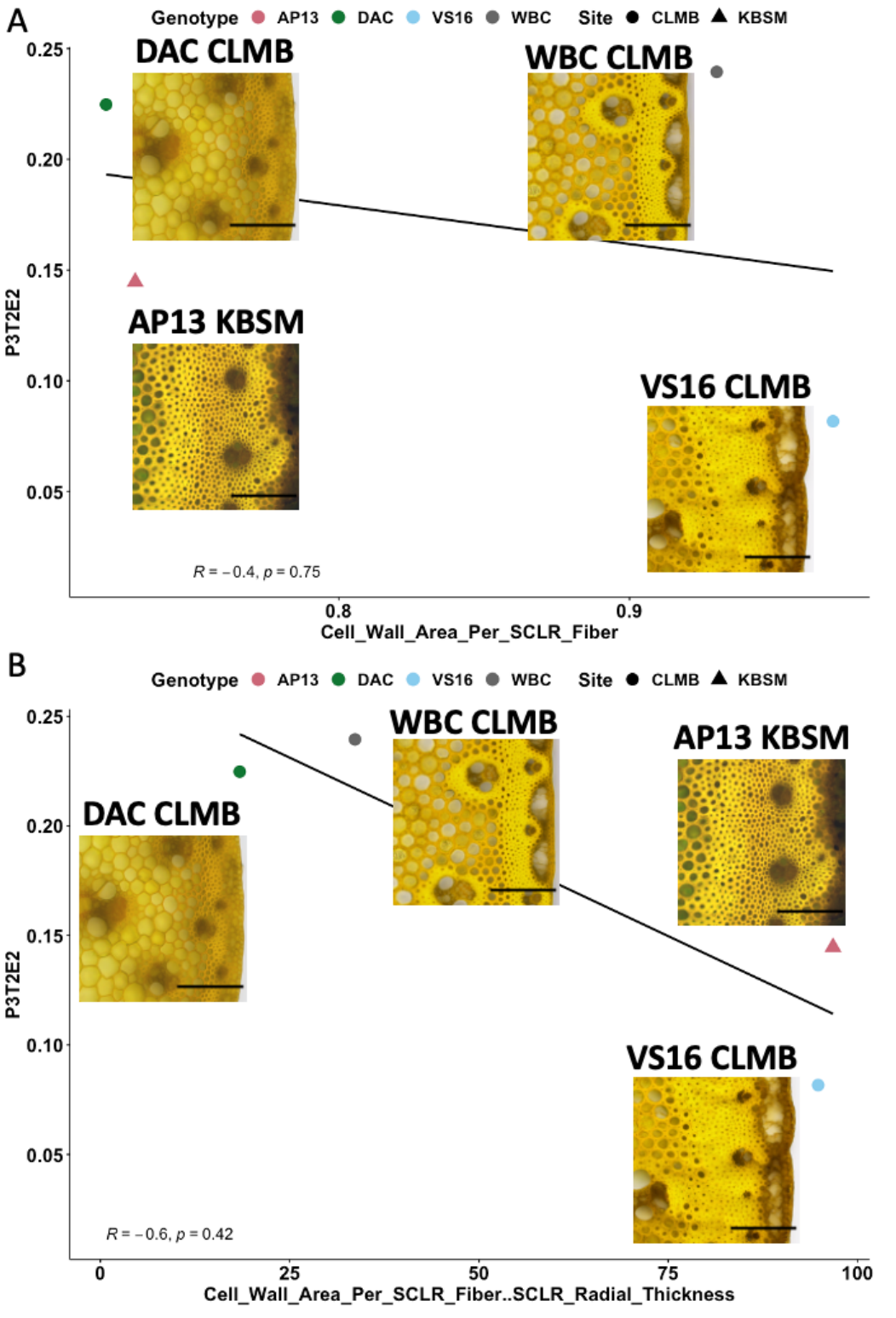
A
Genotype AP13 DAC VS16 WBC Site CLMB KBSM
DAC CLMB
WBC CLMB
AP13 KBSM
VS16 CLMB
P3T2E2
0.25
0.20
0.15
0.10
0.05
R = −0.4, p = 0.75
0.8
0.9
Cell_Wall_Area_Per_SCLR_Fiber
B
Genotype AP13 DAC VS16 WBC Site CLMB KBSM
WBC CLMB
AP13 KBSM
DAC CLMB
VS16 CLMB
P3T2E2
0.25
0.20
0.15
0.10
0.05
R = −0.6, p = 0.42
0
25
50
75
100
Cell_Wall_Area_Per_SCLR_Fiber..SCLR_Radial_Thickness

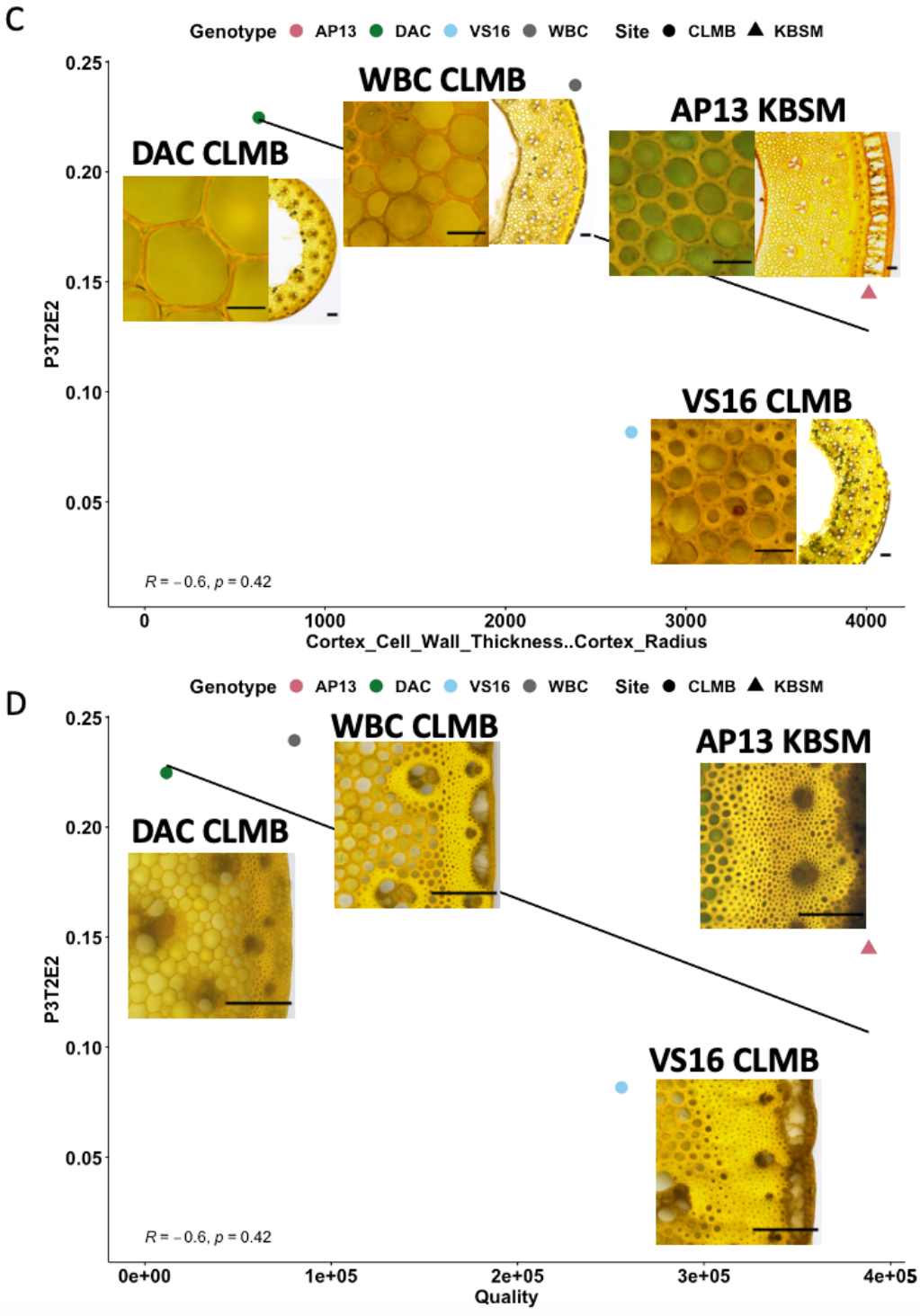

Figure S2.19. Fiber cell wall abundance negatively correlate with % glucose yield by dry weight. (A) Shows that cell wall area per fiber negatively correlates with digestion efficiency, (B) especially when multiplied by the radial thickness of the SCLR. (C) CWT multiplied by cortex radius shows negative correlation with yield, and (B) nearly the same pattern when (CWT x Cortex radius) x (CW per Fiber x SCLR radial thickness) = "Quality".

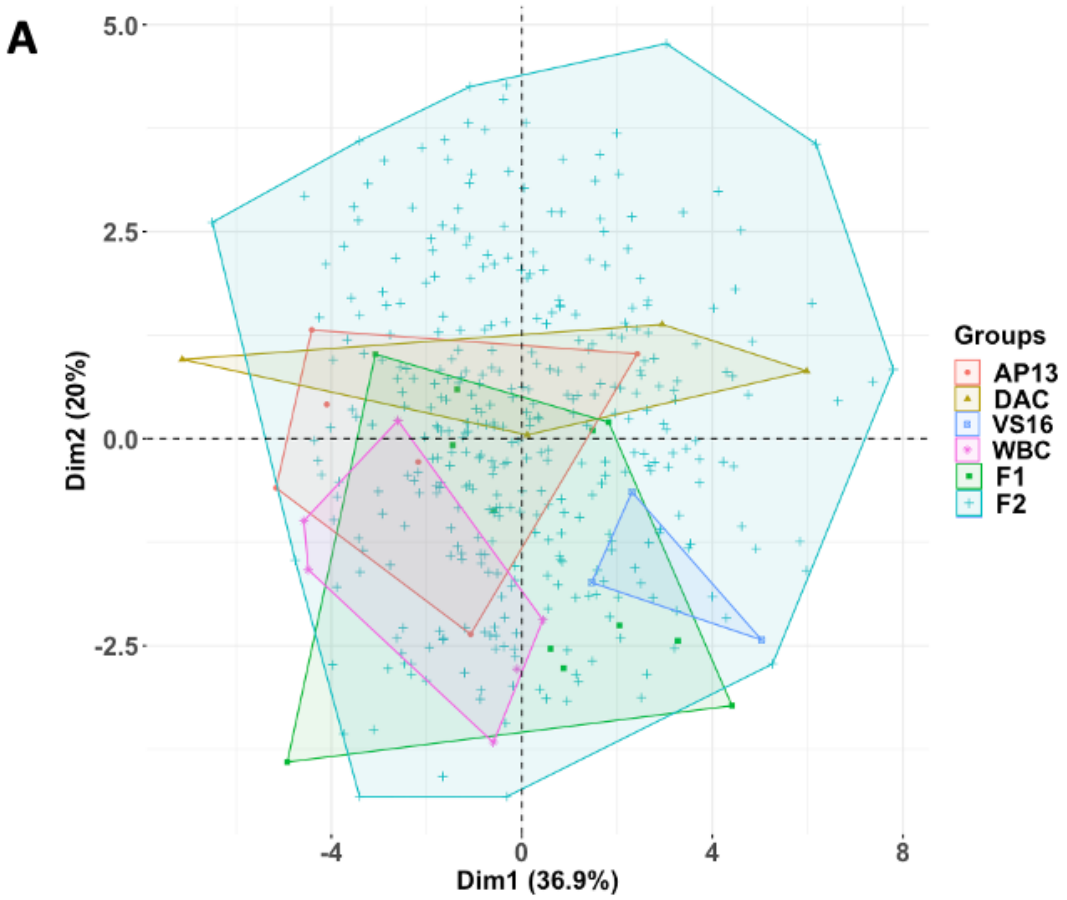
A
5.0
2.5
0.0
-2.5
Dim2 (20%)
-4
0
4
8
Dim1 (36.9%)
Groups
AP13
DAC
VS16
WBC
F1
F2

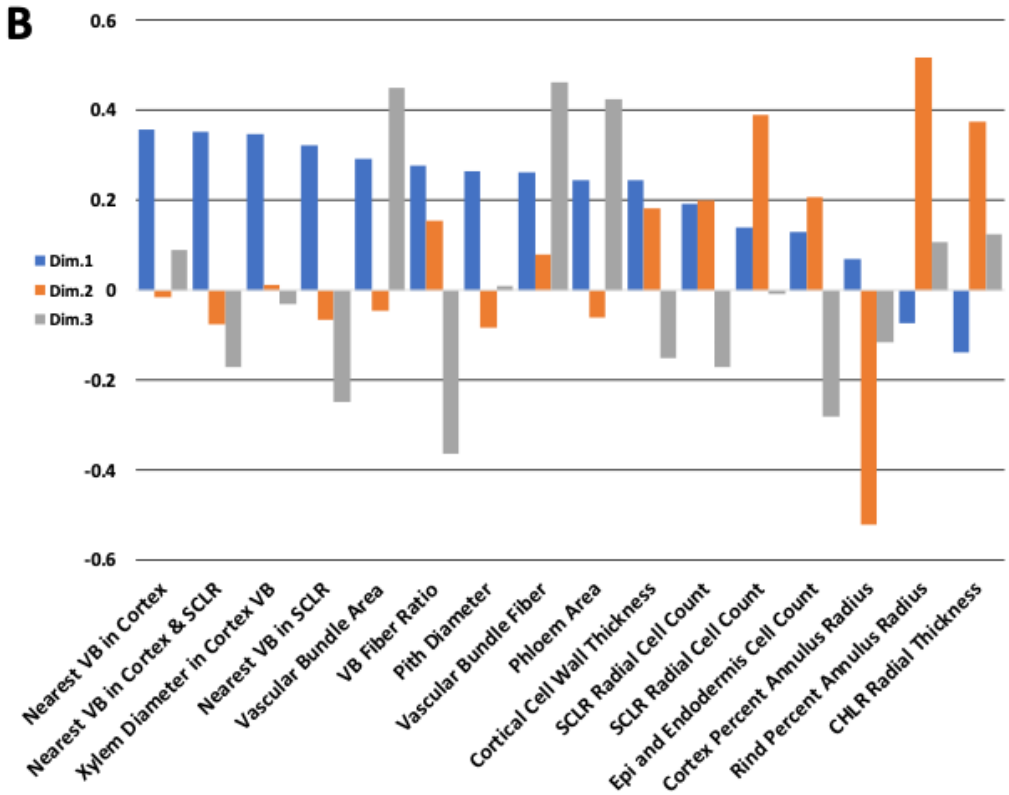
B
0.6
0.4
0.2
0
-0.2
-0.4
-0.6
Dim.1
Dim.2
Dim.3
Nearest VB in Cortex
Nearest VB in Cortex & SCLR
Xylem Diameter in Cortex VB
Nearest VB in SCLR
Vascular Bundle Area
VB Fiber Ratio
Pith Diameter
Vascular Bundle Fiber
Phloem Area
Cortical Cell Wall Thickness
SCLR Radial Cell Count
SCLR Radial Cell Count
Epi and Endodermis Cell Count
Cortex Percent Annulus Radius
Rind Percent Annulus Radius
CHLR Radial Thickness

Figure S3.1. Vascular traits are responsible for the variance explained by the first component after scaling internode anatomy to annulus radius. The first component, which explains 37% of the overall variance, is represented mainly by variation of vascular bundle traits. The second component that is mainly represented by variation in the cell type radii and sclerenchyma radial cell count explain 20% of the overall variance. (A) PCA plot with individuals colored by generation, F0, F1, and F2 compared to figure 3A show the wide variation is still present among F0s and F1s, though reduced slightly, indicating strong variation in anatomy even after scaling to annulus radius. (B) PCA loadings of the F2 mapping population only PCA show that vascular associated traits explain the highest amount of variation in the first dimension.

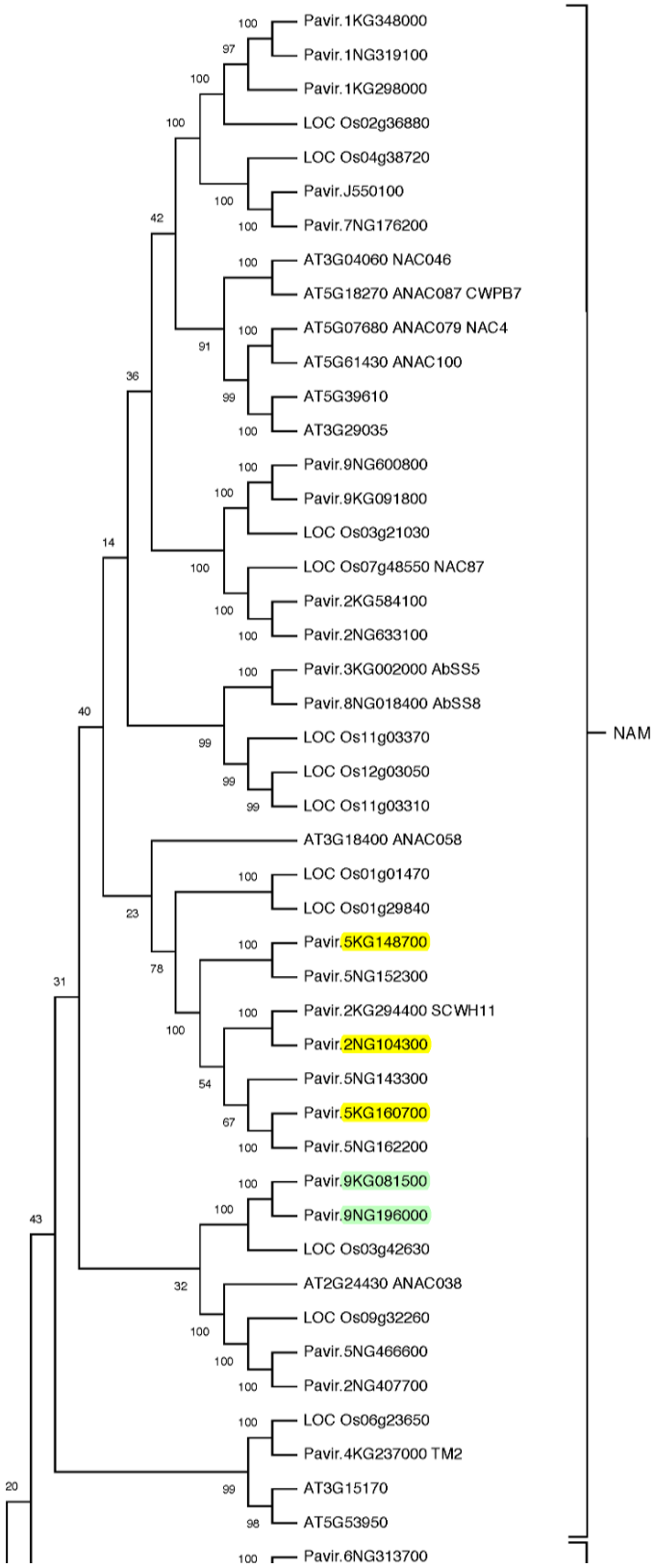
Pavir.1KG348000
Pavir.1NG319100
Pavir.1KG298000
LOC Os02g36880
LOC Os04g38720
Pavir.J550100
Pavir.7NG176200
AT3G04060 NAC046
AT5G18270 ANAC087 CWPB7
AT5G07680 ANAC079 NAC4
AT5G61430 ANAC100
AT5G39610
AT3G29035
Pavir.9NG600800
Pavir.9KG091800
LOC Os03g21030
LOC Os07g48550 NAC87
Pavir.2KG584100
Pavir.2NG633100
Pavir.3KG002000 AbSS5
Pavir.8NG018400 AbSS8
LOC Os11g03370
LOC Os12g03050
LOC Os11g03310
AT3G18400 ANAC058
LOC Os01g01470
LOC Os01g29840
Pavir.5KG148700
Pavir.5NG152300
Pavir.2KG294400 SCWH11
Pavir.2NG104300
Pavir.5NG143300
Pavir.5KG160700
Pavir.5NG162200
Pavir.9KG081500
Pavir.9NG196000
LOC Os03g42630
AT2G24430 ANAC038
LOC Os09g32260
Pavir.5NG466600
Pavir.2NG407700
LOC Os06g23650
Pavir.4KG237000 TM2
AT3G15170
AT5G53950
Pavir.6NG313700
NAM

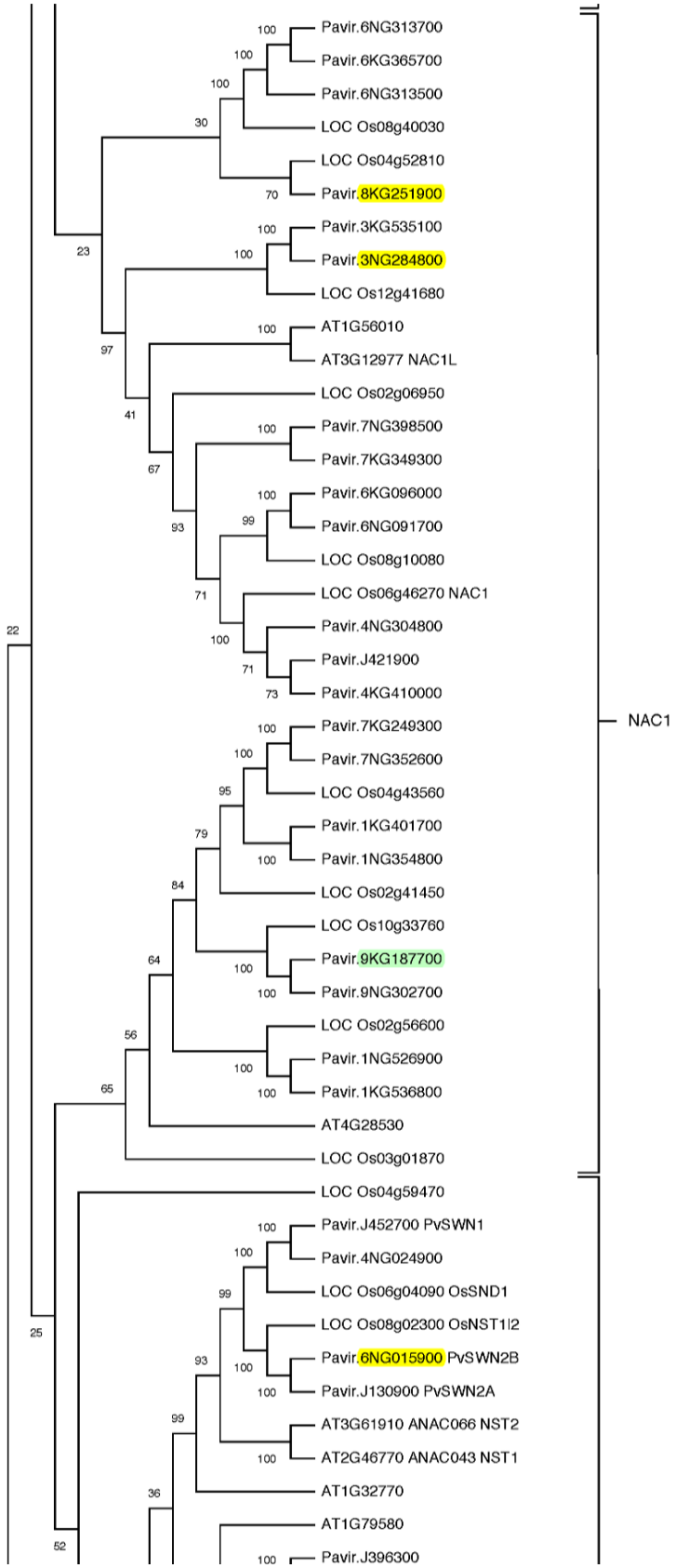
Pavir.6NG313700
Pavir.6KG365700
Pavir.6NG313500
LOC Os08g40030
LOC Os04g52810
Pavir.8KG251900
Pavir.3KG535100
Pavir.3NG284800
LOC Os12g41680
AT1G56010
AT3G12977 NAC1L
LOC Os02g06950
Pavir.7NG398500
Pavir.7KG349300
Pavir.6KG096000
Pavir.6NG091700
LOC Os08g10080
LOC Os06g46270 NAC1
Pavir.4NG304800
Pavir.J421900
Pavir.4KG410000
Pavir.7KG249300
Pavir.7NG352600
LOC Os04g43560
Pavir.1KG401700
Pavir.1NG354800
LOC Os02g41450
LOC Os10g33760
Pavir.9KG187700
Pavir.9NG302700
LOC Os02g56600
Pavir.1NG526900
Pavir.1KG536800
AT4G28530
LOC Os03g01870
LOC Os04g59470
Pavir.J452700 PvSWN1
Pavir.4NG024900
LOC Os06g04090 OsSND1
LOC Os08g02300 OsNST1l2
Pavir.6NG015900 PvSWN2B
Pavir.J130900 PvSWN2A
AT3G61910 ANAC066 NST2
AT2G46770 ANAC043 NST1
AT1G32770
AT1G79580
Pavir.J396300
NAC1

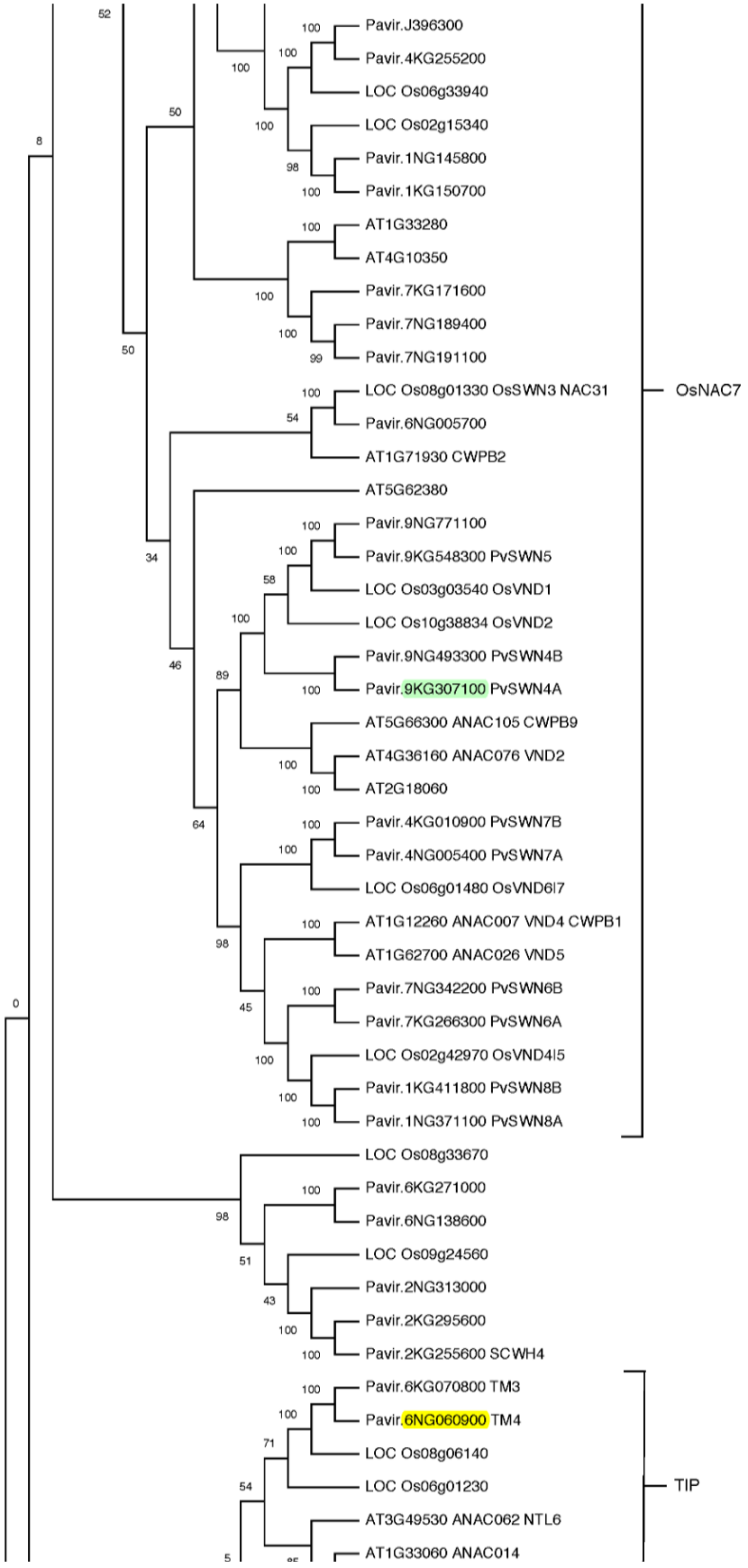
Pavir.J396300
Pavir.4KG255200
LOC Os06g33940
LOC Os02g15340
Pavir.1NG145800
Pavir.1KG150700
AT1G33280
AT4G10350
Pavir.7KG171600
Pavir.7NG189400
Pavir.7NG191100
LOC Os08g01330 OsSWN3 NAC31
Pavir.6NG005700
AT1G71930 CWPB2
AT5G62380
Pavir.9NG771100
Pavir.9KG548300 PvSWN5
LOC Os03g03540 OsVND1
LOC Os10g38834 OsVND2
Pavir.9NG493300 PvSWN4B
Pavir.9KG307100 PvSWN4A
AT5G66300 ANAC105 CWPB9
AT4G36160 ANAC076 VND2
AT2G18060
Pavir.4KG010900 PvSWN7B
Pavir.4NG005400 PvSWN7A
LOC Os06g01480 OsVND6I7
AT1G12260 ANAC007 VND4 CWPB1
AT1G62700 ANAC026 VND5
Pavir.7NG342200 PvSWN6B
Pavir.7KG266300 PvSWN6A
LOC Os02g42970 OsVND4I5
Pavir.1KG411800 PvSWN8B
Pavir.1NG371100 PvSWN8A
LOC Os08g33670
Pavir.6KG271000
Pavir.6NG138600
LOC Os09g24560
Pavir.2NG313000
Pavir.2KG295600
Pavir.2KG255600 SCWH4
Pavir.6KG070800 TM3
Pavir.6NG060900 TM4
LOC Os08g06140
LOC Os06g01230
AT3G49530 ANAC062 NTL6
AT1G33060 ANAC014
OsNAC7
TIP

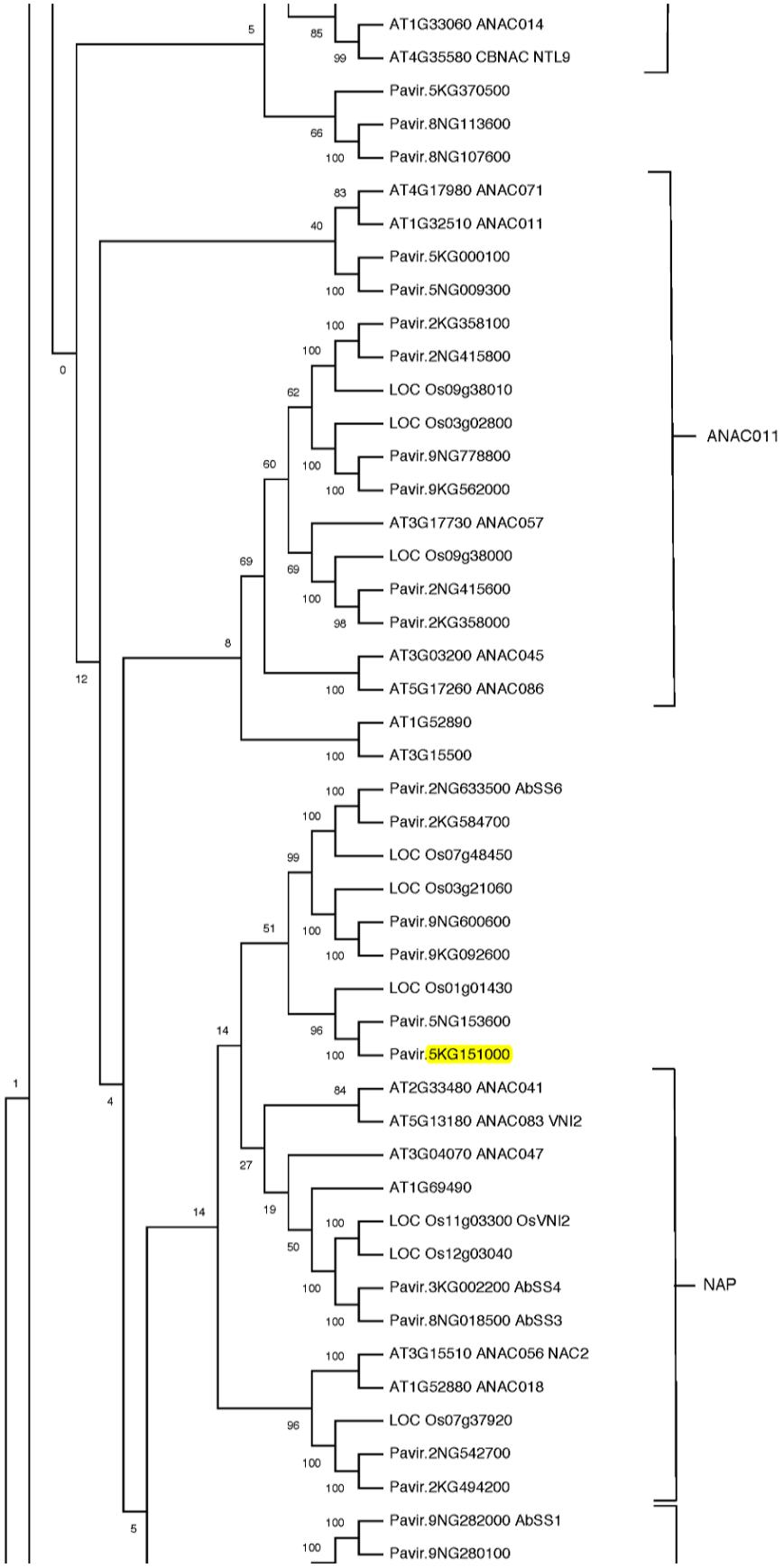
AT1G33060 ANAC014
AT4G35580 CBNAC NTL9
Pavir.5KG370500
Pavir.8NG113600
Pavir.8NG107600
AT4G17980 ANAC071
AT1G32510 ANAC011
Pavir.5KG000100
Pavir.5NG009300
Pavir.2KG358100
Pavir.2NG415800
LOC Os09g38010
LOC Os03g02800
Pavir.9NG778800
Pavir.9KG562000
AT3G17730 ANAC057
LOC Os09g38000
Pavir.2NG415600
Pavir.2KG358000
AT3G03200 ANAC045
AT5G17260 ANAC086
ANAC011
AT1G52890
AT3G15500
Pavir.2NG633500 AbSS6
Pavir.2KG584700
LOC Os07g48450
LOC Os03g21060
Pavir.9NG600600
Pavir.9KG092600
LOC Os01g01430
Pavir.5NG153600
Pavir.5KG151000
AT2G33480 ANAC041
AT5G13180 ANAC083 VNI2
AT3G04070 ANAC047
AT1G69490
LOC Os11g03300 OsVNI2
LOC Os12g03040
Pavir.3KG002200 AbSS4
Pavir.8NG018500 AbSS3
AT3G15510 ANAC056 NAC2
AT1G52880 ANAC018
LOC Os07g37920
Pavir.2NG542700
Pavir.2KG494200
NAP
Pavir.9NG282000 AbSS1
Pavir.9NG280100

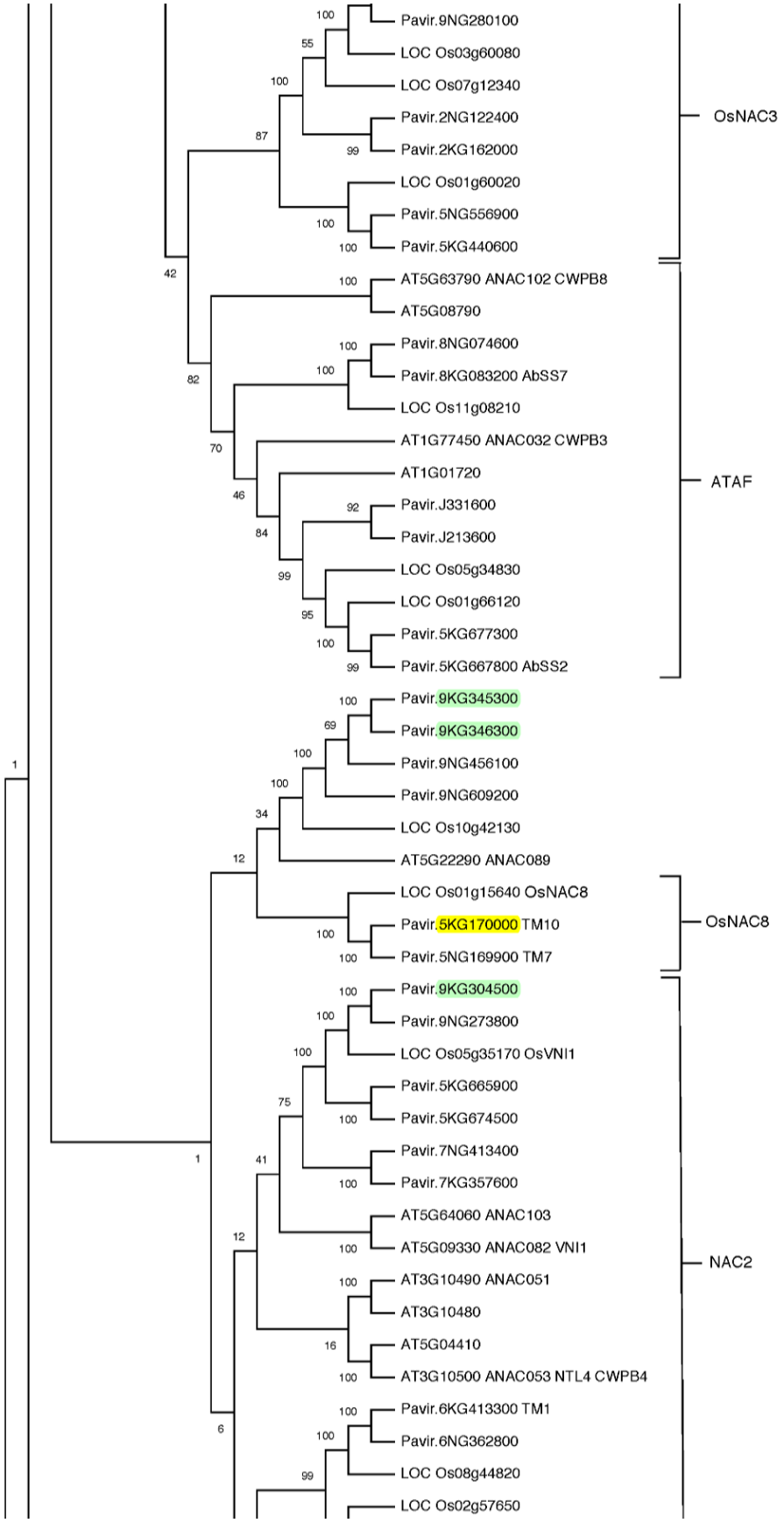
Pavir.9NG280100
LOC Os03g60080
LOC Os07g12340
Pavir.2NG122400
Pavir.2KG162000
LOC Os01g60020
Pavir.5NG556900
Pavir.5KG440600
OsNAC3
AT5G63790 ANAC102 CWPB8
AT5G08790
Pavir.8NG074600
Pavir.8KG083200 AbSS7
LOC Os11g08210
AT1G77450 ANAC032 CWPB3
AT1G01720
Pavir.J331600
Pavir.J213600
LOC Os05g34830
LOC Os01g66120
Pavir.5KG677300
Pavir.5KG667800 AbSS2
ATAF
Pavir.9KG345300
Pavir.9KG346300
Pavir.9NG456100
Pavir.9NG609200
LOC Os10g42130
AT5G22290 ANAC089
LOC Os01g15640 OsNAC8
Pavir.5KG170000 TM10
Pavir.5NG169900 TM7
OsNAC8
Pavir.9KG304500
Pavir.9NG273800
LOC Os05g35170 OsVNI1
Pavir.5KG665900
Pavir.5KG674500
Pavir.7NG413400
Pavir.7KG357600
AT5G64060 ANAC103
AT5G09330 ANAC082 VNI1
AT3G10490 ANAC051
AT3G10480
AT5G04410
AT3G10500 ANAC053 NTL4 CWPB4
Pavir.6KG413300 TM1
Pavir.6NG362800
LOC Os08g44820
LOC Os02g57650
NAC2

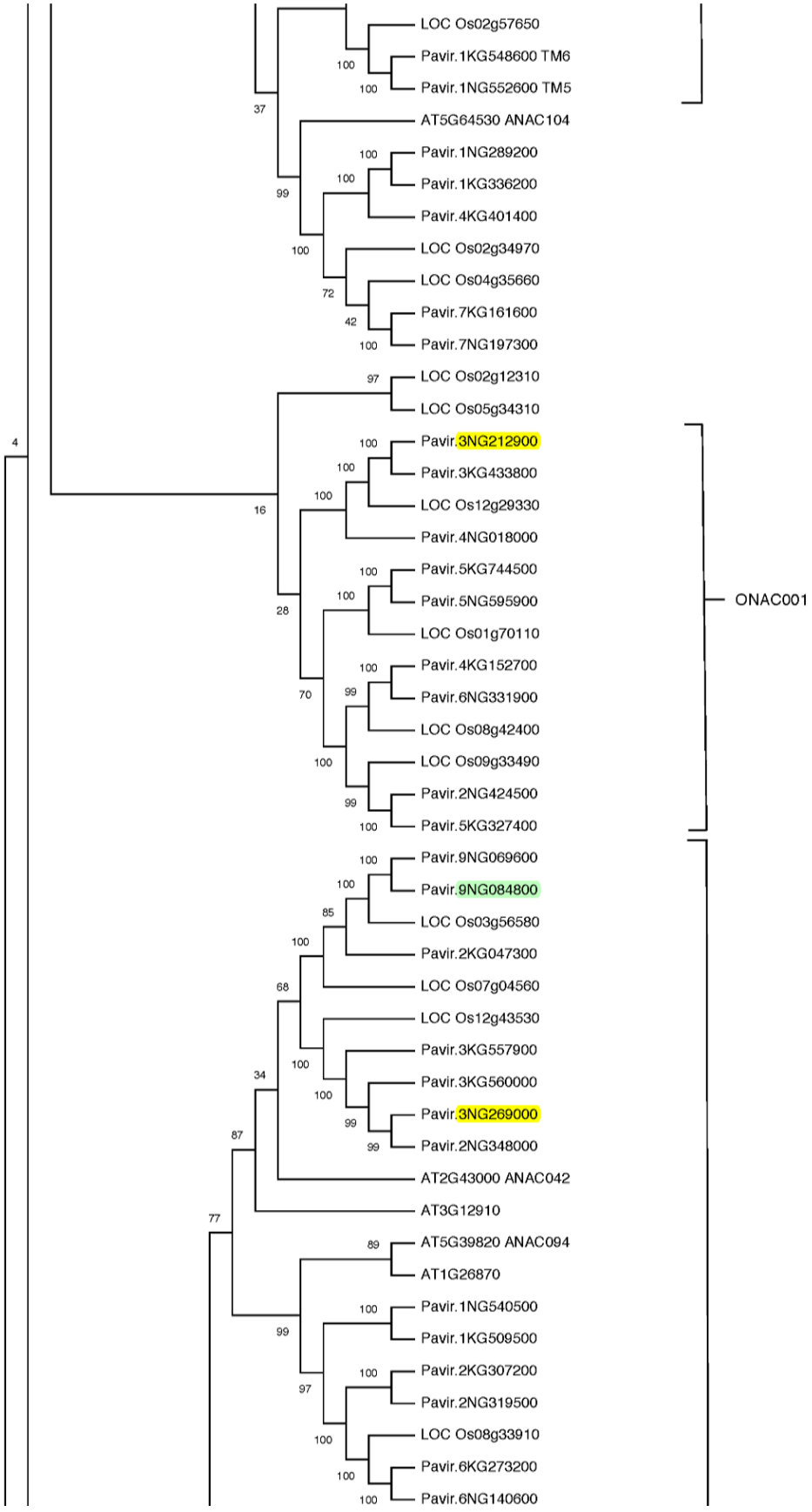
LOC Os02g57650
Pavir.1KG548600 TM6
Pavir.1NG552600 TM5
AT5G64530 ANAC104
Pavir.1NG289200
Pavir.1KG336200
Pavir.4KG401400
LOC Os02g34970
LOC Os04g35660
Pavir.7KG161600
Pavir.7NG197300
LOC Os02g12310
LOC Os05g34310
Pavir.3NG212900
Pavir.3KG433800
LOC Os12g29330
Pavir.4NG018000
Pavir.5KG744500
Pavir.5NG595900
LOC Os01g70110
Pavir.4KG152700
Pavir.6NG331900
LOC Os08g42400
LOC Os09g33490
Pavir.2NG424500
Pavir.5KG327400
Pavir.9NG069600
Pavir.9NG084800
LOC Os03g56580
Pavir.2KG047300
LOC Os07g04560
LOC Os12g43530
Pavir.3KG557900
Pavir.3KG560000
Pavir.3NG269000
Pavir.2NG348000
AT2G43000 ANAC042
AT3G12910
AT5G39820 ANAC094
AT1G26870
Pavir.1NG540500
Pavir.1KG509500
Pavir.2KG307200
Pavir.2NG319500
LOC Os08g33910
Pavir.6KG273200
Pavir.6NG140600
ONAC001

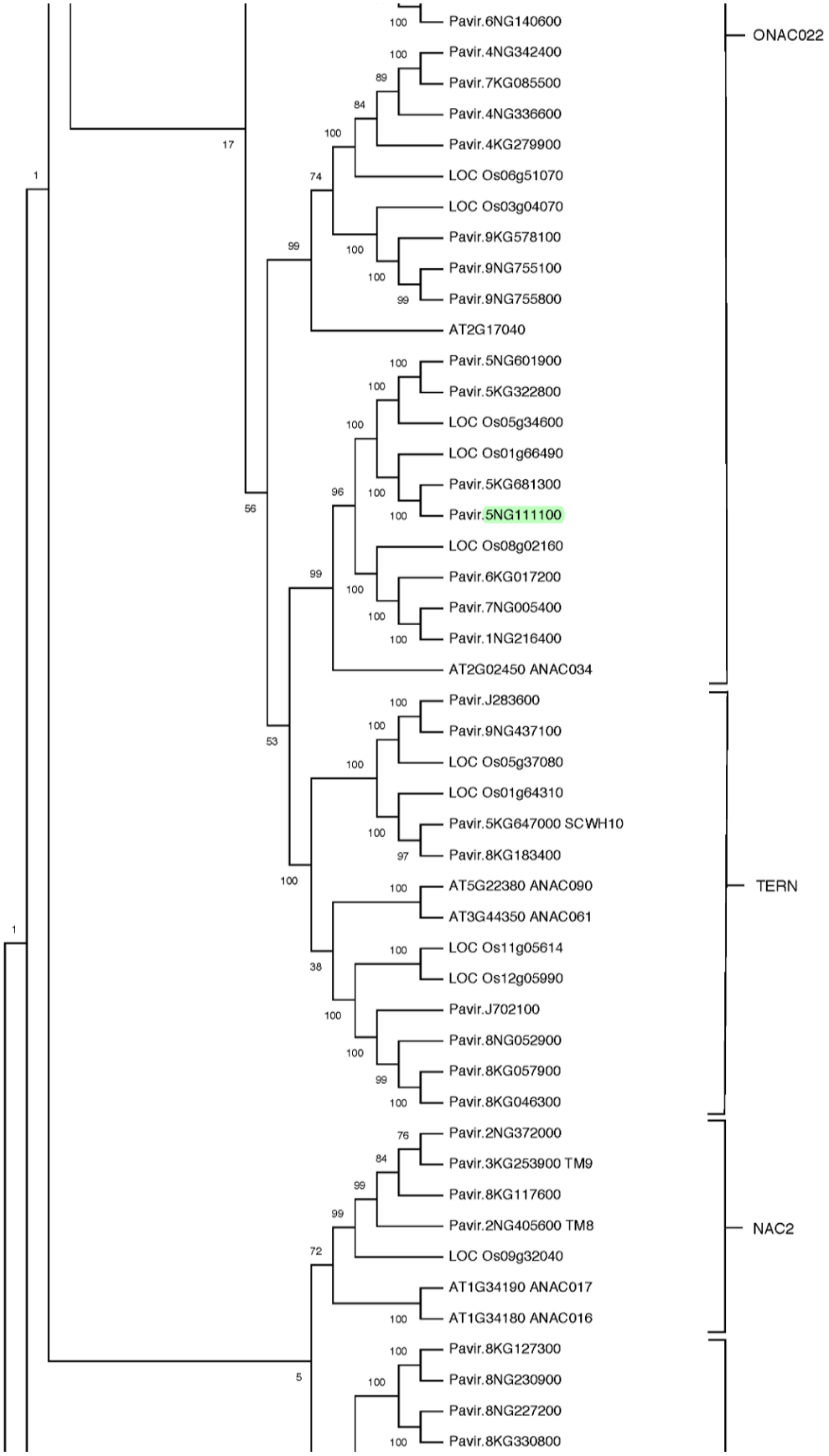
Pavir.6NG140600
Pavir.4NG342400
Pavir.7KG085500
Pavir.4NG336600
Pavir.4KG279900
LOC Os06g51070
LOC Os03g04070
Pavir.9KG578100
Pavir.9NG755100
Pavir.9NG755800
AT2G17040
Pavir.5NG601900
Pavir.5KG322800
LOC Os05g34600
LOC Os01g66490
Pavir.5KG681300
Pavir.5NG111100
LOC Os08g02160
Pavir.6KG017200
Pavir.7NG005400
Pavir.1NG216400
AT2G02450 ANAC034
Pavir.J283600
Pavir.9NG437100
LOC Os05g37080
LOC Os01g64310
Pavir.5KG647000 SCWH10
Pavir.8KG183400
AT5G22380 ANAC090
AT3G44350 ANAC061
LOC Os11g05614
LOC Os12g05990
Pavir.J702100
Pavir.8NG052900
Pavir.8KG057900
Pavir.8KG046300
Pavir.2NG372000
Pavir.3KG253900 TM9
Pavir.8KG117600
Pavir.2NG405600 TM8
LOC Os09g32040
AT1G34190 ANAC017
AT1G34180 ANAC016
Pavir.8KG127300
Pavir.8NG230900
Pavir.8NG227200
Pavir.8KG330800
ONAC022
TERN
NAC2

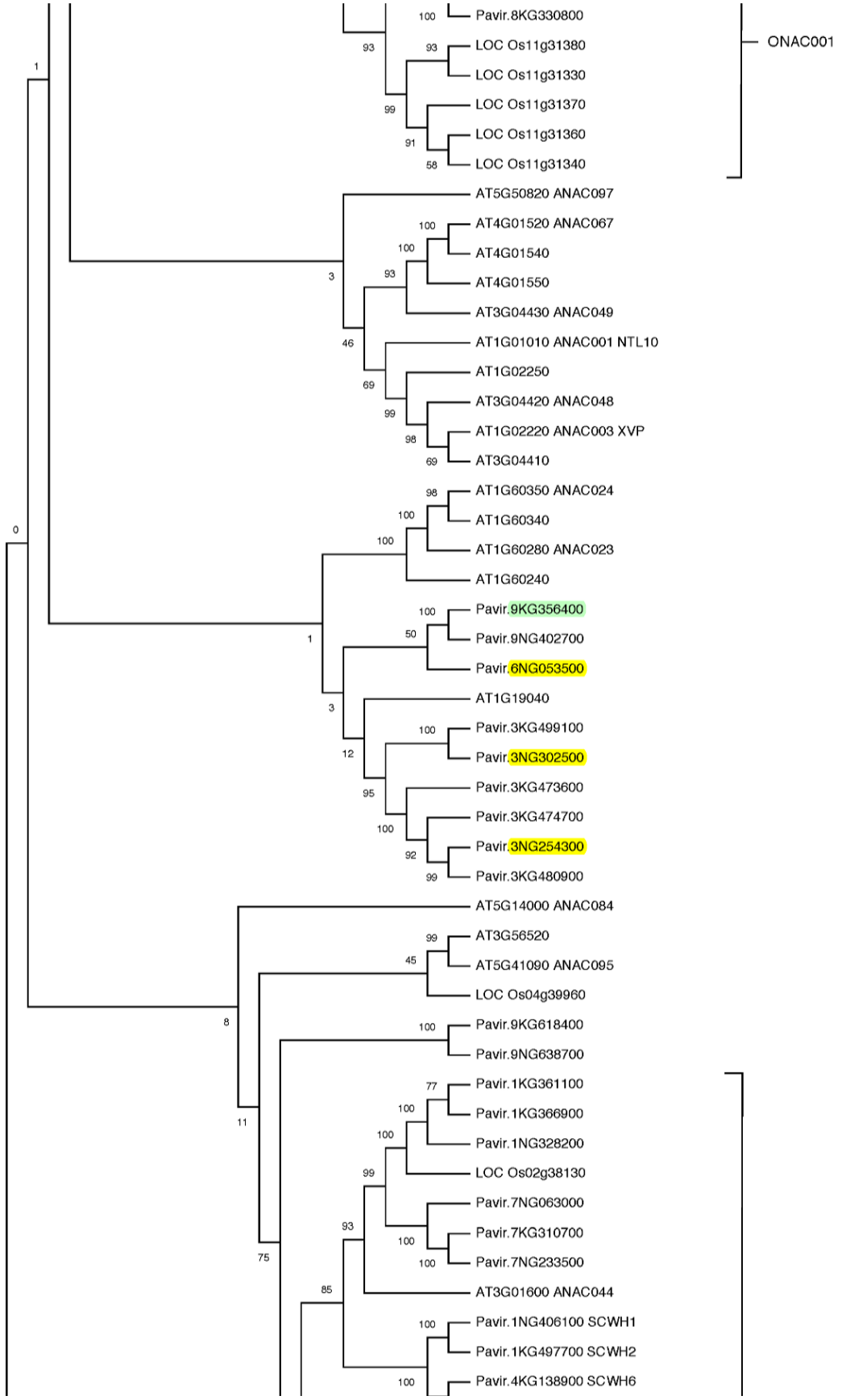
Pavir.8KG330800
LOC Os11g31380
LOC Os11g31330
LOC Os11g31370
LOC Os11g31360
LOC Os11g31340
ONAC001
AT5G50820 ANAC097
AT4G01520 ANAC067
AT4G01540
AT4G01550
AT3G04430 ANAC049
AT1G01010 ANAC001 NTL10
AT1G02250
AT3G04420 ANAC048
AT1G02220 ANAC003 XVP
AT3G04410
AT1G60350 ANAC024
AT1G60340
AT1G60280 ANAC023
AT1G60240
Pavir.9KG356400
Pavir.9NG402700
Pavir.6NG053500
AT1G19040
Pavir.3KG499100
Pavir.3NG302500
Pavir.3KG473600
Pavir.3KG474700
Pavir.3NG254300
Pavir.3KG480900
AT5G14000 ANAC084
AT3G56520
AT5G41090 ANAC095
LOC Os04g39960
Pavir.9KG618400
Pavir.9NG638700
Pavir.1KG361100
Pavir.1KG366900
Pavir.1NG328200
LOC Os02g38130
Pavir.7NG063000
Pavir.7KG310700
Pavir.7NG233500
AT3G01600 ANAC044
Pavir.1NG406100 SCWH1
Pavir.1KG497700 SCWH2
Pavir.4KG138900 SCWH6

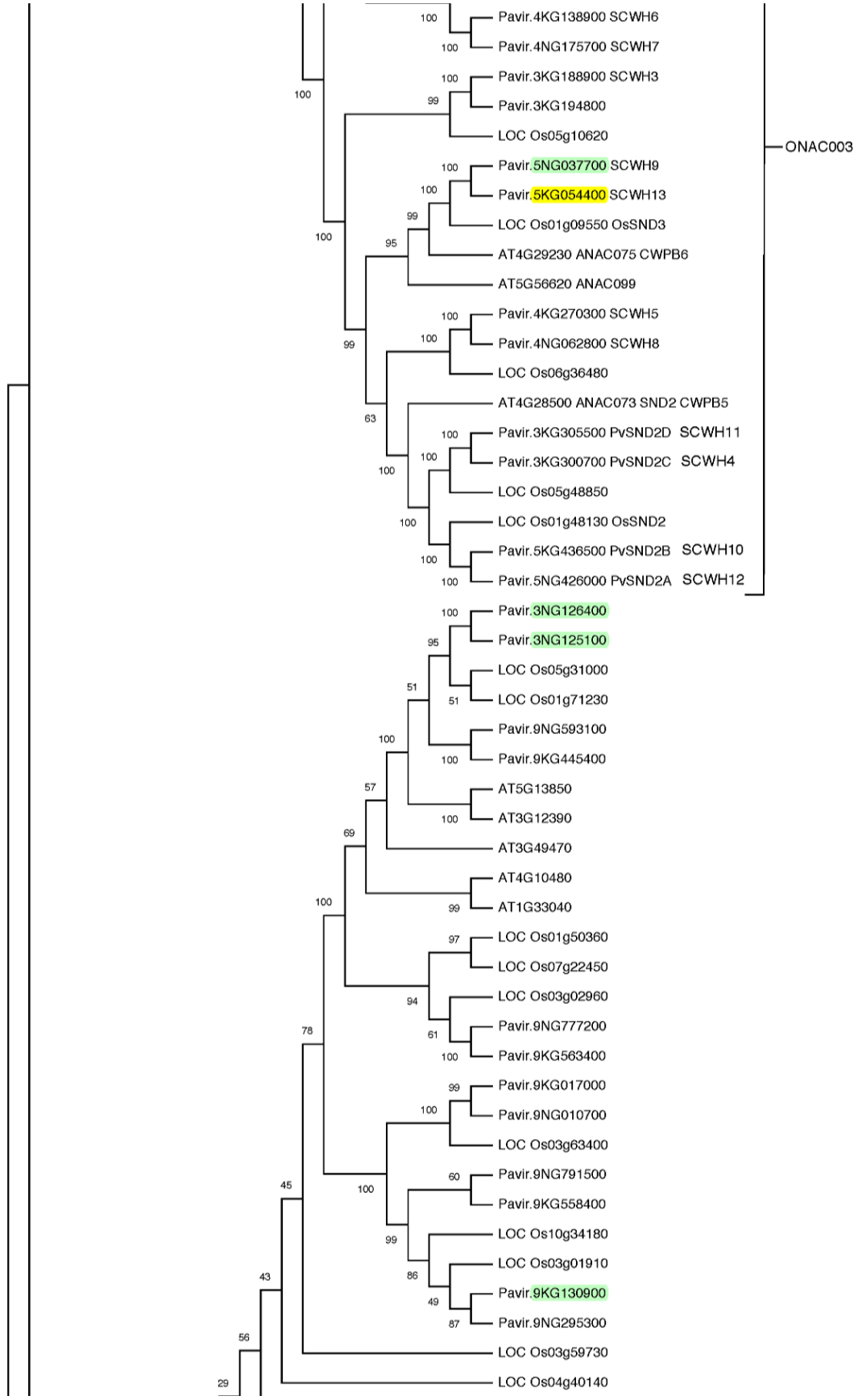
Pavir.4KG138900 SCWH6
Pavir.4NG175700 SCWH7
Pavir.3KG188900 SCWH3
Pavir.3KG194800
LOC Os05g10620
Pavir.5NG037700 SCWH9
Pavir.5KG054400 SCWH13
LOC Os01g09550 OsSND3
AT4G29230 ANAC075 CWPB6
AT5G56620 ANAC099
Pavir.4KG270300 SCWH5
Pavir.4NG062800 SCWH8
LOC Os06g36480
AT4G28500 ANAC073 SND2 CWPB5
Pavir.3KG305500 PvSND2D SCWH11
Pavir.3KG300700 PvSND2C SCWH4
LOC Os05g48850
LOC Os01g48130 OsSND2
Pavir.5KG436500 PvSND2B SCWH10
Pavir.5NG426000 PvSND2A SCWH12
ONAC003
Pavir.3NG126400
Pavir.3NG125100
LOC Os05g31000
LOC Os01g71230
Pavir.9NG593100
Pavir.9KG445400
AT5G13850
AT3G12390
AT3G49470
AT4G10480
AT1G33040
LOC Os01g50360
LOC Os07g22450
LOC Os03g02960
Pavir.9NG777200
Pavir.9KG563400
Pavir.9KG017000
Pavir.9NG010700
LOC Os03g63400
Pavir.9NG791500
Pavir.9KG558400
LOC Os10g34180
LOC Os03g01910
Pavir.9KG130900
Pavir.9NG295300
LOC Os03g59730
LOC Os04g40140

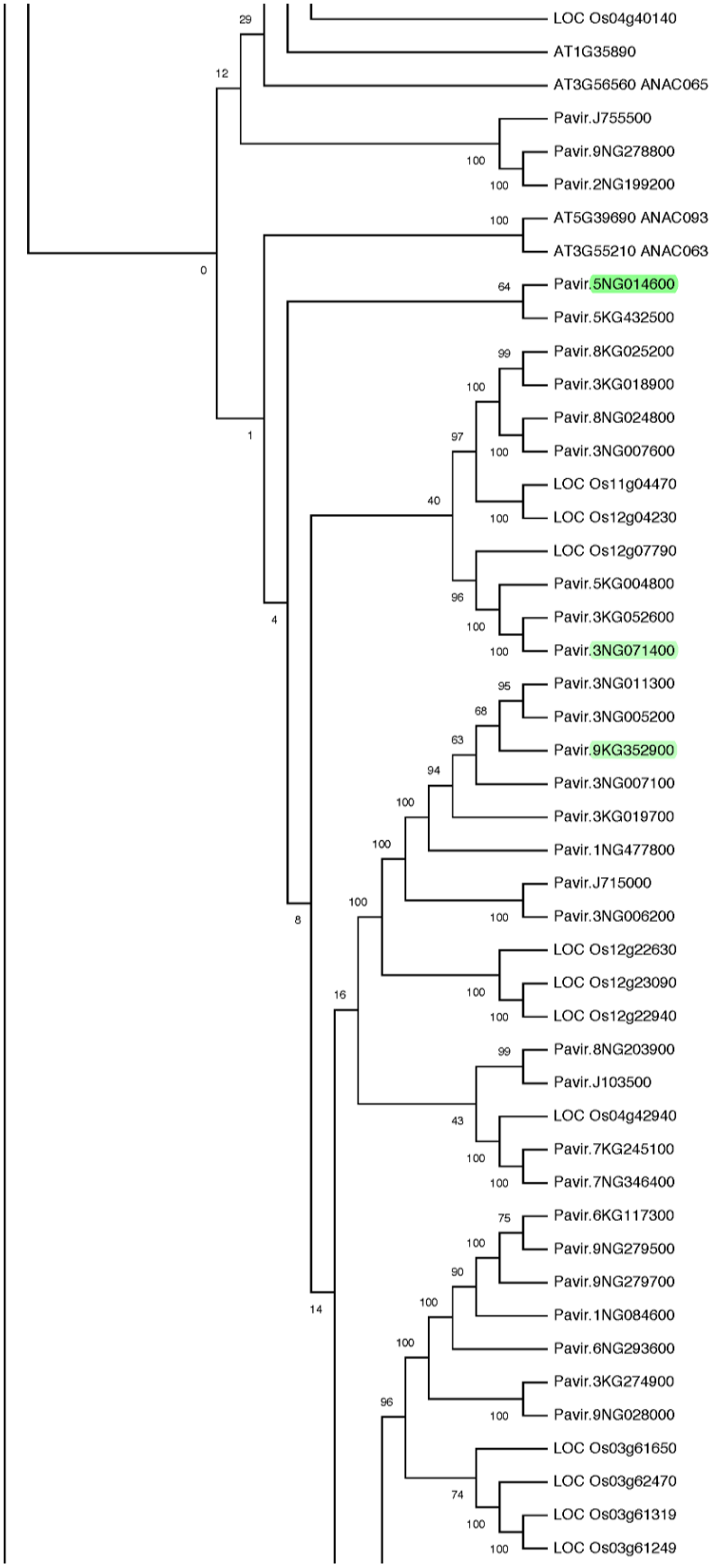
LOC Os04g40140
AT1G35890
AT3G56560 ANAC065
Pavir.J755500
Pavir.9NG278800
Pavir.2NG199200
AT5G39690 ANAC093
AT3G55210 ANAC063
Pavir.5NG014600
Pavir.5KG432500
Pavir.8KG025200
Pavir.3KG018900
Pavir.8NG024800
Pavir.3NG007600
LOC Os11g04470
LOC Os12g04230
LOC Os12g07790
Pavir.5KG004800
Pavir.3KG052600
Pavir.3NG071400
Pavir.3NG011300
Pavir.3NG005200
Pavir.9KG352900
Pavir.3NG007100
Pavir.3KG019700
Pavir.1NG477800
Pavir.J715000
Pavir.3NG006200
LOC Os12g22630
LOC Os12g23090
LOC Os12g22940
Pavir.8NG203900
Pavir.J103500
LOC Os04g42940
Pavir.7KG245100
Pavir.7NG346400
Pavir.6KG117300
Pavir.9NG279500
Pavir.9NG279700
Pavir.1NG084600
Pavir.6NG293600
Pavir.3KG274900
Pavir.9NG028000
LOC Os03g61650
LOC Os03g62470
LOC Os03g61319
LOC Os03g61249

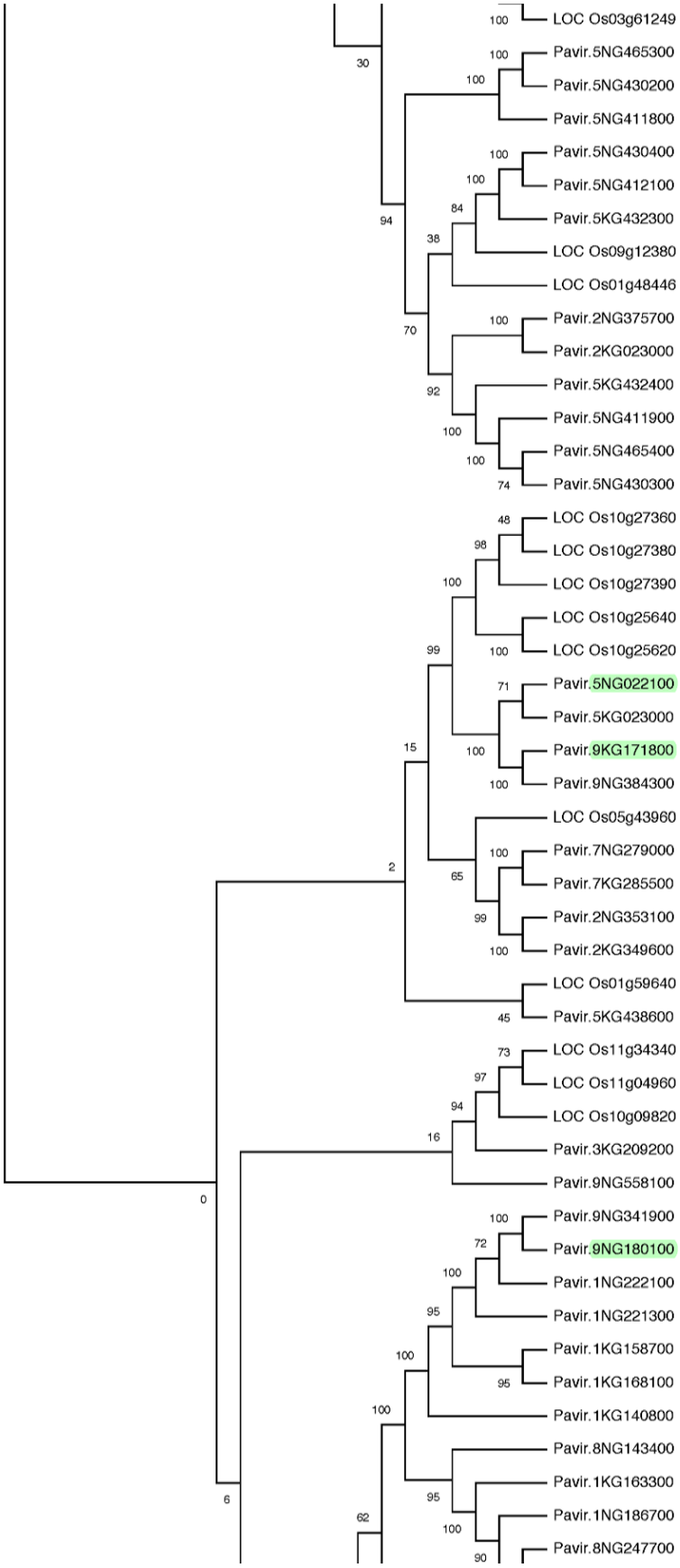
LOC Os03g61249
Pavir.5NG465300
Pavir.5NG430200
Pavir.5NG411800
Pavir.5NG430400
Pavir.5NG412100
Pavir.5KG432300
LOC Os09g12380
LOC Os01g48446
Pavir.2NG375700
Pavir.2KG023000
Pavir.5KG432400
Pavir.5NG411900
Pavir.5NG465400
Pavir.5NG430300
LOC Os10g27360
LOC Os10g27380
LOC Os10g27390
LOC Os10g25640
LOC Os10g25620
Pavir.5NG022100
Pavir.5KG023000
Pavir.9KG171800
Pavir.9NG384300
LOC Os05g43960
Pavir.7NG279000
Pavir.7KG285500
Pavir.2NG353100
Pavir.2KG349600
LOC Os01g59640
Pavir.5KG438600
LOC Os11g34340
LOC Os11g04960
LOC Os10g09820
Pavir.3KG209200
Pavir.9NG558100
Pavir.9NG341900
Pavir.9NG180100
Pavir.1NG222100
Pavir.1NG221300
Pavir.1KG158700
Pavir.1KG168100
Pavir.1KG140800
Pavir.8NG143400
Pavir.1KG163300
Pavir.1NG186700
Pavir.8NG247700

Figure S3.2. NAC transcription factor family neighbor-joining phylogenetic tree of switchgrass (Panicum virgatum), rice (Oryza sativa), and Arabidopsis thaliana suggests expansion of OsNAC7 and ONAC003 subgroups in switchgrass compared to rice. Sub-families that contain genes involved in cell wall formation are based on gene membership set by *Ooka et al 2003*. ANAC numbering obtained from The Arabidopsis Resource (TAIR). CWPB indicates cell wall promoter binding in Yeast 1 hybrid assay (Taylor-Teeples, Lin et al. 2015). SCWH indicates Secondary cell wall homologous genes that contain a motif present in ANAC073/SND2 (Yan 2017 (Yan, Zhang et al. 2017)) and found to belong to the same clade within the ONAC003 subfamily. Eleven switchgrass NACs contain a C-terminal trans membrane (TM) domain that anchors the protein to either

the ER or plasma membrane, rendering it inactive until protease liberation (Yan, Zhang et al. 2017). TM, Abiotic stress response (AbSS), Secondary cell wall homolog (SCWH), described in Yan 2017 based on Panicum virgatum genome version 1.1, Updated here by blasting transcript sequence provided in Yan 2017 against the early release Pv genome v4.1. The evolutionary history was inferred using the Neighbor-Joining method (Saitou and Nei 1987). The bootstrap consensus tree inferred from 1000 replicates (Felsenstein 1985) The percentage of replicate trees in which the associated taxa clustered together in the bootstrap test are shown next to the branches (Felsenstein 1985). This analysis involved 541 amino acid sequences. All ambiguous positions were removed for each sequence pair (pairwise deletion option). Evolutionary analyses were conducted in MEGA X (Kumar, Stecher et al. 2018);(Stecher, Tamura et al. 2020). Switchgrass NACs located within significant internode anatomy QTL intervals are highlighted in yellow, suggestive QTL in blue, and are also described in Table 3.6.

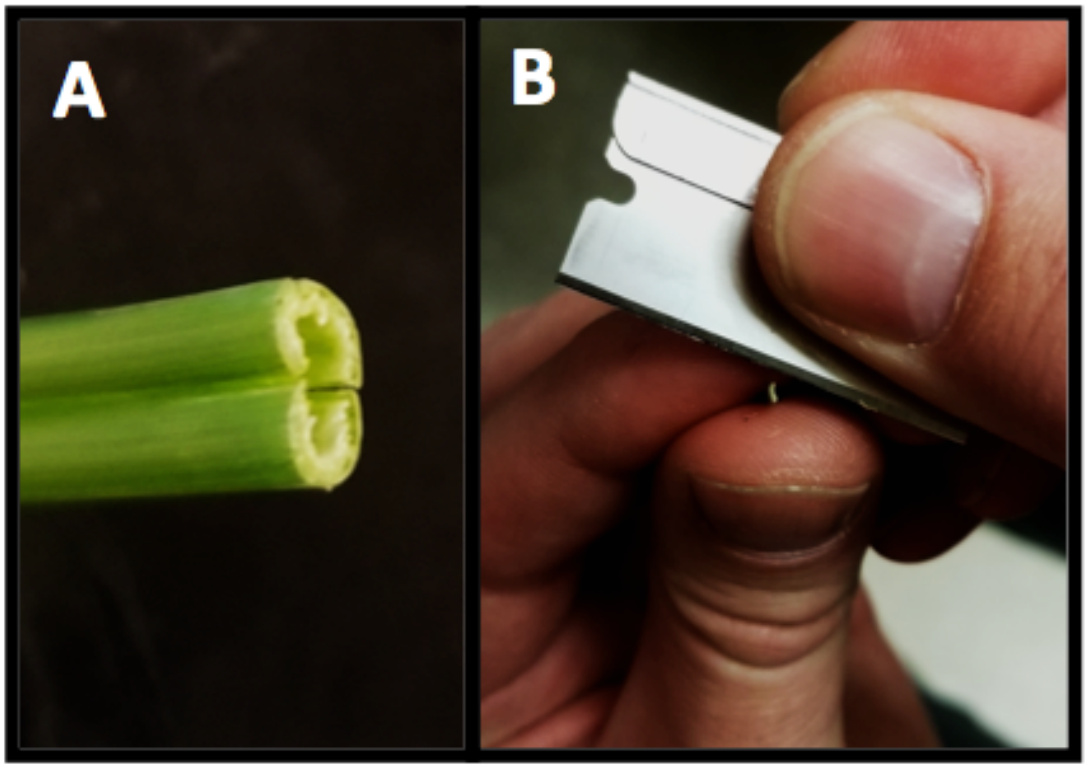

Figure S5.1. How to section a collapsed stem. (A) If the stem is crushed and collapses isolate a single shard and section starting with the short edge shown in (B). This approach is especially useful when samples are extremely valuable and can't be reproduced, such as field harvested samples, etc.

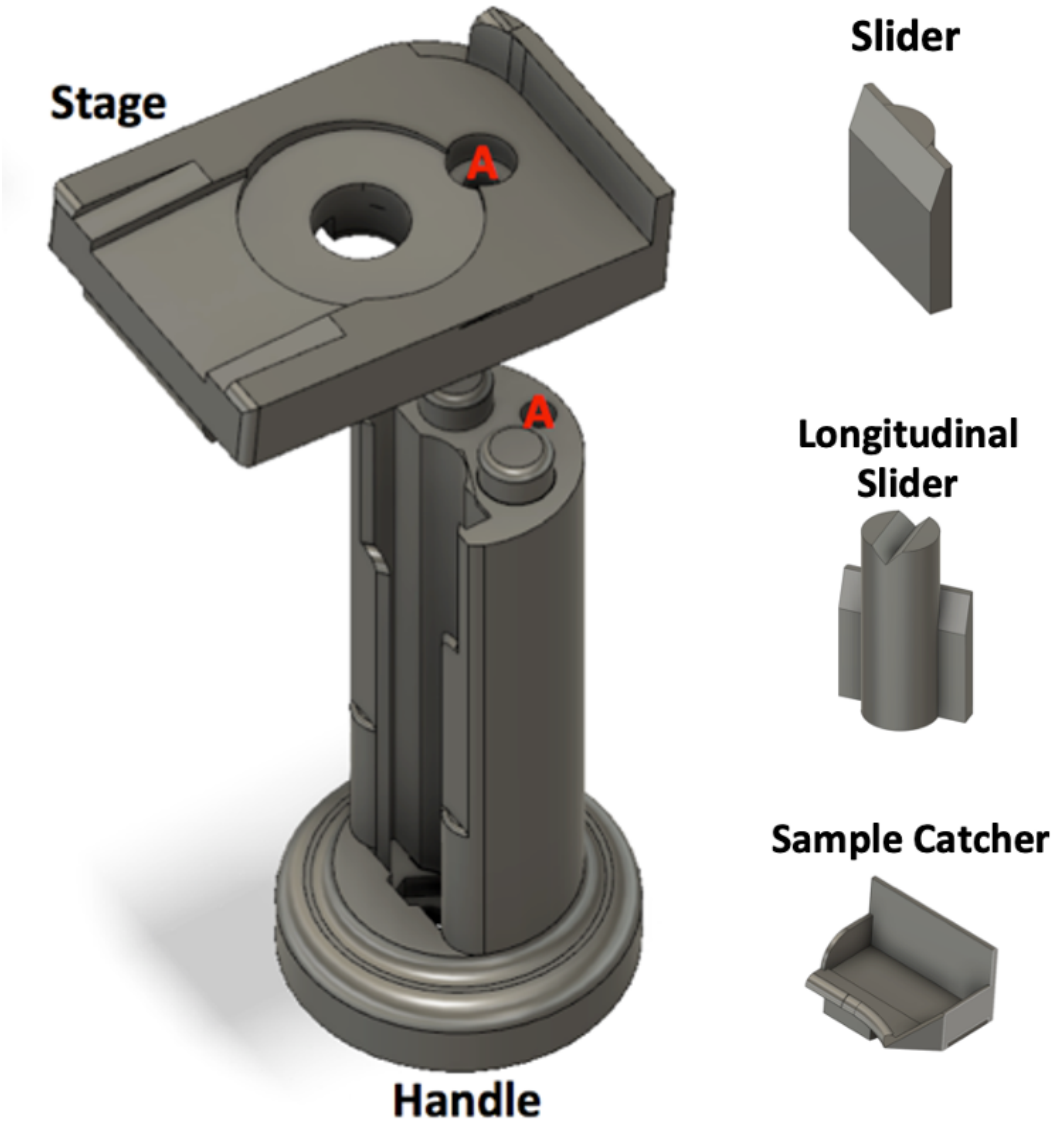

Figure S5.2. Labeled handle and stage assembly models. One or two sliders are slid into the grooves of the handle depending on sample length. A bolt placed through hole A from the top secures the stage to the handle. The sample catcher goes over hole A when sectioning. The longitudinal slider is an option for samples that can easily be glued or affixed to it for sectioning.

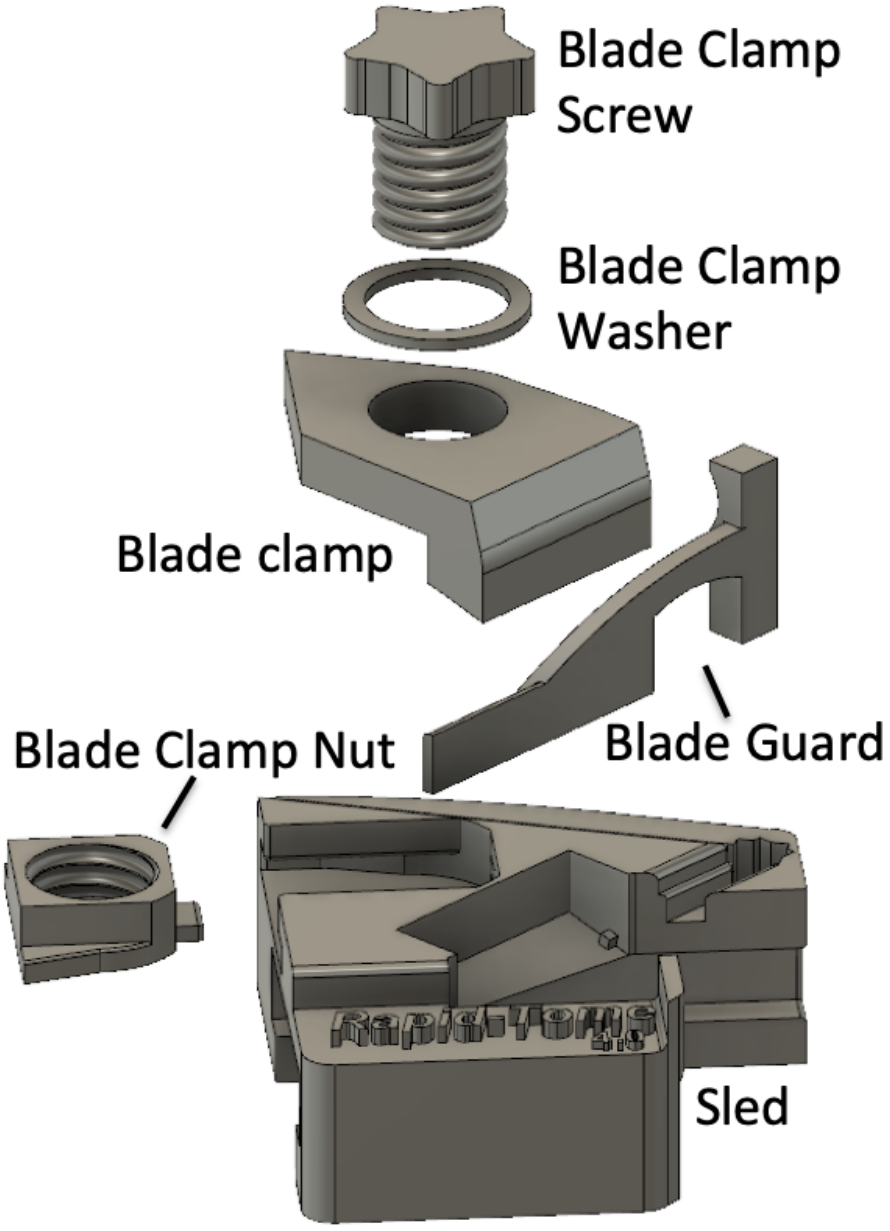

Figure S5.3. Sled and blade clamp models and assembly. The blade clamp nut should be slid into place first. The blade clamp screw is fed through the top of the blade clamp with the blade clamp washer between. The blade guard hooks underneath the bottom side of the sled behind the "Rapid-Tome 4.0" lettering and square base slid down into to opening. When the Rapid-Tome is in use, remove the blade guard and rotate 55 degrees and slide into the holster which is slightly smaller to ensure a secure hold.

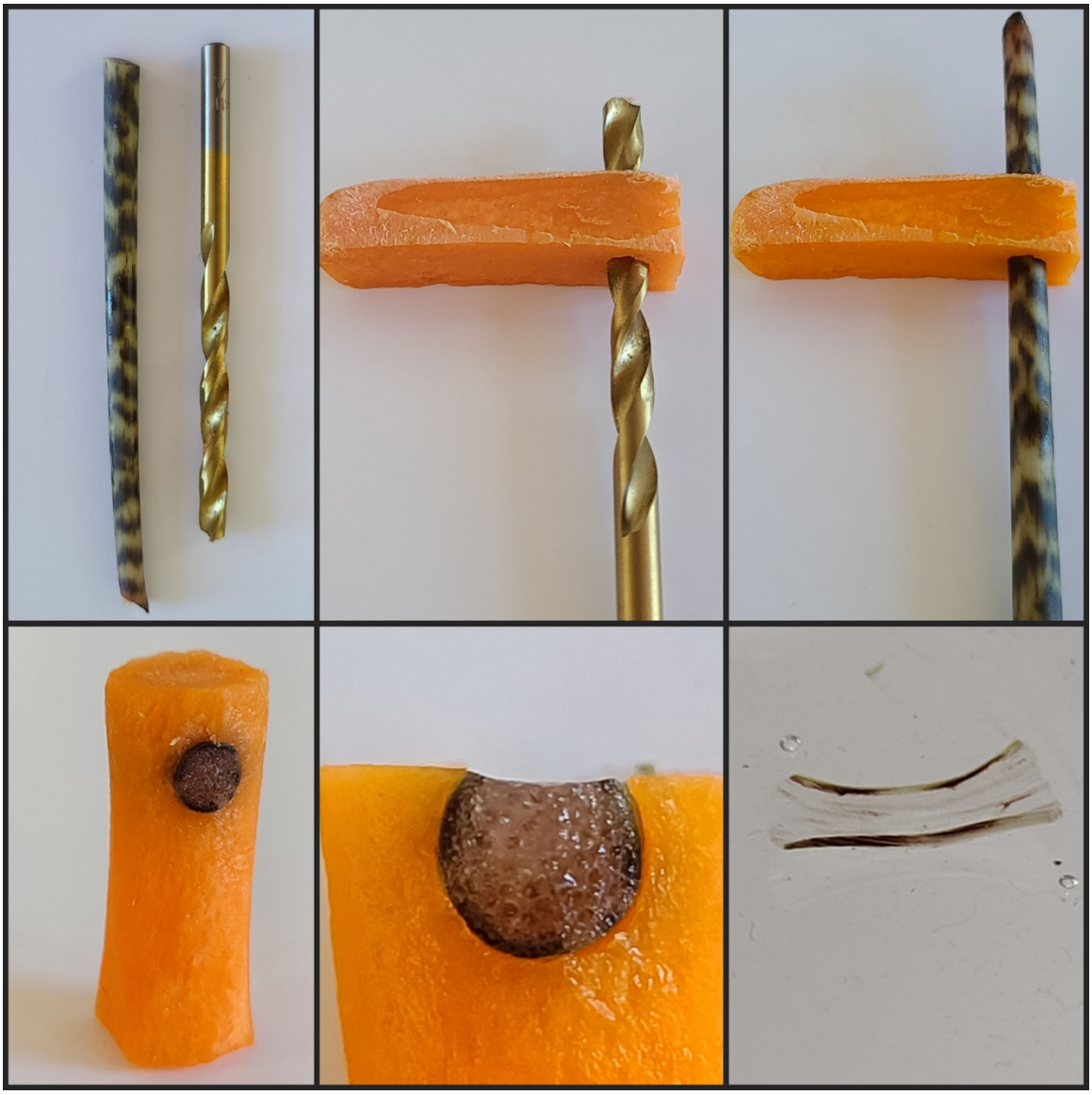

Figure S5.4. Longitudinal sections can be made utilizing a hole cut through a carrot. (A) Select a drill bit that is the same diameter or slightly smaller than the stem segment. (B) Drill a hole through a carrot by hand. (C) Push the stem segment into the carrot until snug. (D) Use a razor blade to remove excess stem segment and carrot so that the carrot fits into the Rapid-Tome stage hole. (E) The carrot effectively holds the stem in place during sectioning. (F) Thin sections are possible even with very fragile stem tissue.

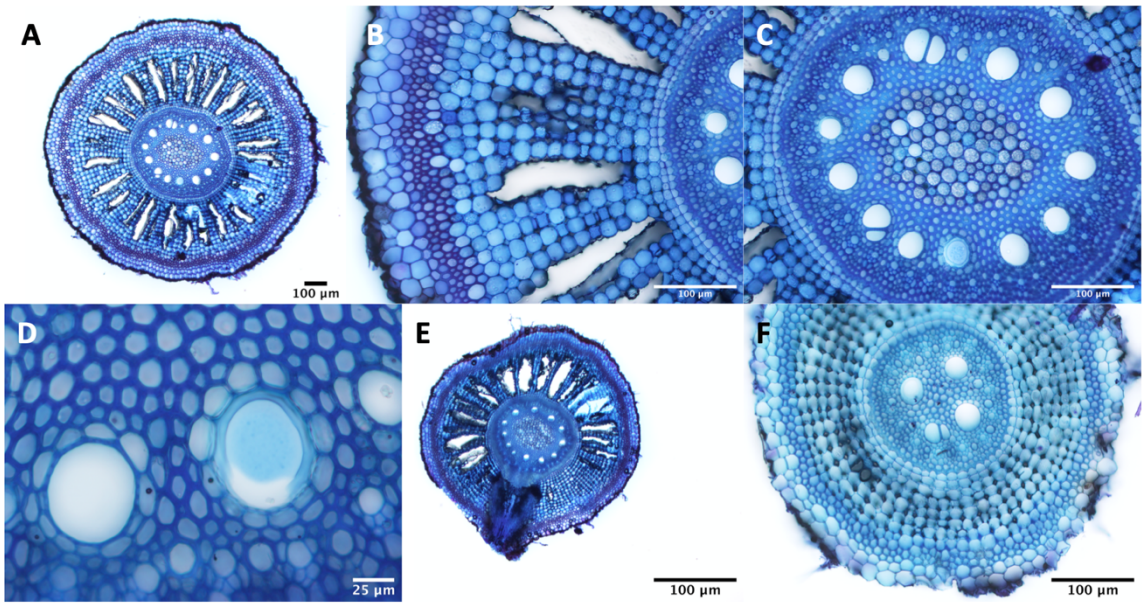

Figure S5.5. Sectioning soft, fresh roots of switchgrass represents the versatility of the Rapid-Tome. (A-D) Large root was sectioned with single cell features intact for analysis and aerenchyma visible. (E) An emerging lateral root from a smaller root was located prior to section to exemplify the ability to section an area of interest. A young secondary root with minimal sclerenchyma fibers was slightly more challenging to section. (F) High quality sections were made possible with the addition of s wrapping the root with three layers of parafilm prior to sectioning. All roots were stained with Toluidine Blue O. Scale bars as labelled.

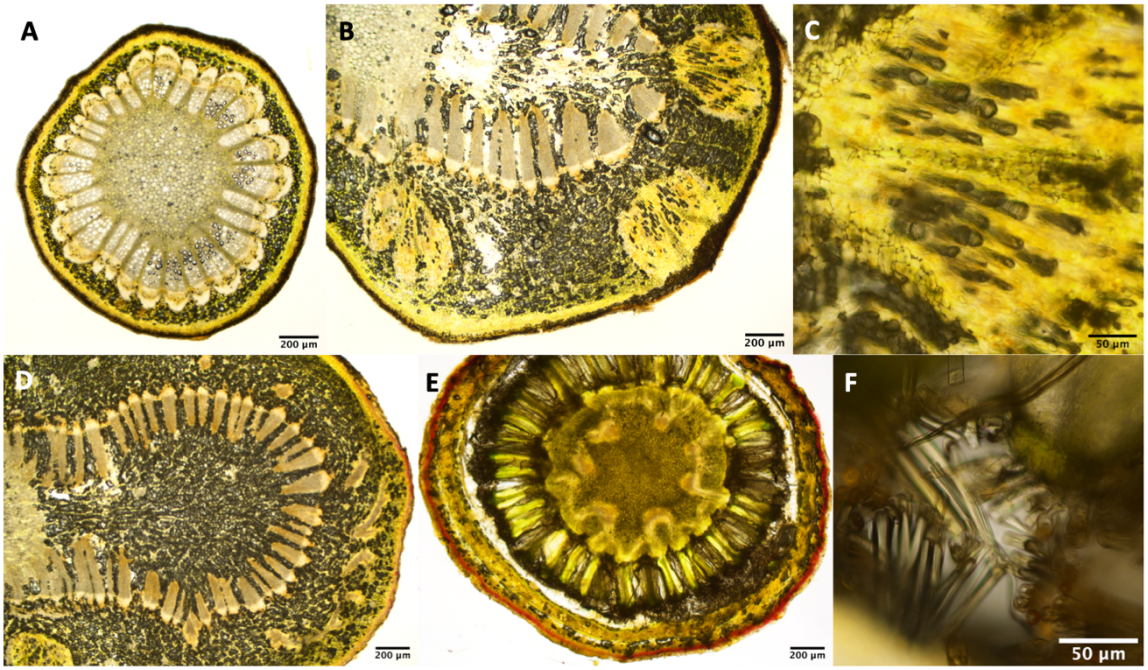

Figure S5.6. Serial sectioning of fresh sycamore terminal bud. Serial section through the tip of a terminal bud shows the quality of sections possible for inconsistent sample structures. This type of sample displays the accuracy of sectioning delicate samples with the Rapid-Tome. Images are presented in reverse order from the tip. Sections were unstained. Sample cut from tree and sectioned fresh the day of harvest. Scale bars as labelled.

Appendix C: Supplementary Text

Text S2.1

Supplemental text: Methods

Segment preparation carried out the day before Hydraulic Conductivity measurement

Segment length removed from full tiller is no less than 150 mm and trimmed to final length of 130 mm once fully prepared. Each segment must contain a single node that is 25 mm from the lower end (closest to the ground). The node must be included to ensure the presence of bordered pits between vessels (Gleason et al., 2017). Entirely remove leaf sheath from the lowest node of the supplied tiller. The lowest usable node to the ground must have a minimum of 3 cm internode length below the node. Remove the leaf sheath form above the node. For larger diameter tillers, typically lowland, a shallow (1-2 mm) cut with a fresh razor blade just above the node was required to facilitate a clean removal. Each location of trimming cuts was wrapped with at least 3 wraps of parafilm that is 3 cm in width, applied over the cut site so that 2 cm of the parafilm width is on the part of the internode closest to the node and 1 cm on the distal part of the internode that will be removed after cutting. With the cut end of the tiller under degassed hydraulic conductivity solution**,** the lower internode below the node was cut to 25mm, cutting through the parafilm. The second (upper) trimming cut was made 125 mm from the node under hydraulic conductivity solution, making the total segment length 150mm. Each segment was labelled with a tape flag label with unique segment ID. Place a tape flag over the parafilm at the end near the node, leaving the cut end exposed. Transfer the labeled segment to vacuum chamber. The vacuum chamber is filled with 4 L of 20 mM KCL nanopure

filtered distilled water. This hydraulic conductivity will be used in subsequent steps of the hydraulic conductivity solution. Segments are rehydrated via vacuum hydration prior to the first hydraulic conductivity measurement at 100% hydration. Segments were held under vacuum for 12 hours.

Gently transfer several segments to the transfer tray and move to the HCA tray. Segments must be kept horizontal. The hydraulic conductivity apparatus tray is filled to a depth of 3 cm with HCS. A 10 x 20 cm silicone mat is submerged and used to hold the segments under the hydraulic conductivity solution after trimming to prevent them from floating and taking in air. Segments should sink after hydration, but smaller segments may float due to the tape and parafilm buoyancy. Also in the hydraulic conductivity tray is a 15 cm ruler and a thin plastic cutting board. Holding the segment horizontally tightly wrap the entire segment in at least 3 wraps of parafilm. Wrapping prevents air seeding through the exposed cut of the leaf sheath and stem stomata that cause premature loss of conductivity during centrifugation. Wraps should be done with a 3 cm width strip of parafilm in a helical manor, working from one end to the other.

Sealing the pith

Polyurethane foam is an open cell foam from earplugs and is ideal for several reasons. Earplugs are designed to have a slow expansion to original size after being compressed, which is helpful to fill the pith after compressing the foam. Additionally, this foam expands past original size when absorbing liquid. Foam strips cut with a razor blade in the absence of moisture to 5-8 mm in length are used to seal the pith in combination with cyanoacrylate Loctite ultra-control gel super glue. The width and length of the foam strips varies with the diameter of the pith. The cyanoacrylate Loctite gel is applied using a micro-

tip applicator so the glue tip can fit into the pith. The cut end closest to the node is triple sealed with foam sandwiched between two glue layers. Sealing steps are carried out while holding the node end just barely out of the hydraulic conductivity solution, with the other end still submerged. Cyanoacrylate cures under water, but all pith steps must be completed before the segment is re-submerged in hydraulic conductivity solution to prevent premature expansion of the foam.

Insert the micro-tip glue applicator into the pith all the way to the node, back off ~ 1 mm and begin to apply the glue. Pull back the glue tip to make room for the glue coming out. The goal is to apply enough glue to span the diameter of the pith for a length of 5-10 mm. Watch for water drops coming out of the pith as the glue displaces it. Remove glue tip and insert the first foam strip with fine point forceps gripping one end of the foam strip. The foam will start to expand rather quickly as it begins to soak up water and glue, move quickly. Use the metal syringe plunger to further push the foam into place. Take care not to push too hard and puncture the foam. Slowly rotate the segment so that the plunger presses against the circumference of the newly forming disc-shaped foam plug within the pith cavity. A little more glue is added after the first foam strip before the second strip is added in the same method as the first. Note: Figure S8B does not show the addition of the second foam that was added to the methods later. There should be at least 1 cm of hollow pith left past the foam plugs. Add another layer of glue ~2 mm thick on top of the foam. It is ok if some glue touches the exposed cut end, 1 cm will be cut off. The foam glue sandwich is designed to ensure that the foam saturates completely and expands to fill the pith cavity, rather than expand into the open end of the pith. The segments then have an

additional 1 cm trimmed from each end to make the final length of 130 mm under the hydraulic conductivity solution in the hydraulic conductivity apparatus tray.

Before the first conductivity measurement was taken, segments were first spun at 500 RPM (-0.03125 MPa) to remove open vessel artifacts by effectively flushing the vessels that span the entire length of the segment. Five or more segments were measured before and after spinning at 500 RPM to assess conductivity losses because of this preventative measure. Percent loss of conductivity of comparing before and after spinning at 500 RPM was less than 2% for all genotypes (+/- 0.5%). Though minimal, the Ks and PLC data in figures 6 and S7 are adjusted to account for this by genotype specific average PLC after spinning at 500 RPM. The other benefit of this approach is to have a proxy measurement of the PLC due to open vessels, and therefore an estimate of the open vessels located in each segment. Each PLC curve was made with 5-12 individual conductivity measurements taken per 13 cm segment after increasingly higher centrifugation RPMs, simulating increasing conditions of water stress.